Hybrid Separations and Adsorption/Reaction Processes: The Case of Isomerization/Separation of Xylenes

Dissertation presented to Faculdade de Engenharia da Universidade do Porto for the degree of PhD in Chemical and Biological Engineering

by

Jonathan Carlos Gonçalves da Silva

Supervised by Professor Alírio Egídio Rodrigues

Laboratory of Separation and Reaction Engineering, Associated Laboratory LSRE/LCM Department of Chemical Engineering, Faculty of Engineering, University of Porto

April 2015

This thesis was financially supported by *Fundação para a Ciência e a Tecnologia* (Portugal) through the PhD grant SFRH/BD/74402/2010. The work was also co-financed by QREN, ON2 and FEDER (Project NORTE-07-0124-FEDER-000007 – Multifunctional Reactors/Process Intensification) and co-financed by FCT/MEC and FEDER under Programe PT2020 (Project UID/EQU/50020/2013).

FEUP-LSRE/LCM - Universidade do Porto

Acknowledgments

In the first place, I would like to thank my supervisor Professor Alírio Rodrigues for giving me the opportunity to come to LSRE and continue my professional formation in chemical engineering. His invaluable guidance and vast experience were an essential keystone in the path for achieving my goals.

I would also like to thank all the professors and colleagues at the LSRE for their patience and willingness to help me anyway they could, whether in terms of basic concepts or experimental work in the lab, they always found the time to assist me. Additionally, all their support outside the LSRE was imperative for me to adapt to a different environment and culture allowing me to grow as a human being as well.

To all family I will always be grateful. Even though they are far away, all their love and support gave me the strength to keep pursuing my goals and dreams. Also to all my Venezuelan friends, here in Porto and those spread around the globe, who gave me the courage to face all the challenges that have presented in this period of my life.

To all and each one of you…

GRACIAS… TOTALES!!!

Abstract

Aromatics and specifically *p*-xylene are building blocks in the production of a variety of products used every day. Since worldwide population increases at exponential rate, the demand of this type of products will increase as well. The demand of *p*-xylene is expected to grow at a rate of 7.4% until 2022; moreover in Portugal the gap between demand and supply in *p*-xylene and benzene is considerably high.

Industrial production of *p*-xylene consists of a cycle loop where *p*-xylene is separated and the other isomers are sent to an isomerization unit where *p*-xylene is produced and recycled back to said separation unit. Since isomerization of xylenes thermodynamically favors the production of *m*-xylene, the energy consumption within the recycle loop is significantly high to fulfill the *p*-xylene demands. In order to overcome the equilibrium constraints, a multifunctional reactor combining separation and isomerization for the production of *p*-xylene together with the modification of the existing aromatics complex in Portugal is proposed to increase the production of benzene and *p*-xylene. The existing simulated moving bed unit for separation of *p*-xylene is turned into a simulated moving bed reactor for separation and production of *p*-xylene at an intermediate concentration which is further purified in a single stage crystallization unit. More *p*-xylene and benzene are produced through selective toluene disproportionation to convert less valuable toluene into said products.

The simulated moving bed reactor is analyzed to determine the appropriate arrangement of columns maintaining the actual dimensions of the unit and the optimal particle size according to the maximum pressure drop that leads to the higher production of *p*-xylene. Calculations based on the true moving bed reactor approach and the actual shifting of the ports leads to two columns, six columns, fourteen columns, and two columns in the first, second, third, and fourth zone respectively where 15% of each column comprises a bed of homogeneous mixture with adsorbent to adsorbent plus catalyst weight ratio of 0.4 followed by a second bed filled with adsorbents using a particle diameter of 0.62 mm. The dual-bed unit allows to obtain in the extract 175% of the *p*-xylene fed to the unit at 200 ºC. The proposed aromatics complex including the dual-bed simulated moving bed reactor, the selective toluene disproportionation, and the single stage crystallization unit results in an increase of 170% and 72% of production of benzene and *p*-xylene respectively.

Finally, three zeolites are experimentally studied with the purpose to be used in the simulated moving bed reactor. Beta zeolite with Si/Al ratio of 35 exhibits the best performance due to its proper balance of acidity.

Resumo

Os aromáticos e especificamente o *p*-xileno atuam como precursores para a produção de uma variedade de produtos usados todos os dias. Uma vez que a população mundial aumenta em ritmo exponencial, a procura deste tipo de produtos também vai aumentar. A procura de *p*-xileno deverá crescer a uma taxa de 7,4% até 2022; além disso, em Portugal a diferencia entre a oferta e a procura de *p*-xileno e benzeno é consideravelmente alta.

A produção industrial do *p*-xileno é constituída por um ciclo em que o *p*-xileno é separado dos outros isómeros os quais são enviados para uma unidade de isomerização onde o *p*-xileno é produzido e reciclado de volta para a referida unidade de separação. Já que o *m*-xileno é favorecido termodinamicamente na isomerização de xilenos o consumo de energia no ciclo é significativamente alto para atender a procura do *p*-xileno. A fim de superar as limitações de equilíbrio, propõe-se a utilização de um reator multifuncional que efetuará simultaneamente a separação e isomerização de *p*-xileno em conjunto com a alteração do complexo aromático existente em Portugal de forma a aumentar a produção do benzeno e *p*-xileno. A unidade de leito móvel simulado existente para a separação do *p*-xileno é substituída por um reator de leito móvel simulado para a separação e produção do *p*-xileno a uma concentração intermédia que é posteriormente purificado numa unidade de cristalização duma etapa. *p*-Xileno e benzeno são também produzidos através da dismutação seletiva de tolueno.

O reator de leito móvel simulado é analisado para determinar a distribuição apropriada de colunas mantendo as dimensões reais da unidade e o tamanho de partícula ótimo de acordo com a queda de pressão máxima que conduz ao aumento da produção do *p*-xileno. Cálculos baseados no reator de leito móvel verdadeiro e no deslocamento real das linhas de entrada e saída conduz a duas, seis, catorze e duas colunas na primeira, segunda, terceira, e quarta zona respetivamente, onde 15% de cada coluna compreende uma primeira camada que consiste numa mistura homogénea com uma relação de adsorvente para adsorvente mais catalisador de 0.4 em peso seguida por uma segunda camada de adsorvente usando um diâmetro de partícula de 0.62 mm. A unidade de duas camadas permite a obtenção no extrato de 175% de *p*-xileno alimentado à unidade a 200 ºC. O complexo aromático proposto, incluindo o reator de leito móvel simulado, a dismutação seletiva de tolueno e a unidade de cristalização resulta num aumento de 170% e 72% na produção de benzeno e *p*-xileno.

Finalmente, três zeólitos são experimentalmente estudados com a finalidade de serem usados no reator de leito móvel simulado. O zeólito Beta com uma relação Si/Al de 35 apresenta o melhor desempenho devido ao seu balaço adequado de acidez.

Table of Contents

List of Figures

List of Tables

Chapter 1: Introduction

This chapter presents the motivation, objectives, and outline of the research involving the development of a process that couples the separation and isomerization in *p*-xylene production. The motivation is based on three aspects: the promising *p*-xylene market behavior, the major importance of the development of sustainable processes in order to follow the environment guidelines that drive the world today, and the necessity of an integrated aromatics plant to match the required aromatics production. Furthermore, the main objective is stated and the rest of the chapters of the thesis are briefly described.

1.1. Relevance and motivation

Xylenes are aromatic hydrocarbons used as raw material for the manufacture of a wide range of products used every day. Xylenes comprise four isomers: *p*-, *m*-, *o*-xylene, and ethylbenzene; the most important due to its application is *p*-xylene. The use of *p*-xylene is mainly the production of polyethylene terephthalate (PET), which is used as polyester fibers, films, and resins for a variety of applications [1]. Particularly PET bottles have received a lot of attention based on their recyclability. The demand is expected to grow at a rate of 7.4% from 2012 to 2022, driven mostly by the production of PTA (Purified Terephthalic Acid – precursor of PET) in China [2].

The production of *p*-xylene is currently performed based on two main operations units: Separation, which is basically the extraction of pure *p*-xylene; and Isomerization, where additional *p*-xylene is produced from the other isomers and recycled back to the separation unit. The most common process for *p*-xylene separation is selective adsorption where an adsorbent retains the *p*-xylene from a liquid mixture of xylenes and a desorbent is used to extract the product. Isomerization is carried out in a gas phase fixed bed catalytic reactor, where the *p*-xylene yield is limited by the thermodynamic equilibrium. Due to the equilibrium constraints a large cycle loop is often required to achieve the desired amount of *p*-xylene; a large loop along with gas phase conditions increase significantly the energy consumption within the process. The aforementioned could be minimized through the ensemble of both units based on the concept of process intensification.

Process intensification, as part of the European Technology Platform on Sustainable Chemistry, indicates the ensemble of technologies that lead to substantially smaller, cleaner, safer, and more energy-efficient processes where lower consumption of raw materials and reduction of emissions of greenhouse gases and pollutants are achieved [3].

The proposed technology for coupling the processes of separation and isomerization in *p*-xylene production is the simulated moving bed reactor (SMBR). As mentioned before, the separation is a selective adsorption process carried out in liquid phase in fixed bed adsorption columns. The concept of simulated moving bed (SMB) is applied to mimic the counter-current flow of the solid adsorbent and liquid flow throughout the switching of inlets and outlets in the column. The SMBR uses the same principle and incorporates the reaction section, the catalyst, within the adsorption columns. In order to combine both processes, isomerization in liquid phase shall be studied. Although the conversion may be lower, it brings other advantages such as better thermal control and longer catalyst life, which allows for off-site catalyst regeneration and therefore easier control of pollution. Furthermore, since the *p*-xylene is withdrawn as it is formed, the equilibrium constraints in the isomerization can be minimized through the SMBR; thus,

reducing the cycle loop and the energy consumption within the process. Recent researches have given promising results, Minceva et al. [4] reported values as high as 1.75 for *p*-xylene deviation from equilibrium (actual *p*-xylene produced to equilibrium *p*-xylene produced ratio) under certain conditions. Bergeot et al. [5] claimed that with this type of technology the recycle feed (cycle loop) is reduced in 54%.

In Portugal, the aromatics are produced within the Matosinhos Refinery located in the northern region of the country; the production capacities of benzene, toluene, *o*- and *p*-xylene are about 43.5, 140, 10, and 92 thousand mtpy respectively [6]. However, start-up of new facilities for the production of nitrobenzene [7] and PTA [8] of 300 and 700 thousand mtpy respectively, establish a considerable difference between supply and demand of benzene and *p*-xylene in the local market. Situations like these shall be seen as an opportunity, a window is opened to improve the processes and increase the production. The high amount of toluene can be used to overcome the deficit, less-valuable toluene can be further processed to obtain valuable products such as benzene and *p*-xylene. Based on the aforementioned, a modified aromatics complex is proposed including Selective Toluene Disproportionation, Single Stage Crystallization, and Simulated Moving Bed Reactor units to increase the production of benzene and *p*-xylene.

1.2. Objectives and outline

The main objective of this thesis is the development of a Simulated Moving Bed Reactor for the production of *p*-xylene in the framework of a proposal to modify the current aromatics complex which allows milder *p*-xylene purity constraints in the extract. The unit shall exhibit optimum arrangement of columns, flow rates, switching time, particle size, and efficient distribution of adsorbents and catalysts based on the existing Simulated Moving Bed facility. In addition, an extensive study on xylene isomerization in liquid phase shall be carried out.

The thesis is divided in ten chapters to reach the aforesaid objectives.

Chapter 2 consists of the discussion of the State-of-the-Art on *p*-xylene production. Starting with the uses, economics, and sources; and then focusing on the current technologies within the aromatics complex, specifically on the processes of *p*-xylene separation and isomerization of xylenes as well as toluene conversion.

The study on xylene isomerization in liquid phase starts with the thermodynamic equilibrium in **Chapter 3**. Based on experiments performed by several researchers in the 1990s, three different expressions are developed to calculate the equilibrium constants as a function of temperature.

In **Chapter 4**, the existing unit for the isomerization of xylenes in gas phase is studied. A mathematical model with optimized kinetic constants is developed based on 34 days of continuous operation of the unit.

The model of the SMBR unit is introduced in **Chapter 5**. A homogeneous mixture of adsorbents and catalyst throughout the columns, with higher proportion of the first, is used to obtain the desired extract and raffinate purities. The system is modeled based on the true moving bed reactor approach for several arrangements of columns under different desorption consumption constraints.

A similar methodology is used in **Chapter 6** to determine the optimum particle size to be used in the unit. Once more, several arrangements of columns comprising a homogeneous mixture with high adsorbent to adsorbent plus catalyst ratio are studied based on the true moving bed reactor approach under maximum allowable pressure drop.

A different distribution of adsorbents and catalysts is analyzed in **Chapter 7**. Every column contains a first bed with a homogeneous mixture where catalyst is present at higher proportion followed by a second bed with just adsorbents. The system is modeled based on the actual shifting of inlet and outlet ports, yet the true moving bed reactor approach is validated for the development of the unit.

The proposed aromatics complex is evaluated in **Chapter 8**. Simplified models for selective toluene disproportionation and single stage crystallization units are used together with more rigorous models for gas phase isomerization and simulated moving bed reactor units, developed in previous chapters, to estimate the increase in production of benzene and *p*-xylene within the complex.

In **Chapter 9**, large-pore zeolites are studied experimentally as possible catalysts for xylene isomerization in liquid phase in the Simulated Moving Bed Reactor unit at three different temperatures and compared to published kinetic data.

Finally, **Chapter 10** presents the major conclusions of this thesis along with recommendations for future work.

1.3. References

[1] Johnson, J. A. 2003. "Aromatics Complexes." In *Handbook of Petroleum Refining Processes*, 2.3-2.11. McGraw-Hill.

[2] Brookes, T. 2012. New Technology Developments in the Petrochemical Industry - Refinery Integration with Petrochemicals to Achieve Higher Value Uplift. In *Egypt Petrochemicals Conference*. Cairo, Egypt: UOP LTD.

[3] Cavani, F., and G. Centi. 2000. "Sustainable Development and Chemistry." In *Kirk-Othmer Encyclopedia of Chemical Technology*. John Wiley & Sons, Inc.

[4] Minceva, M., P. S. Gomes, V. Meshko, and A. E. Rodrigues. 2008. "Simulated moving bed reactor for isomerization and separation of p-xylene." *Chemical Engineering Journal* no. 140 (1-3):305-323.

[5] Bergeot, G., D. Leinekugel-Le-Cocq, L. Wolff, L. Muhr, and M. Bailly. 2010. "Intensification of Paraxylene Production using a Simulated Moving Bed Reactor." *OGST – Revue d'IFP Energies nouvelles* no. 65 (5):721-733.

[6] Galp Energia. *Fábrica de aromáticos e solventes*. http://www.galpenergia.com/PT/agalpenergia/os-nossos-negocios/Refinacao-Distribuicao/ARL/Refinacao/RefinariaMatosinhos/Paginas/FabricaAromaticosSolventes.aspx 2015.

[7] Instituto do Ambiente e Desenvolvimento. 2007. Projecto de Ampliação da CUF-QI Estudo de Impacte Ambiental. Instituto do Ambiente e Desenvolvimento.

[8] Artlant PTA. *Artlant PTA starts production*. http://artlantpta.com/index.php/en/news/126-artlant-pta-starts-production-in-sines 2015.

Chapter 2: State-of-the-Art

This chapter presents the state-of-the-art on *p*-xylene production. A brief introduction on aromatics, including their applications, world and local supply and demand, as well as the economics that drive the production are shown. An overview of an aromatics complex is displayed, starting with the sources and looking over the main units within the complex. Special attention is given to *p*-xylene separation and xylene isomerization, which are the focus of the thesis. Both units are described in detail, types of technologies most employed and the principal suppliers worldwide in these processes are also discussed. The chapter ends with a quick look to the future through a patent review on *p*-xylene production.

2.1. Introduction

Xylenes and ethylbenzene are eight-carbon aromatic isomers (also referred as A_8) that exhibit the molecular formula C_8H_{10}. The xylenes consist of the three isomers depending on the position of the methyl group: *o*-xylene, *m*-xylene, and *p*-xylene. The molecular structures are shown in Figure 2.1.

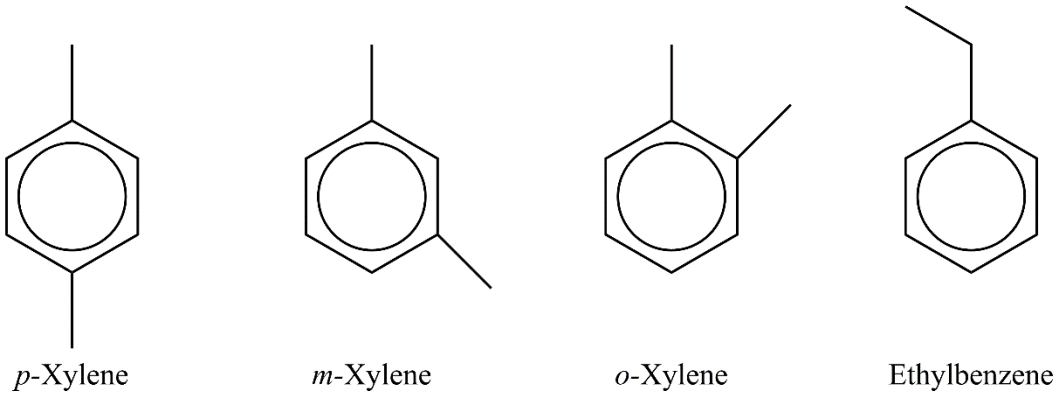

Figure 2.1 Molecular structures of xylene isomers and ethylbenzene

The term mixed xylenes describes a mixture containing the three xylene isomers and usually ethylbenzene and they form a temperature depending equilibrium as it is shown in Figure 2.2.

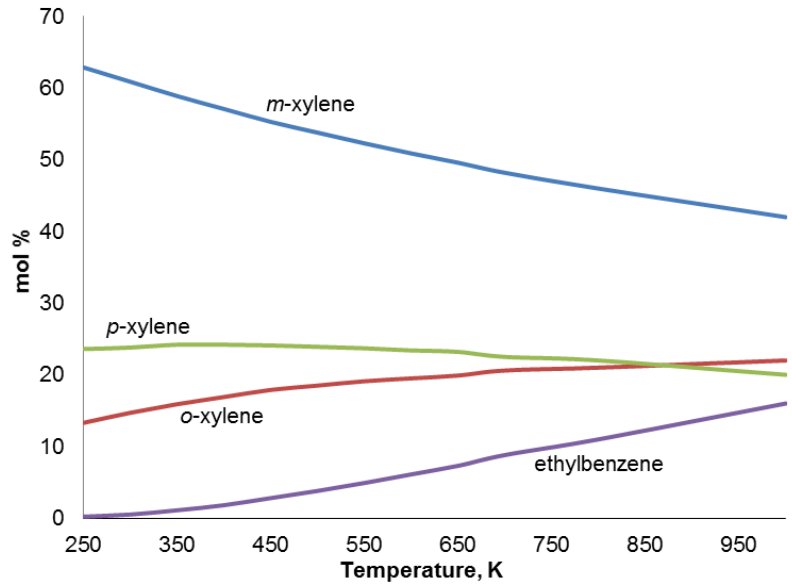

Figure 2.2 Equilibrium product distribution for mixed xylenes at atmospheric pressure [1]

2.2. Derivatives and economics of aromatics

The basic petrochemical intermediates are benzene, toluene, and xylenes. Benzene is a versatile petrochemical building block used in the production of more than 250 different products. The most important benzene derivatives are ethylbenzene, cumene, and cyclohexane (See Figure 2.3).

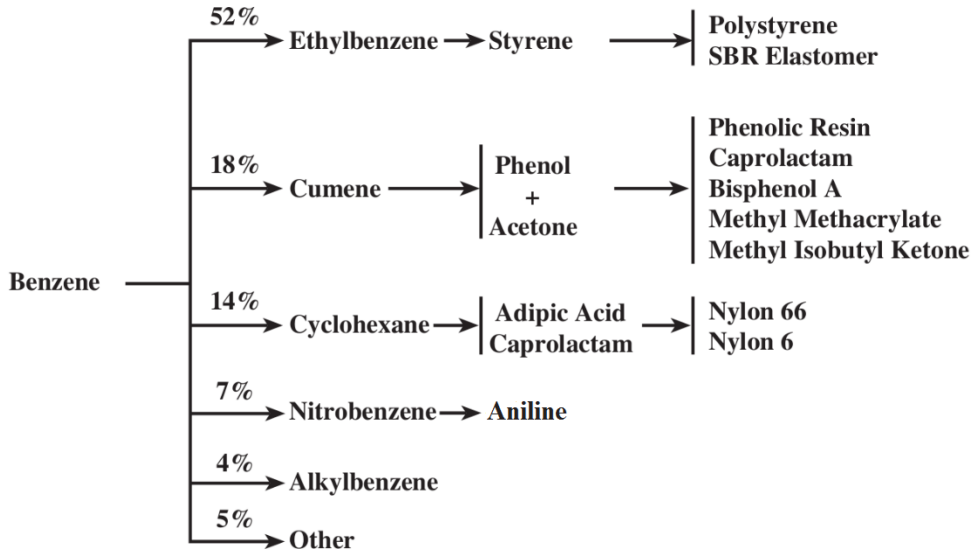

Figure 2.3 Benzene derivatives [2]

Small amounts of mixed xylenes are used for solvent applications, but most xylenes are further processed within the complex to produce one or more of the individual isomers. The most important C_8 aromatic isomer is *p*-xylene, which is used almost exclusively for the production of polyester fibers, polyethylene terephthalate (PET) resins, and films (See Figure 2.4).

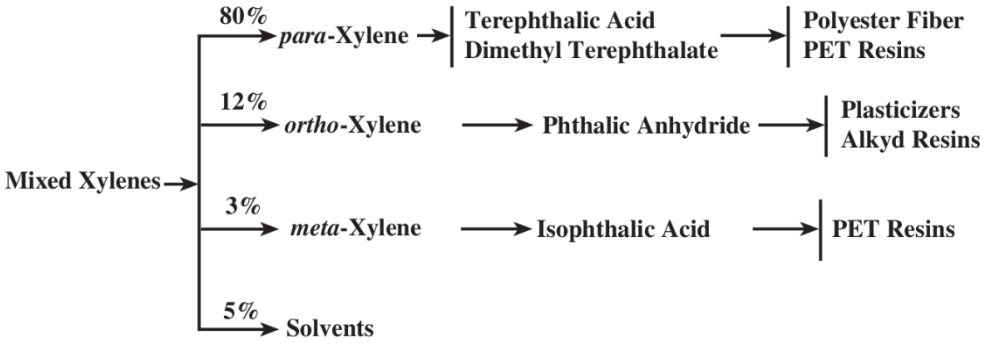

Figure 2.4 Xylenes derivatives [2]

A small amount of toluene is recovered for use in solvent applications and derivatives, e.g., trinitrotoluene and benzoic acid which require relatively smaller amounts; toluene is rather converted to benzene and xylenes [3].

In addition to the previously mentioned applications as building blocks in the petrochemical industry, aromatics are also used as a high octane blending component in gasoline. Regarding the latter, restriction of total aromatic content in the gasoline pool is affecting the market. Moreover, leading economies such as North America and Europe are reducing the gasoline consumption by means of alternative fuels. However, the decrease of aromatics use in gasoline blending is smaller compared to the use as a petrochemical feedstock. A few decades ago the portion of aromatics used in gasoline was significantly higher than that for petrochemical derivatives. Nowadays the growth in petrochemical complexes is remarkable; in fact, China's aromatic capacity has now exceeded the other regions. A substantial portion of China's growth can be attributed to an increased demand to produce purified terephthalic acid (PTA) via *p*-xylene. Emerging regions along with an increasing demand of PET products worldwide have built a robust *p*-xylene market with an expected growth at a rate of 7.4% from 2012 to 2022 [4-6] (see Figure 2.5).

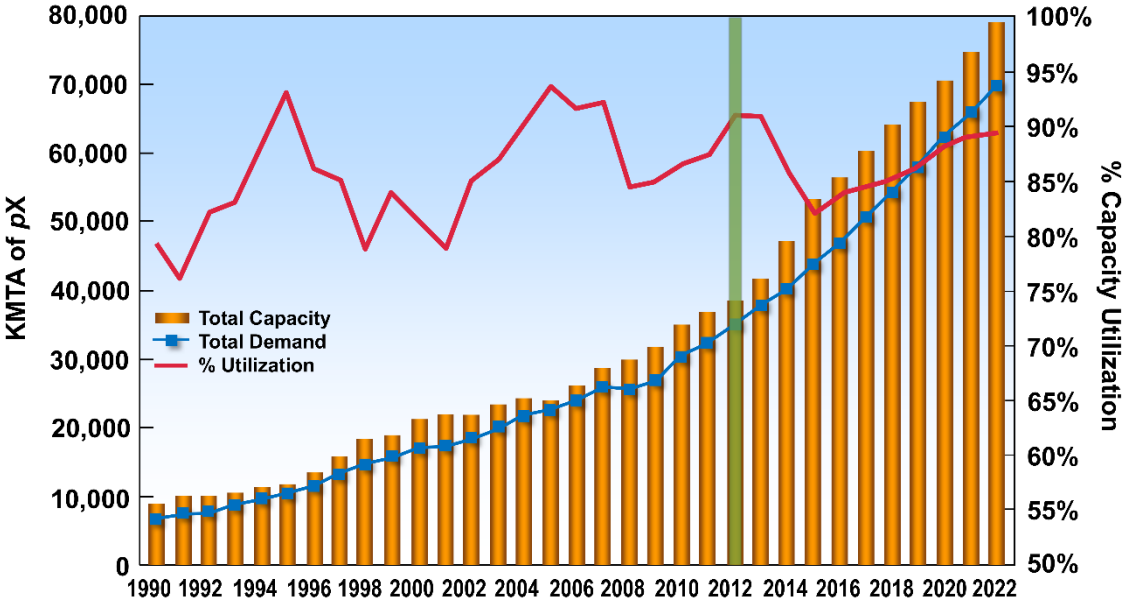

Figure 2.5 World *p*-xylene supply/demand [5]

2.2.1. Aromatics production in Portugal

Matosinhos is one of the main industrial complexes in Portugal owned by Galp Energia. Fuel production, aromatics and solvents, lube oils, paraffins, and sulfur are among the main process units within the complex. The aromatics and solvents unit has a capacity of 440 thousand mtpy, from which the main aromatics products are benzene, toluene, *p*-xylene, and *o*-xylene. A schematic representation of the aromatics plant with nominal capacities is presented in Figure 2.6.

From the flowsheet it can be seen that reformate is the source of aromatics in the complex. Liquid-liquid extraction is performed within the *Arosolvan* unit to separate the non-aromatics and through conventional distillation benzene and toluene are produced with a capacity around of 43.5 and 140 thousand mtpy respectively. A portion of *o*-xylene is separated based on the 5 ºC difference in the boiling points inside the *Xylenes Splitter* unit, approximately 10 thousand mtpy are produced. Finally the *Parex* unit produces 92 thousand mtpy of *p*-xylene [7]. The annual production is based on the nominal capacity with 335 days of operation.

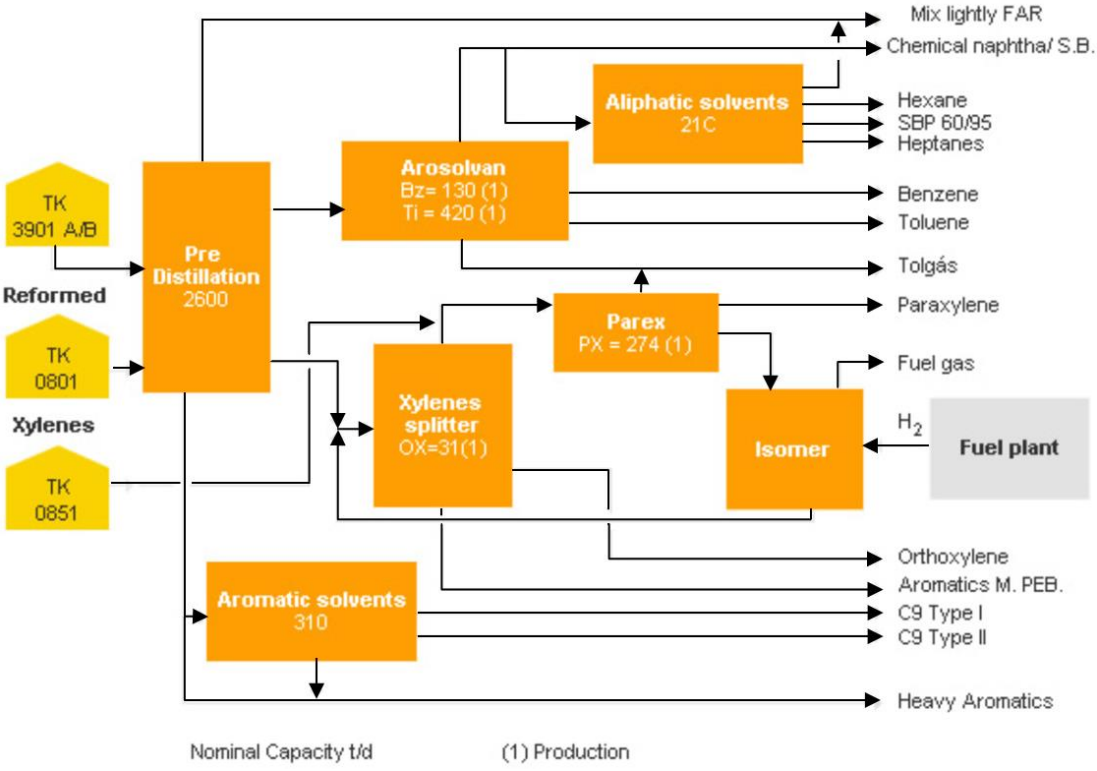

Figure 2.6 Galp aromatics complex [7]

As mentioned before, benzene, toluene, and xylenes are basic intermediates for the petrochemical industry. In Portugal, a high amount of benzene is used in the production of nitrobenzene which is further processed to aniline. The nitrobenzene plant, owned by CUF – Químicos Industriais, started in 1991; after the last expansion project increased their capacity from 175 to 300 thousand mtpy [8]. *p*-Xylene is oxidized to produce PTA which is used as the raw material in the manufacture of polyester polymers. In March 2012 Artlant PTA, located at the south of the country, started the production of PTA with an installed capacity of 700 thousand mtpy [9]. From the aforesaid figures it can be seen that there is a considerable difference between the supply and demand of benzene and *p*-xylene in Portugal.

2.3. Sources of aromatics

The only natural source is petroleum, the fraction varies according to location and geological age; even though the fraction can be as high as 35 wt%, the direct isolation is not economical [10]. Petroleum naphtha is the main feedstock for aromatics production. Reformed naphtha, or reformate, accounts for 70% of total world BTX supply. The pygas by-product from ethylene plants is the next-largest source at 23%. Coal liquids from coke ovens account for the remaining 7%. Pygas and coal liquids are important sources of benzene that may be used only for benzene production or may be combined with reformate and fed to an integrated aromatics complex. Pygas composition varies widely with the type of feedstock being cracked in an ethylene plant, light cracker feeds contain almost no C_8-aromatics. Substantial amounts of C_8-aromatics are found only in pygas from ethylene plants cracking naphtha and heavier feedstocks.

Because reformate is much richer in xylenes than pygas, most *p*-xylene capacity is based on reforming petroleum naphtha. Straight-run naphtha is the material recovered directly from crude oil simple distillation. Hydrocracked naphtha, which is produced in the refinery by cracking heavier streams in the presence of hydrogen, is rich in naphthenes and makes an excellent reforming feedstock. Straight-run naphthas must be hydrotreated before being sent to the aromatics complex, but this pretreatment is not as severe as that required for pygas.

Naphtha is characterized by its distillation curve and is defined by the initial boiling point (IBP) and endpoint (EP). A typical BTX cut has an IBP of 75ºC and an EP of 150ºC. However, many aromatics complexes tailor the cut of the naphtha to fit their particular processing requirements. An IBP of 75-80ºC maximizes benzene production by including all the precursors that form benzene in the reforming unit. Pre-fractionating the naphtha to an IBP of 100-105ºC minimizes the production of benzene by removing the benzene precursors.

If heavy aromatics units are incorporated into the aromatics complex, C_9-aromatics become a valuable source of additional xylenes. Heavier naphtha with an EP of 165-170 ºC maximizes the C_9-aromatic precursors in the feed. A naphtha EP of 150-155 ºC minimizes the C_9-aromatic precursors in the reforming unit feed [2].

2.3.1. Alternative sources

Aromatics can be produced from methane which through dehydroaromatization produces benzene at high temperatures. An alkylating agent is also produced from methane and HBr giving CH_3Br leading to toluene and xylenes [11,12]. Methanol can also be used as raw material to

produce aromatics (MTA – methanol to aromatics), dimethyl ether, C_1-C_5 hydrocarbons, and finally aromatics are formed in fluidized bed reactors at high temperatures [13].

Biomass is also a potential source of aromatics. Catalytic fast pyrolysis (CFP) of lignocellulosic biomass produces oxygenates then converted to aromatics through cracking, deoxygenation, oligomerization, and aromatization. Selectivity to *p*-xylene can be achieved by silylation treatments and deposition of gallium, conversion is increased by employing mesoporous zeolites as catalysts at the expense of losing selectivity [14,15]. Furthermore, glucose can be converted to xylenes by two different paths. Isobutanol is obtained through fermentation, then dehydrated into isobutene followed by oligomerization to isooctane and dehydrocyclizated to xylenes. On the other hand, glucose is isomerized to fructose which is dehydrated to hydroxymethylfurfural (HMF) then hydrodeoxygenated to dimethylfuran (DMF), reaction with ethylene leads to *p*-xylene [16,17]. Acrolein, which is produced with biodiesel, can also be converted with DMF through oxidation, aromatization, and decarboxylation [18].

2.4. Aromatics complex

The following is the description of the process flow of an aromatics complex based on UOP's technologies (see Figure 2.7); special attention is given to the units highlighted inside the rectangle. Other commercial available processes will be described later.

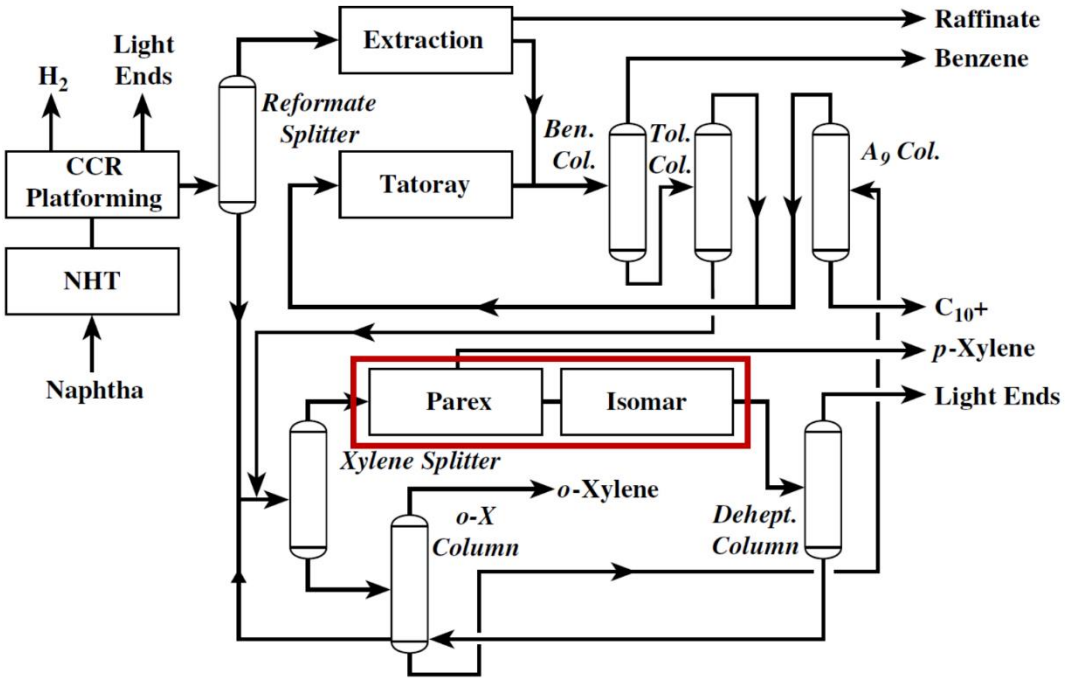

Figure 2.7 Integrated UOP aromatics complex

The naphtha is first hydrotreated to remove sulfur and nitrogen compounds in order to protect the catalysts and then sent to a CCR Platforming unit, where paraffins and naphthenes are converted to aromatics. The CCR Platforming unit is designed to run at high severity, 104 to 106 research octane number clear (RONC), to maximize the production of aromatics.

The reformate product from the CCR Platforming unit is sent to a reformate splitter column. The C_7- fraction from the overhead is sent to the Extraction unit for separation of benzene and toluene. The aromatic extract is clay-treated and then high-purity benzene and toluene products are recovered in the benzene-toluene (BT) fractionation section of the complex. The C_8+ material from the bottom of the toluene column is sent to the xylene recovery section of the complex. The raffinate from the extraction unit may be further refined into paraffinic solvents, blended into gasoline, used as feedstock for an ethylene plant, or converted to additional benzene.

Toluene is usually blended with C_9- and C_{10}-aromatics (A_9+) from the overhead of the A_9 column and charged to a Tatoray unit for the production of additional xylenes and benzene. The effluent is sent to the BT fractionation section, where the benzene product is recovered and the xylenes are fractionated out and sent to the xylene recovery section. The overhead material from the stripper inside the unit is separated into gas and liquid products. The overhead gas is exported to the fuel gas system, and the overhead liquid is normally recycled to the CCR Platforming debutanizer for recovery of residual benzene.

The C_8+ fraction from the bottom of the reformate splitter is clay-treated and then charged to a xylene splitter column. The xylene splitter is designed to withdraw heavy aromatics from the mixed xylenes. The overhead from the xylene splitter is fed directly to the Parex unit, while the bottoms are sent to the A_9 column where the A_9 fraction is recycled to the Tatoray unit. If the complex has no Tatoray unit, the A_9+ material is usually blended into gasoline or fuel oil. Furthermore, if *o*-xylene is to be produced in the complex, the xylene splitter is designed to make a split between *m*- and *o*-xylene. The xylene splitter bottoms are then sent to an o-X column where high-purity *o*-xylene product is recovered overhead. The bottoms are sent to the A_9 column. Even though it is possible to separate *o*-xylene due to the 5 ºC boiling point difference, 120-150 effective plates with high reflux ratio are required leading to excessive operating costs. Very often just a fraction of *o*-xylene is separated.

The xylene splitter overhead is sent directly to the Parex unit, where 99.9 wt% pure *p*-xylene is recovered by adsorptive separation at 97 wt% recovery per pass. Any residual toluene in the Parex feed is extracted along with the *p*-xylene, fractionated out in the finishing column within the Parex unit, and then recycled to the Tatoray unit. The raffinate from the Parex unit is almost entirely depleted of *p*-xylene and is sent to the Isomar unit, where additional *p*-xylene is produced by re-establishing the equilibrium distribution of xylene isomers. Any ethylbenzene present is

either converted to additional xylenes or dealkylated to benzene, depending on the type of catalyst used. The effluent from the Isomar unit is sent to a deheptanizer column in order to continually recycle the C_8-aromatics within the xylene recovery section until they exit the aromatics complex as *p*-xylene, *o*-xylene, or benzene. The overhead from the deheptanizer is split into gas and liquid products. The overhead gas is exported to the fuel gas system, and the overhead liquid is normally recycled to the CCR Platforming debutanizer for recovery of residual benzene [2,10].

2.4.1. Naphtha reforming

In the Platforming process, light petroleum distillate (naphtha) is contacted with a platinum-containing catalyst at elevated temperatures and low pressures. Semi-regenerative, fully regenerative, and continuously regenerative reformers normally operates between 510 and 540 ºC [10]. Platforming produces a high-octane liquid product that is rich in aromatic compounds. Chemical-grade hydrogen, light gas, and liquefied petroleum gas (LPG) are also produced as reaction by-products.

The first UOP Platforming unit went on-stream in 1949. In 1971, Platforming with continuous regeneration, the CCR Platforming was commercialized. The CCR Platforming process has enabled ultralow-pressure operations at 345 kPa (50 psig) and produced product octane levels as high as 108. The continuous regeneration approach has been very successful with more than 95% of the new catalytic reformers being designed as CCR Platforming units. In 2011, UOP started to commercialize the new R-284 catalyst series [5,19].

Aromizing is Axens' CCR reforming technology for aromatics production. The continuous catalyst regeneration system is fully automated, controlling all catalyst circulation and regeneration during start-up, shutdown, and normal operations. The process employs the AR series of catalysts designed to maximize aromatics yield and operates at low pressure and high severity, AR-501 is the latest generation of Aromizing. In the Axens' aromatics complexes there is the Arofining reactor, located upstream of the Aromizing effluent stabilization, which hydrogenates undesirable olefin and diolefin compounds present in the high severity reformate [20].

2.4.2. Aromatic extraction

Axens' Morphylane technology employs the concept of extractive distillation where a solvent is used to modify the relative vapor pressures of various hydrocarbons in such a way that aromatics can be separated from non-aromatics by simple distillation. High purity aromatics is

achieved owing to a carefully selected solvent, NFM is a non-corrosive material, thermally and chemically stable [20].

UOP's Sulfolane process combines both liquid-liquid extraction and extractive distillation in the same process unit. Liquid-liquid extraction is more effective in separating aromatics from the heavy contaminants than from the light ones. Extractive distillation is more effective in separating aromatics from the light contaminants than from the heavy ones [21].

2.4.3. Olefin removal

Olefinic material can interfere with the performance of downstream equipment, adsorbents, and catalysts. The problems associated with the high olefin content in the feeds to adsorbent-type *p*-xylene recovery units, xylene isomerization units, disproportionation units, and others are accelerated catalyst and sieve aging. Clay treaters reduce the olefins content by an acid catalyzed reaction whereby the olefins react with aromatics to form heavy molecules; therefore, they are usually located upstream of fractionation in order to remove the heavier reaction products from the treated streams.

ExxonMobil's Olgone is a new technology that is an alternative to clay treating that is now used to remove olefinic material from, hence reducing the Bromine Index (BI), heavy reformate, aromatic extract, and other streams commonly found in aromatics facilities. Olgone provides higher performance and longer catalyst life [22].

2.4.4. Toluene disproportionation and transalkylation

The two major reactions in the UOP's Tatoray process are disproportionation and transalkylation. Disproportionation is the conversion of toluene alone to an equilibrium mixture of benzene and xylenes. Transalkylation is the conversion of a blend of toluene and heavier aromatics to xylenes through the migration of methyl groups between methyl-substituted aromatics. The Tatoray process effectively converts the ethyl, propyl, and higher alkyl group substituted to lighter single-ring aromatics via dealkylation, while preserving the methyl groups [23].

TransPlus is ExxonMobil's toluene/C_9+ aromatics transalkylation technology which was co-developed with the Chinese Petroleum Corporation (CPC) of Taiwan. The proprietary catalyst is carefully designed to maximize desirable reactions such as disproportionation, transalkylation, and dealkylation. TransPlus technology has the flexibility to process up to 100 wt% of C_9+ aromatics in the fresh feed while maintaining long cycle lengths [24].

2.4.5. Selective toluene disproportionation

The first toluene disproportionation process was introduced by Mobil in 1975 and had a selectivity of about 24% as limited by chemical equilibrium. It was later discovered that pretreatment or selectivation of the catalyst could improve *p*-xylene selectivity beyond the equilibrium limitation [25]. Catalysts with reduced pores favor the transfer of the methyl group to the least hindered position and the *p*-xylene formed diffuses out of the pores faster than the other isomers which isomerize to form *p*-xylene to re-establish the equilibrium [26,27]. Between the zeolites used as catalysts, ZSM-5 is preferred due to high selectivity and slow aging; larger-pore Mordenite is used to convert bulky trimethylbenzenes in disproportionation and transalkylation processes [3,28].

Among the selectivation procedures, chemical liquid deposition (CLD) and chemical vapor deposition (CVD) are the most industrially used methods; the purpose is pore blockage, increase tortuosity, and deactivation of external acid sites [26,28]. See Figure 2.8.

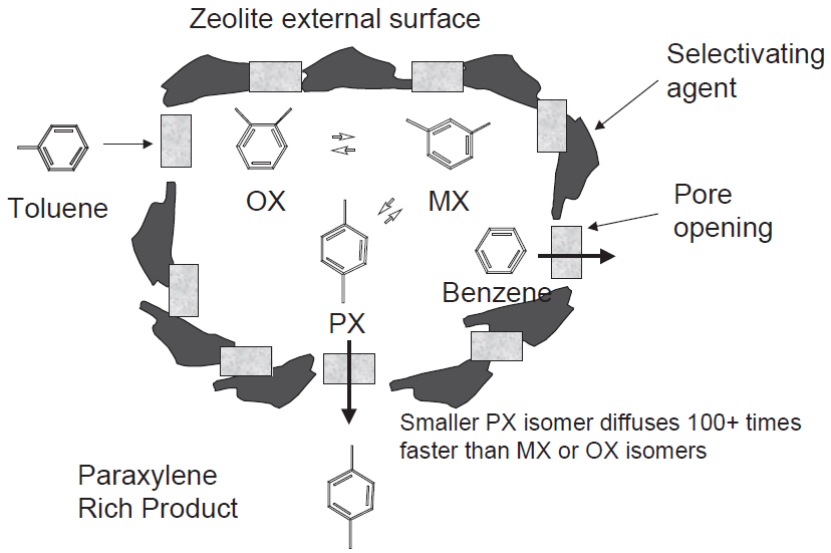

Figure 2.8 Catalyst selectivation in PxMax technology [25]

ExxonMobil's selective toluene disproportionation process based on this development is known as PxMax, which allows *p*-xylene selectivity to be improved to over 90%. Two catalysts technologies are being offered for licensing as part of PxMax process: EM-2200 with in-situ coke selectivation and MTPX with ex-situ permanent selectivation. The process flow scheme (see Figure 2.9) includes a reactor section, fractionation to separate the aromatics products, and a *p*-xylene recovery unit [25].

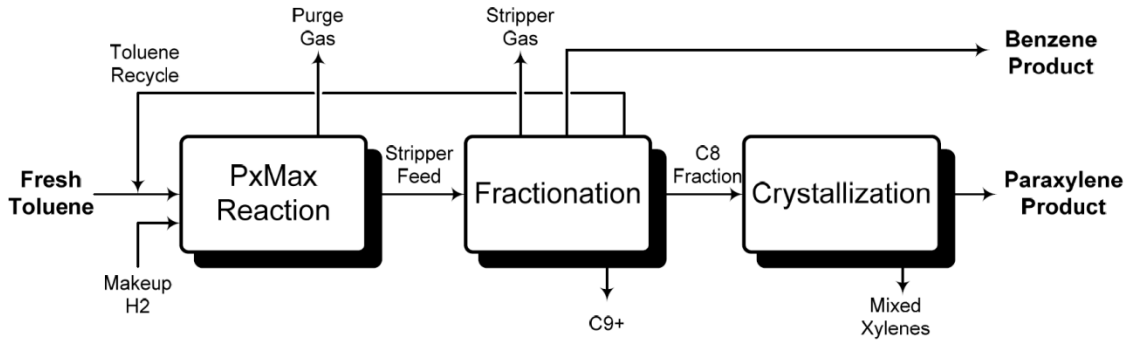

Figure 2.9 Block diagram of PxMax with crystallization [29]

In the UOP aromatics complex, instead of feeding the toluene to Tatoray, another processing strategy for toluene is to feed it to a *p*-xylene catalytic process such as PX-Plus, where the *p*-xylene in the xylene product is enriched to >85%. The concentrated *p*-xylene product could then be easily recovered in a single stage crystallization unit [2].

2.5. *p*-Xylene separation

Ethylbenzene, *p*-xylene, *m*-xylene, and *o*-xylene boil so closely together that separating them by conventional distillation is not practical. Just *o*-xylene can be separated through distillation since there is a 5ºC difference with the next isomer, which is *m*-xylene, although it constitutes an expensive separation as discussed in Section 2.4. Based on the aforementioned, *p*-xylene recovery is typically accomplished either by fractional crystallization or through adsorptive-type processes.

2.5.1. Crystallization

Prior to the 1970's, the typical method for recovering *p*-xylene from mixed xylene streams was low temperature crystallization. These units typically operated at cold stage temperatures of -60 to -65ºC and provided only 60-70% recovery. The situation changed completely with the commercialization of UOP's Parex, a more efficient adsorption-based technology that provides >97% recovery of *p*-xylene (See Figure 2.10).

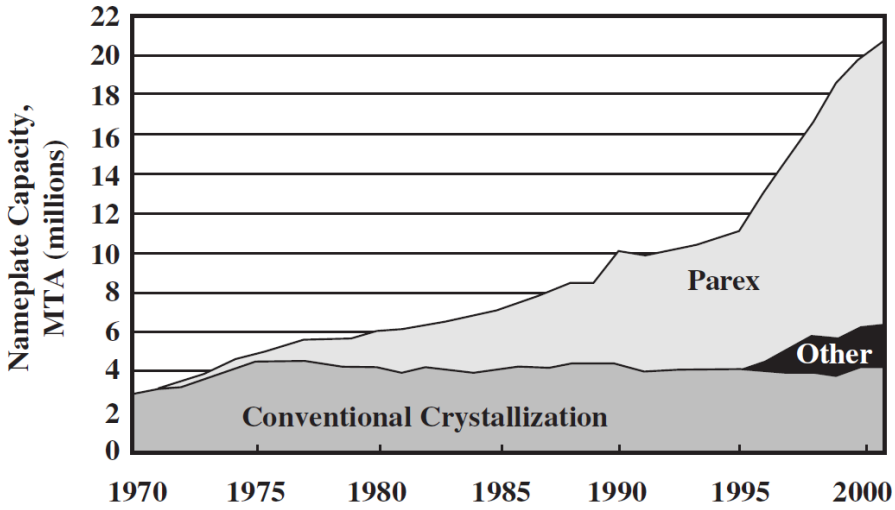

Figure 2.10 *p*-Xylene separation technologies [30]

The crystallization process takes advantage of the large differences between the freezing points of the C_8-aromatic components to separate *p*-xylene from the mixture. C_8-aromatics are known to behave as a eutectic mixture where, as temperature is reduced, one of the components will begin to drop out of the solution as a pure solid phase. The initial composition of the solution determines which component will drop out first. Although *p*-xylene freezing point is the highest, normally it is not present at the highest concentration, resulting in the need of several stages and a recovery of only 60-70%; in recent years, there has been a renewed interest in *p*-xylene crystallization technology in combination with selective toluene disproportionation processes due to the high *p*-xylene content of the C_8-aromatic product, thus, eliminating the eutectic constraints. [29].

Typical process consists of crystallization stages at different temperatures, liquid-solid separation equipment, melting, heat exchangers, and washing streams for purification [31]. Liquid-solid separation depends on the size of the crystals which is governed by crystallization kinetics, the average size of the crystals is set to above 0.5 mm to guarantee good separation [32,33]. Crystallizer may be the suspension or layer type; direct or indirect refrigeration systems can also be used [10].

ExxonMobil's *p*-xylene crystallization process is conducted at three temperature levels: a purity stage at 3 ºC, a scavenger stage at -4 ºC and a recovery stage at -29 ºC to facilitate *p*-xylene crystal separation and washing operations and to maximize *p*-xylene recovery (See Figure 2.11). In suspension type crystallization, the feed is chilled below the equilibrium temperature and held at this temperature for several hours to allow the crystals to grow.

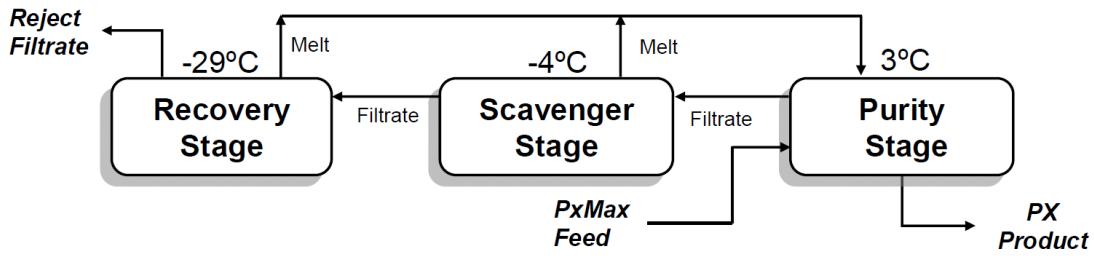

Figure 2.11 Block diagram of ExxonMobil crystallization process [29]

The recovery stage temperature of -29 ºC, which sets the maximum *p*-xylene recovery of the system, was selected based on the practical limitations of a propylene refrigeration system. Conventional crystallization generally required a dual refrigeration system which used ethylene for the cold recovery stages and propylene for the warmer purity stage. A simplified flow diagram of a typical crystallizer stage is given in Figure 2.12.

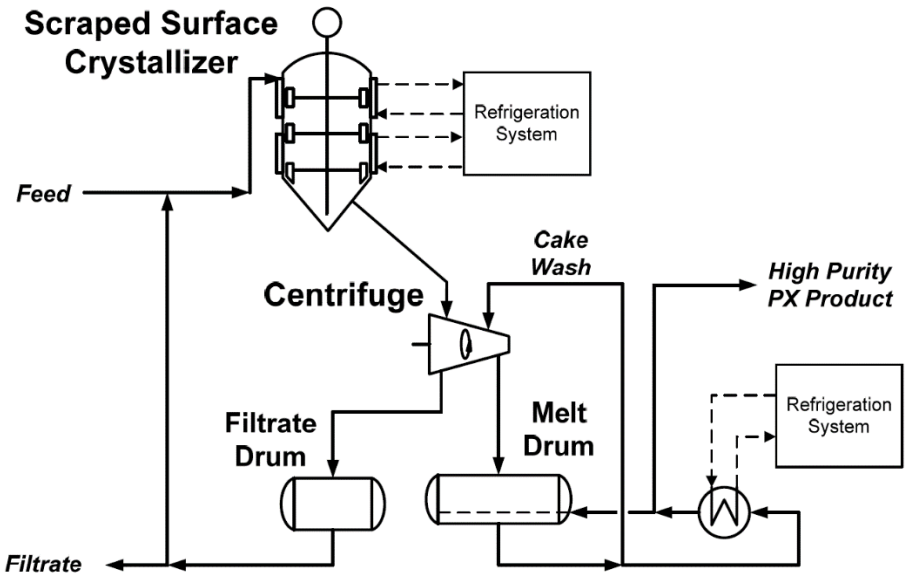

Figure 2.12 Simplified flow diagram of a single crystallization stage [29]

The crystallizer consists of a scraped wall, conical bottom vessel with half-pipe cooling jackets installed along the straight sides of the vessel. Mechanical scrapers are rotated at low rpm to remove the crystals that form at the cold wall surface and to help maintain a uniform slurry in the vessel. After a suitable residence time, the slurry is sent to a high speed centrifuge to separate the filtrate. Washing is required to withdraw remaining mother liquor from the crystals [29].

Other process are the Tsukishima Kikai counter-current crystallization process which replaced the scraped-surface chillers by several cooling crystallizers connected in series [34]. Sulzer Chemtech developed a layer crystallization process limited to 80 wt% of *p*-xylene in the

feed [35]; GTC's CrystPX allows a lower *p*-xylene content in the feed (75 – 95 wt%) with recovery up to 95% in their suspension crystallization process [36].

For equilibrium xylene mixtures, process economics strongly favor adsorption-based processes such as UOP's Parex or Axens' Eluxyl. For this type of unit, a crystallizer unit has 10-30% higher capital cost, higher utility costs, and significantly lower recovery. For the high *p*-xylene concentration feed available from the selective toluene disproportionation processes, the situation is reversed because *p*-xylene recovery and capital and utility costs are strongly related to feed composition [29].

Another similar process, although not used industrially, is stripping crystallization previously known as distillative freezing. The liquid mixture is simultaneously vaporized and crystallized due to the three-phase equilibrium since it operates at the triple point [37].

2.5.2. Adsorption

Sorbex technology, which was invented by UOP in the 1960s [38], was the first large-scale commercial application of continuous adsorptive separation. The first commercial Sorbex unit, a Molex unit for the separation of linear paraffins, came on-stream in 1964 [30]. This technology simulates the counter-current flow of a liquid feed over a solid bed of adsorbent without physically moving the solid. The following are examples of commercially proven UOP technologies based on the Sorbex principle [39]:

- Parex: Separation of *p*-xylene from mixed C_8 aromatic isomers
- MX Sorbex: *m*-Xylene from mixed C_8 aromatic isomers
- Molex: Linear paraffins from branched and cyclic hydrocarbons
- Olex: Olefins from paraffins
- Cresex: *p*-Cresol or *m*-cresol from other cresol isomers
- Cymex: *p*-Cymene or *m*-cymene from other cymene isomers
- Sarex: Fructose from mixed sugars

The process concept is basically the counter-current flow of liquid feed and solid adsorbent, actual movement of the solid is not recommended since mechanical stress tends to destroy the solid. In addition, a homogeneous and tightly packed bed is required for the separation, backmixing of the solid reduces the efficiency of the process [40-42]. The aforementioned is avoided with the simulated moving bed (SMB) technology.

The feed is normally a mixture of components from which one (or more) component would be selectively recovered due to its stronger affinity towards the solid. The positions of injection and withdrawal of four streams divide the adsorbent bed in four zones:

- Zone 1: Regeneration of adsorbent. Located between the point of desorbent injection and extract withdrawal with the purpose of cleaning the adsorbent.
- Zone 2: Desorption of the more adsorbed species. Located between extract port and the point of feed injection where the more adsorbed component is displaced in the pores by the desorbent and recovered in the extract port.
- Zone 3: Adsorption of the more adsorbed species. Located between the point of feed injection and raffinate withdrawal where the more adsorbed compound is retained in the pores allowing to obtain a depleted stream in the raffinate port.
- Zone 4: Regeneration of desorbent. Located between the raffinate port and the point of desorbent injection with the purpose of cleaning the desorbent to be recycled to zone 1.

Counter-current flow is simulated by periodically changing the points of liquid injection and withdrawal along a stationary bed of solid adsorbent. In this SMB technique, the concentration profile actually moves down the adsorbent chamber. As the concentration profile moves, the points of injection and withdrawal of the streams to the adsorbent chamber are moved along with it [39].

In the case of separation of *p*-xylene the four streams are: Feed (mixed-xylenes feed), Extract (*p*-xylene product diluted with desorbent), Raffinate (ethylbenzene, *m*-, and *o*-xylene diluted with desorbent), and Desorbent. At any given time, only four of the bed lines actively carry the streams into and out of the adsorbent chambers. The four-zone system provides a more economical use of desorbent than three-zone units [42]. However, more streams leading to more zones can be used to prevent contamination of the extract or raffinate products; for instance, flushing lines within an industrial *p*-xylene separation unit resulted in a seven-zone system [43].

The desorbent used for separation of *p*-xylene from C_8-aromatics can be either *p*-diethylbenzene or toluene, although the former is preferred. Since it is less volatile, *p*-diethylbenzene can be recovered at the bottom thus reducing the heat load of the associated distillation columns [42]. Moreover, the presence of C_8 non-aromatics or naphthenes, which have a boiling point close to that of toluene, may complicate the recovery of the desorbent in said distillation columns [44].

According to Minceva and Rodrigues [45], separation is accomplished over faujasite-type zeolites, from which prehydrated KY and BaX zeolite are the most employed. The selectivity of these ion exchange zeolites on *p*-xylene depends on the pre-adsorbed water in the zeolite. Maximum selectivity is observed when the water content is between 2 and 6 wt%. The selectivity

also depends on the Si/Al ratio, Rasouli et al. [46] found decreasing selectivity with increasing Si/Al ratio. Moreover, the potential of medium-pore zeolites, such as ZSM-5, instead of large-pore zeolites have also been investigated [47]. Metal organic frameworks (MOF) have also been evaluated, MAF-X8 exhibited selectivity for *p*-xylene [48], MIL-125(Ti)-NH_2 also presented selectivity for *p*-xylene but in the presence of low ethylbenzene concentration [49], *o*-xylene is preferentially adsorbed over MIL-53(Al) [50].

Adsorption in gas phase has also been studied over faujasite Y zeolite [51]. Gas phase operation may provide advantages such as better selectivity, nonetheless higher energy costs and axial dispersion often lead to operation in liquid phase [42].

2.5.2.1. UOP's Parex

UOP Parex units are designed to recover more than 97 wt% of the *p*-xylene from the feed in a single pass. Product purity is 99.9 wt% or better [30], minimum purity specification is 99.7 wt% [52]. The latest generation of adsorbent, ADS-47, leads to a 50% capacity increase in existing units [5].

The flow diagram for a typical Parex unit is shown in Figure 2.13. The separation takes place in the adsorbent chambers, each chamber is divided into a number of adsorbent beds. Each bed is supported by specialized internals that are designed to produce highly efficient flow distribution and are connected to the rotary valve by a bed line. The internals between each adsorbent bed are used to inject or withdraw liquid from the chamber and simultaneously collect liquid from the bed above and redistribute the liquid over the bed below. A typical Parex unit has 24 adsorbent beds and 24 bed lines connecting the beds to the rotary valve. Because of practical construction considerations, most Parex units consist of two adsorption chambers in series with 12 beds in each chamber.

The rotary valve is used to periodically switch the positions of the liquid feed and withdrawal points as the compositions profile moves down the chamber. Pumps provide circulation between the two chambers in order to act as a single unit. The extract from the rotary valve is sent to the extract column for separation of the extract from the desorbent. The overhead from the extract column is sent to a finishing column, where the highly pure *p*-xylene product is separated from any toluene that may have been present in the feed. The raffinate from the rotary valve is sent to the raffinate column for separation of the raffinate from the desorbent. The overhead from the raffinate column is sent to an isomerization unit. The desorbent from the bottom of both the extract and raffinate columns is recycled to the adsorbent chambers through the rotary valve [30].

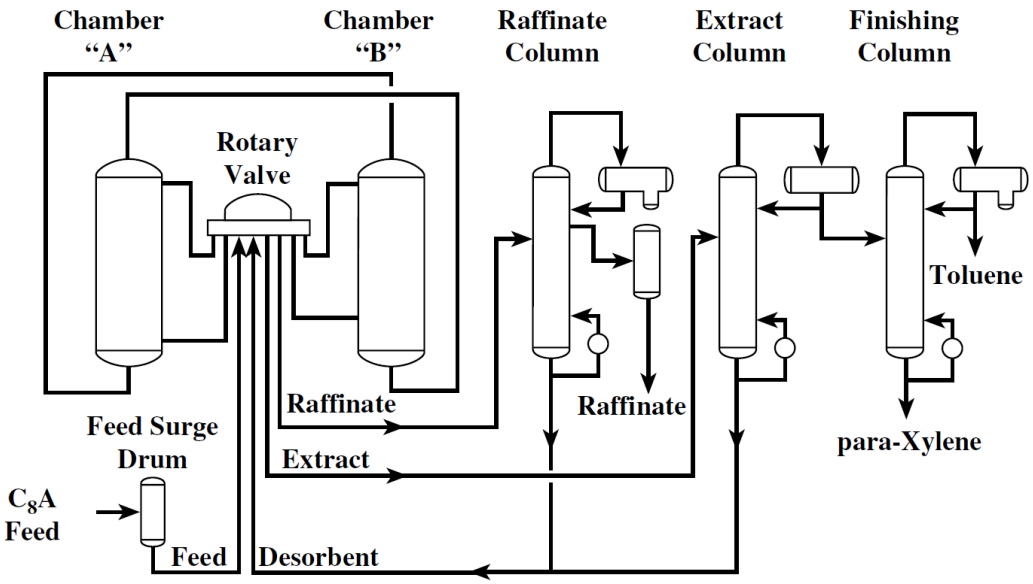

Figure 2.13 Parex flow diagram [30]

2.5.2.2. Axens' Eluxyl

The Eluxyl process is also based on the concept of SMB where liquid circulates in a column containing a stationary adsorbent which is selective for *p*-xylene. Eluxyl offers high purity (up to 99.9%) in its stand-alone version (see Figure 2.14) with high-boiling desorbent, individual on/off valve system, and advanced dynamic control through monitor of concentration profiles by on-line Raman spectroscopy [53].

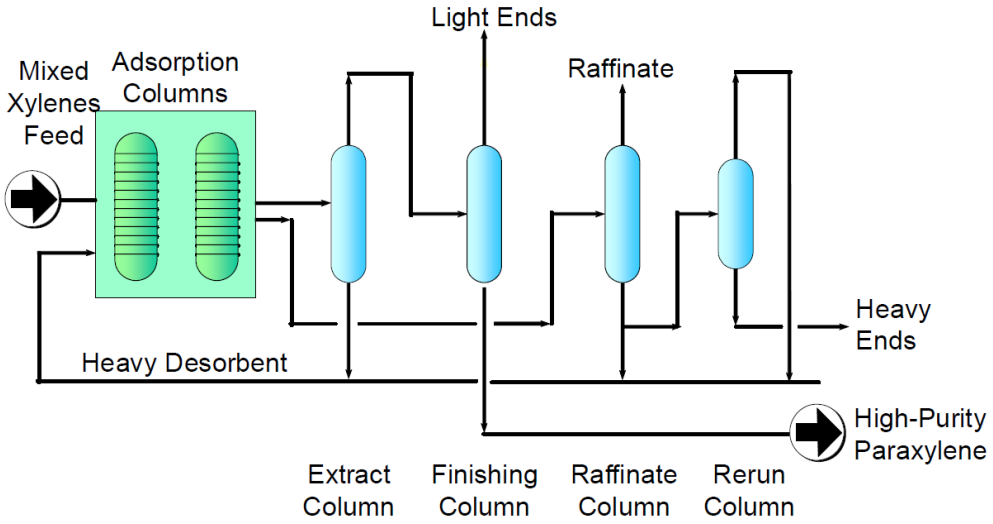

Figure 2.14 Eluxyl stand-alone version [53]

2.5.2.3. Axens' Eluxyl twin raffinate

SMB process may be operated with an additional outlet (second raffinate or second extract) leading to one additional zone. Considering the case of a SMB operated with a second raffinate, the so-called Twin Raffinate mode, former zone located between the feed and the raffinate is subdivided into two zones. By adequately adjusting the flowrate in the subzones, a mixture of *m*- and *o*-xylene can be separated from ethylbenzene.

Maintaining the total number of beds in 24 and the ratio of flowrates of raffinate 2 to raffinate 1 in the range 0.4-0.7 *p*-xylene can still be recovered with high purity and recovery (99.8% and 97%) and a mixture of *o*- and *m*-xylene can be recovered in the second raffinate with purity ranges from 98.0% up to 99.3-99.4%.

In order to produce pure *m*-xylene (and possibly pure *o*-xylene) along with *p*-xylene, two interesting process schemes were investigated by Axens, Eluxyl Twin Raffinate MX/OX splitter Crystallization unit and Eluxyl Twin Raffinate MX SMB unit. In the first one, raffinate 2 coming from the Eluxyl Twin Raffinate is sent to an MX/OX splitter. Then, either the head or the bottom stream is sent to a crystallizer for production of *m*-xylene or *o*-xylene respectively (see Figure 2.15). Therefore, flexibility is offered for either producing *m*- or *o*-xylene. The main parameter is the composition of the stream sent to the crystallization unit from the splitter; depending on the isomer to be produced, the composition has to be in the right part of the *m*-/*o*- binary solid-liquid equilibrium diagram.

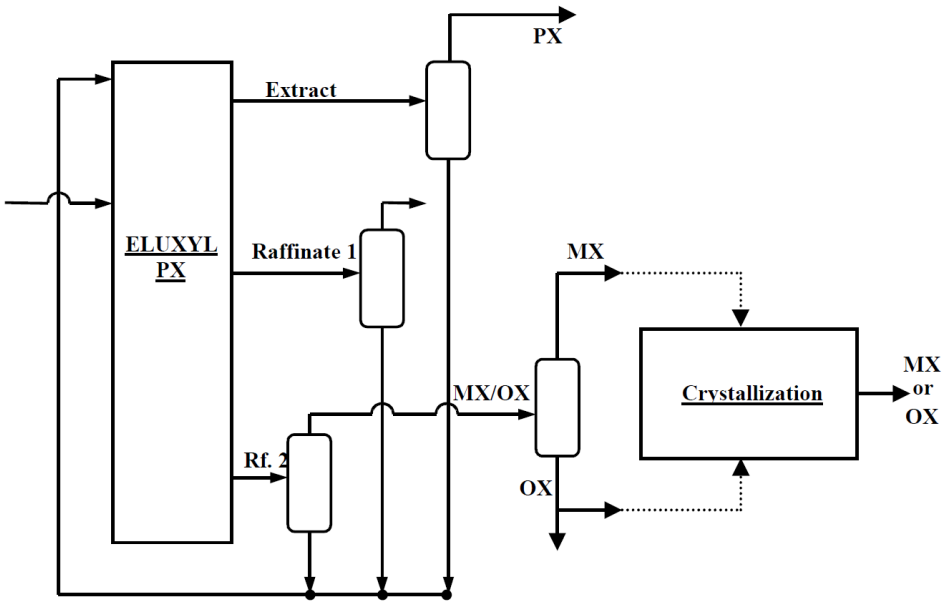

Figure 2.15 Schematic view of Eluxyl twin raffinate MX/OX splitter crystallization unit [54]

The second process is especially dedicated to *m*-xylene production. Raffinate 2 coming from the Eluxyl Twin Raffinate is sent to another SMB unit dedicated to the production of *m*-xylene at high purity (99.5%) and high recovery (see Figure 2.16). It can be noted that raffinate 2 is a better feed for the second SMB unit than a conventional single raffinate stream, as it is more concentrated in *m*-xylene and as it is completely depleted in ethylbenzene which allows the reduction in the amount of adsorbent and desorbent needed in the SMB unit [54].

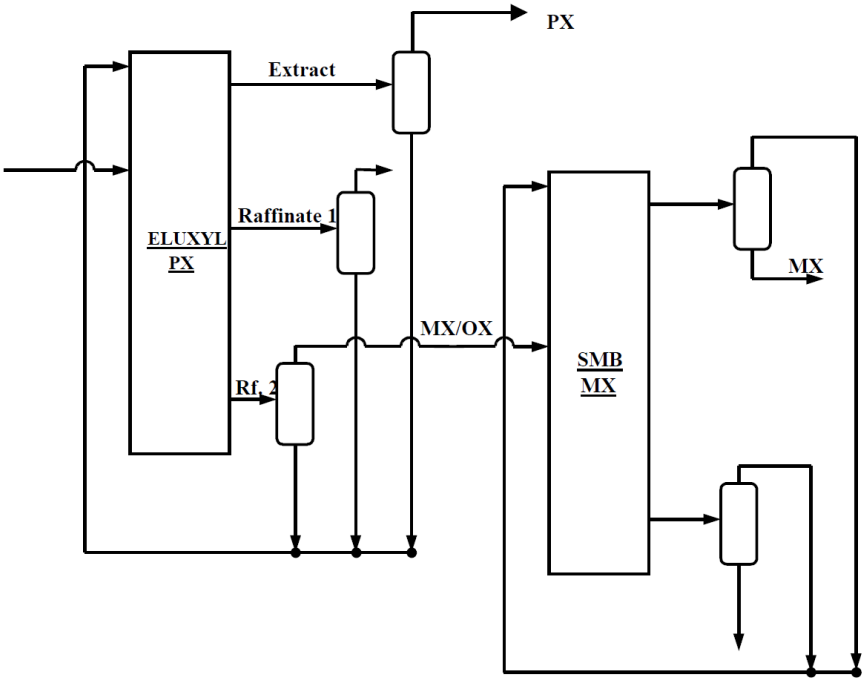

Figure 2.16 Schematic view of Eluxyl twin raffinate MX SMB unit [54]

2.5.3. Crystallization/adsorption hybrid process

The alliance between UOP, Washington Group International, and Niro Process Technology, introduced the HySorb XP process, a simplified, single-chamber, light desorbent adsorption process coupled with single stage crystallization and Niro wash column technology. This combination of technologies when integrated into existing multistage crystallization facilities can increase *p*-xylene production by as much as 500%. The HySorb process produces a 95 wt% *p*-xylene concentrate, eliminating eutectic constraints and enabling single stage crystallization recoveries above 90% [30].

The Axens' hybrid version produces intermediate purity product, ideally suited for a second stage crystallization. Owing to the lower *p*-xylene purity requirement, a smaller amount of sieve is required and only one adsorber is necessary. The hybrid configuration is the most effective way to drastically debottleneck existing crystallization plants [53].

Chevron's hybrid process is currently used in its Pascagoula plant, it is characterized by the use of benzene as desorbent which results in greater boiling point difference leading to easier distillation in the extract and raffinate columns [55]. GTC also offers a hybrid process with a single stage crystallizer as mentioned in Section 2.5.1 and an adsorption process to concentrate the feed to about 90% using Zeosorb PX-200 from Clariant as adsorbent [56].

2.6. Xylene isomerization

The xylene isomerization process is used to maximize the recovery of a particular xylene isomer from a mixture of C_8-aromatic isomers, although is more often applied to *p*-xylene recovery. UOP's Isomar, ExxonMobil's XyMax and Advanced MHAI, and Axens' Oparis are one of the most used technologies worldwide.

The feed is first combined with hydrogen-rich recycle gas and makeup gas to replace the small amount of hydrogen consumed in the reactor (see Figure 2.17). The combined feed is then preheated by exchange with the reactor effluent, vaporized in a fired heater, and raised to reactor operating temperature. The heater is normally a radiant convection-type heater. The process stream is heated in the radiant section, and the convection section is used for a hot-oil system or steam generation. The hot feed gas stream is then sent to the reactor. The reactor effluent is cooled by exchange with the combined feed and then sent to the product separator. The purpose of the product separator is to split the condensed reactor effluent into liquid product and hydrogen-rich recycle gas. The pressure in the product separator determines the pressure in the reactor and is regulated by controlling the rate of hydrogen makeup flow. Hydrogen purity in the recycle gas is monitored by a hydrogen analyzer at the recycle-gas compressor suction. When hydrogen purity gets too low, a small purge is taken from the recycle gas. Liquid from the bottom of the product separator is charged to the deheptanizer column. The C_7- overhead from the deheptanizer is cooled and separated into gas and liquid products. The deheptanizer overhead gas is exported to the fuel gas system. The overhead liquid is recycled to the reforming unit so that any benzene in this stream may be recovered. The C_8+ fraction from the bottom of the deheptanizer is clay-treated, combined with fresh mixed-xylenes feed and recycled [57]. The difference between the technologies lies mainly on the reactor and catalysts used, which will be discussed in the next sections.

2.6.1. Xylene isomerization catalysts

In the reactor two main categories of xylene isomerization catalysts are used, ethylbenzene dealkylation catalysts and ethylbenzene isomerization catalysts. The former converts

ethylbenzene to benzene and the latter to additional xylenes. Since ethylbenzene isomerization is an equilibrium-limited reaction, the conversion of ethylbenzene is usually limited to about 30-35 wt% per pass. Ethylbenzene dealkylation catalyst allows conversion of up to 70 wt% or greater. For a new aromatics complex design, using an ethylbenzene dealkylation catalyst minimizes the size of the xylene column and downstream units required to produce a given amount of *p*-xylene. However, this reduction in size of the xylene loop comes at the expense of lower *p*-xylene yields, because all the ethylbenzene in the feed is being converted to benzene rather than to additional *p*-xylene. Lower *p*-xylene yield means that more feedstock will be required [57]. The reaction is further studied in Chapter 4.

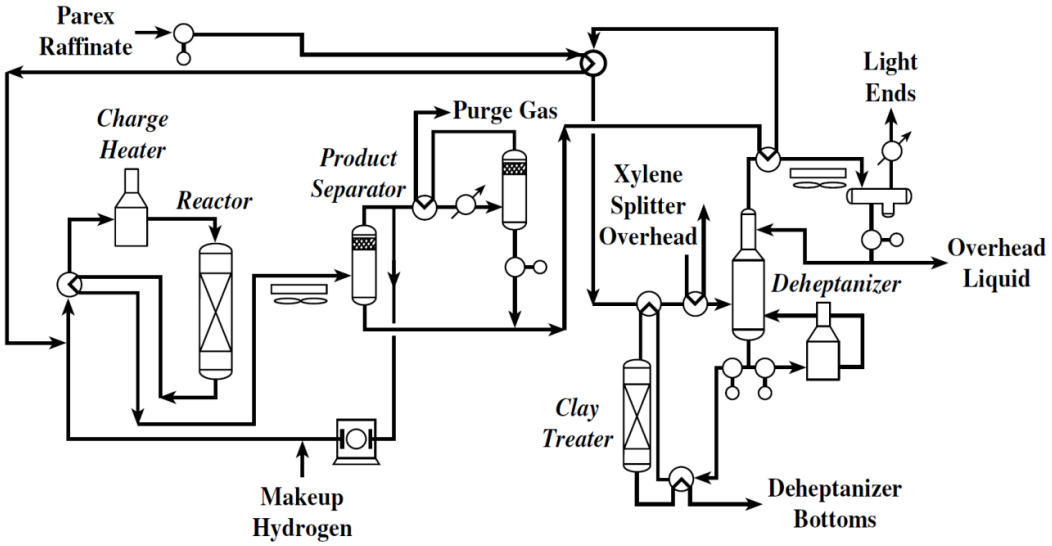

Figure 2.17 UOP's Isomar flow diagram [57]

2.6.2. UOP's Isomar

The Isomar process normally uses a radial-flow reactor. The gas stream enters the top of the reactor and is directed to the sidewall. The fluid then travels radially through the fixed bed and into a center pipe. The reactor effluent then flows down through the center pipe to the reactor outlet. The advantage of the radial-flow reactor is low pressure drop, which is important due to the influence of hydrogen partial pressure on the reaction rates.

UOP offers both types of commercial catalysts; the last catalyst released is I-500 which offers higher selectivity at lower temperatures in dealkylation of ethylbenzene [5]. All xylene isomerization catalysts exhibit some by-product formation across the reactor. The precise level of expected by-product formation varies with catalyst type and operating severity, but it is normally in the range of 1.0 to 4.0 wt% per pass of the feed. By-products are predominantly aromatics, such that overall ring retention is greater than 99%. Moreover, non-aromatic

compounds in the feed to the Isomar unit are primarily cracked to light ends and removed from the Parex-Isomar loop [57].

2.6.3. ExxonMobil's XyMax and Advanced MHAI

Soon after the discovery of ZSM-5 in the early 1970's, Mobil introduced MVPI, the Mobil Vapor Phase Isomerization process. MVPI utilized the first high activity, zeolite based xylene isomerization catalyst. In 1978, Mobil introduced MLPI, the Mobil Low Pressure Isomerization process, which was capable of operating without H_2 recirculation while achieving low xylene losses and long cycle lengths. In 1981, Mobil introduced MHTI, the Mobil High Temperature Isomerization process; and then in 1990 MHAI, the Mobil High Activity Isomerization process. The advances were mainly the higher ethylbenzene conversions with lower xylenes losses [58].

Nowadays ExxonMobil offers XyMax and Advanced MHAI technologies. For sites with lower reactor temperature limitations, and for those that utilize crystallization for *p*-xylene separation, the Advanced MHAI process offers optimum operation. For sites with higher reactor temperature capability, and for those that utilize adsorption-based *p*-xylene separation technology, the XyMax Process is the best choice. Both processes incorporate the latest advances in ExxonMobil's zeolite catalyst technology and are the ethylbenzene dealkylation type [59].

The primary chemical reactions are the conversion of ethylbenzene to benzene and ethylene, cracking of non-aromatics, and isomerization of the *p*-xylene depleted feedstock to an equilibrium mixture of xylenes. These reactions take place in a fixed-bed reactor with two distinct zeolite catalysts. In the top bed, the catalyst is designed to convert ethylbenzene to benzene and ethylene, via dealkylation, and to crack non-aromatics. The ethylene produced is largely hydrogenated to ethane in the top bed also, reducing the likelihood of xylene loss through alkylation to heavy aromatics. The catalyst in the bottom bed is optimized for complete xylene isomerization to near-equilibrium levels of *p*-xylene (see Figure 2.18) [60].

2.6.4. Axens' Oparis

Oparis (OPtimized ARomatics ISomerization) is Axens' new generation catalyst for ethylbenzene and xylenes isomerization. The unique feature of Oparis is its ultra-high selectivity, which allows conversion of xylenes and ethylbenzene to an equilibrium mixture of xylenes with maximum yields at milder operating conditions [61]. The xylenes isomerization reaction is favored by temperature, as are the undesired side reactions. Since ethylbenzene isomerization implies the formulation of hydrogenated, naphthenic intermediate, the reaction is favored by milder temperature and the presence of hydrogen partial pressure. The adjustment of a

C_8-aromatics isomerization unit requires an optimized balance between temperature that drives xylenes isomerization reaction, but results in a higher amount of side reactions, and hydrogen partial pressure, which drives the ethylbenzene isomerization reactions [62].

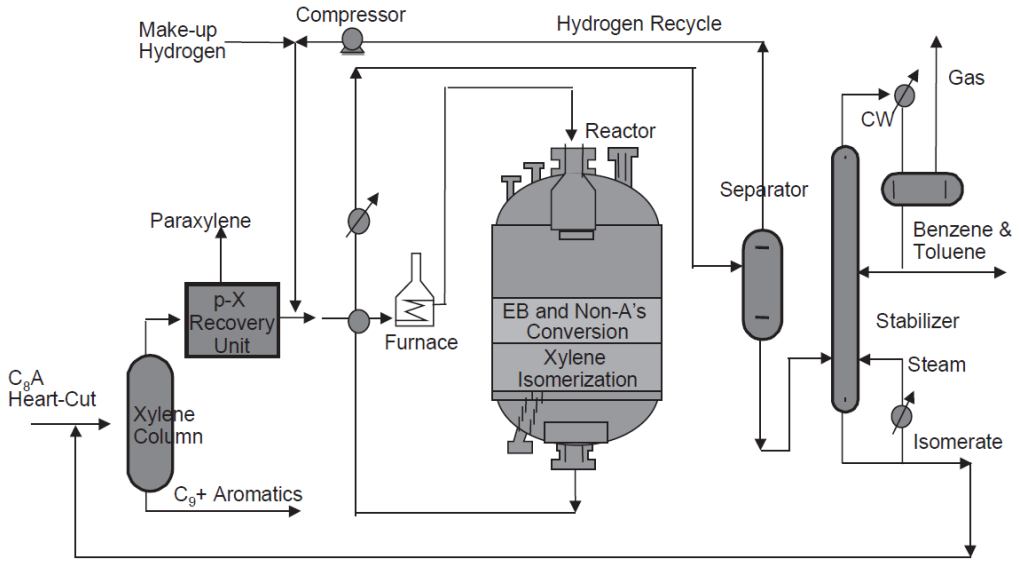

Figure 2.18 ExxonMobil's dual bed catalyst system [25]

The reaction takes place in a conventional gas phase reactor. The liquid effluent from the reaction section is a near-equilibrium mixture of C_8-aromatics which also contains lighter and heavier components resulting from minor side reactions. C_8-naphthenes are also present in equilibrium-related amounts, these are separated and recycled to the isomerization reactor in order to maintain optimum performance. The naphthenes recycle is fine-tuned by employing a small fractionation tower and sent directly to the Oparis isomerization section (see Figure 2.19). In other technologies, the naphthenes are recycled to the xylenes column and *p*-xylene separation section before re-entering the isomerization section [61]. Several technologies are summed up in Table 2.1.

2.7. New trends in xylene production

According to the patent literature of the last few years the new trends in the xylene production, especially in xylene isomerization, are focused on the use of several reactors under different conditions tailored for specific purposes, as well as the use of different catalysts, zeolitic and non-zeolitic. Moreover, productions of other products along with *p*-xylene and process intensification have also attracted attention among the researches worldwide. Some of these patents are presented in Table 2.2.

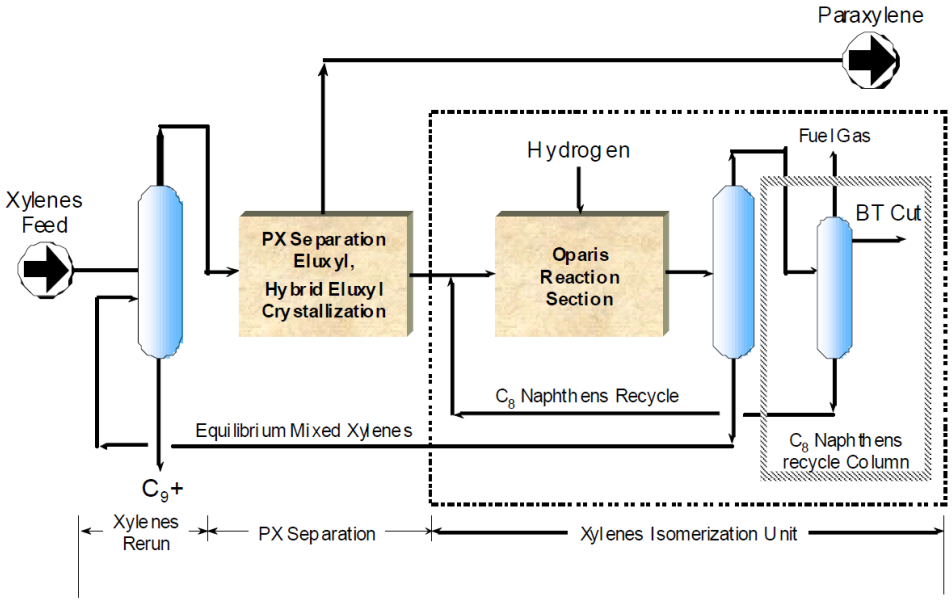

Figure 2.19 Simplified xylenes loop flowscheme including Oparis process [61]

Table 2.1 Xylene isomerization units

Process	Catalyst	Reaction Type[a]	*T*, ºC	*P*, MPa
Octafining	Pt on alumina combined with H-mordenite[b]	Ethylbenzene isomerization in the presence of H_2	425-480	1.14-2.51
Isomar[c]	Pt on alumina	Ethylbenzene isomerization in the presence of H_2	388	1.68
MVPI	NiHZSM-5 with an alumina binder	Ethylbenzene disproportionation in the presence of H_2	315-370	1.48
MLPI	HZSM-5 with an alumina binder	Ethylbenzene disproportionation in the absence of H_2	290-380	0.27
MHTI	Pt on acidic ZSM-5	Ethylbenzene dealkylation in the presence of H_2	427-460	1.48-1.83
XyMax[d]	Noble metal ZSM-5 with amorphous binder	Ethylbenzene dealkylation in the presence of H_2	400-482	0.45-2.87
Oparis[e]	EUO-structural-type zeolite with Pt.	Ethylbenzene isomerization in the presence of H_2	350-420	0.6-1.5

[a] All reactions are in gas phase. [b] Corresponding to O-750 catalyst. [c] Corresponding to I-9 catalyst. [d] From Patent 7,247,762 B2 [63]. [e] From Patent 6,376,734 B1 [64].

2.7.1. Simulated moving bed reactor

Although not industrially proven, simulated moving bed reactor (SMBR) for *p*-xylene production has dragged plenty of attention among researchers. Based on the concept of process intensification, it combines *p*-xylene separation and xylene isomerization in one single unit. Reduction of operating and capital costs, energy consumption, environment impact; are among

Table 2.2 Recent patents in xylene production

Patent No., Date and Title	Inventor/Assignee	Application	Reference
US 6,448,459 B1 Sept 10, 2002 *Process for the Production of Paraxylene that comprises an Adsorption Stage, a Liquid Phase Isomerization Stage and a Gas Phase Isomerization Stage with an EUO-type zeolite*	Julia Magne-Drisch, Fabio Alario, Jean-François Joly, Ari Minkkinen and Elisabeth Merlen / Institut Français du Pétrole	It consists in a combination of stages for isomerization in liquid phase of a fraction that is high in *m*-xylene and *o*-xylene and for isomerization in gas phase of a fraction that is high in ethylbenzene. Ethylbenzene is previously separated by distillation or by adsorption and isomerized at 350-450ºC, 5-20 bar, and with a catalyst that contains EUO-structural-type zeolite. The other fraction with a limited quantity of ethylbenzene is sent to a simulated moving bed with toluene as desorbent which serves as diluent in the isomerization in liquid phase which is carried out at 200-260ºC, 20-30 bar, and with a zeolitic catalyst such as ZSM-5.	[65]
US 2004/0236166 A1 Nov 25, 2004 *Xylene Isomerization*	Gary David Mohr / ExxonMobil Chemical Company	Any ethylbenzene in the feed is removed, either by dealkylation or isomerization, in a separate reactor upstream of the xylene isomerization reactor. The ethylbenzene depleted product is sent to a second reactor, typically the clay treater, as that used to accommodate the olefin removal catalyst. Xylene isomerization is carried out under mild conditions, 160-232ºC and 100-500 psig (liquid phase). This second reactor contains a zeolite catalyst for the xylene isomerization and also another catalyst effective to remove olefins. In certain cases, a single catalyst may be used to effect both xylene isomerization and olefin removal.	[66]
US 2009/0182182 A1 Jul 16, 2009 *Process for Isomerizing a Non-Equilibrium Alkylaromatic Feed Mixture and an Aromatic Production Facility*	John E. Bauer / Honeywell UOP	The C_8 isomerization zone may include a first isomerization stage and a second isomerization stage. At the first isomerization stage, a non-equilibrium alkylaromatic feed mixture is contacted with a zeolite catalyst in the absence of hydrogen at 250-350ºC and enough pressure to keep the mixture in liquid phase for isomerizing at least one isomer. At the second isomerization stage, the intermediate stream from the first stage and a stream rich in one naphthene are contacted with a zeolite catalyst in the presence of hydrogen at 300-500ºC and a pressure less than 2 MPa. The purpose of the second stage is the isomerization of ethylbenzene. Often, C_8 naphthenes can be created in the second isomerization stage; therefore, it is desirable to recycle excess C_8 naphthenes back to the second isomerization stage.	[67]

Patent No., Date and Title	Inventor/Assignee	Application	Reference
US 7,592,499 B2 Sept 22, 2009 *Process for co-Producing para-Xylene and Styrene*	Luc Wolff, Philibert Leflaive and Alain Methivier / Institut Français du Pétrole	The feed of hydrocarbons containing xylenes and ethylbenzene is separated in a simulated moving bed from which an extract rich in *p*-xylene and a raffinate are withdrawn. The ethylbenzene contained in the raffinate is dehydrogenated to styrene with conversion of at least 50 wt%. A stream rich in styrene is separated by means of adsorption, distillation, liquid-liquid extraction, membrane or any combination of said techniques. The unconverted ethylbenzene, *m*-xylene and *o*-xylene is isomerized, preferably in liquid phase (e.g. 200-260ºC and 2-3 MPa), and recycled back to the simulated moving bed unit.	[68]
WO 2009/130402 A1 Oct 29, 2009 *Reactive Simulated Moving Bed for Producing para-Xylene*	Ghislain Bergeot, Catherine Laroche, Philibert Leflaive, Damien Leinekugel Le Cocq and Luc Wolff / Institut Français du Pétrole	Method for producing high-purity *p*-xylene by coupling a step of selective *p*-xylene adsorption and a step of xylene isomerization from an aromatic C_8 mixture optionally containing ethylbenzene. The adsorbent for *p*-xylene separation is BaLSX with a Si/Al ratio of about one, the desorbent is toluene, and the isomerization catalyst is ZSM-5 type. The adsorption is carried out at preferably 200-220ºC and less than 4 MPa. The reactors are located in zone 3 of the SMB unit and the conditions are preferably 180-300ºC and 2-3 MPa at liquid phase.	[69]
US 2010/0152511 A1 Jun 17, 2010 *Hydrocarbon Conversion using an Improved Molecular Sieve*	Hayim Abrevaya, Julio C. Marte, Stephen T. Wilson, Susan C. Koster, John E. Bauer, Wharton Sinkler, Ben A. Wilson and Lance L. Jacobsen / Honeywell UOP	Isomerization of a non-equilibrium C_8 aromatic mixture of xylenes and ethylbenzene with a catalytic composition comprising at least one platinum-group metal component and MgAPSO-31. MgAPSO-31 is a magnesium-containing non-zeolite molecular sieve which has a narrowly defined composition and is particularly useful for isomerization. It contains from about 0.003 to 0.011 mol fraction of magnesium in the microporous crystalline framework structure and comprises crystals with a median diameter of no more than about 1.0 micron. Two isomerization zones can be used. First to isomerize xylenes in the absence of hydrogen over a zeolitic aluminosilicate catalyst; and the second with MgAPSO-31 to isomerize ethylbenzene in the presence of hydrogen to increase the *p*-xylene content of the product. The conditions for the proprietary catalyst comprise a temperature preferably in the range of 300-500ºC and pressure less than about 50 atm.	[70]

the main advantages of these types of process. However, flexibility in operation and control, as well as the lack of past experiences of these type of units constitutes a barrier for being used in the industry [71].

For *p*-xylene separation, SMB is the most employed technique in adsorption-type separations as seen in Section 2.5. The SMBR uses the same principle and incorporates the reaction section within the adsorption columns. There are two possible scenarios: adsorbent and catalyst are two different materials or both are present in the same pellet. For the reversible reaction of the type A↔B, reaction cannot occur near the extract point if high purity is required (otherwise maximum purity obtained is below 99%). To overcome this situation, reactors are inserted between the adsorption columns far from the extract point [72,73]

Minceva et al. [72] proposed a SMBR unit for *p*-xylene production from a mixture of xylene free of ethylbenzene operating in liquid phase. Ba exchanged faujasite type of adsorbent and ZSM-5 catalyst for the reaction section were used in the study. The configuration proposed consisted in six adsorbers in zone 1, nine adsorbers in zone 2, six adsorbers and five reactors in zone 3, and three adsorbers in zone 4. The authors simulated the unit at temperatures between 453 and 573 K for two types of feed: *p*-xylene composition higher than equilibrium (similar to that fed to Parex unit) and one with *p*-xylene composition lower than equilibrium (similar to the raffinate of Parex unit). They found out that for the first type of feed, 1.75 was reached for the *p*-xylene deviation from equilibrium, which is significantly higher than conventional processes. They also concluded that best SMBR performance was achieved with shorter reactors and lower temperatures.

Bergeot et al. [73] followed a similar configuration with six reactors and seven adsorbers between the feed injection and the raffinate withdrawal. They studied the xylene isomerization in liquid phase over HZSM-5 at 523-573 K and came to the conclusion that ethylbenzene cannot be converted. Simulations reported a decrease of more than half within the cycle loop.

2.8. Conclusions

p-Xylene world market is expected to grow in the upcoming years driven by the increasing demand of its derivatives. In Portugal, there is a significant difference between the production of benzene and *p*-xylene and the capacity of recently installed downstream plants that uses said species as raw material; hence, an opportunity to increase the production is identified. Based on the bibliographic research presented in this chapter, several technologies can be used to achieve this goal. In the first place, the conversion of excess toluene to more valuable benzene and *p*-xylene seems to be an understandable option to be considered. In addition, the successful of

hybrid processes combining adsorption and crystallization together with the promising results of recent studies on simulated moving bed reactor for *p*-xylene production constitute a potential alternative to increase the production of benzene and *p*-xylene within the existing aromatics complex of the country.

2.9. Nomenclature

Abbreviations

BTX = Benzene, Toluene, and Xylenes

CCR = Continuous Catalytic Regeneration

CPC = Chinese Petroleum Corporation

CUF = *Companhia União Fabril* (Factory Union Company)

EB = Ethylbenzene

EP = End Point

GTC = Global Technology Licensor

IBP = Initial Boiling Point

IFP = *Institut Français du Pétrole* (French Institute of Petroleum)

MHAI = Mobil High Activity Isomerization

MHTI = Mobil High Temperature Isomerization

MLPI = Mobil Low Pressure Isomerization

MOF = Metal Organic Framework

MVPI = Mobil Vapor Phase Isomerization

MX = *m*-Xylene

OX = *o*-Xylene

PET = Polyethylene Terephthalate

PTA = Purified Terephthalic Acid

PX = *p*-Xylene

RONC = Research Octane Number Clear

SMB = Simulated Moving Bed

SMBR = Simulated Moving Bed Reactor

UOP = Universal Oil Products

2.10. References

[1] Chirico, R. D., and W. V. Steele. 1997. "Thermodynamic Equilibria in Xylene Isomerization. 5. Xylene Isomerization Equilibria from Thermodynamic Studies and Reconciliation of Calculated and Experimental Product Distributions." *J. Chem. Eng. Data* no. 42 (4):784-790.

[2] Johnson, J. A. 2003. "Aromatics Complexes." In *Handbook of Petroleum Refining Processes*, 2.3-2.11. McGraw-Hill.

[3] Kareem, A., S. Chand, and I. M. Mishra. 2001. "Disproportionation of Toluene to Produce Benzene and p- Xylene - A Review." *Journal of Scientific and Industrial Research* no. 60 (4):319-327.

[4] Wantanachaisaeng, P., and K. O'Neil. 2007. Capturing Opportunities for Para-xylene Production. edited by UOP: UOP LLC.

[5] Brookes, T. 2012. New Technology Developments in the Petrochemical Industry - Refinery Integration with Petrochemicals to Achieve Higher Value Uplift. In *Egypt Petrochemicals Conference*. Cairo, Egypt: UOP LTD.

[6] Poparad, A., B. Ellis, B. Glover, and S. Metro. 2011. Reforming Solutions for Improved Profits in an Up-Down World. edited by UOP: UOP LLC.

[7] Galp Energia. *Fábrica de aromáticos e solventes*. http://www.galpenergia.com/PT/agalpenergia/os-nossos-negocios/Refinacao-Distribuicao/ARL/Refinacao/RefinariaMatosinhos/Paginas/FabricaAromaticosSolventes.aspx 2015.

[8] Instituto do Ambiente e Desenvolvimento. 2007. Projecto de Ampliação da CUF-QI Estudo de Impacte Ambiental. Instituto do Ambiente e Desenvolvimento.

[9] Artlant PTA. *Artlant PTA starts production*. http://artlantpta.com/index.php/en/news/126-artlant-pta-starts-production-in-sines 2015.

[10] Fabri, J., U. Graeser, and T. A. Simo. 2012. "Xylenes." In *Ullmann's Encyclopedia of Industrial Chemistry*. Weinheim: Wiley-VCH Verlag GmbH & Co. KGaA.

[11] Ouyang, Q., S.-F. Yin, L. Chen, X.-P. Zhou, and C.-T. Au. 2013. "A new catalytic process for high-efficiency synthesis of p-xylene by methylation of toluene with CH3Br." *AIChE Journal* no. 59 (2):532-540.

[12] Zhang, Y. Y., Y. F. Li, L. Chen, C. T. Au, and S. F. Yin. 2014. "A new catalytic process for the synthesis of para-xylene through benzene methylation with CH3Br." *Catalysis Communications* no. 54:6-10.

[13] Wang, T., X. Tang, X. Huang, W. Qian, Y. Cui, X. Hui, W. Yang, and F. Wei. 2014. "Conversion of methanol to aromatics in fluidized bed reactor." *Catalysis Today* no. 233:8-13.

[14] Cheng, Y. T., Z. Wang, C. J. Gilbert, W. Fan, and G. W. Huber. 2012. "Production of p-xylene from biomass by catalytic fast pyrolysis using ZSM-5 catalysts with reduced pore openings." *Angewandte Chemie - International Edition* no. 51 (44):11097-11100.

[15] Li, J., X. Li, G. Zhou, W. Wang, C. Wang, S. Komarneni, and Y. Wang. 2014. "Catalytic fast pyrolysis of biomass with mesoporous ZSM-5 zeolites prepared by desilication with NaOH solutions." *Applied Catalysis A: General* no. 470:115-122.

[16] Lin, Z., V. Nikolakis, and M. Ierapetritou. 2014. "Alternative approaches for p-xylene production from starch: Techno-economic analysis." *Industrial and Engineering Chemistry Research* no. 53 (26):10688-10699.

[17] Williams, C. L., C. C. Chang, P. Do, N. Nikbin, S. Caratzoulas, D. G. Vlachos, R. F. Lobo, W. Fan, and P. J. Dauenhauer. 2012. "Cycloaddition of biomass-derived furans for catalytic production of renewable p -xylene." *ACS Catalysis* no. 2 (6):935-939.

[18] Shiramizu, M., and F. D. Toste. 2011. "On the Diels-Alder approach to solely biomass-derived polyethylene terephthalate (PET): Conversion of 2,5-dimethylfuran and acrolein into p-xylene." *Chemistry - A European Journal* no. 17 (44):12452-12457.

[19] Lapinski, M., L. Baird, and R. James. 2003. "UOP Platforming Process." In *Handbook of Petroleum Refining Processes*, 4.3-4.31. McGraw-Hill.

[20] Dupraz, C., J. Rault, F. Alario, and S. Ramsey. 2002. Maximizing Paraxylene Production with ParamaX. edited by Axens: Axens.

[21] Stoodt, T. J., and A. Negiz. 2003. "UOP Sulfolane Process." In *Handbook of Petroleum Refining Processes*, 2.13-2.23. McGraw-Hill.

[22] Kerze, A. D., and T. Sato. 2006. Olgone ExxonMobil's New Aromatics Treatment Technology. edited by ExxonMobil: ExxonMobil Chemical.

[23] Negiz, A., and T. J. Stoodt. 2003. "UOP Tatoray Process." In *Handbook of Petroleum Refining Processes*, 2.55-2.63. McGraw-Hill.

[24] ExxonMobil Chemical Technology Licensing LLC. *TransPlus (heavy aromatics transalkylation) advantages* 2011.

[25] Ramsey, S. 2001. PxMax and XyMax - State-of-the-Art Paraxylene Production Technologies from ExxonMobil Chemical. In *2001 World Petrochemical Conference*, edited by ExxonMobil. Texas, USA: ExxonMobil Chemical.

[26] Das, J., Y. S. Bhat, and A. B. Halgeri. 1994. "Selective toluene disproportionation over pore size controlled MFI zeolite." *Industrial and Engineering Chemistry Research* no. 33 (2):246-250.

[27] Chen, N. Y., W. W. Kaeding, and F. G. Dwyer. 1979. "Para-directed aromatic reactions over shape-selective molecular sieve zeolite catalysts." *Journal of the American Chemical Society* no. 101 (22):6783-6784.

[28] Chen, D., J. Wang, X. Ren, H. Teng, and H. Gu. 2010. "Silicalite-1 shell synthesized onto cylinder-shaped ZSM-5 extrudate for disproportionation of toluene into para-xylene." *Catalysis Letters* no. 136 (1-2):65-70.

[29] ExxonMobil Chemical Technology Licensing LLC. 2009. PxMax with Crystallization An Integrated Process for High Purity Paraxylene Production. edited by ExxonMobil: ExxonMobil Chemical.

[30] Commissaris, S. E. 2003. "UOP Parex Process." In *Handbook of Petroleum Refining Processes*, 2.47-2.54. McGraw-Hill.

[31] Lima, R. M., and I. E. Grossmann. 2009. "Optimal synthesis of p-xylene separation processes based on crystallization technology." *AIChE Journal* no. 55 (2):354-373.

[32] Mohameed, H. A., B. A. Jdayil, and K. Takrouri. 2007. "Separation of para-xylene from xylene mixture via crystallization." *Chemical Engineering and Processing: Process Intensification* no. 46 (1):25-36.

[33] De Goede, R., and G. M. Van Rosmalen. 1990. "Crystal growth phenomena of paraxylene crystals." *Journal of Crystal Growth* no. 104 (2):399-410.

[34] Mullin, J. W. 2001. "Industrial techniques and equipment." In *Crystallization*, edited by J. W. Mullin, 315-402. Oxford: Butterworth-Heinemann.

[35] Patience, D. B., J. B. Rawlings, and H. A. Mohameed. 2001. "Crystallization of para-xylene in scraped-surface crystallizers." *AIChE Journal* no. 47 (11):2441-2451.

[36] GTC Technology. 2001. "Paraxylene production." *Hydrocarbon Engineering* no. 6 (9):54-55.

[37] Shiau, L. D., C. C. Wen, and B. S. Lin. 2008. "Separation of p-xylene from the multicomponent xylene system by stripping crystallization." *AIChE Journal* no. 54 (1):337-342.

[38] Broughton, D. B., and C. G. Gerhold. 1961. *Continuous sorption process employing fixed bed of sorbent and moving inlets and outlets.* US 2,985,589. UOP

[39] Johnson, J. A. 2003. "UOP Sorbex Family of Technologies." In *Handbook of Petroleum Refining Processes*, 10.29-10.35. McGraw-Hill.

[40] Beste, Y. A., M. Lisso, G. Wozny, and W. Arlt. 2000. "Optimization of simulated moving bed plants with low efficient stationary phases: Separation of fructose and glucose." *Journal of Chromatography A* no. 868 (2):169-188.

[41] Toumi, A., and S. Engell. 2004. "Optimization-based control of a reactive simulated moving bed process for glucose isomerization." *Chemical Engineering Science* no. 59 (18):3777-3792.

[42] Ruthven, D. M., and C. B. Ching. 1989. "Counter-current and simulated counter-current adsorption separation processes." *Chemical Engineering Science* no. 44 (5):1011-1038.

[43] Silva, M. S. P., A. E. Rodrigues, and J. P. B. Mota. 2015. "Modeling and simulation of an industrial-scale parex process." *AIChE Journal* no. 61 (4):1345-1363.

[44] Neuzil, R. W. 1976. *Process for separating para-xylene.* US 3,997,620. UOP

[45] Minceva, M., and A. E. Rodrigues. 2004. "Adsorption of Xylenes on Faujasite-Type Zeolite: Equilibrium and Kinetics in Batch Adsorber." *Chemical Engineering Research and Design* no. 82 (5):667-681.

[46] Rasouli, M., N. Yaghobi, F. Allahgholipour, and H. Atashi. 2014. "Para-xylene adsorption separation process using nano-zeolite Ba-X." *Chemical Engineering Research and Design* no. 92 (6):1192-1199.

[47] Rasouli, M., N. Yaghobi, S. Chitsazan, and M. H. Sayyar. 2012. "Influence of monovalent cations ion-exchange on zeolite ZSM-5 in separation of para-xylene from xylene mixture." *Microporous and Mesoporous Materials* no. 150:47-54.

[48] Torres-Knoop, A., R. Krishna, and D. Dubbeldam. 2014. "Separating xylene isomers by commensurate stacking of p-xylene within channels of MAF-X8." *Angewandte Chemie - International Edition* no. 53 (30):7774-7778.

[49] Moreira, M. A., J. C. Santos, A. F. P. Ferreira, J. M. Loureiro, F. Ragon, P. Horcajada, P. G. Yot, C. Serre, and A. E. Rodrigues. 2012. "Effect of ethylbenzene in p-xylene selectivity of the porous titanium amino terephthalate MIL-125(Ti)-NH 2." *Microporous and Mesoporous Materials* no. 158:229-234.

[50] Moreira, M. A., J. C. Santos, A. F. P. Ferreira, U. Müller, N. Trukhan, J. M. Loureiro, and A. E. Rodrigues. 2011. "Selective liquid phase adsorption and separation of ortho-xylene with the microporous MIL-53(Al)." *Separation Science and Technology* no. 46 (13):1995-2003.

[51] Kondor, A., and A. Dallos. 2014. "Adsorption isotherms of some alkyl aromatic hydrocarbons and surface energies on partially dealuminated Y faujasite zeolite by inverse gas chromatography." *Journal of Chromatography A.*

[52] Platts. 2012. European Petrochemicals. In *Methodology and Specification Guide*: The McGraw Hill Companies.

[53] Axens Process Licensing. 2005. Eluxyl simulated countercurrent adsorption of paraxylene. edited by Axens: Axens Process Licensing.

[54] Wolff, L., and P. Leflaive. 2004. Eluxyl Twin Raffinate Technology. edited by IFP: IFP.

[55] Cain, J. J. 2001. *Adsorption process for paraxylene purification using CS SSZ-25 adsorbent with benzene desorbent.* US 6,281,406 B1. Chevron Corporation

[56] Gentry, J. 2014. "The petrochemistry of paraxylene." *Hydrocarbon Engineering* no. 19 (9):103-109.

[57] Silady, P. J. 2003. "UOP Isomar Process." In *Handbook of Petroleum Refining Processes*, 2.39-2.46. McGraw-Hill.

[58] Mohr, G. 2002. XyMax: ExxonMobil's State-of-the-Art Xylenes Isomerization Technology. edited by ExxonMobil: ExxonMobil Chemical.

[59] ExxonMobil Chemical Technology Licensing LLC. 2010. XyMax and Advanced MHAI The leading Edge in Xylene Isomerization Technology and Services. edited by ExxonMobil: ExxonMobil Chemical.

[60] Bradley, T. W. 2006. ExxonMobil XyMax Xylene Isomerization Technology Licensing Executive Summary. edited by ExxonMobil: ExxonMobil Chemical.

[61] Axens Process Licensing. 2011. Oparis new isomerization catalyst for maximum xylenes production. edited by Axens: Axens Process Licensing.

[62] Alario, F., and J. Rault. 2002. Boost you Xylene Loop Performance with OPARIS. edited by Axens: Axens.

[63] Stern, D. L. 2007. *Process for xylene isomerization and ethylbenzene conversion.* US 7,247,762-B2. ExxonMobil Chemical Patents Inc.

[64] Magne-Drisch, J., G. Hotier, A. Methivier, J.-F. Joly, F. Alario, and E. Merlen. 2002. *Process for the production of at least one isomer of xylenes that comprise an adsorption stage and an isomerization stage with an EUO-structural-type catalyst.* US 6,376,734-B1. Institut Français du Pétrole

[65] Magne-Drisch, J., F. Alario, J.-F. Joly, A. Minkkinen, and E. Merlen. 2002. *Process for the production of paraxylene that comprises an adsorption stage, a liquid phase isomerization stage and a gas phase isomerization stage with an EUO-type zeolite.* US 6,448,459-B1. Institut Français du Pétrole

[66] Mohr, G. D. 2004. *Xylene isomerization.* US 2004/0236166-A1. ExxonMobil Chemical Company

[67] Bauer, J. E. 2009. *Process for isomerizing a non-equilibrium alkylaromatic feed mixture and an aromatic production facility.* US 2009/0182182-A1. Honeywell/UOP

[68] Wolff, L., P. Leflaive, and A. Methivier. 2009. *Process for co-producing para-xylene and styrene.* US 7,592,499-B2. Institut Français du Pétrole

[69] Bergeot, G., C. Laroche, P. Leflaive, D. Leinekugel-Le-Cocq, and L. Wolff. 2009. *Reactive simulated mobile bed for producing paraxylene.* WO 2009/130402-A1. Institut Français du Pétrole

[70] Abrevaya, H., J. C. Marte, S. T. Wilson, S. C. Koster, J. E. Bauer, W. Sinkler, B. A. Wilson, and L. L. Jacobsen. 2010. *Hydrocarbon conversion using an improved molecular sieve.* US 2010/0152511-A1. Honeywell/UOP

[71] Stankiewicz, A. 2003. "Reactive separations for process intensification: An industrial perspective." *Chemical Engineering and Processing* no. 42 (3):137-144.

[72] Minceva, M., P. S. Gomes, V. Meshko, and A. E. Rodrigues. 2008. "Simulated moving bed reactor for isomerization and separation of p-xylene." *Chemical Engineering Journal* no. 140 (1-3):305-323.

[73] Bergeot, G., D. Leinekugel-Le-Cocq, L. Wolff, L. Muhr, and M. Bailly. 2010. "Intensification of Paraxylene Production using a Simulated Moving Bed Reactor." *OGST – Revue d'IFP Energies nouvelles* no. 65 (5):721-733.

Chapter 3: Thermodynamic equilibrium of xylene isomerization in liquid phase

This chapter deals with the thermodynamic equilibrium for xylene isomerization. Experiments performed by several researchers to calculate the equilibrium in gas phase in the 1990s led to the conclusion that the earlier available thermodynamic data for xylenes, which were mainly based on experimental work performed in the 1940s, were in error. In this work a similar procedure is followed to determine the thermodynamic equilibrium for xylene isomerization in liquid phase. By means of the thermodynamic functions at saturated conditions presented by the previously mentioned studies, the standard free energies of formation are calculated between 250 and 550 K. Three different expressions are developed to calculate the equilibrium constants as a function of temperature.

This chapter is based on: Gonçalves, J. C., and A. E. Rodrigues. 2013. "Thermodynamic equilibrium of xylene isomerization in the liquid phase." *Journal of Chemical and Engineering Data* no. 58 (6):1425-1428.

3.1. Introduction

As previously mentioned, the isomerization reaction involved in the production of *p*-xylene (PX) is limited by the thermodynamic equilibrium which results in a large recycle loop to achieve the desired amount of *p*-xylene. Due to the direct influence of the thermodynamic equilibrium in the process, accurate equilibrium values are of the most importance.

Amelse [1] carried out isomerization experiments over non-shape-selective and shape-selective catalysts and calculated the thermodynamic equilibrium of xylenes at 623 and 673 K. Based on the results obtained, Amelse [1] concluded that xylenes thermodynamic data were erroneous.

According to Chirico et al. [2], available standard thermodynamic properties of formation (e.g. standard Gibbs free energy of formation) for the xylenes were the result of experimental work performed in the 1940s. Those experimental results were obtained only at one temperature, 298.15 K. *p*-Xylene has been studied extensively in the past in order to expand and improve the available data, but *o*-xylene (OX) and *m*-xylene (MX) have been left aside [2]; this was probably due to the higher economic importance of *p*-xylene. Chirico and co-workers [2-5] carried out experimental studies to measure calorimetric and physical properties used to determine standard Gibbs free energies of formation between 250 and 500 K for the three xylenes and ethylbenzene. Furthermore, they developed expressions to evaluate the thermodynamic equilibrium which were in excellent agreement with Amelse [1] results. Chirico and Steele [6] concluded that the largest error was associated with the entropy of *o*-xylene in the liquid and gas phases. Both, Amelse [1] and Chirico et al. [4], highlighted the influence of the rotation of the methyl groups.

Unfortunately, the aforementioned studies presented expressions for the equilibrium constants as a function of temperature only for gas phase; this was probably due to the fact that xylene isomerization occurs industrially under gas phase conditions. However, in the last few years new trends in xylene production are focused on the use of xylene isomerization in liquid phase driven by the environmental benefits of reduction of energy and pollution. Namely, the isomerization is separated in two stages: one in liquid phase for xylenes and one in gas phase for ethylbenzene [7,8]. Moreover, research efforts are being made on process intensification by coupling xylenes isomerization and xylenes separation (both in liquid phase) in a single unit using the Simulated Moving Bed Reactor (SMBR) technology [9,10] and, as previously stated, one of the objectives of this thesis is a complete study on xylene isomerization in liquid phase. This chapter is intended to develop similar expressions of the equilibrium for xylene isomerization in liquid phase based on the thermodynamic functions at saturated conditions presented by Chirico and co-workers [2-4].

3.2. Equilibrium in liquid phase

In order to obtain the standard Gibbs energy of formation to estimate the equilibrium constants in liquid phase, the molar thermodynamic functions at saturation pressure (P^s) are extracted from the studies cited before, for temperatures between 250 and 550 K. The saturation pressure is obtained from the Wagner equation [11] modified to four coefficients into the form (2,4) by Duschek et al. [12]:

$$\ln\left(\frac{P^s}{P_c}\right) = \frac{1}{T_r}\{A(1-T_r) + B(1-T_r)^{1.5} + C(1-T_r)^2 + D(1-T_r)^4\} \tag{3.1}$$

where $T_r = T/T_c$, P_c is the critical pressure, and T_c is the critical temperature. The required equation parameters (A, B, C, and D) of each species are presented in Table 3.1. Critical properties and some other intrinsic properties are shown in Table A.1 (see Annex A).

The molar thermodynamic functions at saturation pressure are presented in Table 3.2; based on those values, the enthalpy (H) and entropy (S) at standard state (i.e., at P^0 = 100 kPa) are calculated at each temperature using Maxwell relations:

$$\left(\frac{\partial S}{\partial P}\right)_T = -\left(\frac{\partial V}{\partial T}\right)_P \tag{3.2}$$

$$\left(\frac{\partial H}{\partial P}\right)_T = V - T\left(\frac{\partial V}{\partial T}\right)_P \tag{3.3}$$

Table 3.1 Wagner parameters for equation (3.1)

	p-Xylene	*m*-Xylene	*o*-Xylene
A	-7.59306	-7.564368	-7.457432
B	1.77964	1.623819	1.519744
C	-1.24526	-1.139601	-1.030912
D	-3.93248	-4.004004	-3.997287

Integrating within the pressure range and assuming no variation of molar volume (V) in liquid phase due to pressure, equations (3.4) and (3.5) are obtained:

$$\Delta S = -\frac{dV}{dT}\Delta P \tag{3.4}$$

$$\Delta H = \left(V - T\frac{dV}{dT}\right)\Delta P \tag{3.5}$$

where $\Delta P = P^0 - P^s$. Following the procedure of Chirico and co-workers [2-4], molar volumes are obtained by means of the molecular weight (MW) and the densities (ρ) calculated with a form of the corresponding-states equation of Riedel:

Table 3.2 Molar thermodynamic functions, enthalpy (H) and entropy (S) at saturation pressure (P^s) at temperatures from 250 to 550 K[d]

	p-Xylene[a]			*m*-Xylene[b]			*o*-Xylene[c]		
T, K	P^s, kPa	$\Delta_0^T H/RT$	$\Delta_0^T S/R$	P^s, kPa	$\Delta_0^T H/RT$	$\Delta_0^T S/R$	P^s, kPa	$\Delta_0^T H/RT$	$\Delta_0^T S/R$
250	0.03907	17.448	26.038	0.03593	15.450	26.616	0.02716	16.129	25.690
260	0.08961	17.553	26.829	0.08300	15.635	27.419	0.06361	16.319	26.517
280	0.3836	17.783	28.368	0.3597	16.001	28.958	0.2827	16.694	28.114
298.15	1.179	18.012	29.721	1.116	16.335	30.307	0.8945	17.031	29.511
300	1.310	18.037	29.857	1.241	16.369	30.442	0.9967	17.066	29.651
320	3.739	18.311	31.304	3.572	16.743	31.884	2.922	17.440	31.138
340	9.225	18.603	32.715	8.878	17.122	33.290	7.379	17.818	32.585
360	20.22	18.913	34.098	19.58	17.510	34.667	16.50	18.201	33.997
380	40.21	19.239	35.454	39.14	17.905	36.020	33.39	18.589	35.380
400	73.78	19.578	36.789	72.15	18.308	37.351	62.20	18.984	36.738
420	126.6	19.932	38.107	124.3	18.719	38.665	108.1	19.384	38.074
440	205.3	20.299	39.409	202.2	19.14	39.96	177.3	19.79	39.39
460	317.5	20.678	40.699	313.6	19.56	41.25	276.8	20.21	40.70
480	471.6	21.069	41.979	467.1	20.00	42.52	414.7	20.63	41.99
500	677.0	21.472	43.249	672.0	20.44	43.79	599.5	21.06	43.27
520	943.9	21.885	44.512	938.8	20.89	45.06	840.8	21.50	44.54
540	1284	22.310	45.771	1279	21.36	46.33	1149	21.95	45.82
550	1485	22.528	46.401	1480	21.61	46.96	1332	22.18	46.45

[a] From Chirico et al. [2]. [b] From Chirico et al. [3]. [c] From Chirico et al. [4]. [d] Values are presented with one digit more than justified.

$$\frac{\rho}{\rho_c} = 1 + 0.85\left(1 - \frac{T}{T_c}\right) + (1.6916 + 0.9845\omega)\left(1 - \frac{T}{T_c}\right)^{1/3} \tag{3.6}$$

Once the thermodynamic functions are obtained in the standard state for each temperature, the formation functions are calculated. Enthalpies of formation include the enthalpies of the reference elements [13]:

$$\Delta_f H^0(T) = \Delta_f H^0(298.15) + [H^0(T) - H^0(298.15)]_{compound} - \sum [H^0(T) - H^0(298.15)]_{elements} \tag{3.7}$$

where $\Delta_f H^0$ at 298.15 K is -24.39±0.63, -25.38±0.37, and -24.39±0.40 kJ kmol^{-1} for *p*-, *m*-, and *o*-xylene respectively [6]. The Gibbs energy of formation is calculated with the enthalpy of formation and the entropies of the reference elements [13]:

$$\Delta_f G^0(T) = \Delta_f H^0(T) - T\left\{S^0(T)_{compound} - \sum S^0(T)_{elements}\right\} \tag{3.8}$$

The enthalpies and entropies of the elements are obtained from Chase [13] and shown in Table 3.3. Table 3.4 presents the Gibbs energy of formation for each xylene species with the corresponding uncertainty; errors associated to pressure and molar volume are not taken into account since they are negligible compared to that of enthalpy and entropy.

Table 3.3 Entropy (S^0) and enthalpy (H^0-$H^0(Tr)$) of reference elements at reference temperature Tr = 298.15 K and standard pressure P^0 = 100 kPa from Chase [13]

	Graphite (C)		Hydrogen (H_2)	
T, K	S^0, J mol^{-1}K^{-1}	$(H^0$-$H^0(Tr))$, kJ mol^{-1}	S^0, J mol^{-1}K^{-1}	$(H^0$-$H^0(Tr))$, kJ mol^{-1}
200	3.082	-0.665	119.412	-2.774
250	4.394	-0.369	125.640	-1.378
298.15	5.740	0	130.680	0
300	5.793	0.016	130.858	0.053
350	7.242	0.487	135.325	1.502
400	8.713	1.039	139.216	2.959
450	10.191	1.667	142.656	4.42
500	11.662	2.365	145.737	5.882
600	14.533	3.943	151.077	8.811

Ethylbenzene cannot be converted in liquid phase because its isomerization to xylenes goes through naphthenes intermediates, which requires the presence of hydrogen. Nevertheless isomerization of xylenes can be carried out in liquid phase over acid catalysts [9,10]. Due to the aforementioned fact, the ethylbenzene is not taken into account in the thermodynamic equilibrium in liquid phase. The equilibrium constants are defined for each isomer pair, according to the reaction scheme in Figure 3.1, as seen in equations (3.9) to (3.11).

Table 3.4 Gibbs energy of formation ($\Delta_f G^0/RT$) of xylene species in liquid phase

T, K	*p*-Xylene	*m*-Xylene	*o*-Xylene
250	42.672 ± 0.019	41.615 ± 0.019	42.866 ± 0.019
260	43.098 ± 0.018	42.050 ± 0.018	43.296 ± 0.018
280	43.882 ± 0.018	42.867 ± 0.018	44.088 ± 0.018
298.15	44.526 ± 0.017	43.537 ± 0.017	44.732 ± 0.017
300	44.589 ± 0.017	43.601 ± 0.017	44.795 ± 0.017
320	45.225 ± 0.017	44.264 ± 0.017	45.430 ± 0.017
340	45.801 ± 0.017	44.861 ± 0.017	46.002 ± 0.017
360	46.320 ± 0.016	45.403 ± 0.016	46.518 ± 0.016
380	46.792 ± 0.016	45.892 ± 0.016	46.983 ± 0.016
400	47.218 ± 0.016	46.336 ± 0.016	47.404 ± 0.016
420	47.604 ± 0.016	46.737 ± 0.016	47.783 ± 0.016
440	47.954 ± 0.016	47.11 ± 0.14	48.13 ± 0.14
460	48.271 ± 0.016	47.43 ± 0.14	48.44 ± 0.14
480	48.559 ± 0.015	47.74 ± 0.14	48.72 ± 0.14
500	48.822 ± 0.015	48.01 ± 0.14	48.98 ± 0.14
520	49.062 ± 0.015	48.25 ± 0.14	49.21 ± 0.14
540	49.282 ± 0.015	48.48 ± 0.14	49.42 ± 0.14
550	49.384 ± 0.015	48.60 ± 0.14	49.53 ± 0.14

Deviations are larger for *m*- and *o*-xylene above 440 K due to the uncertainty of their saturation functions

$$X_{\mathrm{OX}}/X_{\mathrm{MX}} = K_1 = \exp(-\Delta_{R1}G^0/RT) \tag{3.9}$$

$$X_{\mathrm{MX}}/X_{\mathrm{PX}} = K_2 = \exp(-\Delta_{R2}G^0/RT) \tag{3.10}$$

$$X_{\mathrm{PX}}/X_{\mathrm{OX}} = K_3 = \exp(-\Delta_{R3}G^0/RT) \tag{3.11}$$

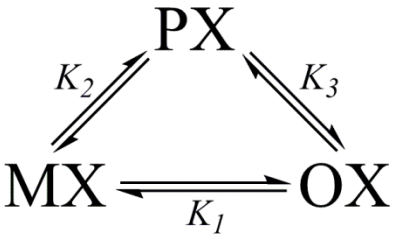

Figure 3.1 Reaction scheme for xylene isomerization. PX = *p*-Xylene, MX = *m*-Xylene, OX = *o*-Xylene. K_1=OX/MX, K_2=MX/PX, K_3=PX/OX. The triangular scheme adds to the mechanism the direct conversion between *o*- and *p*-xylene in order to account for the influence of intracrystalline mass-transfer resistance [14].

Three expression of the form ln*K* = *f(1/T)* are obtained for each equilibrium constant through weighted least squares regression; F-test is used in order to determine the order of the polynomial and the significance of each parameter [15]:

$$\ln K_1 = 4190000_{\pm 130000}(T/\mathrm{K})^{-3} - 259_{\pm 4}(T/\mathrm{K})^{-1} - 0.486_{\pm 0.008};\ R^2_{\mathrm{adj}} = 0.9996 \tag{3.12}$$

$$\ln K_2 = -8700_{\pm 1800}(T/\mathrm{K})^{-2} + 175_{\pm 12}(T/\mathrm{K})^{-1} + 0.500_{\pm 0.018};\quad R^2_{\mathrm{adj}} = 0.9989 \tag{3.13}$$

$$\ln K_3 = -29500_{\pm 600}(T/\mathrm{K})^{-2} + 197_{\pm 4}(T/\mathrm{K})^{-1} - 0.122_{\pm 0.005};\quad R^2_{\mathrm{adj}} = 0.9964 \tag{3.14}$$

The curves obtained by equations (3.12) to (3.14) are depicted in Figure 3.2. The product distribution in thermodynamic equilibrium for the three xylenes is calculated by linear combination of two of the equilibrium constants defined by equations (3.9) to (3.11), and the material balance ($\sum X_i = 1$). The obtained product distribution for several temperatures is presented in Table 3.5.

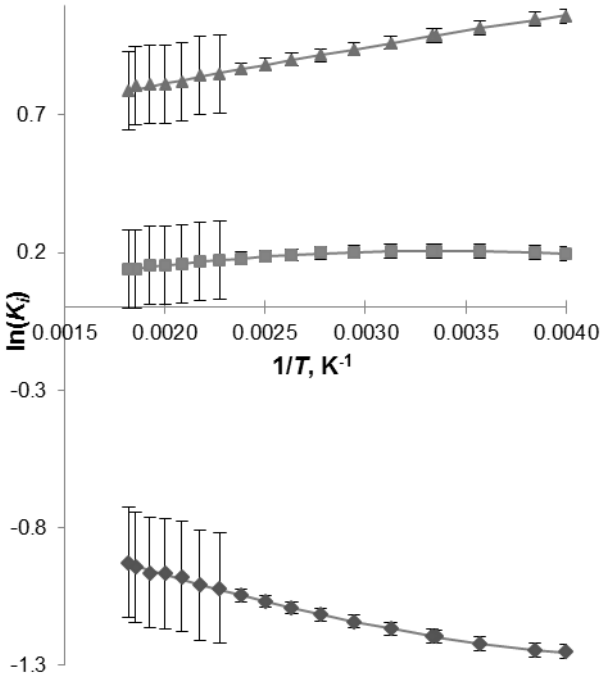

Figure 3.2 Equilibrium constants K_i as a function of temperature according to equations (3.12) to (3.14). (♦) $i = 1$ (▲) $i = 2$ (■) $i = 3$. Error bars are larger for temperatures above 440 K due to the increase in the uncertainty of the saturation functions of *m*-xylene and *o*-xylene.

Table 3.5 Equilibrium product distribution (mol %) based on the equilibrium constants from equations (3.12) to (3.14)[a].

T, K	*p*-Xylene	*m*-Xylene	*o*-Xylene
250	$21._2 \pm 1._1$	$61._3 \pm 2._3$	$17._5 \pm 1._0$
300	$22._2 \pm 1._2$	$59._7 \pm 2._4$	$18._1 \pm 1._0$
350	$23._0 \pm 1._2$	$58._2 \pm 2._5$	$18._8 \pm 1._1$
400	$23._5 \pm 1._2$	$56._9 \pm 2._6$	$19._6 \pm 1._2$
450	$24._0 \pm 1._3$	$55._8 \pm 2._7$	$20._2 \pm 1._2$
500	$24._3 \pm 1._3$	$54._9 \pm 2._8$	$20._8 \pm 1._3$
550	$24._5 \pm 1._3$	$54._2 \pm 2._8$	$21._3 \pm 1._3$

[a] Uncertainties of equilibrium constants from equations (3.12) to (3.14) are calculated based on prediction of new values of the fitted curves and combined in quadrature to obtain the uncertainties within the product distribution

Unfortunately, there are very few references of thermodynamic equilibrium for xylene isomerization in liquid phase in the literature. For instance, Cappellazzo et al. [14] and Norman

et al. [16] carried out experiments on xylene isomerization in liquid phase; they used the equilibrium constants within the kinetic parameters, however they do not show the actual values.

Chirico and Steele [6] only reported isomerization equilibrium in the liquid phase at T = 323 K: ($58._9 \pm 2._9$) % of *m*-xylene, ($18._3 \pm 1._7$) % of *o*-xylene, and ($22._8 \pm 2._4$) % of *p*-xylene. Using the expressions obtained in this study the following equilibrium distribution is obtained: ($59._0 \pm 2._4$) % of *m*-xylene, ($18._4 \pm 1._1$) % of *o*-xylene, and ($22._6 \pm 1._2$) % of *p*-xylene. The aforementioned values show excellent agreement between themselves.

3.3. Conclusions

Three expressions are developed to determine the thermodynamic equilibrium constants for xylene isomerization in liquid phase between 250 and 550 K. A simple procedure is followed based on published thermodynamic functions at saturation pressure.

3.4. Nomenclature

G = Gibbs free energy, J mol^{-1}

H = Enthalpy, J mol^{-1}

K_i = Equilibrium constant i

MW = Molecular weight, g mol^{-1}

P = Pressure, kPa

R = Universal gas constant, J mol^{-1}K^{-1}

R^2_{adj} = Coefficient of determination adjusted R-squared

S = Entropy, J mol^{-1}K^{-1}

T = Temperature, K

V = Molar volume, m^3 mol^{-1}

X_i = Molar fraction of component i

Greek letters

ρ = Density, kg m^{-3}

ω = Acentric factor

Superscripts and subscripts

0 = Standard state conditions

c = Critical

f = Formation property

m = Property on molar basis

r = Reduced property

R_i = Reaction i

s = Saturation conditions

Abbreviations

MX = *m*-Xylene

OX = *o*-Xylene

PX = *p*-Xylene

3.5. References

[1] Amelse, J. A. 1992. The influence of diffusion limitations on xylene isomerization. Paper read at Proceedings from the Ninth International Zeolite Conference, at Montreal.

[2] Chirico, R. D., S. E. Knipmeyer, A. Nguyen, and W. V. Steele. 1997. "Thermodynamic Equilibria in Xylene Isomerization. 1. The Thermodynamic Properties of p-Xylene." *J. Chem. Eng. Data* no. 42 (2):248-261.

[3] Chirico, R. D., S. E. Knipmeyer, A. Nguyen, J. W. Reynolds, and W. V. Steele. 1997. "Thermodynamic Equilibria in Xylene Isomerization. 2. The Thermodynamic Properties of m-Xylene." *J. Chem. Eng. Data* no. 42 (3):475-487.

[4] Chirico, R. D., S. E. Knipmeyer, A. Nguyen, A. B. Cowell, J. W. Reynolds, and W. V. Steele. 1997. "Thermodynamic Equilibria in Xylene Isomerization. 3. The Thermodynamic Properties of o-Xylene." *J. Chem. Eng. Data* no. 42 (4):758-771.

[5] Chirico, R. D., S. E. Knipmeyer, A. Nguyen, and W. V. Steele. 1997. "Thermodynamic Equilibria in Xylene Isomerization. 4. The Thermodynamic Properties of Ethylbenzene." *J. Chem. Eng. Data* no. 42 (4):772-783.

[6] Chirico, R. D., and W. V. Steele. 1997. "Thermodynamic Equilibria in Xylene Isomerization. 5. Xylene Isomerization Equilibria from Thermodynamic Studies and Reconciliation of Calculated and Experimental Product Distributions." *J. Chem. Eng. Data* no. 42 (4):784-790.

[7] Mohr, G. D. 2004. *Xylene Isomerization.* U.S. 6,770,792 B2. ExxonMobil Chemical Company

[8] Abrevaya, H., J. C. Marte, S. T. Wilson, S. C. Koster, J. E. Bauer, W. Sinkler, B. A. Wilson, and L. L. Jacobsen. 2012. *Hydrocarbon Conversion Using an Improved Molecular Sieve.* U.S. Patent 8,304,593 B2.

[9] Minceva, M., P. S. Gomes, V. Meshko, and A. E. Rodrigues. 2008. "Simulated moving bed reactor for isomerization and separation of p-xylene." *Chemical Engineering Journal* no. 140 (1-3):305-323.

[10] Bergeot, G., D. Leinekugel-Le-Cocq, L. Wolff, L. Muhr, and M. Bailly. 2010. "Intensification of Paraxylene Production using a Simulated Moving Bed Reactor." *OGST – Revue d'IFP Energies nouvelles* no. 65 (5):721-733.

[11] Wagner, W. 1973. "New vapour pressure measurements for argon and nitrogen and a new method for establishing rational vapour pressure equations." *Cryogenics* no. 13 (8):470-482.

[12] Duschek, W., R. Kleinrahm, and W. Wagner. 1990. "Measurement and correlation of the (pressure, density, temperature) relation of carbon dioxide II. Saturated-liquid and saturated-vapour densities and the vapour pressure along the entire coexistence curve." *The Journal of Chemical Thermodynamics* no. 22 (9):841-864.

[13] Chase, M. W. J. 1998. *NIST-JANAF Thermochemical Tables*. Fourth ed: American Inst. of Physics.

[14] Cappellazzo, O., G. Cao, G. Messina, and M. Morbidelli. 1991. "Kinetics of Shape-Selective Xylene Isomerization over a ZSM-5 Catalyst." *Industrial & Engineering Chemistry Research* no. 30 (10):2280-2287.

[15] Montgomery, D. C., and G. C. Runger. 2005. *Applied Statistics and Probability for Engineers*: John Wiley & Sons Incorporated.

[16] Norman, G. H., D. S. Shigemura, and J. R. Hopper. 1976. "Isomerization of Xylene over Hydrogen Modernite. A Comprehensive Model." *Industrial & Engineering Chemistry Research* no. 15 (1):41-45.

Chapter 4: Gas phase isomerization unit

A mathematical model based on 34 days of continuous operation of a gas phase isomerization unit is developed in this Chapter. The unit uses a radial-flow reactor with a catalyst capable of converting xylenes and ethylbenzene to mixed xylenes at 365 ºC and 8.4 bar. The catalyst contains EU-1 zeolite, platinum, and alumina used as binder. Two reactions are considered, ethylbenzene isomerization and xylene isomerization; the rates are based on the Hougen-Watson model according to the literature. An optimization procedure is carried out in order to obtain new kinetic constants that minimize the difference between the actual and the calculated values.

This chapter is based on: Gonçalves, J. C., and A. E. Rodrigues. 2013. "Industrial xylene/ethylbenzene isomerization unit using a radial-flow reactor and euo-type zeolite." *Chemical Engineering & Technology* no. 36 (10):1658-1664.

4.1. Introduction

The aromatics complex under study is fed by a mixture of aromatics produced through naphtha catalytic reforming as shown in Figure 4.1. Benzene and toluene from the top of the fractionation column are separated from the non-aromatic compounds using a polar solvent, whereas the bottom is sent to the xylene recovery section. Since xylenes and ethylbenzene form a thermodynamic equilibrium, a separation-isomerization loop is required to increase the production of a certain isomer, which in this case is mainly *p*-xylene and *o*-xylene at a lesser degree. The xylene splitter is designed to make a split between *m*- and *o*-xylene based on the 5 ºC difference in the boiling points separating a fraction of the isomer and producing high purity *o*-xylene by means of further separation of heavy aromatics. The top of the splitter, which consists of non-aromatics, ethylbenzene, *m*-, *p*-, and the remaining *o*-xylene, is sent to the separation unit where high purity *p*-xylene is obtained by means of an adsorptive-type process. The raffinate from the separation unit, almost depleted in *p*-xylene, is fed to the isomerization unit where further production of *p*- and *o*-xylene restores the thermodynamic equilibrium. The addition of hydrogen allows the conversion of ethylbenzene, avoids non-aromatics build up in the loop through cracking, and prevents the catalyst from coking [1,2].

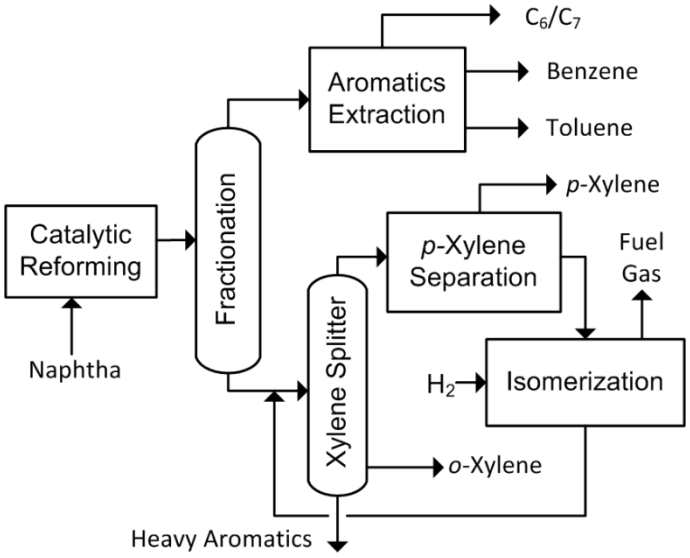

Figure 4.1 Simplified scheme of the aromatics complex under study.

The process flow of an isomerization unit is very standard regardless of the technology supplier (see Figure 4.2). The feed is first combined with hydrogen-rich recycle gas and preheated by exchange with the reactor effluent and vaporized in the fired heater to achieve the reactor operating temperature. The hot feed gas stream is then sent to the reactor. The effluent is cooled by exchange with the combined feed and then sent to the product separator, where the

hydrogen-rich gas is sent back and combined with the feed and the liquid product is charged to a deheptanizer column. The bottom of the column is combined with fresh mixed-xylenes feed and recycled [1,3]. The difference between the technologies lies mainly on the catalysts used as discussed below in Section 4.2.1.

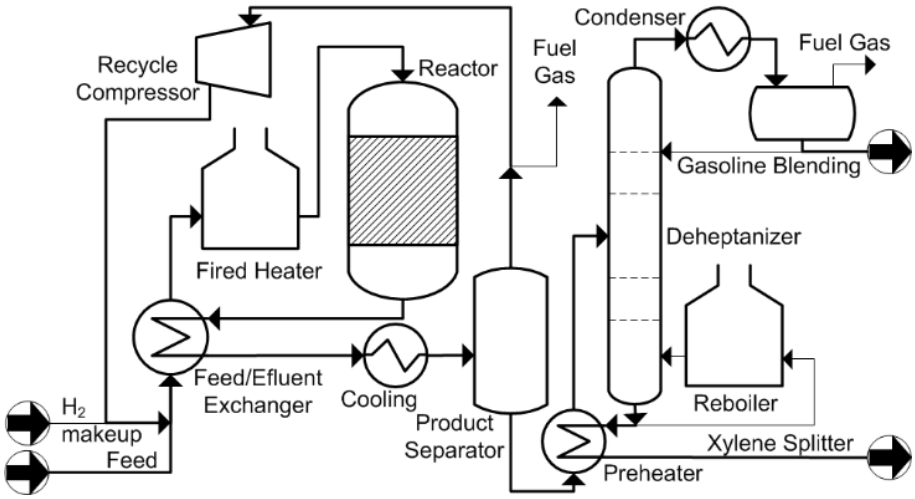

Figure 4.2 Isomerization unit

The purpose of this chapter is to study the isomerization unit with a new type of catalyst running at lower temperatures in the isomerization of ethylbenzene and xylenes. Based on the kinetic models found in the literature supported by reaction mechanisms and the actual performance of the reactor installed inside the unit, a simplified mathematical model with optimized kinetics capable of reproducing the operating data of said reactor is developed.

4.2. Isomerization unit

4.2.1. Catalyst

The catalyst used in this unit is bifunctional-type comprising metal and acidic sites. In the isomerization of xylenes hydrogen and metal sites are not involved, but they do contribute to reduce deactivation by removing the carbonaceous materials from the catalyst surface [4]. Isomerization of xylenes occurs over acid sites following a monomolecular or bimolecular mechanism. The first consists of rapid and reversible addition of a proton to the aromatic ring followed by 1,2-methyl shift, whereas the latter includes disproportionation and transalkylation reactions with diphenylmethane intermediates. The bimolecular reaction is favored at lower temperatures (i.e. below 200 ºC) due to its lower activation energy; above 300 ºC the isomerization is essentially monomolecular. Moreover, the pore structure plays an important role in the mechanism; steric constraints limit the formation of bulky intermediates in small pore-size

catalyst favoring the monomolecular mechanism [5,6]. The reaction scheme presented in Figure 4.3 represents the intramolecular 1,2-methyl shift; however, a triangular scheme, including an apparent direct conversion between *o*- and *p*-xylene, may be used to take into account the fast movement of the *para*-isomer inside small pore-size catalyst [7].

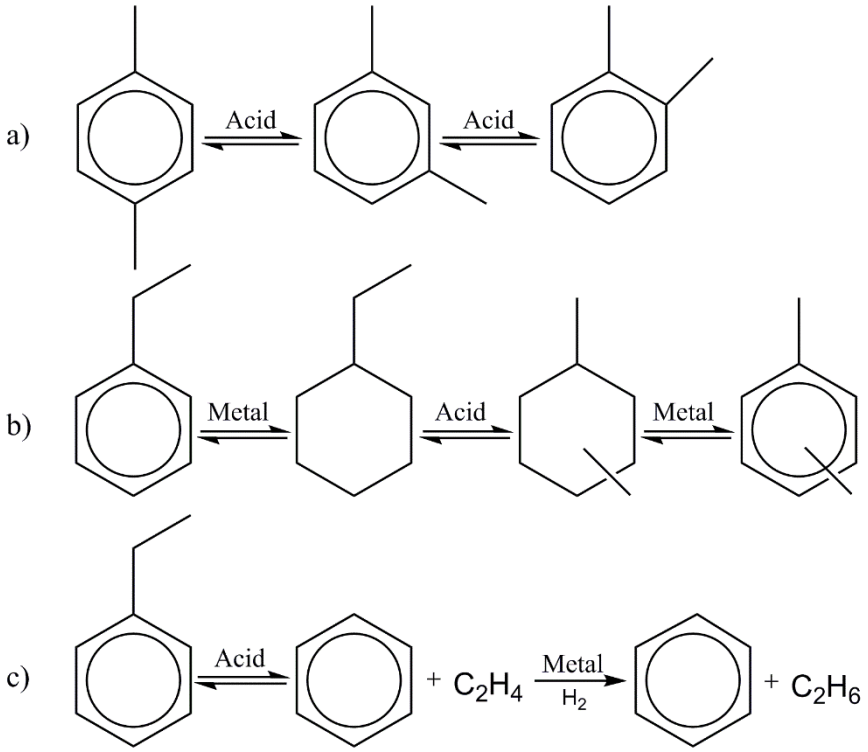

Figure 4.3 Reactions for a) xylene isomerization, b) ethylbenzene isomerization, and c) ethylbenzene dealkylation from Silady [3]

Xylene isomerization catalysts are divided into two main categories based on ethylbenzene conversion: ethylbenzene isomerization catalysts and ethylbenzene dealkylation catalysts. Ethylbenzene isomerization catalysts convert ethylbenzene to xylenes through a naphthene intermediate. The metal function first saturates the ethylbenzene to ethylcyclohexane, then the acid function isomerizes it to dimethylcyclohexane, and finally the metal function dehydrogenates the naphthene to xylene. On low acidic catalyst only *o*-xylene is produced since 1,2-dimethylcyclohexane is the energetically favored intermediate. With high acidic catalyst (e.g. zeolites) and restriction in pores, secondary carbocation leads to a mixture of 1,2-; 1,3-; and 1,4-dimethylcyclohexane producing the three isomers as presented in Figure 4.3 [8]. However, due to equilibrium constraints, the isomerization of ethylbenzene is significantly limited. Ethylbenzene dealkylation is not an equilibrium-constrained reaction; the ethyl group is separated from the aromatic ring by the acid function and hydrogenated by the metal function avoiding further alkylation to heavy aromatics [3].

Both types offer advantages and disadvantages. Through ethylbenzene isomerization, more xylenes are produced from ethylbenzene with the cost of large recycle volume as a result of low conversion of the equilibrium-constrained reaction. The opposite occurs when using dealkylation-type catalyst where higher conversion reduces the recycle at the expense of converting ethylbenzene into benzene instead of xylenes.

Two zeolites are normally used in these type of processes, mordenite isomerizes ethylbenzene into xylene while ZSM-5 dealkylates it into benzene [9]. The difference is mainly based on the pore structure; mordenite possesses large channels being a 12-membered ring zeolite, whereas the smaller pores of ZSM-5 promote dealkylation due to a long residence time of ethylbenzene molecules and stronger acid sites required by the reaction. Particularly, the isomerization-type catalyst is based on partially acidic mordenite with platinum as the hydrogenation component. Mordenite is chosen since disproportionation and transalkylation are limited by steric constraints within the channels. Furthermore, mesopores are formed through dealumination providing easy access of the organic molecules to the protonic sites [10,11].

The reactor studied uses a new generation of this type of catalyst, which comprises 10 wt% of EU-1 (EUO-type) zeolite with Si/Al ratio of 18, 0.3 wt% of platinum, and 89.7 wt% of alumina used as binder. EU-1 is a 10-membered ring zeolite with medium pores (similar to ZSM-5) but with large side pockets [6].

4.2.2. Radial-flow reactor

The unit uses a fixed-bed radial-flow reactor. Radial-flow reactors are usually an alternative when axial reactors cannot meet the demands due to the large amount of catalyst needed when high production is required. Haldor Topsøe proposed this configuration where low pressure drop may be expected owing to the short length of the catalyst bed [12]. The catalyst is placed between two co-axial cylinders; the feed enters at the top of the reactor and is directed to the sidewall. The fluid then travels radially through the fixed bed, and into a center pipe. The reactor effluent then flows down through the center pipe to the reactor outlet according to Figure 4.4. The characteristics and dimensions of the catalyst are shown in Table 4.1.

Table 4.1 Characteristics and dimensions of the catalyst within the reactor

Catalyst diameter, mm	1.6
Total catalyst mass, kg	21120
Catalyst-bed length, m (L)	6.31
Catalyst-bed outer radius, m (R_0)	1.24
Catalyst-bed inner radius, m (R_1)	0.24
Catalyst-bed volume, m^3	29.34

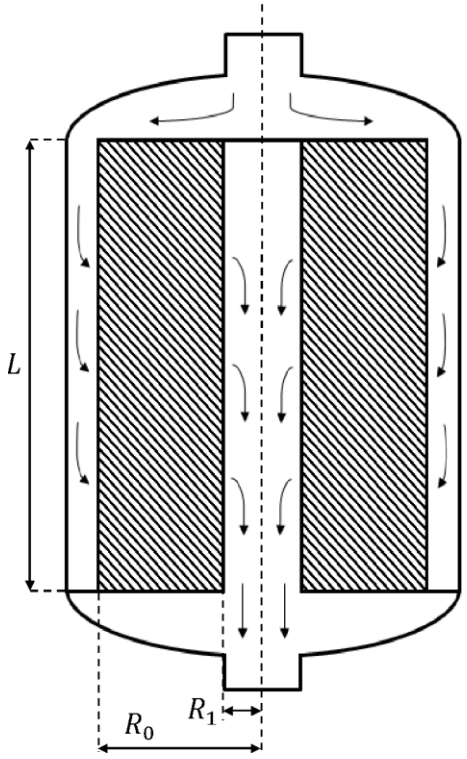

Figure 4.4 Simplified reactor scheme

4.2.3. Reaction system

Reactor data, supplied by GALP personnel, regarding about two months of continuous operation are used in the study; however, data exhibiting deviations from normal operation are ruled out. Reactions involving hydrogen consumption are not considered in the mathematical modeling since hydrogen consumption is less than 2%. These reactions are non-aromatic cracking with the production of light hydrocarbons and hydrodealkylation where xylenes are converted to toluene, which may undergo further hydrodealkylation to benzene over high acidic catalyst, and methane. In normal operation, the naphthene concentration is kept constant for the isomerization of ethylbenzene; loss of naphthenes in the top of the deheptanizer or through cracking leads to a loss of aromatics in order to synthesize more naphthenes. Furthermore, side reactions such as disproportionation and transalkylation are not considered since benzene, toluene, and C_9-aromatic concentrations are below 1%. Table 4.2 summarizes the reactor data to be used in the mathematical modeling. According to the aforementioned, two main reactions are considered: ethylbenzene isomerization and xylene isomerization.

For ethylbenzene isomerization, a bifunctional model is followed according to Roebschlaeger and Christoffel [13]. Ethylbenzene is hydrogenated on platinum sites, then the

Table 4.2 Summarized reactor data used in the mathematical modeling

Day	Flow, ton h^{-1}	Pressure, kPa	H_2, wt%	Inert, wt%	EB_{in}, wt%	PX_{in}, wt%	MX_{in}, wt%	OX_{in}, wt%	EB_{out}, wt%	PX_{out}, wt%	MX_{out}, wt%	OX_{out}, wt%
1	90.31	814	5.79	24.61	10.63	0.90	43.93	14.14	6.97	12.94	34.74	14.96
2	88.21	814	4.45	23.38	11.06	0.92	45.31	14.88	7.18	13.41	36.05	15.53
3	88.83	804	5.47	23.42	10.95	1.06	44.75	14.34	7.08	13.39	35.35	15.29
4	91.52	824	4.95	25.86	10.60	0.92	43.56	14.11	6.93	13.60	34.03	14.63
5	90.22	814	5.35	23.83	10.76	1.00	44.68	14.38	7.19	13.86	34.75	15.01
6	87.86	804	5.10	22.29	10.84	1.04	46.10	14.63	7.43	14.19	35.58	15.41
7	87.79	814	5.12	22.10	10.78	1.11	46.39	14.50	7.40	14.34	35.58	15.46
8	87.77	794	5.06	21.92	10.99	1.02	46.36	14.65	7.33	15.67	34.89	15.13
9	88.19	794	5.65	21.54	11.15	1.10	46.17	14.38	7.35	14.99	35.33	15.15
10	88.57	804	5.04	23.39	10.95	1.21	45.18	14.22	7.71	14.48	34.55	14.83
11	87.09	804	5.22	21.80	10.97	1.25	46.16	14.59	7.83	14.79	35.24	15.11
12	85.81	804	5.02	21.84	11.10	1.18	46.31	14.55	7.70	14.93	35.34	15.16
13	87.37	804	4.60	23.59	10.63	1.08	45.78	14.32	7.27	14.78	34.90	14.86
14	87.09	804	6.26	21.77	10.78	1.03	45.89	14.27	7.27	14.75	34.92	15.04
15	85.97	804	4.45	22.40	11.10	1.10	46.55	14.41	7.48	14.99	35.48	15.22
16	88.66	814	6.32	23.21	10.62	1.05	44.80	14.00	7.20	14.45	34.16	14.66
17	91.03	834	5.52	25.85	10.35	0.95	43.77	13.56	6.98	14.09	33.28	14.29

Day	Flow, ton h^{-1}	Pressure, kPa	H_2, wt%	Inert, wt%	EB_{in}, wt%	PX_{in}, wt%	MX_{in}, wt%	OX_{in}, wt%	EB_{out}, wt%	PX_{out}, wt%	MX_{out}, wt%	OX_{out}, wt%
18	91.30	843	3.94	27.58	10.34	0.98	43.52	13.64	7.00	14.02	33.23	14.24
19	92.39	834	4.40	26.78	10.55	1.03	43.66	13.57	7.01	14.09	33.40	14.32
20	90.54	824	6.40	24.26	10.45	1.16	44.19	13.54	7.09	14.17	33.65	14.42
21	86.41	814	4.91	23.00	10.88	1.21	45.97	14.03	7.38	14.76	35.00	14.95
22	86.64	814	4.65	24.06	10.77	1.22	45.70	13.61	7.22	14.64	34.63	14.81
23	88.40	814	5.02	25.08	10.44	1.22	44.75	13.50	6.99	14.43	34.00	14.48
24	88.84	814	4.24	25.17	10.69	1.31	44.94	13.64	7.03	14.59	34.35	14.62
25	96.05	873	3.85	31.17	9.74	1.37	41.28	12.59	6.64	13.34	31.57	13.43
26	95.52	863	5.36	29.29	9.74	1.32	41.56	12.74	6.68	13.39	31.77	13.52
27	92.14	843	4.64	28.45	10.14	1.42	42.57	12.79	6.88	13.65	32.67	13.72
28	89.99	843	4.18	27.15	10.27	1.57	43.54	13.30	7.01	14.01	33.53	14.12
29	93.31	863	4.29	30.76	10.22	1.67	40.91	12.15	6.62	13.43	31.47	13.42
30	93.58	863	4.51	30.55	10.13	1.67	40.63	12.50	6.71	13.41	31.44	13.38
31	96.40	863	4.22	29.67	10.22	1.78	41.10	13.02	6.88	13.69	31.96	13.58
32	93.33	853	4.93	25.48	11.07	2.27	42.81	13.44	7.52	14.24	33.51	14.32
33	88.28	834	5.74	23.37	11.02	2.22	44.10	13.54	7.48	14.63	34.21	14.57
34	88.85	824	6.08	21.79	11.07	2.68	44.85	13.53	7.77	14.82	34.78	14.76

intermediate is isomerized in the rate controlling step on the acidic sites and very rapidly dehydrogenated producing a mixture of xylene based on the high acidity of the catalyst. According to the authors, there was evidence of competition for adsorption on the acidic sites. Since thermodynamic equilibrium between aromatics and the related naphthenes is rapidly established, naphthene concentrations can be replaced by concentrations of aromatics and hydrogen. Regarding the xylene isomerization, Corma and Cortes [4] presented a consecutive 1,2-methyl shift with single site surface reaction controlling mechanism.

The reaction system to be used in the model is the result of combining both ethylbenzene isomerization and xylene isomerization (see Figure 4.5). According to Bhatia et al. [14], from data on ethylbenzene isomerization, the selectivity of *o*-, *m*-, and *p*-xylene is 0.32, 0.47, and 0.21 respectively. Based on that, the rates are as follows:

$$R_{\mathrm{EB}} = \frac{k_2 P_{\mathrm{H_2}}^2 (P_{\mathrm{OX}} + P_{\mathrm{MX}} + P_{\mathrm{PX}}) - k_1 P_{\mathrm{H_2}}^2 P_{\mathrm{EB}}}{1 + (P_{EB} + P_{OX} + P_{MX} + P_{PX})\left(K_{\mathrm{X}} + K_{\mathrm{H}} P_{\mathrm{H_2}}^2\right)} \tag{4.1}$$

$$R_{\mathrm{OX}} = \frac{k_3 P_{\mathrm{MX}} - k_4 P_{\mathrm{OX}}}{1 + K_{\mathrm{OX}} P_{\mathrm{OX}} + K_{\mathrm{PX}} P_{\mathrm{PX}} + K_{\mathrm{MX}} P_{\mathrm{MX}}} + \frac{0.32 k_1 P_{\mathrm{H_2}}^2 P_{\mathrm{EB}} - k_2 P_{\mathrm{H_2}}^2 P_{\mathrm{OX}}}{1 + (P_{\mathrm{EB}} + P_{\mathrm{OX}} + P_{\mathrm{MX}} + P_{\mathrm{PX}})\left(K_{\mathrm{X}} + K_{\mathrm{H}} P_{\mathrm{H_2}}^2\right)} \tag{4.2}$$

$$R_{\mathrm{MX}} = \frac{k_4 P_{\mathrm{OX}} + k_5 P_{\mathrm{PX}} - k_6 P_{\mathrm{MX}} - k_3 P_{\mathrm{MX}}}{1 + K_{\mathrm{OX}} P_{\mathrm{OX}} + K_{\mathrm{PX}} P_{\mathrm{PX}} + K_{\mathrm{MX}} P_{\mathrm{MX}}} + \frac{0.47 k_1 P_{\mathrm{H_2}}^2 P_{\mathrm{EB}} - k_2 P_{\mathrm{H_2}}^2 P_{\mathrm{MX}}}{1 + (P_{\mathrm{EB}} + P_{\mathrm{OX}} + P_{\mathrm{MX}} + P_{\mathrm{PX}})\left(K_{\mathrm{X}} + K_{\mathrm{H}} P_{\mathrm{H_2}}^2\right)} \tag{4.3}$$

$$R_{\mathrm{PX}} = \frac{k_6 P_{\mathrm{MX}} - k_5 P_{\mathrm{PX}}}{1 + K_{\mathrm{OX}} P_{\mathrm{OX}} + K_{\mathrm{PX}} P_{\mathrm{PX}} + K_{\mathrm{MX}} P_{\mathrm{MX}}} + \frac{0.21 k_1 P_{\mathrm{H_2}}^2 P_{\mathrm{EB}} - k_2 P_{\mathrm{H_2}}^2 P_{\mathrm{PX}}}{1 + (P_{\mathrm{EB}} + P_{\mathrm{OX}} + P_{\mathrm{MX}} + P_{\mathrm{PX}})\left(K_{\mathrm{X}} + K_{\mathrm{H}} P_{\mathrm{H_2}}^2\right)} \tag{4.4}$$

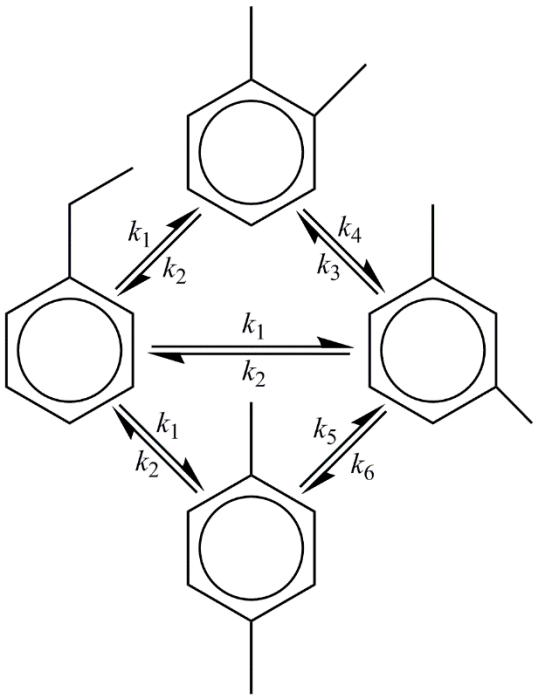

Figure 4.5 Reaction system for ethylbenzene and xylene isomerization

4.2.4. Reactor modeling

The reactor model is based on the following assumptions:

1. Steady state
2. Isothermal conditions.
3. Constant volume.
4. Boundary conditions are of Danckwerts' type.
5. Mass transfer in radial direction can be described by means of the diffusion model.
6. Channeling or shortcut effects do not occur.
7. Absence of gradients in axial direction.
8. Pressure drop is neglected.

Mass balance of component *i* in the volume element for inward-type radial flow:

$$(N_i A_r)_{r+\Delta r} - (N_i A_r)_r + R_i \rho_B A_r \Delta r = 0 \tag{4.5}$$

$$\frac{d}{dr}(N_i A_r) + R_i \rho_B A_r = 0 \tag{4.6}$$

where N_i is the molar flux of component *i*, R_i is the reaction rate defined previously for each species, and ρ_B is the bed density (total catalyst mass / catalyst-bed volume). Convection and dispersion in the radial direction leads to:

$$N_i = vC_i + D\frac{dC_i}{dr} \tag{4.7}$$

Combining equations (4.6) and (4.7):

$$\frac{d}{dr}\left(2\pi r L D \frac{dC_i}{dr}\right) + \frac{d}{dr}(2\pi r L v C_i) + 2\pi r L \rho_B R_i = 0 \tag{4.8}$$

where *D* is the coefficient of turbulent mixing in the radial direction, *u* is the local velocity which depends on the radial coordinate *r*, and C_i is the concentration of component *i*. After rearranging:

$$D\left(\frac{d^2C_i}{dr^2} + \frac{1}{r}\frac{dC_i}{dr}\right) + \frac{C_i}{r}\frac{d}{dr}(vr) + v\frac{dC_i}{dr} + \rho_B R_i = 0 \tag{4.9}$$

Following assumption (3), the continuity equation is in the form:

$$2\pi R_1 v_1 = 2\pi R_0 v_0 = 2\pi r v = const. \rightarrow \frac{d}{dr}(vr) = 0 \tag{4.10}$$

Boundary conditions based on assumption (4):

$$r = R_1 \quad \frac{dC_i}{dr} = 0; \quad r = R_0 \quad v_0\left(C_i^{in} - C_i\right) = D\frac{dC_i}{dr} \tag{4.11}$$

Using dimensionless variables $Y_i = C_i/C$; $\xi = r/R_0$; and introducing the Peclet number $Pe = R_0 v_0/D$, model equations become:

$$\frac{1}{\mathrm{Pe}}\left(\frac{d^2Y_i}{d\xi^2}+\frac{1}{\xi}\frac{dY_i}{d\xi}\right)+\frac{1}{\xi}\frac{dY_i}{d\xi}+\frac{R_0\rho_B}{v_0C}R_i=0 \tag{4.12}$$

$$\frac{dY_i}{d\xi}=0 \text{ at } \xi=\frac{R_1}{R_0};\quad \mathrm{Pe}\left(Y_i^{in}-Y_i\right)=\frac{dY_i}{d\xi}\ at\ \xi=1 \tag{4.13}$$

The parameters and properties of the species involved in the simulation are taken from Green and Perry [15]. The molar volume (V) for the aromatics and naphthenes (inert) is calculated using the virial equation truncated after the second virial coefficient (see Section A.2 in Annex A). At an average temperature 365 ºC (638.15 K) and pressure 8.4 bar (823.8 kPa) the molar volumes of *o*-, *m*-, *p*-xylene, ethylbenzene, and ethylcyclohexane (used for naphthene) are 5.926, 5.938, 5.935, 5.948, and 5.876 $m^3\ kmol^{-1}$ respectively. For hydrogen, ideal gas equation is used since temperature is above critical conditions (V = 6.441 $m^3\ kmol^{-1}$). For the mixture, the molar volume and molecular weight are calculated by means of a weighted mean using the mole fractions. Mole fractions at the reactor inlet are used since naphthene and hydrogen fractions are constant within the reactor and properties of ethylbenzene and xylenes are very similar.

According to Levenspiel [16] and Balakotaiah and Luss [17], for high Reynolds numbers $D/vd_p \approx 1/2$. Based on that, the Peclet number is determined as follows:

$$\mathrm{Pe}=\frac{R_0v_0}{D}=\frac{R_0v_0}{1/2\ v_0d_p}=2\frac{R_0}{d_p} \tag{4.14}$$

4.3. Results and discussion

The second order differential equations are solved through the commercial software gPROMS v.3.7.1 from Process Systems Enterprise (www.psenterprise.com) by the numeric solver DASOLV with a second order orthogonal collocation in finite elements method discretization of the radial domain using 30 uniform intervals with 10^{-5} as tolerance. The kinetic and adsorption constants used, as a first attempt, are obtained from the authors from which the kinetic model is based on. Deviations between the calculated and the actual data are expected since neither the catalysts nor the conditions are the same, Roebschlaeger and Christoffel [13] used Pt/zeolite at 422 ºC and Corma and Cortes [4] worked with Ni/Silica-Alumina at 400 ºC.

Based on the aforementioned, a trust-region reflective least squares procedure [18,19] is carried out with the purpose to obtain new values of kinetic constants in order to minimize the error. The adsorption constants are not included in the optimization (i.e. the adsorption constants are not optimized) based on their small variation among C_8-aromatics and low influence of temperature. The values are taken directly from Roebschlaeger and Christoffel [13], K_X = $6.3\times10^{-3}\ kPa^{-1}$ and K_H = $5\times10^{-7}\ kPa^{-3}$; and from Corma and Cortes [4], K_{OX} = 7.9×10^{-3}

kPa^{-1}, K_{PX} = 1.43×10^{-2} kPa^{-1}, and K_{MX} = 1.14×10^{-2} kPa^{-1}. The function to be minimized is the following:

$$S = \sqrt{\sum_{j=1}^{34}\sum_{i=1}^{4}\left(Y_{j,i}^{actual} - Y_{j,i}^{calculated}\right)^2} \tag{4.15}$$

The new kinetic constants reduce the objective function (S) in about 50%. Table 4.3 presents the kinetic constants for both simulations and the value of the objective function. Moreover, Table 4.4 presents the actual and calculated weight fractions for the species using the kinetics obtained from the optimization for each day. Hydrogen and Inert are not shown since the fractions are constant within the reactor. The gradients for a given day can be seen in Figure 4.6.

Table 4.3 Comparison of kinetic constants[a]

Source	k_1×10^8	k_2×10^9	k_3×10^4	k_4×10^4	k_5×10^4	k_6×10^4	S
Literature	1.8	1.6	2.80	6.76	9.27	3.92	0.066
Optimization[b]	1.62	1.41	2.24	5.82	7.4	3.48	0.033

[a] Units correspond to reaction rate kmol $kg^{-1}h^{-1}$. [b] Values are presented with one digit more than justified

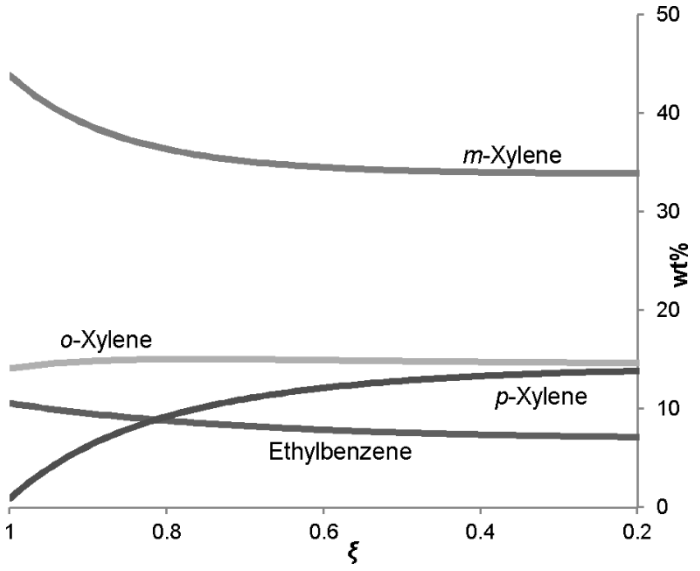

Figure 4.6 Weight fraction of each species against dimensionless radial coordinate for a given day

Moreover, according to Hlavacek [12] the effect of mixing in the flow direction can be disregarded when $\mathrm{Pe}(1-\xi) > 50$. Based on this assumption the reactor model is as follows:

$$\frac{1}{\xi}\frac{dY_i}{d\xi} + \frac{R_0\rho_B}{u_0 C}R_i = 0 \tag{4.16}$$

$$\xi = 1 \quad Y_i = Y_i^{in} \tag{4.17}$$

Table 4.4 Actual and calculated outlet weight fractions. Calculated values are predicted by the model with optimized kinetics

Day	Ethylbenzene		*p*-Xylene		*m*-Xylene		*o*-Xylene	
	actual	calculated	actual	calculated	actual	calculated	actual	calculated
1	6.97	7.15	12.94	13.87	34.74	33.90	14.96	14.67
2	7.18	7.45	13.41	14.61	36.05	34.99	15.53	15.12
3	7.08	7.35	13.39	14.24	35.35	34.59	15.29	14.93
4	6.93	7.13	13.60	13.92	34.03	33.62	14.63	14.52
5	7.19	7.29	13.86	14.17	34.75	34.47	15.01	14.89
6	7.43	7.41	14.19	14.62	35.58	35.36	15.41	15.22
7	7.40	7.40	14.34	14.69	35.58	35.47	15.46	15.22
8	7.33	7.49	15.67	14.68	34.89	35.55	15.13	15.30
9	7.35	7.54	14.99	14.54	35.33	35.48	15.15	15.25
10	7.71	7.38	14.48	14.44	34.55	34.80	14.83	14.94
11	7.83	7.47	14.79	14.72	35.24	35.53	15.11	15.27
12	7.70	7.49	14.93	14.83	35.34	35.56	15.16	15.26
13	7.27	7.28	14.78	14.62	34.90	34.95	14.86	14.97
14	7.27	7.32	14.75	14.36	34.92	35.16	15.04	15.13
15	7.48	7.50	14.99	14.92	35.48	35.54	15.22	15.19
16	7.20	7.18	14.45	14.05	34.16	34.41	14.66	14.82
17	6.98	6.99	14.09	13.81	33.28	33.46	14.29	14.37
18	7.00	6.99	14.02	14.04	33.23	33.24	14.24	14.21
19	7.01	7.10	14.09	13.98	33.40	33.42	14.32	14.31
20	7.09	7.07	14.17	13.83	33.65	33.89	14.42	14.55
21	7.38	7.35	14.76	14.69	35.00	35.08	14.95	14.97
22	7.22	7.26	14.64	14.61	34.63	34.68	14.81	14.74
23	6.99	7.08	14.43	14.24	34.00	34.07	14.48	14.52
24	7.03	7.23	14.59	14.46	34.35	34.30	14.62	14.60
25	6.64	6.60	13.34	13.40	31.57	31.57	13.43	13.41
26	6.68	6.62	13.39	13.23	31.77	31.88	13.52	13.63
27	6.88	6.81	13.65	13.71	32.67	32.55	13.72	13.83
28	7.01	6.96	14.01	14.17	33.53	33.37	14.12	14.17
29	6.62	6.69	13.43	13.42	31.47	31.50	13.42	13.33
30	6.71	6.67	13.41	13.36	31.44	31.50	13.38	13.40
31	6.88	6.85	13.69	13.52	31.96	32.06	13.58	13.69
32	7.52	7.34	14.24	14.13	33.51	33.73	14.32	14.39
33	7.48	7.33	14.63	14.41	34.21	34.48	14.57	14.68
34	7.77	7.46	14.82	14.61	34.78	35.16	14.76	14.90

The results obtained with this simpler model are exactly the same to those obtained with equations (4.12) and (4.13). The optimized kinetic constants are the following: $k_1=(1.6_2\pm1.0_8)\times10^{-8}$ kmol $kg^{-1}kPa^{-3}h^{-1}$; $k_2=(1.4_3\pm1.4_1)\times10^{-9}$ kmol $kg^{-1}kPa^{-3}h^{-1}$; $k_3=(2.2_4\pm0.3_1)\times10^{-4}$ kmol $kg^{-1}kPa^{-1}h^{-1}$; $k_4=(5.8_2\pm0.7_0)\times10^{-4}$ kmol $kg^{-1}kPa^{-1}h^{-1}$; $k_5=(7._4\pm3._8)\times10^{-4}$

kmol $kg^{-1}kPa^{-1}h^{-1}$; and $k_6=(3.4_8\pm1.3_6)\times10^{-4}$ kmol $kg^{-1}kPa^{-1}h^{-1}$. The standard error of each kinetic constant is calculated following the deleted-one Jackknife method as described by Kinsella [20].

According to Al Khattaf [7] shape selectivity in xylene isomerization is observed in medium-pore zeolites such as ZSM-5; this is not the case for large-pore zeolites. The shape selectivity is based on the steric hindrance due to the sizes of the molecules involved. The *p*-xylene critical size is lower than the other xylenes, which enables it to diffuse faster through the catalyst pores. For larger pores, the steric hindrance decreases and the three xylenes diffuse at the same rate. It can be seen in Table 4.3 that k_3, k_4, k_5, and k_6 are slightly reduced by the optimization, probably due to the lower temperature used in the unit. Furthermore, k_5 is reduced at a higher degree than k_6, favoring the formation of *p*-xylene from *m*-xylene; similarly, k_3 is more decreased than k_4, also favoring the formation of *p*-xylene indirectly through *m*-xylene as an intermediate. This may indicate shape selectivity of the catalyst currently used in the isomerization unit. The EU-1 zeolite has a 10-membered ring structure very similar to that of ZSM-5, whereas the catalyst used by Corma and Cortes [4] has large pores. Moreover, the particle size used was very small in order to eliminate the intraparticle diffusion constraints. For larger particles, such as those used in industry applications, the aforementioned diffusion constraints start to appear and increase the reaction rate of *p*-xylene compared to *o*- and *m*-xylene.

Isomerization units normally operate between 380 and 480 ºC [21]; the main advantage of EU-1 zeolite is the possibility to operate at milder conditions, thus reducing C_8-aromatic losses through transalkylation and cracking, which is confirmed by the lower contents of side products in the data used in the modeling. Furthermore, it can be seen in Table 4.3 that the reduction on k_1 and k_2 is low compared to the almost 60 ºC difference between the unit and the work of Roebschlaeger and Christoffel [13]. The higher ethylbenzene isomerization activity observed in this catalyst is due to the easy access by the intermediates to the protonic sites located at the side pockets at the surface of the crystallites and close to the hydrogenation sites (i.e., platinum). This situation is more advantageous than that of the normally used mordenite [10].

The competitive adsorption of product species within the catalyst is evaluated by using a simplified linear kinetic model eliminating the effect of the adsorption constants. In this case the value of *S* is higher, from which it is validated the use of the Hougen-Watson model for the C_8-aromatic isomerization. Furthermore, a triangular scheme for xylene isomerization (considering the direct conversion between *o*- and *p*-xylene) is also evaluated to account for shape selectivity in the catalyst. Although there are signs that may indicate selectivity towards *p*-xylene, *S* is similar for this case; since there is no improvement, the simpler model with less parameters is preferred. Laboratory experiments where intrinsic kinetic data can be obtained are required to choose the model that better fits the data and reduce the uncertainty of the parameters estimated.

4.4. Conclusions

The gas phase isomerization unit with a radial-type reactor and EU-1 zeolite with platinum as catalyst is analyzed. It was confirmed that side reactions and C_8-aromatic losses are significantly reduced by operating at milder conditions due to the higher activity of the catalyst. A mathematical model that effectively simulates the operation of the reactor within the isomerization unit is developed; the model is intended to be used within the simulation of the proposed aromatics complex.

4.5. Nomenclature

A_r = Cross sectional area, m^2

B = Virial coefficient

C = Concentration, kmol m^{-3}

D = Dispersion coefficient in the flow direction, m^2 h^{-1}

d_p = Particle diameter, m

k_l = Kinetic constant on reaction l = 1,2, kmol $kg^{-1}kPa^{-3}h^{-1}$

k_l = Kinetic constant on reaction l = 3-6, kmol $kg^{-1}kPa^{-1}h^{-1}$

K_X = Adsorption constant of C_8-aromatics, kPa^{-1}

K_H = Product of adsorption of naphthenes and hydrogenation, kPa^{-3}

K_m = Adsorption constant of species m = OX, MX, PX, kPa^{-1}

L = Catalyst-bed length, m

N_i = Surface molar flow, kmol $m^{-2}h^{-1}$

P = Pressure, kPa

Pe = Peclet number

r = Radial coordinate, m

R = Universal gas constant, m^3kPa $kmol^{-1}K^{-1}$

R_0 = Catalyst-bed outer radius, m

R_1 = Catalyst-bed inner radius, m

R_i = Reaction rate of component i, kmol $kg^{-1}h^{-1}$

S = Objective function

T = Temperature, K

v = Superficial velocity, m h^{-1}

V = Molar volume, m^3 $kmol^{-1}$

Y = Mole fraction

Greek letters

ξ = Dimensionless radial coordinate

ρ_B = Catalyst-bed density, kg m^{-3}

Abbreviations

EB = Ethylbenzene

MX = *m*-Xylene

OX = *o*-Xylene

PX = *p*-Xylene

Superscripts and subscripts

i = Component i

in = Inlet

j = Day, number of run

out = Outlet

4.6. References

[1] Cannella, William J. 2000. "Xylenes and Ethylbenzene." In *Kirk-Othmer Encyclopedia of Chemical Technology*. John Wiley & Sons, Inc.

[2] Johnson, James A. 2003. "Aromatics Complexes." In *Handbook of Petroleum Refining Processes*, 2.3-2.11. McGraw-Hill.

[3] Silady, Patrick J. 2003. "UOP Isomar Process." In *Handbook of Petroleum Refining Processes*, 2.39-2.46. McGraw-Hill.

[4] Corma, Avelino, and Antonio Cortes. 1980. "Kinetics of the Gas-Phase Catalytic Isomerization of Xylenes." *Industrial & engineering chemistry process design and development* no. 19 (2):263-267.

[5] Guisnet, M., N. S. Gnep, and S. Morin. 2000. "Mechanisms of xylene isomerization over acidic solid catalysts." *Microporous and Mesoporous Materials* no. 35-36:47-59.

[6] Perego, C., and P. Pollesel. 2009. "Advances in Aromatics Processing Using Zeolite Catalysts." In *Advances in Nanoporous Materials*, edited by Stefan Ernst, 97-149. Amsterdam: Elsevier.

[7] Al Khattaf, S. 2005. "Modeling xylene reactions over ZSM-5 zeolite in a riser simulator: 1,3- versus 1,2-methyl shift." *Industrial & Engineering Chemistry Research* no. 44 (21):7957-7968.

[8] Hsu, Y. S., T. Y. Lee, and H. C. Hu. 1988. "Isomerization of ethylbenzene and m-xylene on zeolites." *Industrial & Engineering Chemistry Research* no. 27 (6):942-947.

[9] Marcilly, C. 2003. "Present status and future trends in catalysis for refining and petrochemicals." *Journal of Catalysis* no. 216 (1-2):47-62.

[10] Moreau, F., S. Bernard, N. S. Gnep, S. Lacombe, E. Merlen, and M. Guisnet. 2006. "Ethylbenzene isomerization over bifunctional platinum alumina-EUO catalysts: Location of the active sites." *Microporous and Mesoporous Materials* no. 90 (1):327-338.

[11] Moreau, F., S. Bernard, N. S. Gnep, S. Lacombe, E. Merlen, and M. Guisnet. 2001. "Ethylbenzene Isomerization on Bifunctional Platinum Alumina–Mordenite Catalysts: 1. Influence of the Mordenite Si/Al Ratio." *Journal of Catalysis* no. 202 (2):402-412.

[12] Hlavacek, Vladimir. 1972. "Modeling of Chemical Reactors - XXV. Cylindrical and Spherical Reactor with Radial Flow." *Chemical Engineering Science* no. 27 (2):177-186.

[13] Roebschlaeger, Karl, and Erhard Christoffel. 1980. "Kinetic Investigation of the Isomerization of C_8-Aromatics." *The Canadian journal of chemical engineering* no. 58 (4):517-520.

[14] Bhatia, Subhash, Sudeep Chandra, and Tathagata Das. 1989. "Simulation of the xylene isomerization catalytic reactor." *Industrial & Engineering Chemistry Research* no. 28 (8):1185-1190.

[15] Green, Don W., and Robert H. Perry. 2008. *Perry's Chemical Engineers' Handbook*. 8th ed: McGraw-Hill.

[16] Levenspiel, Octave. 1999. *Chemical Reaction Engineering*. Third ed: John Wiley & Sons.

[17] Balakotaiah, Vemuri, and Dan Luss. 1981. "Effect of Flow Direction on Conversion in Isothermal Radial Flow Fixed-Bed Reactors." *AIChE Journal* no. 27 (3):442-450.

[18] Coleman, Thomas F., and Yuying Li. 1994. "On the convergence of interior-reflective Newton methods for nonlinear minimization subject to bounds." *Math. Program.* no. 67 (2):189-224.

[19] Coleman, T. F. 1996. "An interior trust region approach for nonlinear minimization subject to bounds." *SIAM journal on optimization* no. 6 (2):418-45.

[20] Kinsella, A. 1986. "Numerical methods for error evaluation." *American journal of physics* no. 54 (5):464-6.

[21] Minceva, Mirjana, Pedro Sá Gomes, Vera Meshko, and Alírio E. Rodrigues. 2008. "Simulated moving bed reactor for isomerization and separation of p-xylene." *Chemical Engineering Journal* no. 140 (1-3):305-323.

Chapter 5: Simulated moving bed reactor: Adsorbent and catalyst homogeneous mixture

This chapter analyzes the use of process intensification in the production of *p*-xylene. Both separation and isomerization processes are combined in the simulated moving bed unit currently used for *p*-xylene separation. In addition, based on larger yields required for *p*-xylene and benzene, a modification to the aromatics complex is proposed including a new single stage crystallization unit allowing further purification of high *p*-xylene content streams. Based on the aforementioned, a lower *p*-xylene purity is defined in the extract (0.70) along with a purity of 0.95 of the rest of the aromatics in the raffinate; a simulated moving bed reactor unit combining adsorbent and catalyst within the columns is designed instead of the commonly used simulated moving bed facility. Keeping the same physical characteristics of the unit, several configurations with different flow rates are analyzed with the purpose of obtaining the highest productivity by means of simulations using a commercial software and the true moving bed reactor approach.

This chapter is based on: Gonçalves, J. C., and A. E. Rodrigues. 2014. "Simulated moving bed reactor for p-xylene production: Adsorbent and catalyst homogeneous mixture." *Chemical Engineering Journal* no. 258:194-202.

5.1. Introduction

As discussed in Chapter 2, the production of *p*-xylene is currently performed based on two main operation units: Separation, which is basically the extraction of pure *p*-xylene; and Isomerization, where additional *p*-xylene is produced in gas phase from the other isomers and recycled back to the separation unit. The *p*-xylene yield is limited by the thermodynamic equilibrium, which results in large cycle loops to achieve the desired amount of *p*-xylene; a large loop along with gas phase conditions increase significantly the energy consumption within the process. The aforementioned could be minimized through the ensemble of both units based on the concept of process intensification. Process intensification, as part of sustainable process development, indicates the ensemble of technologies that leads to a substantially smaller, cleaner, safer, and more energy-efficient process where lower consumption of raw materials and reduction of emissions of greenhouse gases and pollutants are achieved [1].

The most common process for *p*-xylene separation is selective adsorption in fixed bed columns using the concept of simulated moving bed (SMB) where the counter-current flow of the solid adsorbent and liquid flow is simulated by the switching of inlets and outlets in the unit [2]. The proposed technology for coupling the processes of separation and isomerization is the simulated moving bed reactor (SMBR). The SMBR uses the principle of SMB and incorporates the reaction section, the catalyst, within the adsorption columns. The main obstacle is the different conditions, phases, where the separation and isomerization are carried out. Between the two options, adsorption in gas phase and isomerization in liquid phase, the latter is chosen since, although the conversion may be lower, it brings other advantages such as better thermal control and longer catalyst life, which allows for off-site catalyst regeneration and therefore easier control of pollution. Furthermore since *p*-xylene is withdrawn as it is formed, the equilibrium constraints in the isomerization can be minimized through the SMBR; thus reducing the cycle loop and the energy consumption within the process.

The objective of this chapter is to determine the best arrangement of columns with optimized flow rates and switching time in the SMBR unit, based on the existing SMB unit, for *p*-xylene production in the framework of a proposal to modify the current aromatics complex which allows milder *p*-xylene purity constraints in the extract.

5.2. Proposed aromatics complex

In recent years, the demand for aromatic derivatives has led to steady growth rate of *p*-xylene and benzene, while demand for toluene based derivatives has been historically much lower. This

pushes producers to convert toluene to higher value *p*-xylene and benzene. Moreover, toluene constitutes an alternative feed source to debottleneck of existing aromatics complexes to increase production capacity [3,4]. A new configuration for the existing aromatics plant, consisting of minor modifications to existing units and a couple of new ones, is proposed with the purpose of further processing toluene to match the higher demand on *p*-xylene and benzene (see Figure 5.1). The current aromatics complex is described in Chapter 4.

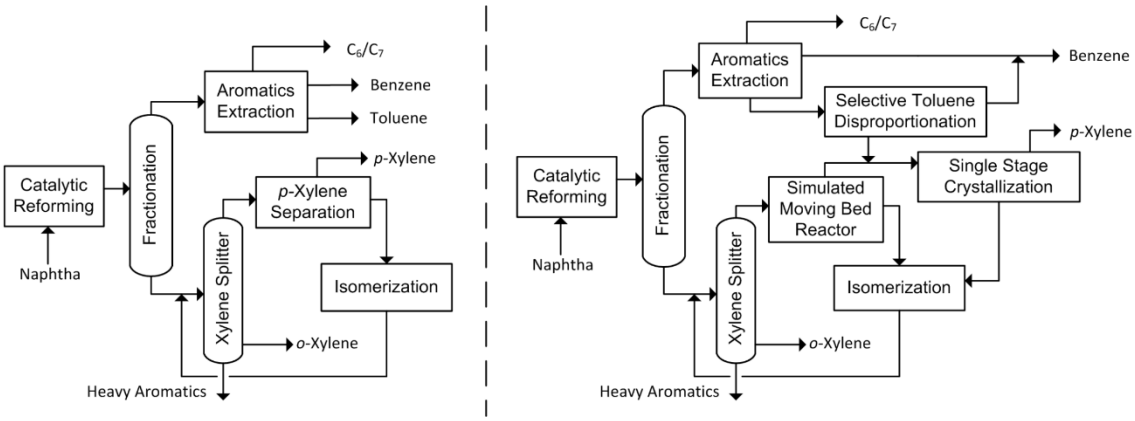

Figure 5.1 Current (left) and proposed (right) aromatics complex.

In the new configuration, toluene produced in the Aromatics Extraction unit is sent to a new Selective Toluene Disproportionation unit. In the presence of acid catalyst, toluene may go through a disproportionation reaction producing benzene and an equilibrium mixture of xylenes; however, by using a modified catalyst it is possible to obtain a 90 wt% or higher *p*-xylene stream (see Chapter 2).

The high *p*-xylene content places the crystallization technology in advantage over adsorption-type processes because capital and utility costs are strongly related to feed composition. The significantly lower recovery in conventional crystallization is due to eutectic constraints in equilibrium mixture of xylenes; these constraints are eliminated with higher *p*-xylene fractions leading to higher recovery values (see Chapter 2). GTC's CrystPX is designed to process a range of feed concentrations (75-95 wt% of *p*-xylene) in a single stage crystallization unit with purity higher than 99.8 wt% and up to 95% recovery [5]. The aforesaid allows *p*-xylene concentration down to 70 wt% in the extract of the SMBR unit. Both streams depleted on *p*-xylene, from SMBR and Single Stage Crystallization, are sent to the Isomerization unit where the thermodynamic equilibrium is re-established and ethylbenzene is converted in gas phase. This new configuration allows the increase of *p*-xylene and benzene production by means of less valuable toluene conversion; a global mass balance is calculated in Chapter 8.

5.3. Simulated moving bed reactor

Xylene isomerization is a reaction of the type $A \leftrightarrow B$. In this case, reaction cannot occur near the extract point if high purity is required, otherwise the reverse reaction will pollute the product and purity will always be below 99%. To overcome this situation, reactors are inserted between the adsorption columns far from the extract point [6,7]. However, since the minimum concentration required in the extract for this new configuration is about 70 wt%, a much simpler configuration can be employed. Keeping the catalyst and adsorbent mixed inside the columns, it may produce a high enough *p*-xylene concentration stream to be further processed by the crystallization unit. This approach involves simpler operation and allows the direct contact between catalyst and adsorbent resulting in more efficient *p*-xylene withdraw as it is formed to overcome the thermodynamic equilibrium constraints.

One of the most employed SMB based technologies for *p*-xylene separation is UOP's Parex. The studied aromatics complex uses this technology consisting of 24 adsorbent beds with length and diameter of 1.14 and 4.12 m respectively, *p*-diethylbenzene as desorbent, particle diameter of 0.62 mm, and a switching time of 1.15 min [2]. The SMBR unit will keep the geometric characteristics of the Parex unit, i.e., 24 adsorbent beds, with the possibility to modify the location of inlets and outlets in order to use the appropriate number of columns in each zone since column configuration plays an important role when dealing with different product concentrations [8]. Moreover, *p*-diethylbenzene cannot be used since it isomerizes into *o*- and *m*-diethylbenzene over acid catalysts; toluene, which has been used in the industry, is used as desorbent [7,9].

Generally, the feed to the Parex unit contains a naphthenic fraction which is involved in the ethylbenzene isomerization in the Isomar unit. These non-aromatic compounds increase the utility consumption of the unit; however, they do not affect the xylene adsorption [10]. The feed used, as a first attempt, is that used by Minceva et al. [6]: 23.6 wt% *p*-xylene; 49.7 wt% *m*-xylene; 12.7 wt% *o*-xylene; 14 wt% ethylbenzene.

This work is foreseen as a modification of the current aromatics complex; that is the main reason to maintain the physical dimensions of the equipment. In case that the resulting flow rates are below or above the downstream units, a second train with the same characteristics could be installed to guarantee optimal operation of said units. It is strongly recommended, whenever possible, to use similar units to the original ones while installing second trains in revamp and/or expansion projects in order to keep operation simplicity.

5.3.1. Adsorption and reaction data

The normal operating conditions for the Parex process is around 180 ºC and 9 bar [11]. Pressure shall be high enough to maintain the operation in liquid phase and to avoid failure of associated equipment (e.g., pump cavitation) due to pressure drop in lines and columns; in other words, the influence on adsorption and reaction data is neglected. Temperature, on the other hand, definitely affects the reaction and adsorption data. According to Minceva et al. [6], increase in temperature leads to lower adsorption capacity and faster isomerization, which means that a compromise shall exist somewhere above normal Parex operation.

Bergeot [12] carried out adsorption and reaction experiments of xylenes at 200 ºC in liquid phase. The adsorbent used was low silica X zeolite exchanged with barium (BaLSX); the author claimed that the adsorbent presented better selectivity compared to that of BaX, specifically on ethylbenzene. The adsorption equilibrium is described with the generalized Langmuir isotherm:

$$q_i = q_{sat}\frac{b_i C_i}{1+\sum_j b_j C_j} \tag{5.1}$$

The catalyst used in the isomerization tests was HZSM-5, which is industrially used in xylene isomerization in gas phase. The reaction scheme followed is presented in Figure 5.2. According to Cappellazzo et al. [13], the triangular scheme adds to the mechanism the direct conversion between *o*- and *p*-xylene, which actually does not occur, to account for the influence of intracrystalline mass-transfer resistance. Following the triangular scheme, the reaction rates for each species are given by equations (5.2) to (5.4).

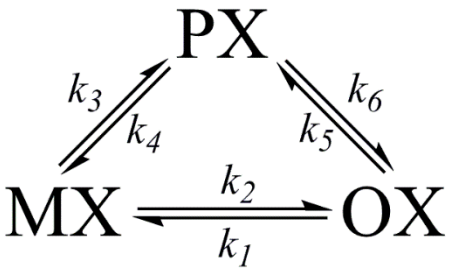

Figure 5.2 Xylene isomerization reaction scheme

$$R_{\mathrm{PX}} = k_5 C_{\mathrm{OX}} + k_3 C_{\mathrm{MX}} - k_6 C_{\mathrm{PX}} - k_4 C_{\mathrm{PX}} \tag{5.2}$$

$$R_{\mathrm{MX}} = k_1 C_{\mathrm{OX}} + k_4 C_{\mathrm{PX}} - k_2 C_{\mathrm{MX}} - k_3 C_{\mathrm{MX}} \tag{5.3}$$

$$R_{\mathrm{OX}} = k_2 C_{\mathrm{MX}} + k_6 C_{\mathrm{PX}} - k_5 C_{\mathrm{OX}} - k_1 C_{\mathrm{OX}} \tag{5.4}$$

Table 5.1 presents adsorption, reaction, and physical data used in the mathematical modeling of the SMBR unit. Figure 5.3 presents the adsorption isotherms for each species; it can be seen that toluene is a suitable desorbent since it is adsorbed less strongly that *p*-xylene but more than the rest of the isomers [9].

Table 5.1 Thermodynamic and physical parameters from Bergeot [12]

Adsorption Data		Reaction Data		Physical Data	
q_{sat}	0.148 kg kg^{-1}	k_1	2.1859×10^{-8} m^3 kg^{-1}s^{-1}	ρ_{ads}	2013 kg m^{-3}
b_{PX}	5.1 m^3 kg^{-1}	k_2	7.7491×10^{-9} m^3 kg^{-1}s^{-1}	ρ_{cat}	1150 kg m^{-3}
b_{MX}	1.5883 m^3 kg^{-1}	k_3	1.1544×10^{-4} m^3 kg^{-1}s^{-1}	ε	0.32
b_{OX}	1.5883 m^3 kg^{-1}	k_4	2.5742×10^{-4} m^3 kg^{-1}s^{-1}	ε_p	0.352
b_{EB}	1.7647 m^3 kg^{-1}	k_5	3.6647×10^{-7} m^3 kg^{-1}s^{-1}	R_p[a]	3.1×10^{-4} m
b_{Tol}	3.4 m^3 kg^{-1}	k_6	2.8973×10^{-7} m^3 kg^{-1}s^{-1}		

[a] Particle size currently used within the SMB unit [2].

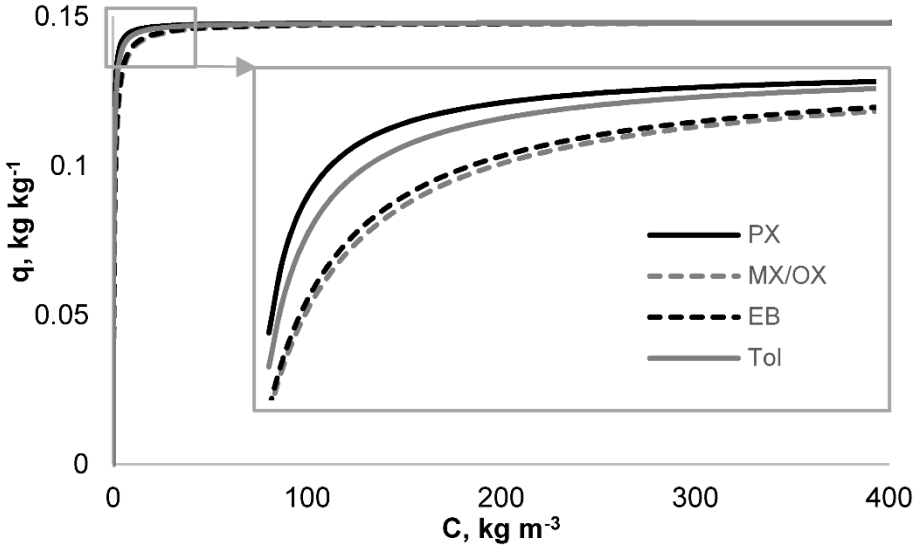

Figure 5.3 Adsorption isotherms for each species. Isotherms for *m*- and *o*-xylene are the same [12]

5.3.2. Mathematical model

The SMB process (and analogously the SMBR process) can be modeled by means of a continuous TMB (True Moving Bed) model or by simulating the actual shifting of the inlet and outlet ports along the unit. The equivalent TMB approaches the SMB when a large number of columns are involved (e.g., 24 columns) and provides a fast way to obtain product yields for different configurations and parameters at steady-state [14].

Regardless of the methodology used to model the SMBR, the assumptions are the following:

1. Isothermal conditions.
2. Axial dispersed plug flow for the fluid phase.
3. Plug flow for the solid phase (just for TMBR).
4. Constant flow rate in each zone.
5. Mass transfer described by linear driving force (LDF) approximation.
6. Adsorbents and catalysts are mixed homogeneously and possess similar physical characteristics.

7. Pressure drop is not considered.

Mass balances for species i in the bulk phase, adsorbent particle phase, and catalyst particle phase are given by equations (5.5) to (5.7) respectively:

$$\frac{\partial C_i}{\partial t} = D_{ax}\frac{\partial^2 C_i}{\partial z^2} - u\frac{\partial C_i}{\partial z} - \frac{1-\varepsilon}{\varepsilon}\frac{3}{R_p}K_l\left[\varphi\left(C_i - \overline{C_{pi}}_{ads}\right) + (1-\varphi)\left(C_i - \overline{C_{pi}}_{cat}\right)\right] \tag{5.5}$$

$$\begin{aligned}\varepsilon_p\frac{\partial \overline{C_{pi}}_{ads}}{\partial t} + (1-\varepsilon_p)\rho_{ads}\frac{\partial \overline{q}_i}{\partial t} \\ = u_s\left[\varepsilon_p\frac{\partial \overline{C_{pi}}_{ads}}{\partial z} + (1-\varepsilon_p)\rho_{ads}\frac{\partial \overline{q}_i}{\partial z}\right] + \frac{3}{R_p}K_l\left(C_i - \overline{C_{pi}}_{ads}\right)\end{aligned} \tag{5.6}$$

$$\varepsilon_p\frac{\partial \overline{C_{pi}}_{cat}}{\partial t} = u_s\varepsilon_p\frac{\partial \overline{C_{pi}}_{cat}}{\partial z} + \frac{3}{R_p}K_l\left(C_i - \overline{C_{pi}}_{cat}\right) + \rho_{cat}R_i \tag{5.7}$$

where C_i is the concentration of each species in the bulk phase, the axial dispersion coefficient D_{ax} is estimated through the particle Peclet number ($\mathrm{Pe} = 2uR_p/D_{ax}$), which is about 0.45 for low Reynolds in liquids [15], with constant interstitial velocity u throughout each zone. Physical properties such as bed porosity ε, particle porosity ε_p, particle radius R_p, density of adsorbent ρ_{ads} and catalyst ρ_{cat} are given in Table 5.1. The average mass adsorbed $\overline{q_i}$ is described by the equilibrium isotherm as a function of the average particle concentration in the adsorbents $\overline{C_{pi}}_{ads}$; the reaction rate R_i is a function of the average particle concentration in the catalysts $\overline{C_{pi}}_{cat}$, and φ represents the adsorbent to adsorbent plus catalyst weight ratio ($\varphi = m_{ads}/m_{ads} + m_{cat}$).

The axial derivative terms in the particle balances represent the movement of the solid, these terms do not exist when using the SMBR method. Moreover, all time derivative terms are set to zero for steady state using the TMBR method resulting in a simpler and faster model; this reduction cannot be done while using SMBR method since the model is intrinsically dynamic leading towards a cyclic steady state after a certain number of cycles.

The boundary condition for the particle phase, both adsorbent and catalyst, is given by setting the outlet concentration within the particles equal to that entering the previous zone due to the countercurrent movement of the solid. For the bulk phase, Danckwerts boundary conditions for species i are used:

$$z = 0 \;\rightarrow\; D_{ax}\frac{\partial C_i}{\partial z} = u\left(C_i - C_i^{in}\right); \quad z = L \;\rightarrow\; \frac{\partial C_i}{\partial z} = 0 \tag{5.8}$$

where C_i^{in} depends on the specific zone within the unit. The inlet concentration is determined by mass balances in each inlet and outlet port:

Desorbent (D) port: $$Q_4 + Q_D = Q_1; \quad C_{i,4}^{out} Q_4 + C_{i,D} Q_D = C_{i,1}^{in} Q_1 \tag{5.9}$$

Extract (X) port: $$Q_1 = Q_2 + Q_X; \quad C_{i,1}^{out} = C_{i,2}^{in} = C_{i,X} \tag{5.10}$$

Feed (F) port: $$Q_2 + Q_F = Q_3; \quad C_{i,2}^{out} Q_2 + C_{i,F} Q_F = C_{i,3}^{in} Q_3 \tag{5.11}$$

Raffinate (R) port: $$Q_3 = Q_3 + Q_R; \quad C_{i,3}^{out} = C_{i,4}^{in} = C_{i,R} \tag{5.12}$$

where Q_1, Q_2, Q_3, and Q_4 are the flow rates for each zone.

Normally, the value of an SMB facility is measured through the following performance parameters: purity (desorbent free), recovery, desorbent consumption, and productivity. These parameters can also be calculated for the SMBR; although, deviation from the equilibrium is commonly used instead of recovery since the reaction involved is limited by the thermodynamic equilibrium. The performance parameters, considering *p*-xylene as the desired product, are defined as follows:

Extract Purity: $$\mathrm{PurX} = \frac{C_{\mathrm{PX},X}}{C_{\mathrm{PX},X} + C_{\mathrm{MX},X} + C_{\mathrm{OX},X} + C_{\mathrm{EB},X}} \tag{5.13}$$

Raffinate Purity: $$\mathrm{PurR} = \frac{C_{\mathrm{MX},X} + C_{\mathrm{OX},X} + C_{\mathrm{EB},X}}{C_{\mathrm{PX},X} + C_{\mathrm{MX},X} + C_{\mathrm{OX},X} + C_{\mathrm{EB},X}} \tag{5.14}$$

Deviation from the Equilibrium: $$\mathrm{DE} = \frac{C_{\mathrm{PX},X} Q_X + C_{\mathrm{PX},R} Q_R}{C_{\mathrm{PX},eq} Q_F} \tag{5.15}$$

Desorbent Consumption: $$\mathrm{DC} = \frac{Q_D}{C_{\mathrm{PX},X} Q_X} \tag{5.16}$$

Productivity: $$\mathrm{PR} = \frac{C_{\mathrm{PX},X} Q_X}{V_{ads+cat}} \tag{5.17}$$

where $C_{\mathrm{PX},eq}$ is the *p*-xylene concentration in equilibrium at operating conditions estimated with the expressions developed in Chapter 3.

As stated before, LDF is used for the mass transfer resistance. Instead of calculating the gradient of the particle concentration, an average is used; the transfer between phases will then be proportional to the concentration difference. External and internal mass transfer resistances are coupled in a single global mass transfer coefficient [16]:

$$\frac{1}{K_l} = \frac{1}{k_{ext}} + \frac{1}{\varepsilon_p k_{int}} \tag{5.18}$$

where for consistency with the LDF approximation, the internal coefficient is calculated as $k_{int} = 5\, D_m/\tau R_p$, for which the correlation proposed by Wakao and Smith is used to estimate

the tortuosity factor as $\tau = 1/\varepsilon_p$ [17]. The external mass transfer coefficient is estimated by the Wilson and Geankoplis correlation valid for 0.0016 < Re < 55 [18]:

$$\mathrm{Sh} = \frac{1.09}{\varepsilon}(\mathrm{ReSc})^{0.33} \quad \text{with} \quad \mathrm{Sh} = \frac{2k_{ext}R_p}{D_m};\ \ \mathrm{Re} = \frac{2\rho R_p v}{\mu};\ \ \mathrm{Sc} = \frac{\mu}{\rho D_m} \qquad (5.19)$$

where the molecular diffusivity D_m (cm^2 s^{-1}) is calculated through the Wilke-Chang method modified to include the mixed solvent case by Perkins and Geankoplis [19]. Properties are presented in Section A.3 in Annex A.

5.4. Results and discussion

The SMBR unit is modeled through the continuous TMBR approach since a large number of simulations are required and some optimization are foreseen to adjust several operation parameters. The simulation comprises a numerical solution using the commercial software gPROMS v3.7.1 from Process Systems Enterprise (www.psenterprise.com). The numerical method involves the discretization of the axial domain using second-order orthogonal collocation on 50 finite elements with 10^{-5} as tolerance. In the first simulations it was noticed that the adsorbent to adsorbent plus catalyst ratio shall be at least 0.9 in order to reach the desired purity in the extract (0.70); it was also noticed that the maximum purity in the raffinate is slightly above 0.95; therefore, those values are fixed in the entire study.

5.4.1. Separation regions and separation volumes

Normally in this type of unit, the flow rates of each zone are expressed as velocity ratios ($\gamma_j = u_j/u_s$) using the interstitial velocity in zone j and the solid velocity (column length / switching time). In pure separation systems, the flow rates in zone 1 and 4 shall guarantee the regeneration of the adsorbent and desorbent respectively, while the actual separation occurs in zones 2 and 3. In the absence of mass-transfer resistances, the region of separation in the plane $\gamma_2 \times \gamma_3$ is constant regardless the value of γ_1 and γ_4 (given the previous constraints fulfilled); in the presence of mass-transfer effects, the region is expected to become smaller and somehow dependent on γ_1 and γ_4 and shall be evaluated through successive simulations [20].

The steady-state TMBR model is successively solved for several values of γ_2 and γ_3 for given γ_1 and γ_4. Starting from a small enough value for the feed flow rate, flow rate in zone 2 is increased until the purity constraints are no longer satisfied; afterwards, the feed flow rate is increased and the procedure is repeated as long as the said constraints are not violated. The whole process is

repeated for different values of γ_1 and γ_4. A simplified diagram to determine the separation regions is presented in Figure 5.4.

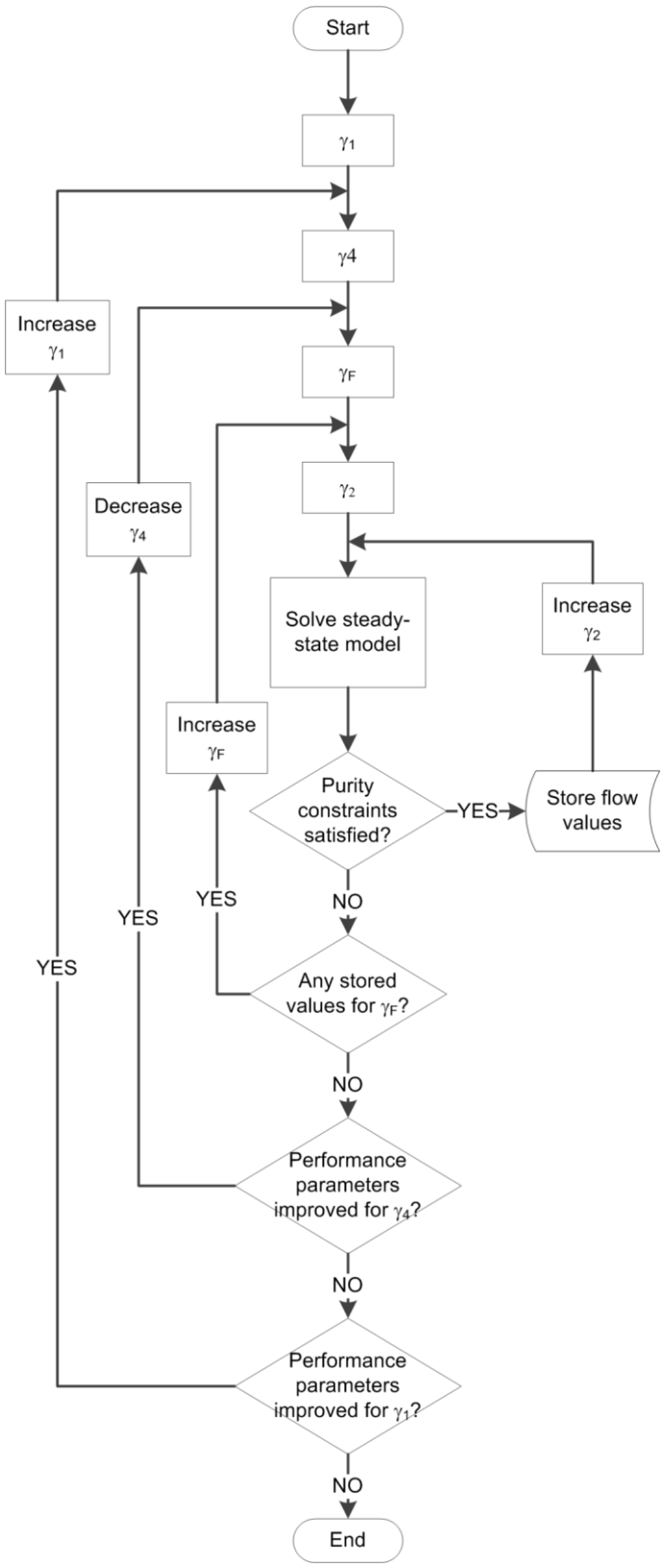

Figure 5.4 Flow diagram to determine separation regions for different flow conditions

Since the reverse reaction is present in every zone of the unit, a larger amount of desorbent (i.e., higher γ_1 - γ_4) is expected comparing to that of TMB. In each separation region in the plane $\gamma_2 \times \gamma_3$, the best flow rate in zones 2 and 3 is that which provides higher feed flow rate (i.e., higher γ_3 - γ_2). Figure 5.5 shows the influence of γ_4 and γ_1 in the separation regions with fixed γ_1 and γ_4 and 69 s switching time. Table 5.2 presents the optimum point for each separation region with the corresponding productivity, desorbent consumption, and deviation from the equilibrium for the Parex configuration (6-9-6-3) for γ_1 values between 3.0 and 6.0 and γ_4 values between 0.3 and 1.0.

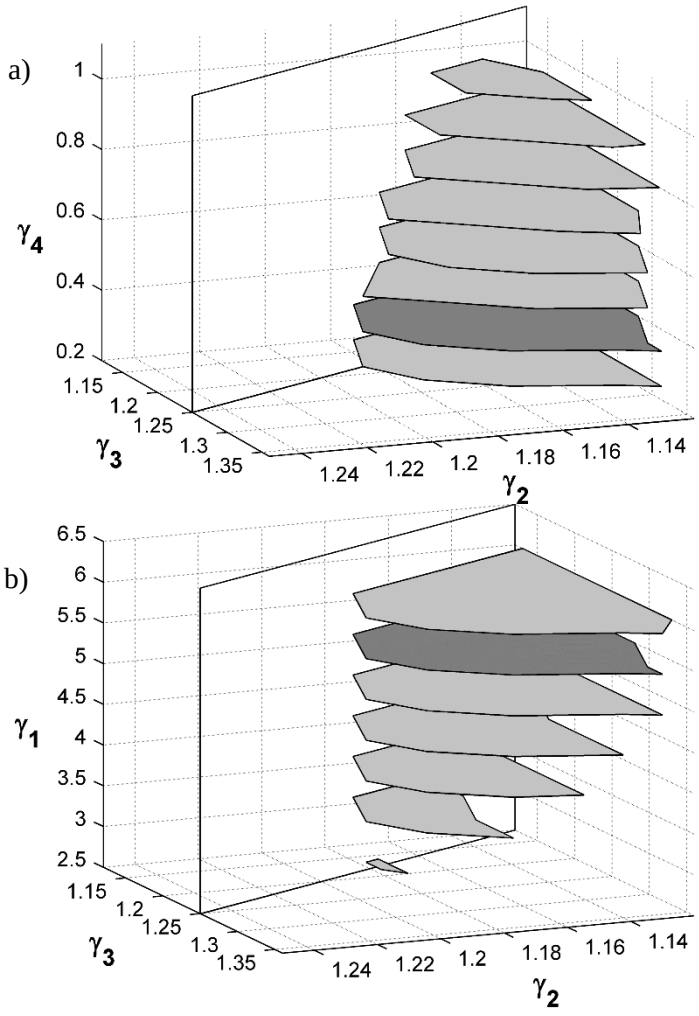

Figure 5.5 Separation regions of 6-9-6-3 configuration and 69 s switching time for: a) several values of γ_4 and fixed γ_1 = 5.5 b) several values of γ_1 and fixed γ_4 = 0.4. Darker region indicates optimum value.

It can be seen that the separation region increases as flow rate in zone 1 increases and flow rate in zone 4 decreases. This is referred to as transition region by Azevedo and Rodrigues [20] and is dependent on the mass-transfer effects. Outside the transition region (i.e., higher γ_1 and lower γ_4) the separation region is fairly constant, from which the optimum point is chosen as the boundaries of said transition region that provides higher productivity. For this SMBR unit, the

optimum point corresponds to a value of γ_1 and γ_4 of 5.5 and 0.4 respectively (see Table 5.2); although there is an increase in productivity for a γ_1 value from 5.5 to 6.0, it is very small (around 1%) compared to the 10% higher desorbent consumption. Figure 5.6 depicts the profiles within the columns at those operating conditions.

Table 5.2 Optimum points for γ_1 values between 3.0 and 6.0 and γ_4 values between 0.3 and 1.0 for 6-9-6-3 configuration and 69 s switching time.

γ_4	γ_2	γ_3	PR, kg $m^{-3}h^{-1}$	DC, m^3 kg^{-1}	DE
			$\gamma_1 = 3.0$		
0.3	1.20	1.30	59.73	0.145	1.52
0.4	1.20	1.30	65.89	0.126	1.58
0.5	1.19	1.29	64.18	0.125	1.61
0.6	1.19	1.28	62.30	0.123	1.65
0.7	1.19	1.26	44.60	0.165	1.63
			$\gamma_1 = 3.5$		
0.3	1.17	1.34	121.55	0.084	1.74
0.4	1.17	1.34	127.71	0.078	1.77
0.5	1.16	1.33	126.80	0.076	1.80
0.6	1.16	1.32	121.19	0.076	1.83
0.7	1.16	1.31	116.81	0.077	1.88
0.8	1.16	1.29	107.20	0.081	1.92
0.9	1.16	1.27	89.43	0.093	1.97
			$\gamma_1 = 4.0$		
0.3	1.15	1.35	153.28	0.077	1.80
0.4	1.15	1.35	159.41	0.072	1.82
0.5	1.15	1.35	158.86	0.070	1.85
0.6	1.15	1.34	153.75	0.071	1.88
0.7	1.15	1.32	145.47	0.073	1.93
0.8	0.14	1.31	141.10	0.073	1.98
0.9	1.14	1.28	124.44	0.080	2.04
1.0	1.16	1.24	72.34	0.133	2.08
			$\gamma_1 = 4.5$		
0.3	1.14	1.36	173.23	0.078	1.84
0.4	1.14	1.36	179.35	0.073	1.86
0.5	1.14	1.35	174.67	0.073	1.89
0.6	1.13	1.34	171.48	0.073	1.94
0.7	1.13	1.33	167.79	0.072	1.98
0.8	1.13	1.31	157.38	0.075	2.02
0.9	1.13	1.29	144.43	0.080	2.07
1.0	1.14	1.25	102.51	0.109	2.13
			$\gamma_1 = 5.0$		
0.3	1.13	1.37	186.59	0.081	1.85
0.4	1.13	1.36	186.33	0.079	1.89
0.5	1.13	1.35	185.93	0.077	1.92
0.6	1.13	1.34	181.03	0.078	1.95

γ_4	γ_2	γ_3	PR, kg $m^{-3}h^{-1}$	DC, m^3 kg^{-1}	DE
0.7	1.13	1.33	177.54	0.077	2.00
0.8	1.13	1.32	168.91	0.079	2.04
0.9	1.13	1.30	156.04	0.084	2.10
1.0	1.13	1.26	123.14	0.104	2.16
			$\gamma_1 = 5.5$		
0.3	1.13	1.37	193.35	0.086	1.88
0.4	**1.13**	**1.36**	**193.02**	**0.084**	**1.91**
0.5	1.13	1.36	190.73	0.084	1.93
0.6	1.12	1.34	187.68	0.083	1.97
0.7	1.12	1.33	182.53	0.084	2.01
0.8	1.12	1.32	175.63	0.086	2.07
0.9	1.12	1.30	162.80	0.090	2.13
1.0	1.13	1.27	133.59	0.108	2.18
			$\gamma_1 = 6.0$		
0.3	1.13	1.37	195.74	0.093	1.90
0.4	1.12	1.36	195.25	0.092	1.93
0.5	1.12	1.35	192.94	0.091	1.94
0.6	1.12	1.35	192.18	0.090	1.98
0.7	1.12	1.33	184.57	0.092	2.02
0.8	1.12	1.31	177.50	0.094	2.09
0.9	1.12	1.30	168.01	0.097	2.14
1.0	1.12	1.27	140.10	0.114	2.20

Bold indicates optimum

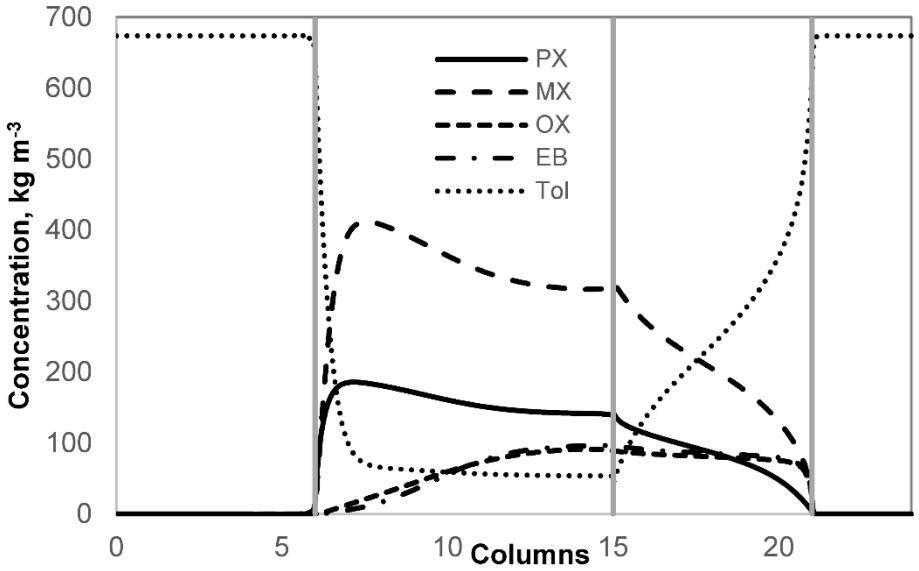

Figure 5.6 Bulk concentration profiles for $\gamma_1 = 5.5$; $\gamma_2 = 1.13$; $\gamma_3 = 1.36$; $\gamma_4 = 0.4$ in 6-9-6-3 configuration and 69 s switching time.

5.4.2. Arrangement of columns

The length of zones 1 and 4 seems excessive for their regeneration purposes, the profiles are almost constant within those zones. This is due to the higher amount of desorbent used compared to a normal Parex unit, where, for instance, the value of γ_1 is below 2 [11]. The flow rates in zones 1 and 4 are already fixed while the number of columns in each section can be varied in order to optimize the section length in each zone. For comparison purposes, separation regions for different configurations maintaining the same flow rates in zones 1 and 4 are estimated, the results are presented in Figure 5.7. The best configurations provide larger areas with the highest peaks; Table 5.3 presents the optimum point for each separation region with the corresponding productivity, desorbent consumption, and deviation from the equilibrium.

The highest productivities are provided by configurations with less columns in zones 1 and 4 as expected. Figure 5.8 shows the profiles within the columns for the configuration 2-6-14-2. In addition to the reduction of zones 1 and 4, higher amounts of aromatics are observed in zones 2 and 3 leading to an increase in xylene isomerization. Since *p*-xylene concentration is lower in zone 3 than in zone 2, it is expected that zone 3 favors the production of *p*-xylene while zone 2 favors the consumption. Moreover, the purity required in the raffinate is more difficult to reach compared to that of the extract (i.e., 0.95 vs 0.70 respectively); from which the highest productivities are obtained by units with more columns in zone 3.

Table 5.3 Optimum points for several configurations and 69 s switching time (γ_1 = 5.5 and γ_4 = 0.4).

Config	γ_2	γ_3	PR, kg $m^{-3}h^{-1}$	DC, m^3 kg^{-1}	DE
2-4-16-2	1.12	1.46	234.69	0.069	1.64
2-5-15-2	1.12	1.44	231.68	0.070	1.71
3-4-15-2	1.12	1.44	231.63	0.070	1.71
3-4-14-3	1.12	1.43	229.71	0.071	1.75
3-5-14-2	1.12	1.43	229.52	0.071	1.74
2-6-14-2	1.12	1.43	229.25	0.071	1.74
3-6-13-2	1.12	1.42	226.74	0.072	1.78
4-5-13-2	1.12	1.41	224.58	0.073	1.81
4-5-12-3	1.12	1.40	221.58	0.074	1.84
3-7-12-2	1.12	1.40	220.66	0.074	1.84
4-7-11-2	1.12	1.39	217.02	0.075	1.87
3-8-11-2	1.13	1.39	205.49	0.079	1.84
3-9-10-2	1.13	1.39	204.16	0.080	1.84
4-8-9-3	1.13	1.38	200.48	0.081	1.87
5-9-7-3	1.13	1.36	188.98	0.086	1.91

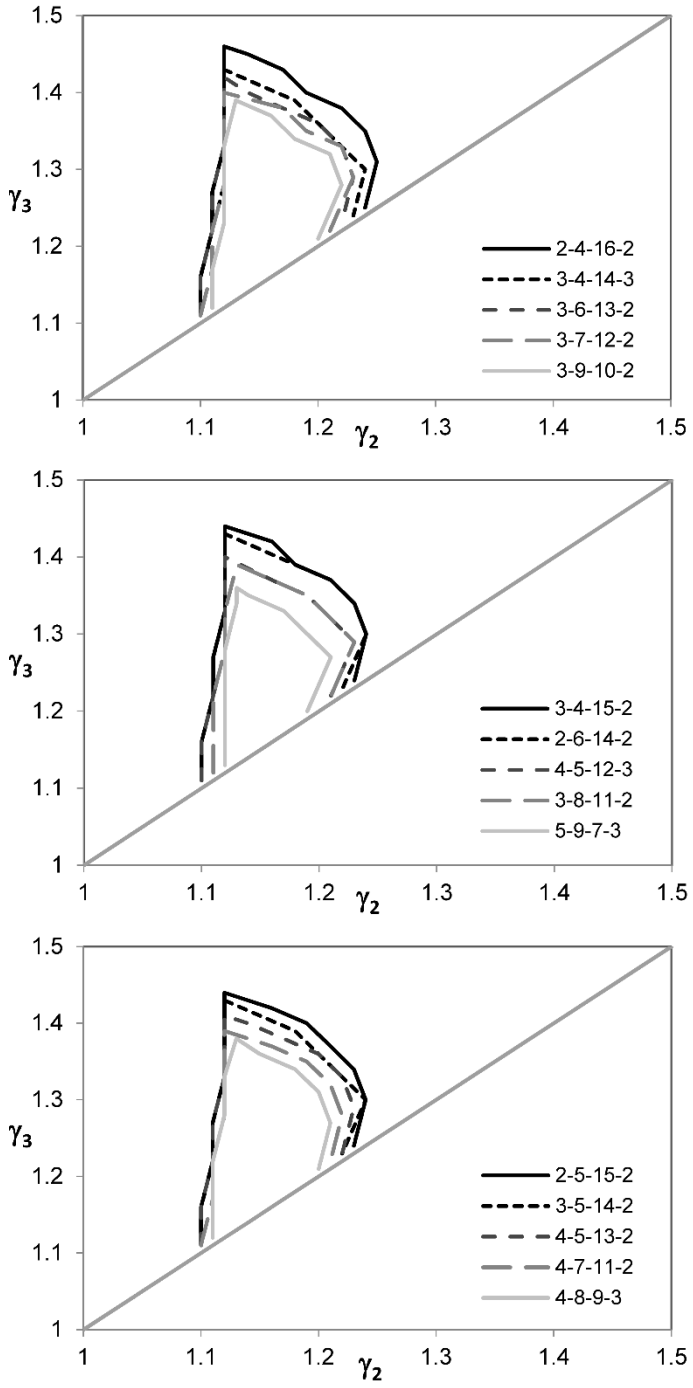

Figure 5.7 Separation regions for different configurations and 69 s switching time (γ_1 = 5.5 and γ_4 = 0.4).

5.4.3. Optimization of flow rates and switching times

The flow rates used for the previous configurations are not necessarily the best conditions; however, they should be close enough to perform an optimization procedure. An optimization solver (CVP_SS) of the commercial software gPROMS is used for this purpose. Along with the flow rates in each zone, the switching time is included as a decision variable in the optimization.

According to Sá Gomes et al. [14], the influence of switching time is not straightforward, it is possible to process more feed at the expense of higher mass-transfer resistances.

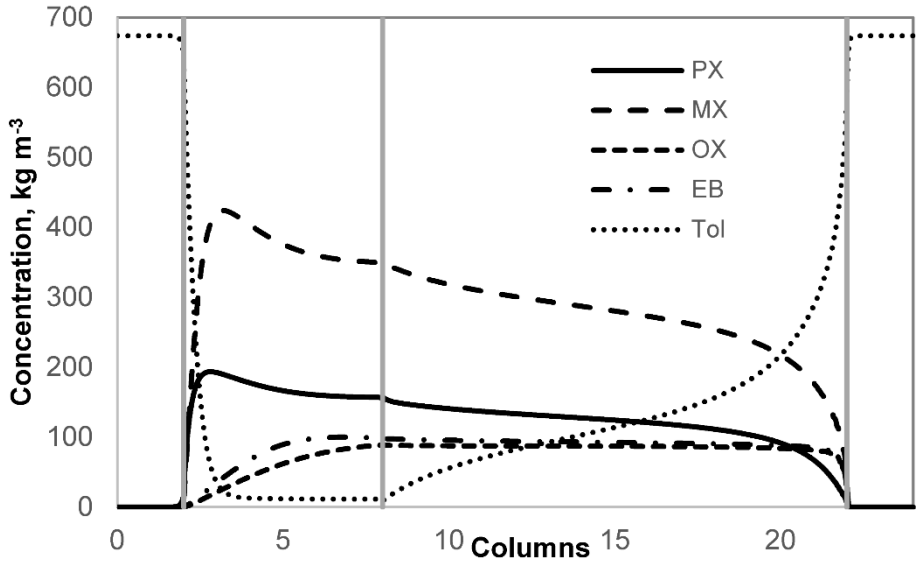

Figure 5.8 Bulk concentration profiles for $\gamma_1 = 5.5$; $\gamma_2 = 1.12$; $\gamma_3 = 1.43$; $\gamma_4 = 0.4$ in 2-6-14-2 configuration and 69 s switching time.

A single-objective optimization procedure is used to maximize productivity. Although the desorbent consumption is a unit performance parameter, the actual desorbent recovery units (distillation columns for this case) shall be considered in order to optimize the whole SMBR unit. A compromise may exist between operating at maximum productivity with diluted products (higher recovery duty) and lower productivities using less desorbent [14]. Following the aforementioned, several maximum DC values are used as constraints in the optimization procedure along with the purity in the extract and the raffinate (0.70 and 0.95 respectively). The best six configurations are chosen for the optimization and the results are presented in Table 5.4.

The columns arrangement that offered better performance is 2-6-14-2. In order to achieve lower desorbent consumption it is necessary to use longer switching times, hence increasing contact time up to a certain point, corresponding to desorbent consumption lower than 0.05 $m^3\ kg^{-1}$, where significant mass-transfer resistances prevent the unit from achieving the desired product purities.

The behavior of productivity as function of desorbent consumption for each configuration can be seen in Figure 5.9. In the graph it can be spotted a change around DC = 0.06 $m^3\ kg^{-1}$. The productivity increases faster for desorbent consumptions lower than 0.06 $m^3\ kg^{-1}$. In other words, for each 0.01 $m^3\ kg^{-1}$ in desorbent consumption, which can be seen as operation cost, the gain in productivity is higher than that operating above 0.06 $m^3\ kg^{-1}$. Therefore, it would be recommended to operate around said value. However, a decision cannot be made without the

study of the recovery units where a somewhat similar relation between desorbent consumption and the duty of recovery units can be obtained.

Table 5.4 Optimization for several configurations at different desorbent consumption

Configuration	γ_1	γ_2	γ_3	γ_4	PR, kg $m^{-3}h^{-1}$	DE	Switching time, s
DC = 0.08 m^3 kg^{-1}							
2-6-14-2	4.48	1.12	1.32	0.32	580.11	2.01	20
2-5-15-2	4.48	1.13	1.32	0.31	552.02	2.01	21
3-5-14-2	4.45	1.13	1.32	0.31	532.50	2.01	21
2-4-16-2	4.48	1.13	1.33	0.28	507.83	2.00	23
3-4-15-2	4.45	1.13	1.32	0.30	490.64	2.00	23
3-4-14-3	4.46	1.13	1.32	0.33	471.78	2.01	24
DC = 0.07 m^3 kg^{-1}							
2-6-14-2	4.08	1.13	1.32	0.43	514.28	2.00	22
2-5-15-2	4.08	1.13	1.33	0.37	489.11	1.99	24
3-5-14-2	4.03	1.13	1.32	0.39	469.39	1.99	24
2-4-16-2	4.09	1.13	1.34	0.35	449.74	1.97	26
3-4-15-2	4.08	1.13	1.33	0.36	432.69	1.98	27
3-4-14-3	4.07	1.13	1.33	0.39	415.48	1.99	28
DC = 0.06 m^3 kg^{-1}							
2-6-14-2	**3.74**	**1.13**	**1.33**	**0.49**	**412.32**	**1.98**	**29**
2-5-15-2	3.74	1.13	1.34	0.46	394.61	1.96	31
3-5-14-2	3.74	1.13	1.34	0.48	373.85	1.97	32
2-4-16-2	3.75	1.14	1.35	0.41	364.74	1.93	34
3-4-15-2	3.73	1.14	1.35	0.43	347.15	1.94	35
3-4-14-3	3.74	1.14	1.34	0.46	330.94	1.95	36
DC = 0.05 m^3 kg^{-1}							
2-6-16-2	3.47	1.14	1.41	0.45	227.85	1.72	58
2-5-15-2	3.48	1.14	1.40	0.48	222.54	1.76	59
3-4-15-2	3.47	1.15	1.41	0.47	194.06	1.69	68
2-4-14-2	3.46	1.15	1.40	0.51	183.36	1.72	71
3-5-14-2	3.48	1.15	1.41	0.49	172.24	1.69	76
3-4-14-3	3.47	1.15	1.42	0.52	154.15	1.67	84

Bold indicates optimum

5.5. Conclusions

A hybrid unit combining separation and isomerization of xylenes using the concept of simulated moving bed is analyzed. The unit is foreseen as part of the modified aromatics complex containing a single stage crystallization to further purify the *p*-xylene, from which purity down to 0.70 is accepted in the extract. After several simulations and optimizations, it is concluded that the best configuration is 2-6-14-2 operating at corresponding desorbent consumption of 0.06 m^3 kg^{-1} with a productivity of 412.32 kg $m^{-3}h^{-1}$.

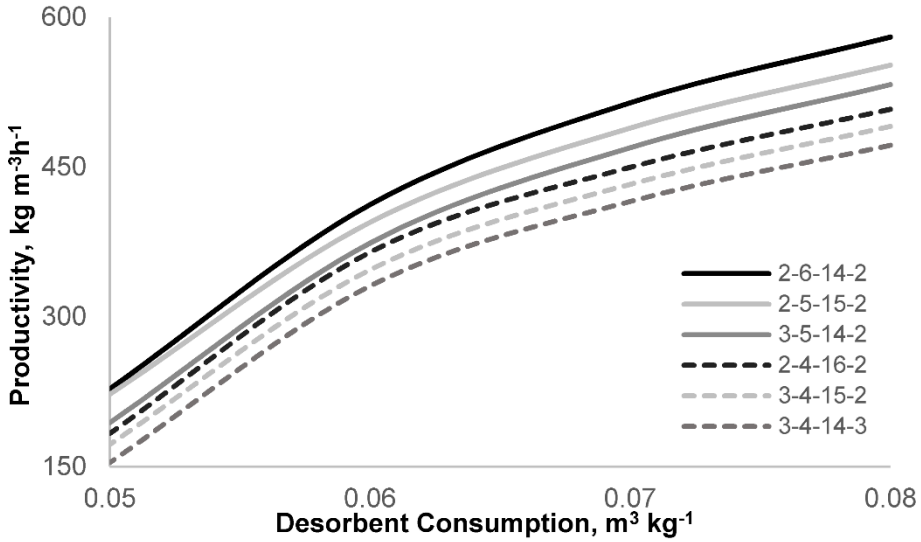

Figure 5.9 Variation of productivity with desorbent consumption for different configurations

5.6. Nomenclature

b_i = Adsorption equilibrium constant of component i, m^3 kg^{-1}

C_i = Concentration of component i, kg m^{-3}

$C_{i,j}$ = Concentration of component i in zone j, kg m^{-3}

$\overline{C_{pi}}_{ads}$ = Average particle concentration of component i in the adsorbent, kg m^{-3}

$\overline{C_{pi}}_{cat}$ = Average particle concentration of component i in the catalyst, kg m^{-3}

$C_{\mathrm{PX},eq}$ = p-Xylene concentration in equilibrium, kg m^{-3}

D_{ax} = Axial dispersion coefficient, m^2 s^{-1}

DC = Desorbent consumption, m^3 kg^{-1}

DE = Deviation from the equilibrium

D_m = Molecular diffusivity, m^2 s^{-1}

k_{ext} = External mass-transfer coefficient, m s^{-1}

k_n = Kinetic constant of reaction n, m^3 $kg^{-1}s^{-1}$

k_{int} = Internal mass-transfer coefficient, m s^{-1}

K_l = Global mass-transfer coefficient, m s^{-1}

L = Length, m

Pe = Peclet number

PR = Productivity, kg $m^{-3}h^{-1}$

PurX = Extract purity

PurR = Raffinate purity

Q_j = Volumetric flow rate in zone j, m^3 kg^{-1}

q_i = Adsorbed concentration of component i, kg kg^{-1}

q_{sat} = Saturated adsorbed concentration, kg kg^{-1}

Re = Reynolds number

R_i = Reaction rate of component i, s^{-1}

R_p = Particle radius, m

Sc = Schmidt number

Sh = Sherwood number

T = Temperature, K

t = time, s

u = Interstitial velocity, m s^{-1}

u_s = Solid velocity, m s^{-1}

v = Superficial velocity, m s^{-1}

z = Axial coordinate, m

Greek letters

γ_j = Velocity ratio in zone j

ε = Bed porosity

ε_p = Particle porosity

μ = Viscosity, cP

ρ = Fluid density, kg m^{-3}

ρ_{ads}= Density of adsorbent, kg m^{-3}

ρ_{cat}= Density of catalyst, kg m^{-3}

τ = Tortuosity factor

φ = Adsorbent to adsorbent plus catalyst weight ratio

Abbreviations

EB = Ethylbenzene

D = Desorbent

F = Feed

LDF = Linear Driving Force

MX = *m*-Xylene

OX = *o*-Xylene

PX = *p*-Xylene

R = Raffinate

SMB = Simulated Moving Bed

SMBR = Simulated Moving Bed Reactor

TMB = True Moving Bed

TMBR = True Moving Bed Reactor

Tol = Toluene

X = Extract

Superscripts and subscripts

in = Inlet

out = Outlet

5.7. References

[1] Cavani, F., and G. Centi. 2000. "Sustainable Development and Chemistry." In *Kirk-Othmer Encyclopedia of Chemical Technology*. John Wiley & Sons, Inc.

[2] Minceva, M., and A. E. Rodrigues. 2005. "Two-level optimization of an existing SMB for p-xylene separation." *Computers and Chemical Engineering* no. 29 (10):2215-2228.

[3] Starkey, D. R., J. L. Andrews, S. L. Luo, and K. J. Knob. 2009. PxMax with Crystallization. An Integrated Process for High Purity Paraxylene Production. edited by ExxonMobil: ExxonMobil Chemical Technology Licensing LLC.

[4] Bass, G., and T. Kinn. 2005. Enhancing Para-xylene Production by Utilizing ExxonMobil's PxMax Process. edited by ExxonMobil: ExxonMobil Chemical Company.

[5] GTC Technology. 2001. "Paraxylene production." *Hydrocarbon Engineering* no. 6 (9):54-55.

[6] Minceva, M., P. S. Gomes, V. Meshko, and A. E. Rodrigues. 2008. "Simulated moving bed reactor for isomerization and separation of p-xylene." *Chemical Engineering Journal* no. 140 (1-3):305-323.

[7] Bergeot, G., D. Leinekugel-Le-Cocq, L. Wolff, L. Muhr, and M. Bailly. 2010. "Intensification of Paraxylene Production using a Simulated Moving Bed Reactor." *OGST – Revue d'IFP Energies nouvelles* no. 65 (5):721-733.

[8] Mun, S. 2012. "Consideration of a target product concentration level in the optimal design of a four-zone simulated moving bed process for binary separation." *Chemical Engineering Journal* no. 204–206 (0):179-187.

[9] Ruthven, D. M., and C. B. Ching. 1989. "Counter-current and simulated counter-current adsorption separation processes." *Chemical Engineering Science* no. 44 (5):1011-1038.

[10] Silva, M. S. P., J. P. B. Mota, and A. E. Rodrigues. 2012. "Fixed-bed adsorption of aromatic C 8 isomers: Breakthrough experiments, modeling and simulation." *Separation and Purification Technology* no. 90:246-256.

[11] Minceva, M. 2004. *Separation/Isomerization of Xylenes by Simulated Moving Bed Technology*, Departamento de Engenharia Química, Universidade do Porto, Portugal.

[12] Bergeot, G. 2010. *Extension du concept "One-column" au lit mobile simulé réactif. Application à la séparation réactive des C_8 aromatiques*, École doctorale Sciences et Ingénierie des Ressources, Procédés, Produits, Environnement, Institut National Polytechnique de Lorraine, France.

[13] Cappellazzo, O., G. Cao, G. Messina, and M. Morbidelli. 1991. "Kinetics of Shape-Selective Xylene Isomerization over a ZSM-5 Catalyst." *Industrial & Engineering Chemistry Research* no. 30 (10):2280-2287.

[14] Sá Gomes, P., N. Lamia, and A. E. Rodrigues. 2009. "Design of a gas phase simulated moving bed for propane/propylene separation." *Chemical Engineering Science* no. 64 (6):1336-1357.

[15] Knaebel, K. S. 2008. "Adsorption." In *Albright's Chemical Engineering Handbook*, edited by L. Albright. Boca Raton: Taylor & Francis Group, LLC.

[16] Santacesaria, E., M. Morbidelli, P. Danise, M. Mercenari, and S. Carrà. 1982. "Separation of xylenes on Y zeolites. 1. Determination of the adsorption equilibrium parameters, selectivities, and mass transfer coefficients through finite bath experiments." *Industrial and Engineering Chemistry Process Design and Development* no. 21 (3):440-445.

[17] Do, D. D. 1998. *Adsorption Analysis: Equilibria and Kinetics*. London: Imperial College Press.

[18] Ruthven, D. M. 1984. *Principles of Adsorption and Adsorption Processes*. First ed. New York: John Wiley & Sons, cop.

[19] Poling, B. E., J. M. Prausnitz, and J. J. P. O'Connell. 2001. *The Properties of Gases and Liquids*. 5th ed. New York: The McGraw-Hill Companies.

[20] Azevedo, D. C. S., and A. E. Rodrigues. 1999. "Design of a simulated moving bed in the presence of mass-transfer resistances." *AIChE Journal* no. 45 (5):956-966.

Chapter 6: Simulated moving bed reactor: Optimal particle size

In this chapter a similar study as in the previous one is carried out with four particle diameters: 0.5, 0.7, 0.8, and 0.9 mm, maintaining the extract and raffinate purity in 0.70 and 0.95 respectively, and adsorbent to adsorbent plus catalyst weight ratio of 0.9. After performing simulations using the true moving bed approach, it is verified that the high amount of desorbent is mainly caused by the reverse reaction in the isomerization of xylenes. Furthermore, the highest productivity is offered by the 2-6-14-2 configuration for every particle size studied. The system is then analyzed with that arrangement of columns and the aforesaid particle diameters together with the currently used 0.62 mm under the maximum pressure drop of the existing Simulated Moving Bed unit (685 kPa). The optimal particle diameter is 0.62 mm exhibiting the highest productivity. The results also show that a single study with a small particle size is sufficient to accurately determine the best configuration of the system.

This chapter is based on: Gonçalves, J. C., and A. E. Rodrigues. 2015. "Simulated Moving Bed Reactor for *p*-xylene production: Optimal particle size." *Canadian Journal of Chemical Engineering*. In press.

6.1. Introduction

The core of this thesis is the development of a Simulated Moving Bed Reactor (SMBR) for the production of *p*-xylene in the framework of a proposal to modify the aromatics complex. In the previous chapter, a complete analysis with the currently used particle diameter (i.e., 0.62 mm) was carried out at 200 ºC and milder extract purity constraint (i.e., 0.70) provided by further purification through a crystallization unit. The purpose of this chapter is to follow a similar methodology for different particle diameters (i.e., 0.5, 0.7, 0.8, and 0.9 mm) to determine the optimal size of adsorbents and catalysts with their corresponding flow rates and switching time to be used in the SMBR unit operating at the same temperature subject to the maximum pressure drop constraint of the existing Simulated Moving Bed (SMB) facility.

6.2. Mathematical model

As in the previous chapter, the system is modelled by means of a continuous True Moving Bed Reactor (TMBR). This model is simpler, less time-consuming, and suitable for optimizations [1]. The assumptions, mass balances, and boundary conditions are the same; the performance parameters to assess the SMBR unit – productivity (PR), desorbent consumption (DC), and deviation from the equilibrium (DE) – are defined in the same manner, considering *p*-xylene in the extract point as the desired product.

The adsorption isotherms and reaction kinetics are again taken from Bergeot [2] and assumed to be constant for different particle diameters. Based on the aforementioned, the particle size only affects the dispersion, pressure drop, and the mass-transfer resistance which is described by the linear driving force (LDF) approximation.

6.2.1. Pressure drop

The pressure drop in SMBR units is normally estimated by the sum of the pressure drop in each zone of the unit [3-5]. Ergun [6] developed an equation to calculate the pressure drop (ΔP) in fixed beds that covers laminar and turbulent flow conditions:

$$\Delta P = \frac{150\mu u L_c}{d_p^2}\left(\frac{1-\varepsilon}{\varepsilon}\right)^2 + \frac{1.75\rho u^2 L_c}{d_p}\left(\frac{1-\varepsilon}{\varepsilon}\right) \tag{6.1}$$

where μ and ρ are the mixture viscosity and density flowing through the fixed bed with interstitial velocity u, L_c is the length of a single column with bed porosity ε and particle diameter d_p.

The properties of the mixture are estimated by the same methods (see Annex A) and assumed constant since they are very similar among the isomers and do not change significantly with pressure in liquid phase; consequently, the interstitial velocity is taken as constant in each zone.

The bed porosity is also assumed constant since the particles are rigid and spherical and so deformation due to process conditions is not expected; moreover, the column to particle diameter ratio is large enough (i.e. >> 10) for the particles sizes studied [7]. For lower ratios the bed porosity becomes a function of said ratio, particularly below 10 when shortcutting may occur at the wall [8]. Additionally, the size of the adsorbent and catalyst are equal for every case in order to prevent the smaller particles of being dragged to the bottom by the liquid displacing the larger particles to the top leading to variable porosity throughout the column and, more importantly, losing of homogeneity in the adsorbent-catalyst mixture.

It is important to highlight that the value from equation (6.1) must be multiplied by the number of columns to obtain the pressure drop of a certain zone. Moreover, since the expression was developed for fixed beds, the interstitial velocity shall be the one that corresponds to the actual SMBR unit although the model is solved using the TMBR approach. Both velocities are related through the velocity of solid phase based on the concept of relative velocity ($u^{\mathrm{SMBR}} = u^{\mathrm{TMBR}} + u_s$).

6.3. Results and discussion

The system is solved numerically using the commercial software gPROMS v3.7.1 from Process Systems Enterprise (www.psenterprise.com). The axial domain is discretized by the second-order orthogonal collocation method on 50 finite elements with 10^{-5} as tolerance. The values of extract and raffinate purity and adsorbent to adsorbent plus catalyst weight ratio are not modified (0.70; 0.95; and 0.9 respectively).

6.3.1. Separation regions and separation volumes

For each particle diameter, the steady-state TMBR model is solved for several values of γ_2 and γ_3 to evaluate the influence of γ_1 and γ_4 for the configuration and switching time currently used in the SMB unit (6-9-6-3 and 69 s respectively) as described in Chapter 5. Figure 6.1 shows the influence of γ_4 and γ_1 in the separation regions for each particle size. For the four diameters

the transition region described by Azevedo and Rodrigues [9], where the separation region increases as flow rate in zone 1 increases and flow rate in zone 4 decreases, is clearly identified.

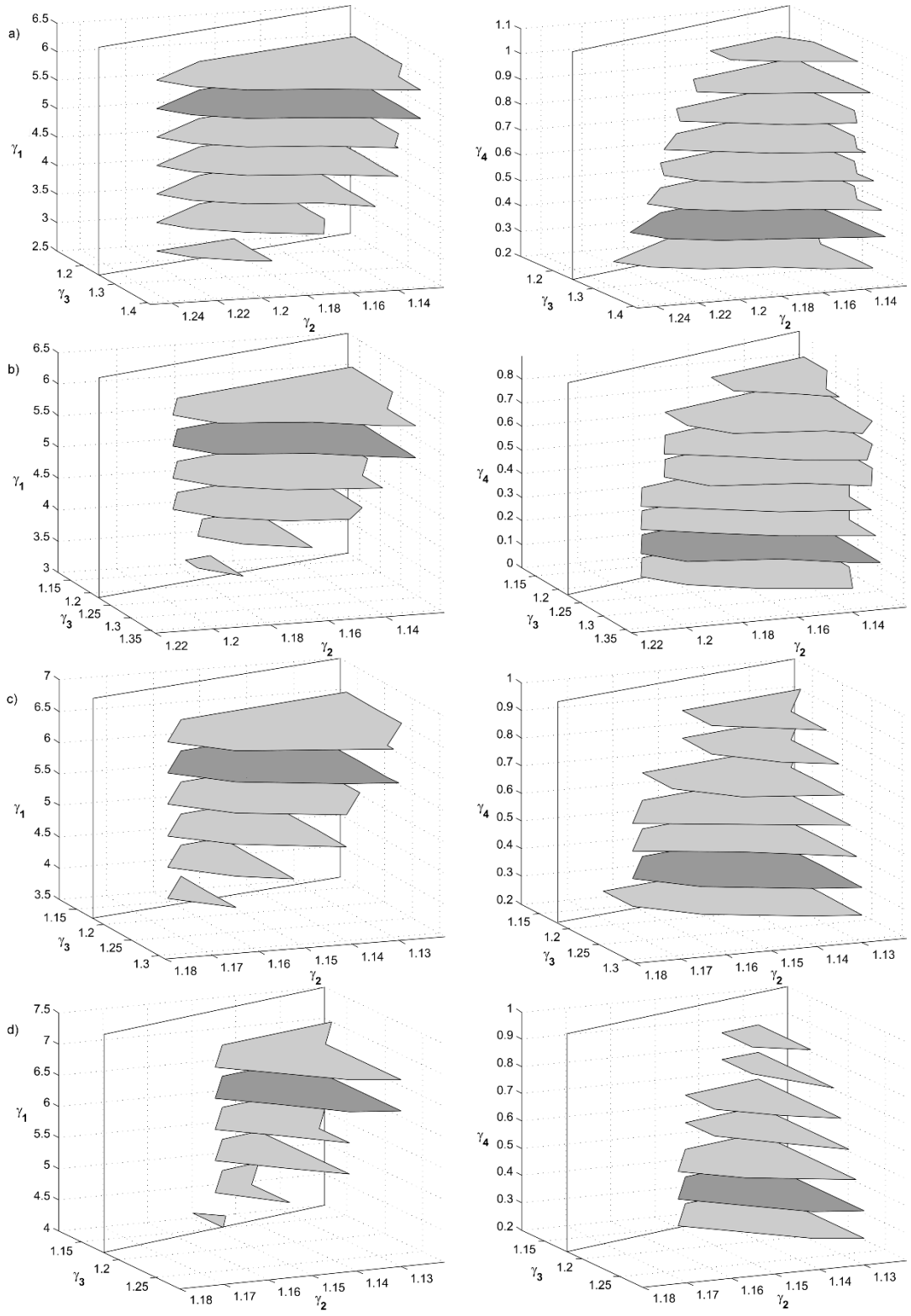

Figure 6.1 Separation regions for 6-9-6-3 configuration and 69 s switching time with several values of γ_1 and fixed γ_4 (left) and several values of γ_4 and fixed γ_1 (right) for particle diameter: a) 0.5 mm (γ_1=5.5 and γ_4=0.4) b) 0.7 mm (γ_1=5.5 and γ_4=0.2) c) 0.8 mm (γ_1=6.0 and γ_4=0.4) d) 0.9 mm (γ_1=6.5 and γ_4=0.4). Darker regions indicate the optimum values for γ_1 and γ_4.

Moreover, from smaller to larger particles it can be seen a significant reduction in the separation volume due to the greater influence of the particle diameter in the mass-transfer resistance. For instance the intraparticle mass-transfer coefficient, calculated by $k_p = 15D_{\text{eff}}/\left(d_p/2\right)^2$ to keep consistency with the LDF approximation, presents values of 0.320, 0.163, 0.125, and 0.099 s^{-1} for particle diameter 0.5, 0.7, 0.8, and 0.9 mm respectively.

Table 6.1 presents the optimum point (i.e., peak of the darker separation region in Figure 6.1) for each particle size with the corresponding productivity, desorbent consumption, and deviation from the equilibrium. The optimum point is chosen at the boundary of the previously mentioned transition region (i.e., region fairly constant for higher values of γ_1 and/or lower values of γ_4); in other words, the point at which higher desorbent consumption does not lead to a significant increase in productivity is selected as optimum for each size (see Tables B.1 to B.4 in Annex B). The optimum point for diameters 0.5, 0.62 (see Table 5.2 in Chapter 5), 0.7, 0.8, and 0.9 mm corresponds to a value of γ_1 and γ_4 of 5.5 and 0.4, 5.5 and 0.4, 5.5 and 0.2, 6.0 and 0.4, and 6.5 and 0.4 respectively. As expected for larger particles higher flow rates of desorbent (i.e., higher γ_1 - γ_4) are needed to compensate the increase in the mass-transfer resistance. On the other hand, for smaller particles the amount of desorbent tends to a constant yet still high value, this is due to the reverse reaction rather than the mass-transfer.

Table 6.1 Optimum points for 6-9-6-3 configuration and 69 s switching time for each particle diameter

Size, mm	γ_1	γ_2	γ_3	γ_4	PR, kg $m^{-3}h^{-1}$	DC, m^3 kg^{-1}	DE
0.5	5.5	1.13	1.41	0.4	209.99	0.078	1.76
0.7	5.5	1.13	1.36	0.2	187.52	0.090	1.90
0.8	6.0	1.13	1.31	0.4	151.10	0.118	1.95
0.9	6.5	1.13	1.28	0.4	126.75	0.154	1.96

6.3.2. Arrangement of columns

Normally, higher desorbent flow rates are needed to regenerate the solid and desorbent when section lengths of zones 1 and 4 are shorter [10], a trade-off analysis between the amount of desorbent and the number of columns determines the proper configuration of the unit [11]. However, as indicated in the previous chapter and verified in the last section, the higher desorbent flow rates are mainly due to the presence of the reverse reaction in each section of the SMBR unit. Based on the aforesaid, separation regions for different configurations with fixed flow rates in zone 1 and 4 and 69 s switching time corresponding to each diameter are estimated and presented in Figure 6.2; as usual, the best configurations provide larger separation regions. The vertices of separation regions for several configurations with the corresponding productivity, desorbent consumption, and deviation from the equilibrium for each particle diameter are presented in Table B.5 in Annex B.

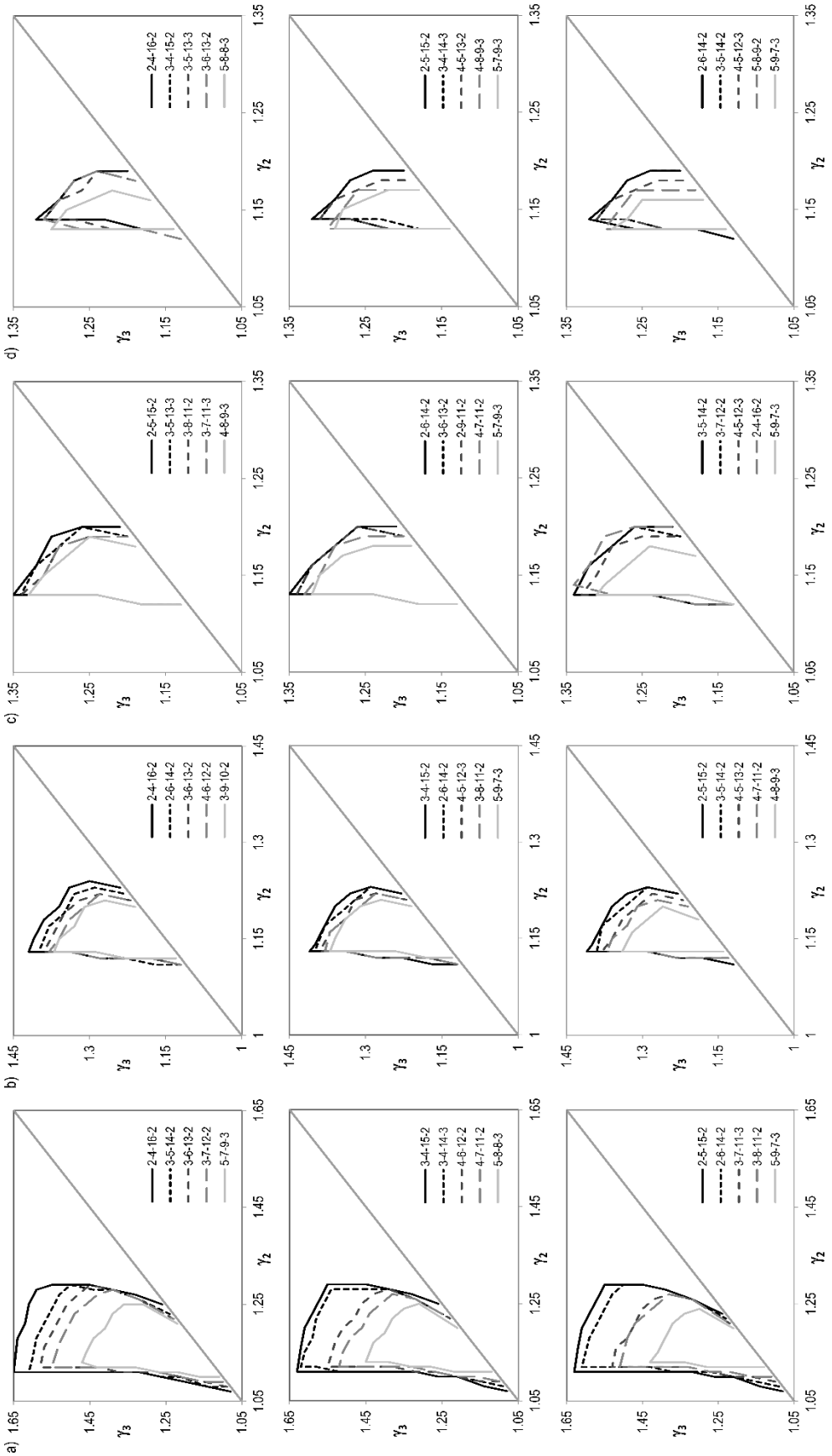

Figure 6.2 Separation regions for different configurations and 69 s switching time for particle diameter: a) 0.5 mm (γ_1=5.5 and γ_4=0.4) and b) 0.7 mm (γ_1=5.5 and γ_4=0.2) c) 0.8 mm (γ_1=6.0 and γ_4=0.4) d) 0.9 mm (γ_1=6.5 and γ_4=0.4).

As expected, fewer columns in zones 1 and 4 provide higher productivities. Regardless the particle diameter, configurations with larger zone 3 exhibit better performances since in this zone *p*-xylene is produced in the isomerization reaction due to its lower concentration. However, the difference between the regions of the analyzed columns arrangements is smaller for larger particles; as the particle size increases the mass-transfer resistance becomes more important reducing the influence of the length of each zone in the performance of the SMBR [12].

6.3.3. Optimization without maximum pressure drop constraint

The best six configurations for each particle size are included in an optimization procedure using the solver (CVP_SS) of the commercial software gPROMS. The flow rates for each zone and the switching times are optimized to maximize the productivity through a single-objective optimization procedure. Several values of desorbent consumption are used as constraints along with the purity in the extract and raffinate port (i.e., 0.70 and 0.95 respectively) as the procedure followed in Chapter 5.

Table B.6 in Annex B presents the optimization results for each particle diameter. It can be seen that 2-6-14-2 is the best configuration for every size, as for 0.62 mm. As expected, for larger particles the feasible DC values for the unit increases due to the mass-transfer resistance. In addition, the switching time also increases with higher desorbent consumption constraints; as pointed out by Sá Gomes et al. [1], longer switching times allow to process more feed by increasing contact time with the disadvantage of higher mass-transfer resistance.

The productivity as function of desorbent consumption for the four particle diameters studied can be seen in Figure 6.3. Similarly to 0.62 mm, a change in the profile can be pinpointed at a specific value of desorbent consumption: 0.05; 0.07; 0.09; and 0.10 $m^3\ kg^{-1}$ for 0.5; 0.7; 0.8; and 0.9 mm respectively. It is recommended to operate around said values since the gain in productivity for desorbent consumption is the highest. Moreover, the difference between the configurations is shorter for larger particles as noted in Section 6.3.2; some overlapping is even observed for 0.7 mm and larger. Based on the aforementioned, it is recommended to use smaller particles when choosing the appropriate configuration for an SMBR unit.

Based on the previous results, the configuration chosen for further studies considering the pressure drop within the unit is 2-6-14-2. Figure 6.4 presents the productivity, pressure drop, and desorbent consumption for the particle diameters studied including the currently size used (0.62 mm). On the absence of pressure drop constraints it can be seen that below 0.62 mm the increase in pressure drop outweighs that of productivity, while above 0.7 mm a faster increase in desorbent consumption is noticed. In case of a new unit, the proper particle size would be around 0.6 – 0.7

mm avoiding significant pressure drop. High pressure drop considerably affects the cost of this type of units, from which it is not recommended to set excessive values of allowable pressure drop early in the design and without any preliminary study of the system [13].

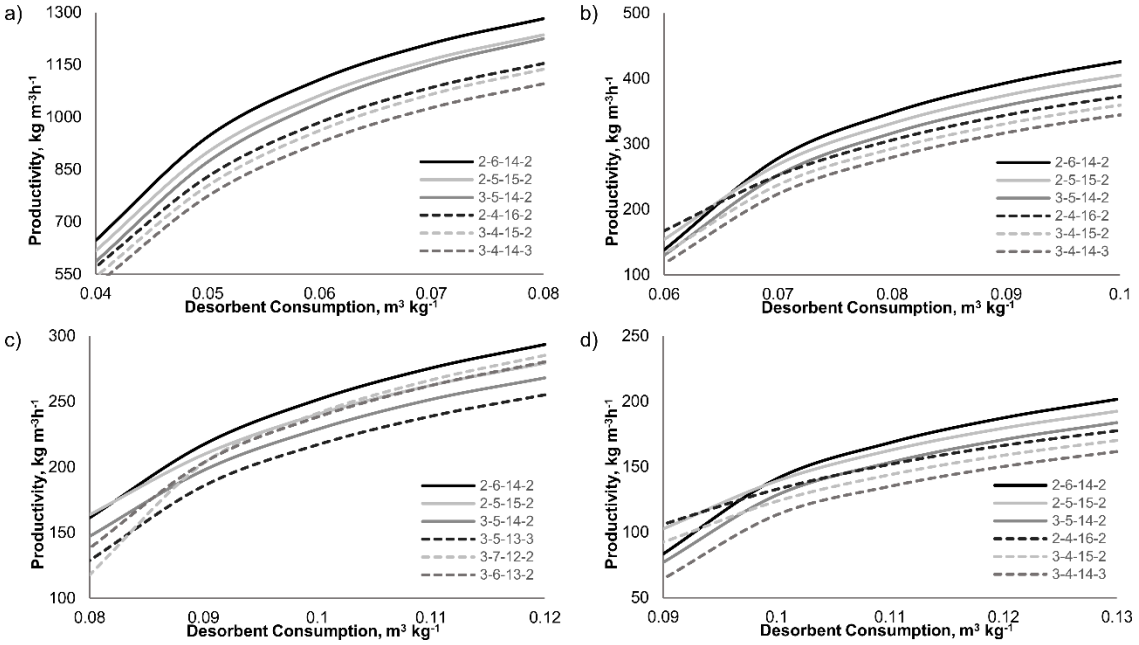

Figure 6.3 Variation of productivity with desorbent consumption for different configurations for particle diameter: a) 0.5 mm b) 0.7 mm c) 0.8 mm d) 0.9 mm.

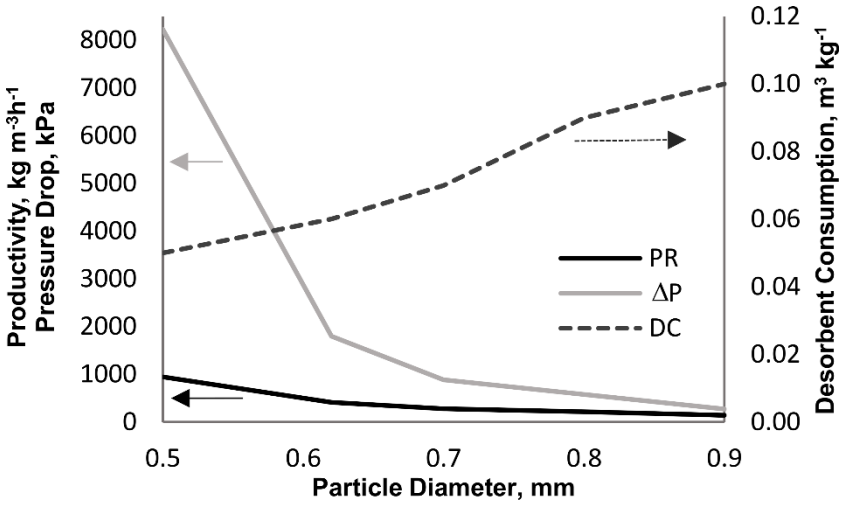

Figure 6.4 Productivity (PR), pressure drop (ΔP), and desorbent consumption (DC) with 2-6-14-2 configuration for particle diameters: 0.5, 0.62, 0.7, 0.8, and 0.9 mm without maximum pressure drop constraint.

6.3.4. Optimization subject to maximum pressure drop constraint

As mentioned before, the SMBR development is based on an existing SMB unit with its corresponding maximum allowable pressure drop defined by the construction material, thickness,

among others. Operating beyond said pressure drop may cause significant damage on the equipment [4,14]. The maximum pressure drop in the 24 beds of the SMB unit shall not exceed 824 kPa. In this study a safety margin of 20% is used to provide operational flexibility and to take into account the potential presence of a naphthenic fraction which affects neither the adsorption nor the isomerization but does increase the pressure drop within the unit [15]; hence, the maximum allowable pressure drop is set to 685 kPa (i.e., 25 kPa by meter of column bed).

In addition to the pressure drop constraint, a minimum switching time is included in this optimization procedure. In the previous section, short switching times are obtained for small particles since the contact time required to ensure the mass transfer from the liquid to the solid phase is lower [16]. Switching times lower than 30 seconds makes the operation of the recycle pump difficult and prevent the system from stabilize between switches [5,14,17]. Furthermore, the switching time is normally used as a controlled variable of the process [18]; therefore, it is not advisable to use short values to guarantee correct operation of the controlling system.

The flow rates with the corresponding productivity, desorbent consumption, switching time, and pressure drop are presented in Table 6.2 for each particle size. Generally, in this type of system there are two regions delimited by the particle diameter: for lower particles the system is limited by the pressure drop while for larger particles is limited by mass-transfer resistance. The optimal particle size which gives the maximum productivity is between the two limiting regions [3,12,17,19,20]. Up to 0.7 mm the system reaches the maximum allowed pressure drop and for larger particles it is controlled by mass-transfer.

Table 6.2 Optimization for 2-6-14-2 configuration with different particle sizes under the maximum pressure drop restriction (685 kPa).

Size, mm	γ_1	γ_2	γ_3	γ_4	PR, kg $m^{-3}h^{-1}$	DC, m^3 kg^{-1}	Switching time, s	ΔP, kPa
0.50	3.52	1.13	1.47	0.65	219.63	0.04	72	685
0.62	**4.37**	**1.13**	**1.43**	**0.21**	**267.40**	**0.06**	**57**	**685**
0.70	4.37	1.13	1.36	0.28	259.41	0.07	50	685
0.80	4.72	1.14	1.32	0.34	217.43	0.09	49	580
0.90	4.98	1.15	1.33	0.30	140.72	0.10	73	271

Bold indicates optimum

The two limiting regions can be seen in Figure 6.5. The maximum productivity is given by 0.62 mm particle size, which is the actual size currently used in the existing SMB unit. A larger particle was expected since a higher flow rate of desorbent due to the reverse reaction is employed in the SMBR unit. However, the highest pressure drop normally occurs in section 1 [18,19], and the SMBR has a shorter section than the existing SMB unit (i.e., 2 columns in SMBR compared to 6 columns in the existing SMB), which somehow compensates for the higher desorbent flow rate.

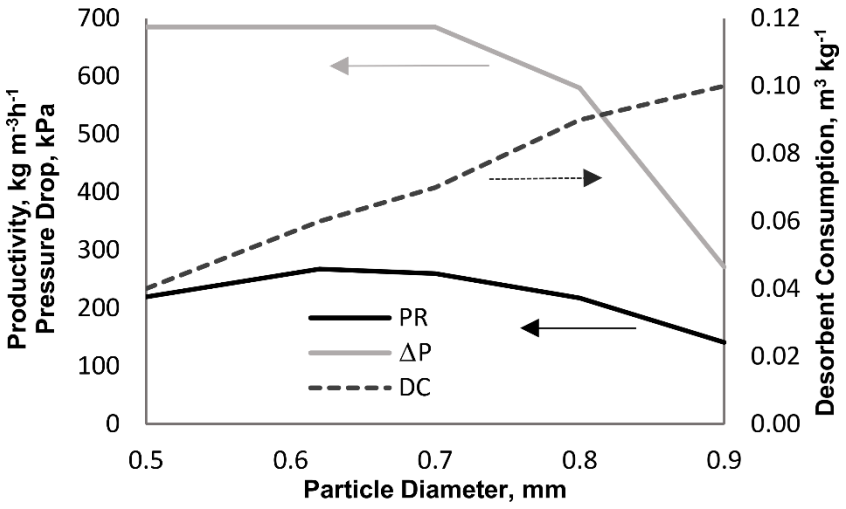

Figure 6.5 Productivity (PR), pressure drop (ΔP), and desorbent consumption (DC) with 2-6-14-2 configuration for particle diameters: 0.5, 0.62, 0.7, 0.8, and 0.9 mm subject to maximum pressure drop constraint of 685 kPa.

The simulations considering pressure drop have only been carried out for the configuration 2-6-14-2. In order to verify that the optimal configuration is maintained regardless the pressure drop constraint, a new optimization is performed with the optimal particle diameter (0.62 mm), its corresponding desorbent consumption (0.06 m^3 kg^{-1}), and 685 kPa as maximum pressure drop for the best configurations obtained in Section 6.3.3; the results are presented in Table 6.3. The difference in productivity among the first three configurations (including 2-6-14-2) is about 0.5%, from which it can be assumed that a single study with a relative small particle size is enough to determine the best arrangement of columns for this type of unit saving a significant amount of computing-time.

Table 6.3 Optimization for several configurations with 0.62 mm particle size, 0.06 m^3 kg^{-1} of desorbent consumption, and a maximum pressure drop of 685 kPa.

Config	γ_1	γ_2	γ_3	γ_4	PR, kg $m^{-3}h^{-1}$	DE	Switching time, s
2-5-15-2	4.46	1.13	1.45	0.23	268.01	1.67	58
2-6-14-2	4.37	1.13	1.43	0.21	267.40	1.71	57
2-4-16-2	4.52	1.13	1.46	0.27	266.41	1.64	59
3-5-14-2	4.39	1.13	1.44	0.22	251.97	1.68	61
3-4-15-2	4.45	1.13	1.45	0.24	251.02	1.64	62
3-4-14-3	4.39	1.13	1.42	0.31	249.35	1.74	60

An alternative approach where several values of productivity, instead of desorbent consumption as described in the previous sections, are used as constraints can be followed. In this case the desorbent consumption is minimized for each productivity while satisfying the other constraints (i.e., minimum purity, switching time, and maximum pressure drop). The optimization is repeated until the maximum feasible productivity is found for a given particle size and/or unit configuration. The results obtained following this procedure, presented in Table B.7 in Annex B

and similar to those calculated with the first approach, also verify that the high amount of desorbent needed is due to the isomerization of xylenes which combined with small particles (i.e., < 0.5 mm) leads to high pressure drop within the unit.

6.4. Conclusions

A thorough study with different particle diameters is carried out for the Simulated Moving Bed Reactor unit. It is verified that the high amount of desorbent needed is due to the reverse reaction in the isomerization of xylenes rather than mass-transfer resistances; therefore, particles smaller than 0.5 mm do not bring significant advantages to the process. Moreover, for each particle size the best arrangement of columns is fairly constant although the difference became shorter for larger particles due to the mass-transfer in the solid phase. From the aforesaid it can be concluded that a relative small particle must be used when determining the proper configuration for this type of service. Finally, under a maximum allowable pressure drop of 685 kPa within the unit, the optimal particle diameter found is 0.62 mm with a productivity of 267.40 kg $m^{-3}h^{-1}$ and desorbent consumption of 0.06 m^3 kg^{-1}.

6.5. Nomenclature

DC = Desorbent consumption, m^3 kg^{-1}

DE = Deviation from the equilibrium

D_{eff} = Effective pore diffusivity, m^2 s^{-1}

d_p = Particle diameter, m

k_p = Intraparticle mass-transfer coefficient, s^{-1}

P = Pressure, kPa

PR = Productivity, kg $m^{-3}h^{-1}$

u = Interstitial velocity, m s^{-1}

u_s = Solid velocity, m s^{-1}

Greek letters

γ_j = Velocity ratio in zone j

ε = Bed porosity

μ = Viscosity, cP

ρ = Fluid density, kg m^{-3}

Abbreviations

SMB = Simulated Moving Bed

SMBR = Simulated Moving Bed Reactor

TMBR = True Moving Bed Reactor

6.6. References

[1] Sá Gomes, P., N. Lamia, and A. E. Rodrigues. 2009. "Design of a gas phase simulated moving bed for propane/propylene separation." *Chemical Engineering Science* no. 64 (6):1336-1357.

[2] Bergeot, G. 2010. *Extension du concept "One-column" au lit mobile simulé réactif. Application à la séparation réactive des C_8 aromatiques*, École doctorale Sciences et Ingénierie des Ressources, Procédés, Produits, Environnement, Institut National Polytechnique de Lorraine, France.

[3] Mun, S. 2013. "Improving performance of a tandem simulated moving bed process for sugar separation by making a difference in the adsorbents and the column lengths of the two subordinate simulated moving bed units." *Journal of Chromatography A* no. 1277:48-57.

[4] Jo, S. H., Q. Han, Y. W. Suh, J. B. Ryu, S. C. Yi, K. B. Lee, and S. Mun. 2009. "Particle-size optimization for a polymer coated silica gel in SMB chromatography for amino acid separation." *Journal of Liquid Chromatography and Related Technologies* no. 32 (19):2822-2838.

[5] Zhang, Z., M. Mazzotti, and M. Morbidelli. 2003. "Multiobjective optimization of simulated moving bed and Varicol processes using a genetic algorithm." *Journal of Chromatography A* no. 989 (1):95-108.

[6] Ergun, S. 1952. "Fluid flow through packed columns." *Chemical Engineering Progress* no. 48:89-94.

[7] Kim, J. K., and P. C. Wankat. 2003. "Scaling and Intensification Procedures for Simulated Moving-Bed Systems." *AIChE Journal* no. 49 (11):2810-2821.

[8] De Klerk, A. 2003. "Voidage variation in packed beds at small column to particle diameter ratio." *AIChE Journal* no. 49 (8):2022-2029.

[9] Azevedo, D. C. S., and A. E. Rodrigues. 1999. "Design of a simulated moving bed in the presence of mass-transfer resistances." *AIChE Journal* no. 45 (5):956-966.

[10] Wu, D. J., Z. Ma, and N. H. L. Wang. 1999. "Optimization of throughput and desorbent consumption in simulated moving-bed chromatography for paclitaxel purification." *Journal of Chromatography A* no. 855 (1):71-89.

[11] Ruthven, D. M., and C. B. Ching. 1989. "Counter-current and simulated counter-current adsorption separation processes." *Chemical Engineering Science* no. 44 (5):1011-1038.

[12] Houwing, J., H. A. H. Billiet, and L. A. M. Van der Wielen. 2003. "Mass-transfer effects during separation of proteins in SMB by size exclusion." *AIChE Journal* no. 49 (5):1158-1167.

[13] Jupke, A., A. Epping, and H. Schmidt-Traub. 2002. "Optimal design of batch and simulated moving bed chromatographic separation processes." *Journal of Chromatography A* no. 944 (1-2):93-117.

[14] Nam, H. G., M. G. Han, S. C. Yi, Y. K. Chang, S. Mun, and J. H. Kim. 2011. "Optimization of productivity in a four-zone simulated moving bed process for separation of succinic acid and lactic acid." *Chemical Engineering Journal* no. 171 (1):92-103.

[15] Silva, M. S. P., J. P. B. Mota, and A. E. Rodrigues. 2012. "Fixed-bed adsorption of aromatic C 8 isomers: Breakthrough experiments, modeling and simulation." *Separation and Purification Technology* no. 90:246-256.

[16] Minceva, M., and A. E. Rodrigues. 2005. UOP's Parex: Modeling, Simulations and Optimization. In *4th Mercosur Congress on Process Systems Engineering and 2nd Mercosur Congress on Chemical Engineering*. Rio de Janeiro, Brazil.

[17] Biressi, G., O. Ludemann-Hombourger, M. Mazzotti, R. M. Nicoud, and M. Morbidelli. 2000. "Design and optimisation of a simulated moving bed unit: Role of deviations from equilibrium theory." *Journal of Chromatography A* no. 876 (1-2):3-15.

[18] Toumi, A., and S. Engell. 2004. "Optimization-based control of a reactive simulated moving bed process for glucose isomerization." *Chemical Engineering Science* no. 59 (18):3777-3792.

[19] Zabka, M., P. S. Gomes, and A. E. Rodrigues. 2008. "Performance of simulated moving bed with conventional and monolith columns." *Separation and Purification Technology* no. 63 (2):324-333.

[20] Kim, S. G., H. G. Nam, J. H. Kim, and S. Mun. 2011. "Optimal design of a four-zone simulated moving bed process for separation of homoharringtonine and harringtonine." *Canadian Journal of Chemical Engineering* no. 89 (2):304-313.

Chapter 7: Simulated moving bed reactor: Dual-bed column

A dual-bed Simulated Moving Bed Reactor comprising an adsorbent/catalyst homogeneous mixture bed followed by just adsorbents within the columns is developed under the framework of the proposed aromatics complex. A method comprising dynamic optimizations of a single column is followed to estimate the optimum proportion of adsorbents and catalyst within the first bed in such a way that the rate of production of *p*-xylene is equal to its rate of adsorption. Afterwards, the switching time and the first bed length are optimized through successive simulations using the simulated moving bed reactor approach. Finally, an integrated method that combines less time-consuming true moving bed reactor results with rigorous simulated moving bed reactor calculations to accurate develop a dual-bed Simulated Moving Bed Reactor unit is proposed.

This chapter is based on: Gonçalves, J. C., and A. E. Rodrigues. 2015. "Simulated moving bed reactor for p-xylene production: Dual-bed column." Submitted to *Computers & Chemical Engineering*

7.1. Introduction

In Chapter 5 and 6 it was used the True Moving Bed Reactor (TMBR) simplified model to determine the optimum arrangement of columns, flow rates, particle size, and switching time of the Simulated Moving Bed Reactor (SMBR); however, the results were not obtained using the SMBR actual model. Generally, True Moving Bed (TMB) models provide fast and precise results of the real Simulated Moving Bed (SMB) unit, especially when a large number of columns are involved [1-3]. However, small deviations may cause large errors with very steep profiles at the outlet ports [4]; moreover, large oscillations in the products of SMB, due to high mass-transfer coefficients, are not properly reproduced by the TMB approach [5,6]. In the SMBR, the presence of catalysts throughout the columns increases said oscillations preventing the TMBR model to match the results of the actual SMBR unit. The aforesaid can be overcome by using a different distribution of adsorbents and catalysts that reduces the oscillations in the outlet ports and at the same time provides better interaction between both solids enhancing the performance of the unit.

Multilayer configurations alternating catalysts and adsorbents have been used in steam reforming of methane [7] and ethanol [8]; even layers of different adsorbents have been used in pressure swing adsorption units [9]. In the same spirit, an SMBR comprising dual-bed columns as shown in Figure 7.1 is proposed. The purpose of this chapter is then to study this innovative dual-bed SMBR for *p*-xylene production taking into account previous results obtained using the TMBR approach. Evidently, 24 adsorbent beds with length and diameter of 1.14 and 4.12 m are taken from the existing SMB facility; the unit operates at 200 ºC with a particle size of 0.62 mm as calculated in the previous chapter.

7.2. Mathematical model

7.2.1. Dual-bed column system

The system is modeled by means of the actual SMBR instead of a continuous TMBR as in the previous chapters. Since there are two different beds in each column, the counter-current movement of the solid phase does not provide constant product yields in the outlet ports at steady-state. The system must be simulated by the actual shifting of the inlet and outlet ports along the unit; nevertheless, the assumptions followed are those used in Chapter 5: isothermal operation, axial dispersed plug flow, constant flow rate in each zone, mass transfer described by linear driving force approximation, and similar physical characteristics for adsorbents and catalysts.

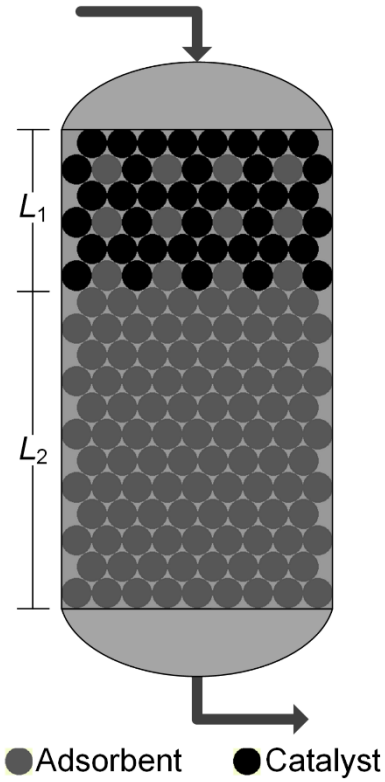

Figure 7.1 Distribution of adsorbents and catalysts within the columns of the simulated moving bed reactor. L_1 represents the length of the first bed with homogeneous mixture of adsorbent and catalyst; L_2 corresponds to the second bed with just adsorbents

Mass balances in the first bed (i.e., $0 < z < L_1$) for species i in the bulk phase, adsorbent particle phase, and catalyst particle phase are given by equations (7.1) to (7.3) respectively:

$$\frac{\partial C_i}{\partial t} = D_{ax}\frac{\partial^2 C_i}{\partial z^2} - u\frac{\partial C_i}{\partial z} - \frac{1-\varepsilon}{\varepsilon}\frac{3}{R_p}K_l\left[\varphi\left(C_i - \overline{C_{pi}}_{ads}\right) + (1-\varphi)\left(C_i - \overline{C_{pi}}_{cat}\right)\right] \quad (7.1)$$

$$\varepsilon_p\frac{\partial \overline{C_{pi}}_{ads}}{\partial t} + (1-\varepsilon_p)\rho_{ads}\frac{\partial \overline{q_i}}{\partial t} = \frac{3}{R_p}K_l\left(C_i - \overline{C_{pi}}_{ads}\right) \quad (7.2)$$

$$\varepsilon_p\frac{\partial \overline{C_{pi}}_{cat}}{\partial t} = \frac{3}{R_p}K_l\left(C_i - \overline{C_{pi}}_{cat}\right) + \rho_{cat}R_i \quad (7.3)$$

while in the second bed (i.e., $L_1 < z < L_c$) the catalyst is not present, which leads to mass balances for species i in just the bulk phase and adsorbent particle phase:

$$\frac{\partial C_i}{\partial t} = D_{ax}\frac{\partial^2 C_i}{\partial z^2} - u\frac{\partial C_i}{\partial z} - \frac{1-\varepsilon}{\varepsilon}\frac{3}{R_p}K_l\left(C_i - \overline{C_{pi}}_{ads}\right) \quad (7.4)$$

$$\varepsilon_p\frac{\partial \overline{C_{pi}}_{ads}}{\partial t} + (1-\varepsilon_p)\rho_{ads}\frac{\partial \overline{q_i}}{\partial t} = \frac{3}{R_p}K_l\left(C_i - \overline{C_{pi}}_{ads}\right) \quad (7.5)$$

where C_i is the concentration of each species in the bulk phase, D_{ax} is the axial dispersion coefficient, and u is the interstitial velocity. Physical properties such as bed porosity ε, particle porosity ε_p, particle radius R_p, density of adsorbent ρ_{ads} and catalyst ρ_{cat} are given in Chapter

5. The average mass adsorbed $\overline{q_i}$ and the reaction rate R_i are obtained from Bergeot [10] and used as function of the average particle concentration in the adsorbents ($\overline{C_{pi}}_{ads}$) and catalysts ($\overline{C_{pi}}_{cat}$) respectively as in the previous chapters. The adsorbent to adsorbent plus catalyst weight ratio ($\varphi = m_{ads}/m_{ads} + m_{cat}$) is calculated in the next section. The properties are calculated in the same manner and presented in Annex A; similarly, the internal mass-transfer coefficient is calculated using molecular diffusivity estimated by the Wilke-Chang method modified to include the mixed solvent case by Perkins and Geankoplis [11], and the external mass-transfer coefficient is estimated by the Wilson and Geankoplis correlation [12]. Danckwerts boundary conditions for species i are used for the bulk phase in equation (7.6) at the inlet and outlet of the column, while equation (7.7) guarantees continuity between the two beds providing the other boundary conditions in the bulk phase:

$$z = 0 \quad D_{ax}\frac{\partial C_i}{\partial z} = u\left(C_i - C_i^{in}\right); \quad z = L_c \quad \frac{\partial C_i}{\partial z} = 0 \tag{7.6}$$

$$C_i|_{L_1^-} = C_i|_{L_1^+}; \quad \left.\frac{\partial C_i}{\partial z}\right|_{L_1^-} = \left.\frac{\partial C_i}{\partial z}\right|_{L_1^+} \tag{7.7}$$

where the inlet concentration (C_i^{in}) depends on the specific zone within the unit and is determined by mass balances in each inlet and outlet port as in the previous studies (see Chapter 5). Furthermore, the performance parameters to assess the SMBR unit – productivity (PR), desorbent consumption (DC), and deviation from the equilibrium (DE) – are defined in the same manner, considering *p*-xylene in the extract point as the desired product. However, since the system is intrinsically dynamic, an average of the concentrations is calculated over the last cycle when the system has reached the cyclic steady-state:

Extract Purity:
$$\mathrm{PurX} = \frac{\int_t^{t+N_c t_s} C_{\mathrm{PX},X}\, dt}{\int_t^{t+N_c t_s}\left(C_{\mathrm{PX},X} + C_{\mathrm{MX},X} + C_{\mathrm{OX},X} + C_{\mathrm{EB},X}\right)dt} \tag{7.8}$$

Raffinate Purity:
$$\mathrm{PurR} = \frac{\int_t^{t+N_c t_s}\left(C_{\mathrm{MX},X} + C_{\mathrm{OX},X} + C_{\mathrm{EB},X}\right)dt}{\int_t^{t+N_c t_s}\left(C_{\mathrm{PX},X} + C_{\mathrm{MX},X} + C_{\mathrm{OX},X} + C_{\mathrm{EB},X}\right)dt} \tag{7.9}$$

Deviation from the Equilibrium:
$$\mathrm{DE} = \frac{Q_X \int_t^{t+N_c t_s} C_{\mathrm{PX},X} dt + Q_R \int_t^{t+N_c t_s} C_{\mathrm{PX},R} dt}{N_c t_s C_{\mathrm{PX},eq} Q_F} \tag{7.10}$$

Desorbent Consumption:
$$\mathrm{DC} = \frac{Q_D N_c t_s}{Q_X \int_t^{t+N_c t_s} C_{\mathrm{PX},X} dt} \tag{7.11}$$

Productivity:
$$\mathrm{PR} = \frac{Q_X \int_t^{t+N_c t_s} C_{\mathrm{PX},X} dt}{V_{ads+cat} N_c t_s} \tag{7.12}$$

where a cycle length is given by the number of columns (N_c) times the switching time (t_s). The SMBR unit is assumed to operate under cyclic steady state when the average concentrations of each species do not differ from those in the preceding cycle for more than 1 %.

7.2.2. Equivalence between TMBR and SMBR

As discussed in Chapter 5 and 6, in TMBR the flow rates are expressed as ratios of interstitial velocity to solid velocity (u^{TMBR}/u_s) where column length divided by the switching times gives the velocity of solid ($u_s = L_c/t_s$). Moreover, in TMBR the solid moves counter-currently while it is actually fixed in SMBR; hence, both models are related through the solid velocity: $u^{\mathrm{SMBR}} = u^{\mathrm{TMBR}} + u_s$. The equivalent SMBR flow rate is then calculated using the corresponding interstitial velocity.

7.2.3. Optimum adsorbent to adsorbent plus catalyst weight ratio

The adsorbent to adsorbent plus catalyst weight ratio to be used in the model is determined by minimizing the following objective function:

$$\min_{\varphi}\left\{\int_0^{t_s}\left(R_{ads,\mathrm{PX}} - R_{cat,\mathrm{PX}}\right)^2 dt\right\} \tag{7.13}$$

where $R_{ads,\mathrm{PX}}$ and $R_{cat,\mathrm{PX}}$ represent the average rate of adsorption and production of *p*-xylene as shown in equations (7.14) and (7.15). In other words, the optimal ratio is that where the amount of *p*-xylene entering into the adsorbents equals that leaving the catalysts:

$$R_{ads,\mathrm{PX}} = \varphi\int_o^{L_1}\left(C_{\mathrm{PX}} - \overline{C_{p,\mathrm{PX}}}_{ads}\right)dz \tag{7.14}$$

$$R_{cat,\mathrm{PX}} = -(1-\varphi)\int_0^{L_1}\left(C_{\mathrm{PX}} - \overline{C_{p,\mathrm{PX}}}_{cat}\right)dz \tag{7.15}$$

The optimizations are conducted in a single column using equations (7.1) to (7.3). Due to the dynamic behavior of the system an average over time must be used, in this case the switching time of the TMBR from Chapter 6 is used (i.e., 57 s). The flow and concentrations are also taken from said TMBR; the values of zone 3 are used since this zone favors the production of *p*-xylene. The inlet flow and concentrations are those entering to one of the columns in zone 3 while the initial concentration corresponds to the concentration of the next column which is what actually occurs within the columns of the simulated moving bed reactor; the process is repeated for each column in zone 3. Unfortunately up to this point L_1 is not known, the procedure must then be repeated for several values provided $L_1 < L_c$. Figure 7.2 presents the diagram to determine the optimum adsorbent to adsorbent plus catalyst weight ratio.

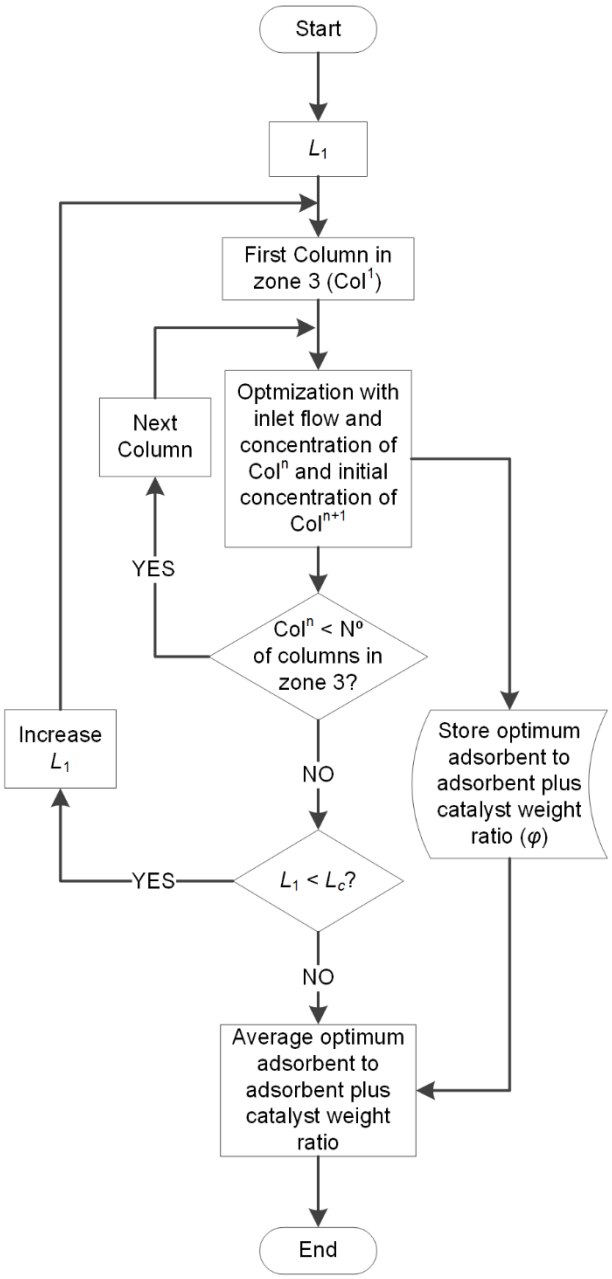

Figure 7.2 Flow diagram to determine the optimum adsorbent to adsorbent plus catalyst weight ratio (φ)

7.3. Results and discussion

All simulations are conducted with the commercial software gPROMS v.3.7.1 from Process Systems Enterprise (www.psenterprise.com). The numerical method involves the discretization of the axial domain of each column by the second-order orthogonal collocation method on 10 and 20 finite elements in the first and second bed respectively with 10^{-5} as tolerance. The extract and raffinate purity are set to 0.70 and 0.95 throughout the study as in the previous simulations.

7.3.1. Optimum adsorbent to adsorbent plus catalyst weight ratio

The dynamic optimizations are carried out using the solver (CVP_SS) of the commercial software gPROMS. The concentrations of each component in zone 3 to be used in the estimation of the optimum adsorbent to adsorbent plus catalyst weight ratio are presented in Table 7.1. The SMBR equivalent flow rate of zone 3 of the TMBR, which corresponds to configuration 2-6-14-2 with optimized flow and switching time (57 s) from Chapter 6, is used as inlet flow for each column (i.e., 747 $m^3\ h^{-1}$).

Table 7.1 Mass concentration (kg m^{-3}) at the inlet of each column in zone 3 for configuration 2-6-14-2 with optimized flow conditions from Chapter 6

Column	*p*-Xylene	*m*-Xylene	*o*-Xylene	Ethylbenzene	Toluene
1	157.44	346.95	86.67	97.08	9.28
2	146.59	334.06	86.48	96.10	33.95
3	141.65	321.38	86.17	95.05	52.84
4	137.83	311.98	86.00	94.30	66.94
5	134.40	303.86	85.86	93.67	79.23
6	131.15	296.41	85.73	93.10	90.63
7	127.66	288.65	85.57	92.51	102.63
8	124.22	281.21	85.37	91.96	114.29
9	120.37	273.14	85.09	91.36	127.12
10	115.43	263.12	84.68	90.63	143.29
11	109.47	251.50	84.13	89.80	162.37
12	101.11	235.92	83.32	88.72	188.40
13	87.94	212.79	82.08	87.21	227.90
14	61.18	168.99	79.34	83.87	305.83
15[a]	5.98	37.76	24.57	23.85	594.62

[a] To be used only for initial concentration of column 14

Table 7.2 presents the optimized φ for each column and the average value at several lengths values of L_1. Due to the feed concentration to the unit, there is not an optimum value that balances adsorption and reaction rates in the first column; thus, the value of φ is zero. A similar phenomena is observed for the last column at high L_1. The total average corresponds to a ratio of 0.35; however, the first bed is not expected to occupy a significant portion of the column bed since the reverse reaction may prevent the system from satisfying the purity requirements. The first bed fraction can be quickly estimated using the ratios of TMBR (φ^{TMBR}) and SMBR (φ^{SMBR}) by keeping the same amount of catalyst within the bed column: $L_1 = 100\left(1-\varphi^{\mathrm{TMBR}}\right)/\left(1-\varphi^{\mathrm{SMBR}}\right)$. The length of the first bed, using 0.9 and 0.35 for the ratios of TMBR and SMBR respectively, is about 15% of the length of the column; based on this value it would be more reasonable to use the average of just 10 and 20 %L_c giving a ratio of 0.4 corresponding to L_1 of 17 %L_c (rounded up to 20 %L_c).

Table 7.2 Optimum adsorbent to adsorbent plus catalyst weight ratio (φ) in each column for several lengths of the first bed (L_1) as percentage of column length (L_c)

Column	10 %L_c	20 %L_c	30 %L_c	40 %L_c	50 %L_c	60 %L_c	70 %L_c	80 %L_c	90 %L_c
1	0.00	0.00	0.00	0.00	0.00	0.00	0.00	0.00	0.00
2	0.58	0.57	0.55	0.50	0.47	0.44	0.42	0.41	0.41
3	0.59	0.58	0.55	0.51	0.48	0.46	0.45	0.45	0.45
4	0.58	0.57	0.53	0.50	0.47	0.45	0.44	0.44	0.44
5	0.55	0.53	0.50	0.47	0.44	0.42	0.42	0.42	0.43
6	0.49	0.46	0.41	0.37	0.34	0.34	0.35	0.36	0.37
7	0.49	0.47	0.43	0.39	0.37	0.37	0.39	0.40	0.41
8	0.49	0.46	0.43	0.39	0.38	0.38	0.39	0.41	0.42
9	0.41	0.38	0.33	0.30	0.30	0.32	0.34	0.36	0.38
10	0.42	0.40	0.36	0.34	0.34	0.36	0.38	0.40	0.42
11	0.39	0.37	0.33	0.32	0.33	0.35	0.38	0.40	0.43
12	0.35	0.31	0.28	0.29	0.31	0.34	0.37	0.40	0.43
13	0.22	0.18	0.17	0.20	0.24	0.28	0.32	0.36	0.39
14	0.22	0.04	0.00	0.00	0.00	0.00	0.00	0.00	0.00
Average	0.41	0.38	0.35	0.33	0.32	0.32	0.33	0.34	0.36

7.3.2. Configurations from TMBR to SMBR

Once the adsorbent to adsorbent plus catalyst weight ratio and the length of the first bed have been defined (i.e., $\varphi = 0.4$ and $L_1 = 20\ \%L_c$), the SMBR unit can be simulated based on the results using the TMBR approach from the previous chapter (see Table 6.3). Six configurations are taken with the corresponding flow rates in zones 1 and 4 and switching time from the optimization conducted using the TMBR approach. Table 7.3 presents the performance of said configurations at the peak of their separation regions which are depicted in Figure 7.3.

Table 7.3 Performance of the best configurations based on TMBR approach from Table 6.3 calculated using the SMBR approach. Flow rates in zones 1 and 4 (Q_1 and Q_4) and switching time (t_s) are those equivalent to TMBR while flow rates in zones 2 and 3 (Q_2 and Q_3) corresponds to the peak within the separation region.

Config	Q_1, $m^3\ h^{-1}$	Q_2, $m^3\ h^{-1}$	Q_3, $m^3\ h^{-1}$	Q_4, $m^3\ h^{-1}$	PR, $kg\ m^{-3}h^{-1}$	DC, $m^3\ kg^{-1}$	t_s, s
2-4-16-2	1640	641	682	380	136.53	0.12	59
2-5-15-2	1650	653	694	370	133.80	0.12	58
2-6-14-2	1650	665	707	370	133.58	0.12	57
3-4-15-2	1540	610	649	350	129.28	0.12	62
3-5-14-2	1550	621	661	350	128.93	0.12	61
3-4-14-3	1570	632	668	380	118.72	0.13	60

In the previous chapter, 2-6-14-2 was the optimum configuration as opposed to the results presented in Table 7.3. Nevertheless, the higher switching time of 2-4-16-2 shifts the separation

region (see Figure 7.3) to the left resulting in lower flow rate in zone 2 which in turns increases the flow rate in the extract leading to a higher productivity despite of the lower peak. Based on the aforementioned, the switching time must be adjusted.

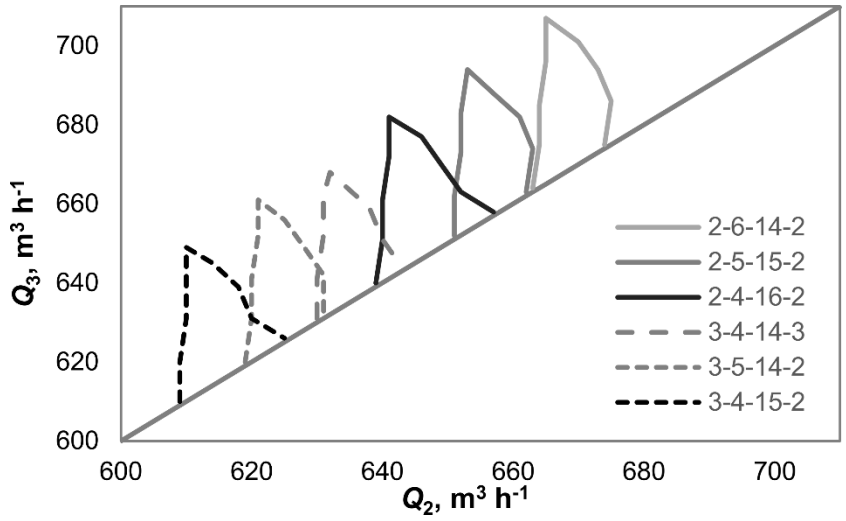

Figure 7.3 Separation regions of the best configurations based on TMBR approach from Table 6.3 calculated using the SMBR approach. Flow rates in zones 1 and 4 (Q_1 and Q_4) and switching time (t_s) are those equivalent to TMBR

7.3.3. Optimization of switching time

As stated before, in TMBR the flow rates are expressed as interstitial velocity to solid velocity ratio where the solid velocity depends on the switching time. The switching times presented in Table 7.3 are the result of simultaneous optimizations of said ratios and switching time; in other words, they affected the flow rates in each zone of the unit. In this case, several switching times are studied in the best three configurations maintaining the flow rates in zone 1 and 4 constant. Table 7.4 presents the performance at the peak of the separation region for switching times from 55 to 75 s.

Configuration 2-6-14-2 exhibits the best performance at 70 s switching time as it can be seen in Figure 7.4, which is higher than the 57 s switching time from the TMBR studies. As indicated by Sá Gomes et al. [1] and verified for this type of system in prior chapters, longer switching times result in higher feed flow rate due to the increased contact time up to a certain point where mass-transfer resistance limits the capacity of the unit causing a reduction in productivity. The flow rates in zones 2 and 3 for these units are slightly higher than those obtained with TMBR at the same switching time; higher rates pushes the optimum switching times to higher values in order to balance the contact time and mass-transfer resistance as previously indicated. Based on the aforementioned, it is expected to obtain longer switching times in SMBR compared to those obtained using the TMBR approach.

Table 7.4 Performance of configurations 2-6-14-2, 2-5-15-2, and 2-4-16-2 for several switching times (t_s) and fixed flow rates in zones 1 and 4 (Q_1 and Q_4). Flow rates in zones 2 and 3 (Q_2 and Q_3) corresponds to the peak within the separation region

Config	Q_1, $m^3 h^{-1}$	Q_2, $m^3 h^{-1}$	Q_3, $m^3 h^{-1}$	Q_4, $m^3 h^{-1}$	PR, kg $m^{-3}h^{-1}$	DC, $m^3 kg^{-1}$	t_s, s
2-6-14-2	1650	691	730	370	122.15	0.13	55
2-6-14-2	1650	629	674	370	147.35	0.11	60
2-6-14-2	1650	577	625	370	162.01	0.10	65
2-6-14-2	**1650**	**533**	**581**	**370**	**167.14**	**0.10**	**70**
2-6-14-2	1650	496	542	370	164.25	0.10	75
2-5-15-2	1650	691	730	370	123.43	0.13	55
2-5-15-2	1650	629	673	370	145.95	0.11	60
2-5-15-2	1650	577	624	370	160.38	0.10	65
2-5-15-2	1650	533	579	370	163.24	0.10	70
2-5-15-2	1650	496	541	370	162.31	0.10	75
2-4-16-2	1640	692	727	380	111.81	0.14	55
2-4-16-2	1640	630	670	380	134.60	0.12	60
2-4-16-2	1640	578	622	380	151.87	0.11	65
2-4-16-2	1640	534	578	380	156.58	0.10	70
2-4-16-2	1640	496	539	380	157.85	0.10	75

Bold indicates optimum

It is important to note that the optimum configuration based on the TMBR approach was also 2-6-14-2, which validates the use of equivalent TMBR as a preliminary study in the development of a dual-bed SMBR unit. This configuration is used in the rest of this thesis.

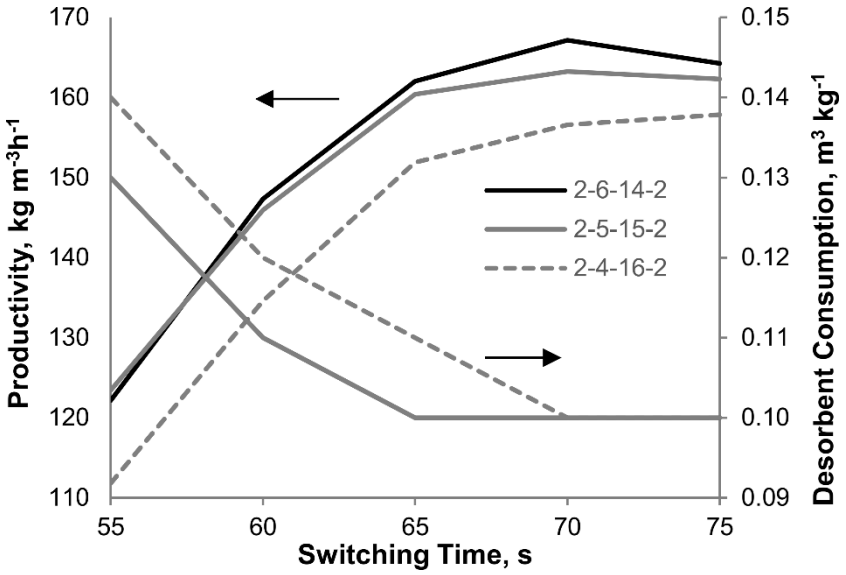

Figure 7.4 Variation of productivity and desorbent consumption of configurations 2-6-14-2, 2-5-15-2, and 2-4-16-2 for several switching times. Desorbent consumption of 2-6-14-2 and 2-5-15-2 are overlapped

7.3.4. Optimization of first-bed length

Up to this point the length of the first bed used, estimated in Section 7.3.1, was 20 %L_c. Table 7.5 presents the performance at the highest feed flow rate of 2-6-14-2 with 70 s switching time for first bed lengths from 5 to 25 %L_c.

Table 7.5 Performance of configuration 2-6-14-2 with 70 s switching time for several lengths of the first bed (L_1) as percentage of column length (L_c) and fixed flow rates in zones 1 and 4 (Q_1 and Q_4). Flow rates in zones 2 and 3 (Q_2 and Q_3) corresponds to the peak within the separation region

Q_1, $m^3 h^{-1}$	Q_2, $m^3 h^{-1}$	Q_3, $m^3 h^{-1}$	Q_4, $m^3 h^{-1}$	PR, kg $m^{-3}h^{-1}$	DC, $m^3 kg^{-1}$	DE	L_1, %L_c
1650	518	673	370	380.94	0.04	1.50	5
1650	526	609	370	287.89	0.06	2.02	10
1650	529	592	370	226.27	0.07	2.08	15
1650	533	581	370	167.14	0.10	2.02	20
1650	540	563	370	73.23	0.22	1.87	25

Higher values of productivity are obtained as the first bed length decreases, lower values of L_1 leads to higher amount of adsorbent allowing to process more feed within the unit. However, the optimum L_1 corresponds to appropriate balance between adsorbent and catalyst that maximizes the production of *p*-xylene while fulfilling the purity requirements, L_1 is then given by the highest DE value. For a 15 %L_c first bed the deviation from the equilibrium is 2.08; this value corresponds to a *p*-xylene in the extract to *p*-xylene in the feed ratio of 1.75, the highest among the lengths studied. One of the main purposes of this type of units is to produce more out of less; in fact, feed costs in *p*-xylene production could be as high as 80% [13]. Nevertheless, feedstock availability and downstream requirements could justify to operate with 10 %L_c which allows to process about 32% more feed with still high value of DE (2.02) that corresponds to 1.69 *p*-xylene in the extract to *p*-xylene in the feed ratio. Actually, these figures verify the superior performance of the dual-bed SMBR compared to that of homogeneous mixture; in Chapter 6, the optimum unit exhibited lower productivity and deviation from the equilibrium (267.40 kg $m^{-3}h^{-1}$ and 1.71 respectively) with higher feed flow rate (92 $m^3 h^{-1}$).

7.3.5. Influence of different adsorbent to adsorbent plus catalyst weight ratios

Several weight ratios of adsorbent to adsorbent plus catalyst are evaluated for a SMBR with 2-6-14-2 configuration, 70 s switching time, and 15 %L_c first bed length in order to validate the procedure followed in Section 7.2.3. The results for ratios from 0.3 to 0.6 are presented in Table 7.6.

Table 7.6 Performance of configuration 2-6-14-2 for several adsorbent to adsorbent plus catalyst weight ratio (φ) and fixed flow rates in zones 1 and 4 (Q_1 and Q_4). Flow rates in zones 2 and 3 (Q_2 and Q_3) corresponds to the peak within the separation region

Q_1, $m^3\ h^{-1}$	Q_2, $m^3\ h^{-1}$	Q_3, $m^3\ h^{-1}$	Q_4, $m^3\ h^{-1}$	PR, $kg\ m^{-3}h^{-1}$	DC, $m^3\ kg^{-1}$	DE	φ
1650	530	588	370	206.08	0.08	2.06	0.3
1650	529	592	370	226.27	0.07	2.08	0.4
1650	529	600	370	250.21	0.06	2.05	0.5
1650	527	609	370	282.92	0.06	2.01	0.6

Similarly to the first bed length optimization, the productivity increases for higher ratios due to the higher amount of adsorbent present within the columns. A ratio of 0.4 provides the most efficient distribution of adsorbents and catalysts giving the highest deviation from the equilibrium validating the proposed method; although the difference on DE between the ratios studied is very small. As in the case of L_1, 12% more feed can be processed with 0.5 adsorbent to adsorbent plus catalyst weight ratio.

7.3.6. SMBR/TMBR integrated method

Due to the dynamic nature of the dual-bed SMBR unit, it is not possible to carry out fast optimizations at steady-state as in TMBR studies; therefore, it is mandatory to find analogies and develop an integrated method involving both approaches for the design of the SMBR for the production of *p*-xylene. Actually, a single run of a dual-bed SMBR initially filled with toluene takes on average 5.5 hours to reach cyclic steady-state (about 27 cycles) compared to just a few seconds for the equivalent TMBR.

A methodology to determine the optimum configuration and operating conditions of a dual-bed SMBR for *p*-xylene production can be summarized as follows:

1. Determine optimum arrangement of columns, flow rates, switching time, and particle size of the SMBR with homogeneous mixture containing a high adsorbent to adsorbent plus catalyst weight ratio (e.g., 0.9) using TMBR approach as shown in Chapter 6.
2. Determine optimum adsorbent to adsorbent plus catalyst weight ratio using the concentration profiles and flow rates of the optimum unit from TMBR through dynamic optimizations as presented in Section 7.2.3
3. Optimize switching time in the dual-bed SMBR using constant flow rates in zones 1 and 4 and arrangement of columns from TMBR results maximizing productivity through SMBR approach.

4. Finally, adjust the length of the first bed according to feed and product requirements through SMBR approach.

Concentration profiles of the dual-bed SMBR developed in this work (2-6-14-2, 15 %L_c, 0.4 ratio, 70 s switching time) under cyclic steady-state at the middle of the switching time and its equivalent TMBR (2-6-14-2, 0.9 ratio, 70 s switching time), with flow rates calculated accordingly based on SMBR flow rates, are displayed in Figure 7.5. Even though TMBR present a steeper profile (as expected), both models are remarkable similar. Very often, controllers for SMB units are based on its TMB model [14]; in this case, TMBR may be used in the development of controllers of the dual-bed SMBR unit.

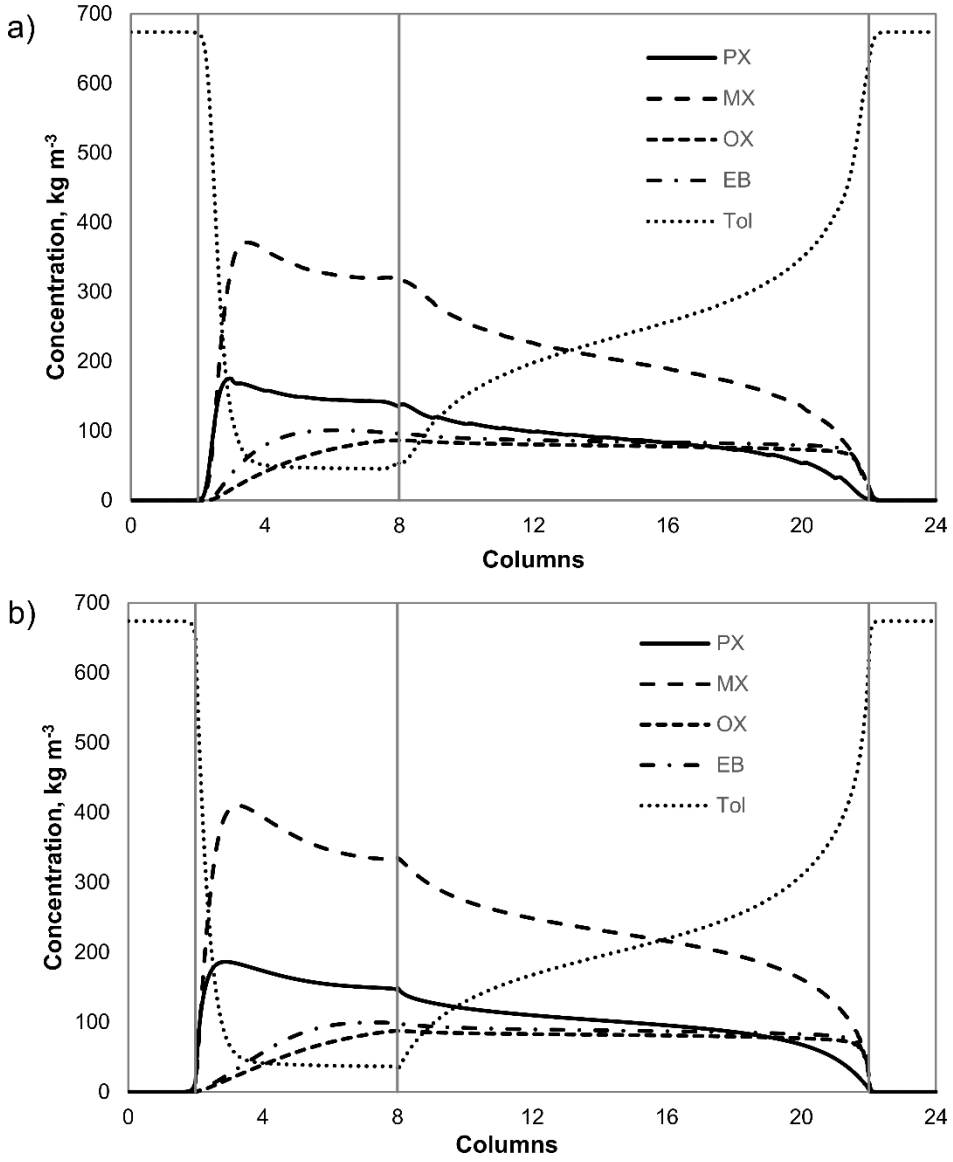

Figure 7.5 Concentration profile for a) SMBR under cyclic steady-state at the middle of the switching time and b) equivalent TMBR

7.4. Conclusions

A dual-bed SMBR is developed comprising 15% of column bed filled with homogeneous mixture of adsorbent and catalyst with a ratio of 0.4 and the rest of the column filled just with adsorbents, column configuration of 2-6-14-2 and a switching time of 70 s. The unit exhibits a productivity of 226.27 kg $m^{-3}h^{-1}$, a desorbent consumption of 0.07 m^3 h^{-1}, and an interesting deviation from the equilibrium of 2.08 that allows to obtain in the extract 175% of the *p*-xylene fed to the unit under the studied conditions. An integrated method is proposed to efficiently use the results from less time-consuming TMBR in the development of the dual-bed SMBR. Additionally, a simplified procedure to estimate optimum adsorbent to adsorbent plus catalyst weight ratio for the adsorption and reaction of *p*-xylene is validated.

7.5. Nomenclature

C_i = Concentration of component i, kg m^{-3}

$\overline{C_{pi}}_{ads}$ = Average particle concentration of component i in the adsorbent, kg m^{-3}

$\overline{C_{pi}}_{cat}$ = Average particle concentration of component i in the catalyst, kg m^{-3}

$C_{\mathrm{PX},eq}$ = p-Xylene concentration in equilibrium, kg m^{-3}

D_{ax} = Axial dispersion coefficient, m^2 s^{-1}

DC = Desorbent consumption, m^3 kg^{-1}

DE = Deviation from the equilibrium

L_1 = Length of first bed, m

L_2 = Length of second bed, m

L_c = Length of column, m

m_{ads} = Mass of adsorbent, kg

m_{cat} = Mass of catalyst, kg

N_c = Number of columns

PR = Productivity, kg $m^{-3}h^{-1}$

PurX = Extract purity

PurR = Raffinate purity

Q_j = Volumetric flow rate in zone j, $m^3\ s^{-1}$

q_i = Adsorbed concentration of component i, $kg\ kg^{-1}$

R_p = Particle radius, m

$R_{ads,i}$ = Adsorption rate of component i, $kg\ m^{-2}s^{-1}$

$R_{cat,i}$ = Reaction rate of component i, $kg\ m^{-2}s^{-1}$

t = Time, s

t_s = Switching time, s

u = Interstitial velocity, $m\ s^{-1}$

u_s = Solid velocity, $m\ s^{-1}$

$V_{ads+cat}$ = Adsorbent plus catalyst volume, m^3

z = Axial coordinate, m

Greek letters

ε = Bed porosity

ε_p = Particle porosity

ρ_{ads}= Density of adsorbent, $kg\ m^{-3}$

ρ_{cat}= Density of catalyst, $kg\ m^{-3}$

φ = Adsorbent to adsorbent plus catalyst weight ratio

Abbreviations

D = Desorbent

F = Feed

MX = *m*-Xylene

OX = *o*-Xylene

PX = *p*-Xylene

R = Raffinate

SMB = Simulated Moving Bed

SMBR = Simulated Moving Bed Reactor

TMB = True Moving Bed

TMBR = True Moving Bed Reactor

X = Extract

Superscripts and subscripts

in = Inlet

7.6. References

[1] Sá Gomes, P., N. Lamia, and A. E. Rodrigues. 2009. "Design of a gas phase simulated moving bed for propane/propylene separation." *Chemical Engineering Science* no. 64 (6):1336-1357.

[2] Pais, L. S., J. M. Loureiro, and A. E. Rodrigues. 1998. "Modeling Strategies for Enantiomers Separation by SMB Chromatography." *AIChE Journal* no. 44 (3):561-569.

[3] Ruthven, D. M., and C. B. Ching. 1989. "Counter-current and simulated counter-current adsorption separation processes." *Chemical Engineering Science* no. 44 (5):1011-1038.

[4] Beste, Y. A., M. Lisso, G. Wozny, and W. Arlt. 2000. "Optimization of simulated moving bed plants with low efficient stationary phases: Separation of fructose and glucose." *Journal of Chromatography A* no. 868 (2):169-188.

[5] Grosfils, V., C. Levrie, M. Kinnaert, and A. Vande Wouwer. 2007. "On simplified modelling approaches to SMB processes." *Computers & Chemical Engineering* no. 31 (3):196-205.

[6] Zhong, G., and G. Guiochon. 1997. "Simulated moving bed chromatography. Effects of axial dispersion and mass transfer under linear conditions." *Chemical Engineering Science* no. 52 (18):3117-3132.

[7] Oliveira, E. L. G., C. A. Grande, and A. E. Rodrigues. 2011. "Effect of catalyst activity in SMR-SERP for hydrogen production: Commercial vs. large-pore catalyst." *Chemical Engineering Science* no. 66 (3):342-354.

[8] Cunha, A. F., Y. J. Wu, F. A. Díaz Alvarado, J. C. Santos, P. D. Vaidya, and A. E. Rodrigues. 2012. "Steam reforming of ethanol on a Ni/Al 2O 3 catalyst coupled with a hydrotalcite-like sorbent in a multilayer pattern for co 2 uptake." *Canadian Journal of Chemical Engineering* no. 90 (6):1514-1526.

[9] Bárcia, P. S., J. A. C. Silva, and A. E. Rodrigues. 2010. "Octane Upgrading of C5/C6 Light Naphtha by Layered Pressure Swing Adsorption." *Energy & Fuels* no. 24 (9):5116-5130.

[10] Bergeot, G. 2010. *Extension du concept "One-column" au lit mobile simulé réactif. Application à la séparation réactive des C_8 aromatiques*, École doctorale Sciences et Ingénierie des Ressources, Procédés, Produits, Environnement, Institut National Polytechnique de Lorraine, France.

[11] Poling, B. E., J. M. Prausnitz, and J. J. P. O'Connell. 2001. *The Properties of Gases and Liquids*. 5th ed. New York: The McGraw-Hill Companies.

[12] Ruthven, D. M. 1984. *Principles of Adsorption and Adsorption Processes*. First ed. New York: John Wiley & Sons, cop.

[13] Alario, F., and J. Rault. 2002. Boost you Xylene Loop Performance with OPARIS. edited by Axens: Axens.

[14] Haag, J., A. Vande Wouwer, S. Lehoucq, and P. Saucez. 2001. "Modeling and simulation of a SMB chromatographic process designed for enantioseparation." *Control Engineering Practice* no. 9 (8):921-928.

Chapter 8: Proposed aromatics complex

The proposed aromatics complex is analyzed quantitatively in this chapter. Two cases are studied with different flow rates of reformate fed to the complex to obtain the increase in the production of *p*-xylene and benzene. The mass balance is calculated considering complete separation within the distillation columns and more rigorous models for the isomerization and simulated moving bed reactor unit developed in previous chapters. The performance of the selective toluene disproportionation unit is estimated based on conversion and selectivity reported in the literature while solid-liquid equilibria is used to determine the theoretical recovery of the crystallization unit.

8.1. Introduction

The main objective of this thesis is the development of a simulated moving bed reactor (SMBR) unit for the production of *p*-xylene in the framework of a modified aromatics complex leading to an increase in the production of *p*-xylene and benzene. The proposed aromatics complex is described in Chapter 5 and is analyzed in this Chapter. Models and results obtained in previous chapters along with simplified models for the rest of the units are used with the purpose of calculating the mass balance of the complex and determining the increase in the production of *p*-xylene and benzene.

8.2. Mathematical modeling

The most employed separation unit within the complex is the distillation column, throughout the calculations the outlet streams of said units are estimating assuming complete separation of the corresponding key components. The SMBR unit is taken from Chapter 7 with a first bed length of 15% and adsorbent to adsorbent plus catalyst weight ratio of 0.4 and the isomerization unit corresponds to that of Chapter 4 assuming 5 and 25 wt% of hydrogen and naphthenes respectively. The models for the selective toluene disproportionation (STDP) and the crystallization unit are described in detail further on. Moreover, the non-aromatic components and heavy aromatics (i.e., C_9+) are not taken into account.

8.2.1. Selective toluene disproportionation

This unit is intended to convert toluene in more valuable *p*-xylene and benzene through disproportionation of two molecules of toluene. Normally, the reaction is carried out in the presence of hydrogen to extend the catalyst life by suppressing cracking; therefore, benzene is also produced by the dealkylation of toluene [1,2]. The parameters used for this unit are presented in Table 8.1:

Table 8.1 Selective toluene disproportionation unit parameters

Toluene conversion, %	25[a]
Benzene / Xylenes, molar	1.5[a]
Xylene distribution, %	
p-Xylene	89.8[b]
m-Xylene	9.4[b]
o-Xylene	0.8[b]

[a] from Beck et al. [3]. [b] from Ji et al. [4]

8.2.2. Single stage crystallization

Crystallization processes are based on solid-liquid equilibria [5]; as the temperature is reduced the solute solubility decreases resulting in saturation and, subsequently, precipitation of pure component crystals for eutectic mixtures [6,7]. The solubility of xylenes is calculated by equation (8.1) from Hildebrand et al. [8] assuming ideal behavior, i.e., the influence of activity coefficients is neglected [9,10]:

$$\ln x_i = \frac{\Delta H_i^{fusion}}{R}\left(\frac{1}{T_{m,i}} - \frac{1}{T}\right) + \frac{\Delta C_{p,i}}{R}\left(\ln\frac{T}{T_{m,i}} + \frac{T_{m,i}}{T} - 1\right) \tag{8.1}$$

where x_i is the molar fraction of component *i* in liquid phase at temperature *T*, and ΔH_i^{fusion} and $\Delta C_{p,i}$ are the heat of fusion and the difference of the liquid and solid capacities for pure component *i* at its melting point $T_{m,i}$; the values are reported in Section A.4 in Annex A. The procedure consists of reducing the temperature until a second component reaches saturation (i.e., eutectic point), which is calculated through equation (8.2) based on a simple mass balance:

$$x_{i,T-1} = x_{i,T}\frac{1 - x_{\mathrm{PX},T-1}}{1 - x_{\mathrm{PX},T}} \tag{8.2}$$

where $x_{i,T}$ is the molar fraction of component *i* in the mother liquor at temperature *T* and $x_{i,T-1}$ is its molar fraction at a lower temperature; x_{PX} is obtained from equation (8.1) at the corresponding temperature. The eutectic point corresponds to the temperature when the molar fraction from equation (8.2) is higher than that calculated with equation (8.1). Normally, *p*-xylene is the first component to precipitate and the eutectic point is determined by *m*-xylene [9,11].

8.3. Results and discussion

The block diagram of the proposed aromatics complex is presented in Figure 8.1 along with the mass balance for two cases. Case I corresponds to the current feed of reformate (stream 1) to the aromatics complex based on the 90% of the nominal capacity by Galp Energia [12], the double is used in Case II.

The reformate is sent to the fractionation column where benzene, toluene, and non-aromatics are separated through the top and sent to the aromatics extraction unit where non-aromatics are separated and benzene and toluene (stream 2) is mixed with the outlet of the STDP unit and sent to the benzene column to obtain benzene as final product (stream 11). The bottom of the fractionation is mixed with the recycle from the isomerization unit and fed to the xylene splitter. Composition of xylenes in stream 1 is estimated assuming equilibrium in gas phase at 525 ºC

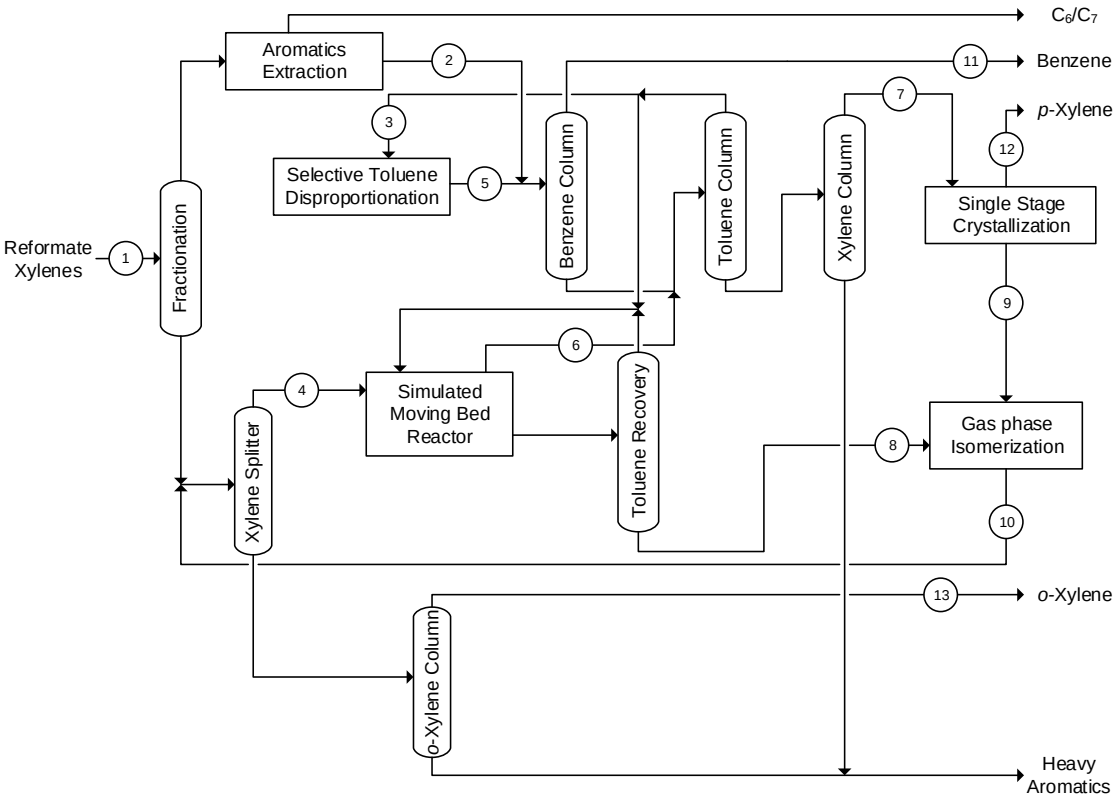

Stream	1	2	3	4	5	6	7	8	9	10	11	12	13
Case I													
Flow, ton h^{-1}	32.00	20.60	64.60	23.95	64.60	567.03	24.53	6.84	6.81	13.65	13.18	17.72	1.10
Ben,wt%	15.31	23.79	0.00	0.00	12.81	0.00	0.00	0.00	0.00	0.00	100.00	0.00	0.00
Tol, wt%	49.06	76.21	100.00	0.00	75.58	97.00	0.00	0.00	0.00	0.00	0.00	0.00	0.00
PX, wt%	7.81	0.00	0.00	23.53	10.43	2.10	76.04	2.83	13.74	22.98	0.00	100.00	0.00
MX, wt%	16.52	0.00	0.00	50.16	1.09	0.88	23.24	14.06	83.66	49.28	0.00	0.00	0.00
OX, wt%	7.49	0.00	0.00	16.60	0.09	0.01	0.54	50.36	1.95	19.63	0.00	0.00	100.00
EB, wt%	3.81	0.00	0.00	9.71	0.00	0.01	0.18	32.75	0.65	8.11	0.00	0.00	0.00
Case II													
Flow, ton h^{-1}	64.00	41.20	131.47	58.16	131.47	757.95	47.99	24.72	12.84	37.56	26.65	35.15	2.20
Ben,wt%	15.31	23.79	0.00	0.00	12.81	0.00	0.00	0.00	0.00	0.00	100.00	0.00	0.00
Tol, wt%	49.06	76.21	100.00	0.00	75.58	95.68	0.00	0.00	0.00	0.00	0.00	0.00	0.00
PX, wt%	7.81	0.00	0.00	23.43	10.43	3.07	76.93	5.12	13.74	22.98	0.00	100.00	0.00
MX, wt%	16.52	0.00	0.00	50.01	1.09	1.09	20.19	39.34	75.47	49.28	0.00	0.00	0.00
OX, wt%	7.49	0.00	0.00	17.14	0.09	0.06	1.23	37.01	4.61	19.63	0.00	0.00	100.00
EB, wt%	3.81	0.00	0.00	9.42	0.00	0.10	1.65	18.53	6.18	8.11	0.00	0.00	0.00

Figure 8.1 Block diagram and mass balance of the proposed aromatics complex

(operating condition in naphtha reforming) using the expressions developed by Chirico and Steele [13]. A portion of *o*-xylene is separated in the splitter and sent to the *o*-xylene column to obtain the final product (stream 13). The top of the splitter is sent to the SMBR unit where a high *p*-xylene stream with desorbent toluene (stream 6) is obtained and mixed with also a high *p*-xylene mixture of xylene with non-reacted toluene from the STDP unit. Toluene is separated in the toluene column and recycled back to be used as desorbent and the rest (stream 3) is sent to disproportionation to be converted into benzene and xylenes. Heavy aromatics formed in the reactions are withdrawn in the xylene column and the high *p*-xylene stream (stream 7) is sent to

the single stage crystallization unit where *p*-xylene is obtained as final product (stream 12). Toluene in the low *p*-xylene content stream from the SMBR is separated in the toluene recovery column, the xylene mixture is then sent to the gas phase isomerization unit (stream 8) along with the outlet from the crystallization (stream 9) where thermodynamic equilibrium is re-established by producing *p*-xylene out of *o*- and *m*-xylene and ethylbenzene and recycled back (stream 10) to the xylene splitter. The gas phase isomerization unit includes a dedicated fractionation tower to separate the naphthenes required for the isomerization of ethylbenzene as presented in Section 2.6.4 in order to prevent the unnecessarily circulation of said species in the SMBR and crystallization units.

8.3.1. Case I

The production of benzene corresponds to 117.5 thousand mtpy (based on 335 days of operation per year) which represents an improvement of 170% compared to the current production. In the case of *p*-xylene, 158 thousand mtpy is obtained representing 72% more *p*-xylene within the proposed aromatics complex. The production of *o*-xylene is not modified.

The *p*-xylene concentration fed to the crystallization unit is above the minimum set in Chapter 5 (75%). The temperature at which *m*-xylene starts to drop out of the mother liquor is 219 K, the operating temperature is therefore fixed at 220 K. It can be seen in Table 8.2 that *m*-xylene fraction in the mother liquor exceeds its solubility at 219 K, therefore the operation must be carried out above this point. *o*-Xylene has the highest melting point after *p*-xylene, however it is not the second species to crystallize since its molar fraction is significantly lower than that of *m*-xylene. Moreover, ethylbenzene presents unrealistic values of solubility at these temperatures because its melting point is very distant. Even though the temperature is higher than the colder stage of the conventional crystallization (213 K), is not high enough to use only one refrigeration system. Practical limitations of propylene refrigeration systems limit the temperature to 244 K [14]; a two stage crystallization unit might be more energetically efficient. Nevertheless, the recovery in the crystallization unit is 95%.

The increment in the production of *p*-xylene in the SMBR compared to the current separation unit is only 15% while the rest is provided by selective toluene disproportionation. This is due to a considerably reduction in the outlet stream from the isomerization unit leading to lower feed to the SMBR unit. It has been seen that for the SMBR the extract flow rate is significantly higher than the raffinate due to the continuous production of *p*-xylene, this results in lesser xylenes sent to the isomerization unit. Minceva and Rodrigues [15] used a feed of 87 m^3 h^{-1} in their optimization studies of the existing separation unit; in this case the feed is reduced to about 35 m^3 h^{-1}. Furthermore, since the feed is considerably lower less amount of desorbent can be used;

the equivalent true moving bed approach model is used to calculate the corrected flow rates in zones 1 and 4 of the SMBR unit maintaining the same switching time, Table 8.3 presents the parameters and performances of the SMBR unit for each case.

Table 8.2 Solubility and actual molar fractions of the mother liquor at several temperatures for cases I and II

	T, K	222	221	220	219	218	217	216
	Solubility from equation (8.1)							
	OX	0.474	0.460	0.446	0.432	0.418	0.405	0.392
	MX	0.913	0.888	0.863	0.839	0.816	0.793	0.771
	PX	0.148	0.143	0.138	0.133	0.128	0.124	0.119
	EB	3.998	3.884	3.773	3.665	3.559	3.456	3.356
	Molar fraction in the mother liquor from equation (8.2)							
	OX	0.019	0.019	0.019	0.020	0.020	0.020	0.020
Case I	MX	0.826	0.831	0.836	0.841	0.846	0.850	0.854
	PX	0.148	0.143	0.138	0.133	0.128	0.124	0.119
	EB	0.006	0.006	0.006	0.006	0.007	0.007	0.007
	Molar fraction in the mother liquor from equation (8.2)							
	OX	0.046	0.046	0.046	0.046	0.047	0.047	0.047
Case II	MX	0.746	0.750	0.754	0.759	0.763	0.767	0.771
	PX	0.148	0.143	0.138	0.133	0.128	0.124	0.119
	EB	0.061	0.061	0.062	0.062	0.062	0.063	0.063

The aforementioned indicates that the SMBR and isomerization units are now oversized for their corresponding services, the reformate supplied to the aromatics complex must be increased in order to provide more efficient use of the existing said units assuming appropriate upstream equipment to handle the increased rates.

Table 8.3 Configuration of the SMBR unit for cases I and II with 70 s switching time

Case	Q_1, $m^3\ h^{-1}$	Q_2, $m^3\ h^{-1}$	Q_3, $m^3\ h^{-1}$	Q_4, $m^3\ h^{-1}$	PR, $kg\ m^{-3}h^{-1}$	DC, $m^3\ kg^{-1}$	DE	L_1, $\%L_c$
I	1370	529	564	480	150.68	0.07	2.32	15
II	1650	526	610	370	293.35	0.06	1.94	10

8.3.2. Case II

The production now corresponds to 238 thousand mtpy which represents an improvement of 447% in benzene and 314 thousand mtpy representing 241% in *p*-xylene using the double of the current feed within the aromatics complex. The production of *o*-xylene in this case is also doubled. Even though 300 and 700 thousand mtpy of benzene and *p*-xylene are not achieved, the increase in production of said products is still very remarkable.

The ratio of benzene to xylene from STDP can be modified through the catalyst employed. Low Si/Al ratio increases dealkylation of toluene leading to more production of benzene; if an equimolar mixture is desired high Si/Al ratio should be used [1]. Even more *p*-xylene can be produced by alkylation of toluene with methanol where also a high *p*-xylene content stream can be sent to a crystallization unit [16].

In case II the eutectic point in the crystallization unit is 216 K due to the slightly higher concentration of *p*-xylene with consequently lower amount of *m*-xylene which is the second compound to crystallize (see Table 8.2). However, the operating temperature is maintained at 220 K corresponding to a recovery of 95% since no significant improvement is observed between the two temperatures.

The feed to the SMBR is higher than that in case I as expected, around 84 $m^3\ h^{-1}$ are sent to the unit due to the doubled rate from the fractionation bottom and the increased recycle from the isomerization unit. Moreover, the unit configuration used in case I shall be modified to handle the larger feed; a first bed of 10% is now used as it was discussed in Section 7.3.4 in Chapter 7. It can be seen in Table 8.3 that the productivity in case II is considerably higher due to the larger feed involved; however, case I SMBR seems to be more efficient regarding the process intensification since it possesses higher deviation from the equilibrium, in fact, case II SMBR doubles the production of *p*-xylene with a feed higher by 2.4 times.

8.4. Conclusions

The proposed aromatics complex is analyzed and mass balances for the currently feed to the system and a hypothetically two fold feed are presented. In both cases the production of benzene and *p*-xylene is significantly enhanced, a 170% and 72% respectively for the first case and 447% and 241% respectively for the second case compared to the current production. It is verified that an extract purity of 0.70 in the SMBR unit guarantees *p*-xylene content higher than 75% leading to a 95% recovery within the single stage crystallization unit. Moreover the SMBR unit proves to be flexible to handle different feed flow rates and the flow in the gas phase isomerization unit is significantly reduced.

8.5. Nomenclature

C_p = Heat capacity, $J\ mol^{-1}K^{-1}$

DC = Desorbent consumption, $m^3\ kg^{-1}$

DE = Deviation from the equilibrium

H^{fusion} = Heat of fusion, kJ mol^{-1}

L_1 = Length of first bed, m

L_c = Length of column, m

PR = Productivity, kg m^{-3}h^{-1}

Q_j = Volumetric flow rate in zone j, m^3 s^{-1}

R = Universal gas constant, kJ mol^{-1}K^{-1}

T = Temperature, K

T_m = Melting point, K

x_i = Mole fraction of component i

Abbreviations

Ben = Benzene

EB = Ethylbenzene

MX = *m*-Xylene

OX = *o*-Xylene

PX = *p*-Xylene

SMBR = Simulated moving bed reactor

STDP = Selective toluene disproportionation

Tol = Toluene

Superscripts and subscripts

T = At temperature *T*

8.6. References

[1] Kareem, A., S. Chand, and I. M. Mishra. 2001. "Disproportionation of Toluene to Produce Benzene and p- Xylene - A Review." *Journal of Scientific and Industrial Research* no. 60 (4):319-327.

[2] Das, J., Y. S. Bhat, and A. B. Halgeri. 1994. "Selective toluene disproportionation over pore size controlled MFI zeolite." *Industrial and Engineering Chemistry Research* no. 33 (2):246-250.

[3] Beck, J. S., D. H. Olson, and S. B. McCullen. 1994. *Selective toluene disproportionation process (STDP) with ex situ selectivated zeolite catalyst.* US 5,367,099 A. Mobil Oil Corp.

[4] Ji, Y. J., B. Zhang, L. Xu, H. Wu, H. Peng, L. Chen, Y. Liu, and P. Wu. 2011. "Core/shell-structured Al-MWW@B-MWW zeolites for shape-selective toluene disproportionation to para-xylene." *Journal of Catalysis* no. 283 (2):168-177.

[5] Jakob, A., R. Joh, C. Rose, and J. Gmehling. 1995. "Solid-liquid equilibria in binary mixtures of organic compounds." *Fluid Phase Equilibria* no. 113 (1-2):117-126.

[6] Mullin, J. W. 2001. "Industrial techniques and equipment." In *Crystallization*, edited by J. W. Mullin, 315-402. Oxford: Butterworth-Heinemann.

[7] Radhakrishnan, K. B., and A. R. Balakrishnan. 2001. "Kinetics of melt crystallization of organic eutectic forming binary mixtures in non-flow systems." *Chemical and Engineering Processing* no. 40 (1):71-81.

[8] Hildebrand, J. H., J. M. Prausnitz, and R. L. Scott. 1970. *Regular and Related Solutions: the solubility of gases, liquids, and solids*. First ed. New York: Van Nostrand Reinhold Co.

[9] Patience, D. B., J. B. Rawlings, and H. A. Mohameed. 2001. "Crystallization of para-xylene in scraped-surface crystallizers." *AIChE Journal* no. 47 (11):2441-2451.

[10] Beierling, T., R. Gorny, and G. Sadowski. 2013. "Modeling growth rates in static layer melt crystallization." *Crystal Growth and Design* no. 13 (12):5229-5240.

[11] Seki, H., S. Amano, and G. Emoto. 2010. "Modeling and control system design of an industrial crystallizer train for para-xylene recovery." *Journal of Process Control* no. 20 (9):999-1008.

[12] Galp Energia. *Fábrica de aromáticos e solventes*. http://www.galpenergia.com/PT/agalpenergia/os-nossos-negocios/Refinacao-Distribuicao/ARL/Refinacao/RefinariaMatosinhos/Paginas/FabricaAromaticosSolventes.aspx 2015.

[13] Chirico, R. D., and W. V. Steele. 1997. "Thermodynamic Equilibria in Xylene Isomerization. 5. Xylene Isomerization Equilibria from Thermodynamic Studies and Reconciliation of Calculated and Experimental Product Distributions." *J. Chem. Eng. Data* no. 42 (4):784-790.

[14] Starkey, D. R., J. L. Andrews, S. L. Luo, and K. J. Knob. 2009. PxMax with Crystallization. An Integrated Process for High Purity Paraxylene Production. edited by ExxonMobil: ExxonMobil Chemical Technology Licensing LLC.

[15] Minceva, M., and A. E. Rodrigues. 2005. "Two-level optimization of an existing SMB for p-xylene separation." *Computers and Chemical Engineering* no. 29 (10):2215-2228.

[16] Alabi, W., L. Atanda, R. Jermy, and S. Al-Khattaf. 2012. "Kinetics of toluene alkylation with methanol catalyzed by pure and hybridized HZSM-5 catalysts." *Chemical Engineering Journal* no. 195–196 (0):276-288.

Chapter 9: Xylene isomerization in liquid phase

Three large-pore zeolites are evaluated in liquid phase at low temperatures with the purpose of maximizing conversion instead of selectivity. Zeolites Beta with a Si/Al ratio of 25 and 35 and Mordenite with a ratio of 30 are studied in the conversion of *o*-xylene at 493 K. Maximum conversion is achieved by the catalyst with the highest Si/Al ratio due to faster diffusion of the isomer inside the zeolite channels because of the lower acidity of the solid. A kinetic study is then carried out over said catalyst between 473 and 513 K above 9 bar to maintain liquid phase operation in a batch reactor in the presence of toluene. The activation energies obtained do not indicate the presence of diffusional constraints towards any isomer; moreover, the results suggest the influence of the apparent direct conversion between *o*- and *p*-xylene only at higher temperatures. Finally, the kinetic model obtained is simulated in a fixed-bed catalytic reactor exhibiting higher performance compared to that of ZSM-5 in the temperature range from 493 to 533 K.

This chapter is based on: Gonçalves, J. C., and A. E. Rodrigues. 2015. "Xylene isomerization in liquid phase using large-pore zeolites." Submitted to *Chemical Engineering & Technology*

9.1. Introduction

Zeolites are porous crystalline aluminosilicates built from silica and alumina tetrahedra; they have been used in acid-catalyzed processes instead of previously employed corrosive catalyst in refineries and petrochemical industries worldwide [1,2]. Particularly, xylene isomerization is industrially carried out in gas phase in the presence of hydrogen over bifunctional-type zeolite catalysts comprising metal sites which do not actually participate in the isomerization but do reduce deactivation by removing carbonaceous materials from the catalyst surface [3]. Furthermore, the metal sites are required for the conversion of ethylbenzene which may be isomerized to xylenes or dealkylated to benzene [4].

The conversion of aromatics requires the formation of carbocations by protonation of the aromatic ring; the proton donors in the zeolites are the Brønsted acid sites, provided by the bridging OH linking Si to Al within the framework, while Lewis sites are electron donors constituted by extra-framework Al [5]. Xylene isomerization, disproportionation, and dealkylation are catalyzed by Brønsted acid sites [6-8], where disproportionation needs higher concentration of acid sites [9] and the strength of said sites follows the trend: isomerization < dealkylation < disproportionation [10,11]. The acidity of zeolites is determined by the Si/Al ratio, total acid sites decrease with increasing said ratio [2,5,12,13]; on the other hand, the strength is provided by their separation with a maximum depending on the specific topology of the zeolite [5,14].

Since xylene isomerization is normally performed in gas phase, the information available in the literature in liquid phase is very scarce; the catalysts used are essentially Mordenite (large-pore zeolite) [15] and ZSM-5 (medium-pore zeolite) [16-19]. Nonetheless, there are examples in the industry of process of xylene isomerization in liquid phase in the past. Low Temperature Isomerization was carried out at low temperatures and without hydrogen [20]. The process was particularly effective when the zeolite catalyst employed was ZSM-4 (large-pore zeolite) which aged very slowly [21]. According to Morrison and Tabak [22], catalysts present long cycle life in liquid phase because precursors to coke are dissolved by the reactant liquid and flushed out from the reactor. The main disadvantage of the process was the incapability of transforming ethylbenzene forcing the use of expensive distillation to prevent the compound from building up in the system; the aforementioned pushed the aromatics plants to implement the xylene isomerization in gas phase. However, in the recent years there has been a new interest in xylene isomerization in liquid phase probably due to the reduction of energy and pollution. Generally, the process is separated into two stages where xylenes are isomerized in liquid phase while

ethylbenzene is converted in gas phase; the catalysts employed for the liquid-phase stage are MCM-21 (medium-pore zeolite) [23] and ZSM-5 [24,25].

Other processes involving aromatics have also attracted attention to be implemented in liquid phase. A successful example is the production of ethylbenzene through alkylation of benzene; in gas phase the reaction was performed over ZSM-5 but due to diffusion problems, medium-pore zeolites were not suitable in liquid phase [1,26]. Diffusion in liquid phase is slower than in gas phase, the molecule requires energy equivalent to its latent heat to enter into the channels and the degree of freedom for appropriate orientation is less due to its lower entropy [27]. Large-pore zeolites, such as Y and Beta, were used instead being the latter more selective because of the absence of cavities that allow space for bulky intermediates and prevent the molecules from diffusing within the solid [28-30].

Very often activity and selectivity have contradictory requirements which provide an optimization challenge of the catalyst to be used in a specific process [31]. Normally, medium-pore zeolites provide higher selectivity while higher conversions are achieved over large-pore zeolites; the purpose of this chapter is to evaluate large-pore zeolites as potential catalysts to be used in the Simulated Moving Bed Reactor (SMBR) for the production of *p*-xylene where higher conversion is wanted from the catalyst since selectivity to the *para*-isomer is provided by the adsorbent. Based on the aforementioned, large-pore zeolites Beta with Si/Al ratio of 25 (H-BEA 25) and 35 (H-BEA 35) and Mordenite with a ratio of 30 (H-MOR 30) are studied in xylene isomerization in liquid phase at low temperatures.

9.2. Experimental

9.2.1. Materials

The reagents in the experiments, *o*-xylene (OX, purity ≥ 99.0 %), *m*-xylene (MX, purity ≥ 99.0 %), *p*-xylene (PX, purity ≥ 99.0 %), and toluene (Tol, purity ≈ 99.8 %), were purchased from Sigma-Aldrich® and used without further purification. The three catalysts were kindly supplied by Clariant® in the powder form and used after dried overnight.

9.2.2. Experimental set-up and procedure

The experiments are carried out in the batch mode by means of an autoclave reactor (HP reactor 4575A, Parr®) provided with a controlled stirrer and electrical heated jacket. The catalyst is added into the reactor along with the reagent to be used in the experiment (e.g., pure OX) and

closed; helium is introduced to maintain inert atmosphere and enough pressure to keep the reagents in the liquid form (i.e., > 9 bar). The reactor is then heated up to the desired temperature while agitating in order to keep uniform temperature in the mixture (small extent of the reaction might occur during this procedure). The stirrer is set to a sufficient speed to avoid settling of the catalyst (i.e., 300 rpm) in order to avoid influence of mass-transfer resistance [32]; this is verified by obtaining the same results at a higher speed (i.e., 460 rpm). Once the mixture has reached the desired temperature, the samples are collected after passing through a sintered filter and a serpentine in cold water to avoid powder loss and vaporization.

The samples are analyzed by a gas chromatographer (GC2010 plus, Shimadzu®) equipped with a fused silica capillary column WCOT-CP XYLENES (0.53 mm × 50 m) and flame ionization detector (FID).

9.2.3. *o*-Xylene conversion over the three catalysts

Each catalyst is evaluated in the conversion of *o*-xylene at 493 K and 9 bar after 8 hours. Each run consists of 250 ml of pure *o*-xylene and 10 g of the corresponding catalyst. *o*-Xylene is selected for these reaction tests since the proximity of the methyl groups leads to steric hindrance reducing the access of the proton in the isomerization reaction [33]. Moreover, it has been reported that *o*-xylene exhibits the lowest diffusion coefficient in large-pore zeolites [30], suggesting it to be the less reactive isomer under the reaction test conditions.

9.2.4. Kinetic study

The catalyst presenting the highest *o*-xylene conversion is used in a kinetic study at 473, 493 and 513 K above 9 bar. At each temperature three experiments are carried out with 9 g of catalyst and 220 ml corresponding to each isomer in the presence of toluene (i.e., 40 vol%) for 8 hours. Very often toluene is included to suppress xylene disproportionation reactions [15]; additionally, as indicated before the solid is foreseen as catalyst in the SMBR where toluene is used as desorbent and thus mixed with the xylene isomers within the unit.

9.3. Kinetic modeling

The isomerization of xylenes may go through a bimolecular or monomolecular mechanism, the former has a lower activation energy but restricted to catalysts with large space around the active sites to accommodate the bulky intermediates [1]. At 493 K the bimolecular mechanism partially contributes to the reaction over zeolite Y and is significantly less important over

Mordenite; over zeolite Beta the isomerization follows only the monomolecular route due to its tortuous pore system [34-36].

The monomolecular mechanism consists of rapid and reversible addition of a proton to the aromatic ring followed by 1,2-methyl shift. Following this mechanism the reaction scheme comprises interconversion between *o*- and *m*-xylene and between *m*- and *p*-xylene, this scheme is often called linear scheme; however, a triangular scheme including a direct conversion between *o*- and *p*-xylene is frequently used to account for the faster diffusion of *p*-xylene inside the pores [18,37]. Both schemes are presented in Figure 9.1.

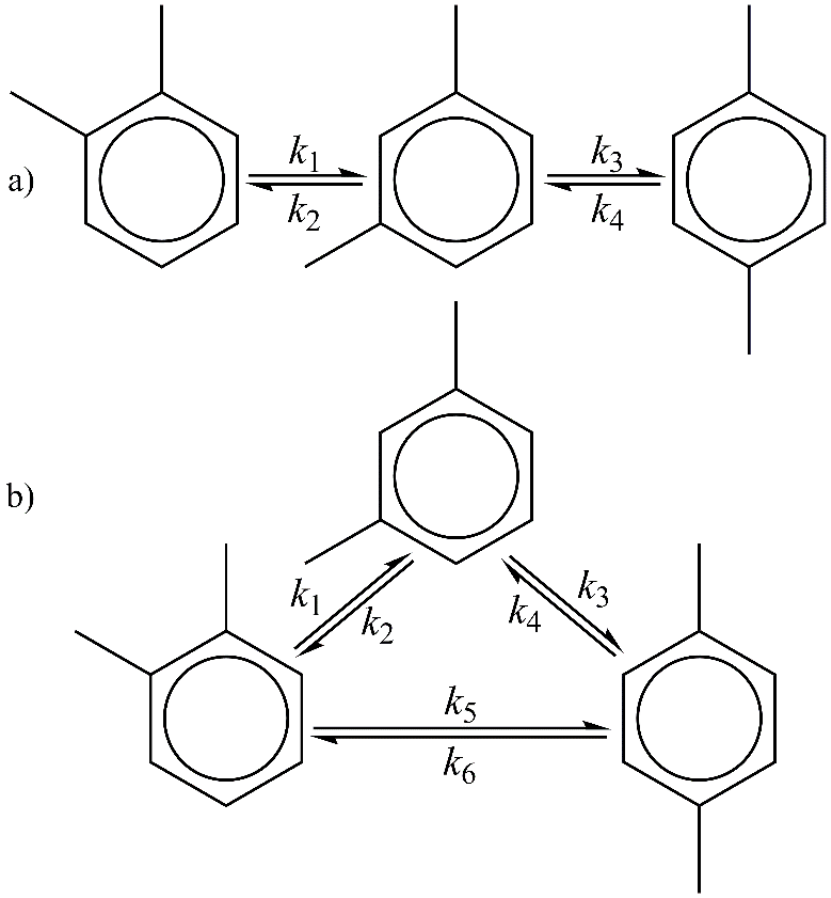

Figure 9.1 Reaction schemes for xylene isomerization: a) linear b) triangular

Following the triangular scheme, the reaction rates for each isomer are given by equations (9.1) to (9.3). The adsorption constants are not included in the reaction rates since full coverage in adsorption sites is very common in liquids [38].

$$R_{\mathrm{OX}} = k_2 C_{\mathrm{MX}} + k_6 C_{\mathrm{PX}} - k_5 C_{\mathrm{OX}} - k_1 C_{\mathrm{OX}} \tag{9.1}$$

$$R_{\mathrm{MX}} = k_1 C_{\mathrm{OX}} + k_4 C_{\mathrm{PX}} - k_2 C_{\mathrm{MX}} - k_3 C_{\mathrm{MX}} \tag{9.2}$$

$$R_{\mathrm{PX}} = k_5 C_{\mathrm{OX}} + k_3 C_{\mathrm{MX}} - k_6 C_{\mathrm{PX}} - k_4 C_{\mathrm{PX}} \tag{9.3}$$

Clearly, for the linear scheme k_5 and k_6 are eliminated since there is no direct conversion between *o*- and *p*-xylene. The mass balance for species i in a batch reactor with constant volume V_l, mass of catalyst W_c, and reaction rate R_i (defined by equations (9.1) to (9.3)) is given by equation (9.4) considering isothermal operation and absence of mass-transfer resistance:

$$\frac{V_l}{W_c}\frac{\mathrm{d}C_i}{\mathrm{d}t} = R_i \qquad i = \mathrm{OX, MX, PX} \tag{9.4}$$

The influence of temperature on the kinetic constant is taken into account through the centered temperature form of the Arrhenius equation:

$$k_j = k_{0,j}\exp\left[-\frac{E_{a,j}}{R}\left(\frac{1}{T}-\frac{1}{T_0}\right)\right] \qquad j = 1,3,6 \qquad T_0 = 493\ \mathrm{K} \tag{9.5}$$

The kinetic constants corresponding to j = 2,4,5 are calculated based on the reverse reaction and the equilibrium constant at the corresponding temperature in order to guarantee thermodynamic consistency. The equilibrium constants are obtained from the expressions developed in Chapter 3.

9.4. Results and discussion

9.4.1. Catalyst characterization

9.4.1.1. Scanning electron microscopy

Figures 9.2 to 9.4 present the scanning electron microscopy (SEM) for H-BEA 25, H-MOR 30, and H-BEA 35 respectively. It can be seen that the particle size increases with the Si/Al ratio; according to Shirazi et al. [12], increasing the silica content leads to larger surface area and crystal size.

9.4.1.2. X-ray diffraction

Figures 9.5 and 9.6 present the x-ray diffraction (XRD) for zeolites Beta and Mordenite compared to those reported by the International Zeolite Association (www.iza-structure.org), the samples present good match with the corresponding reference pattern.

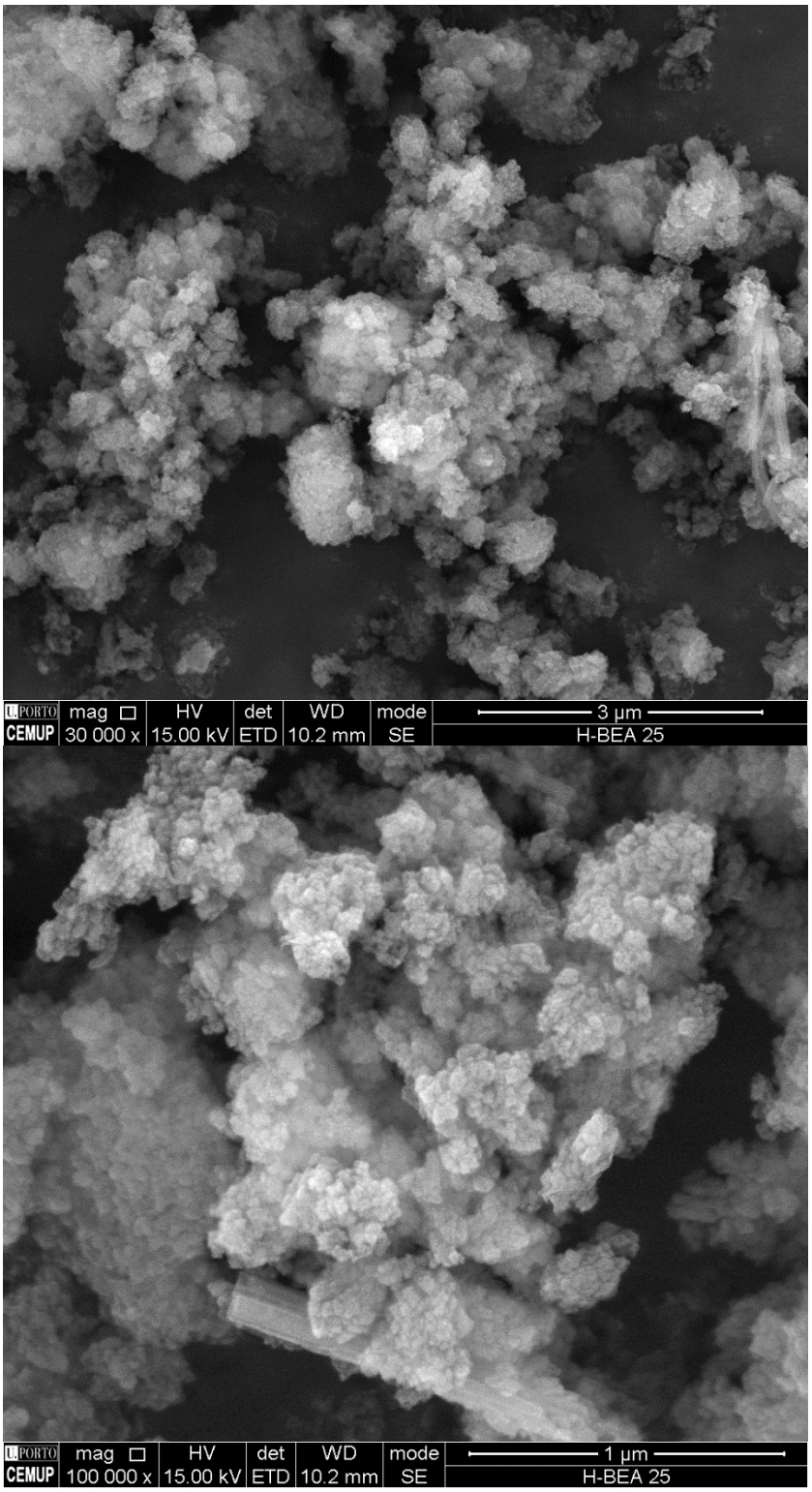

Figure 9.2 Scanning electron microscopy images of H-BEA 25

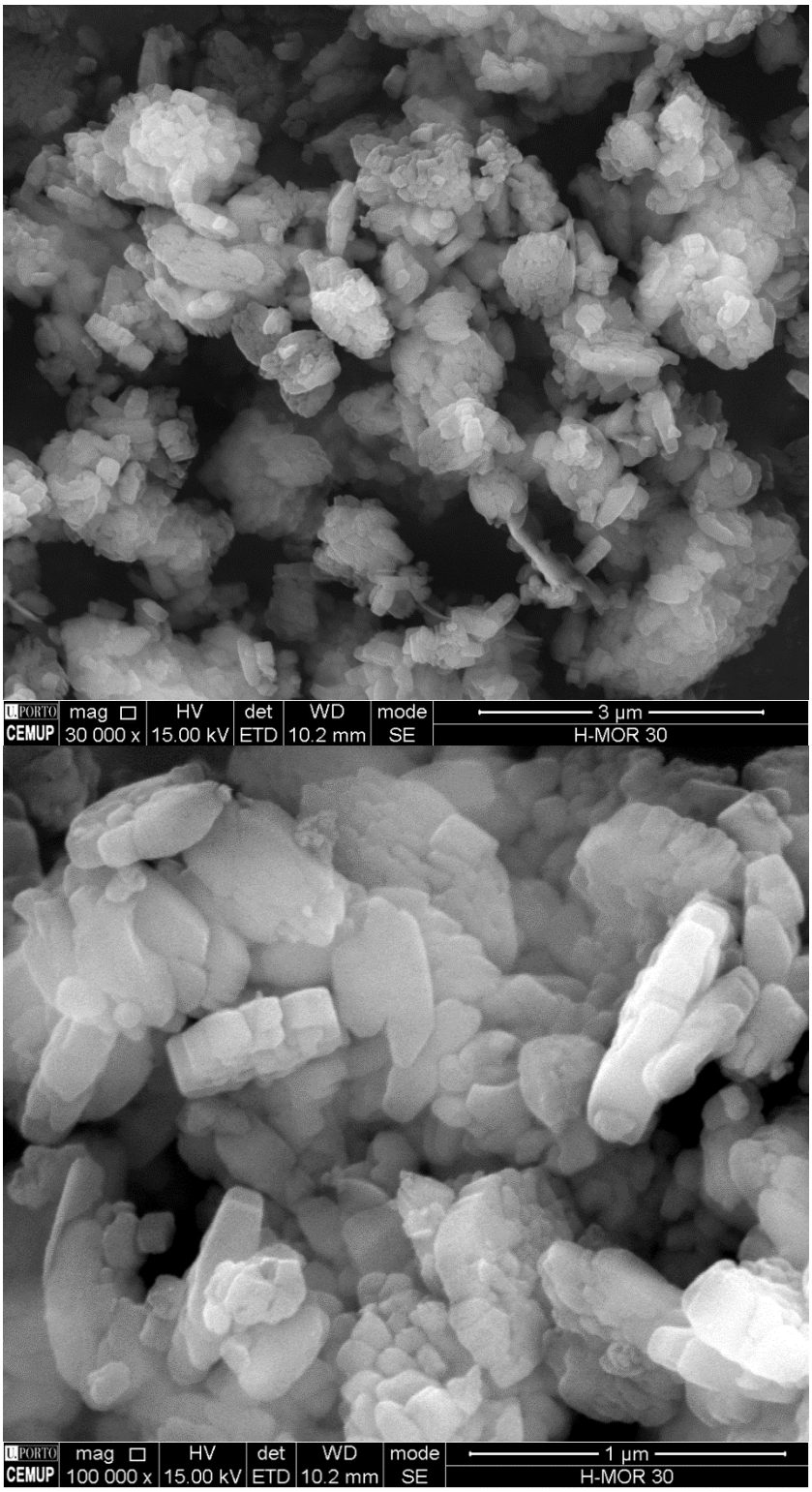

Figure 9.3 Scanning electron microscopy images of H-MOR 30

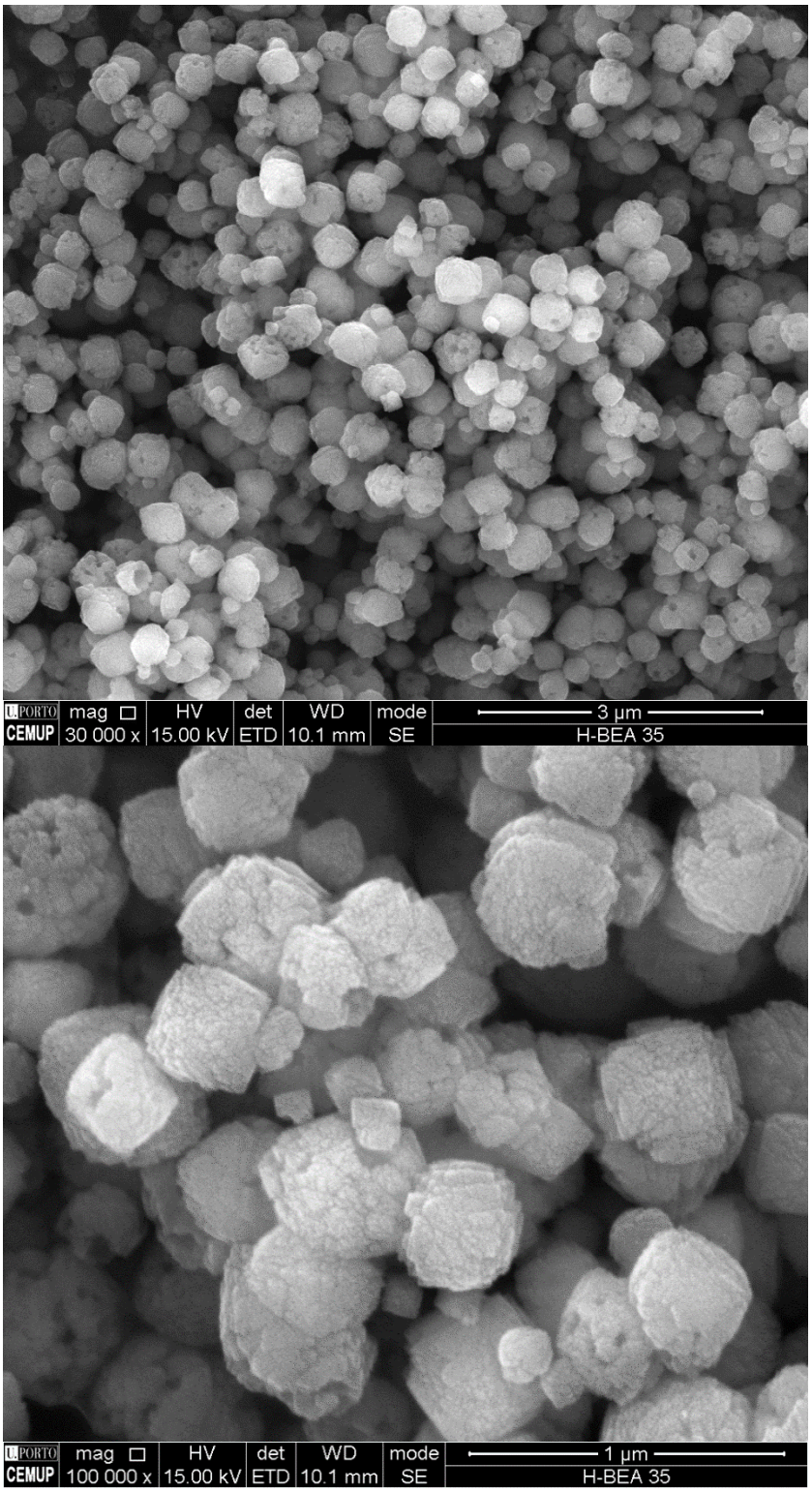

Figure 9.4 Scanning electron microscopy images of H-BEA 35

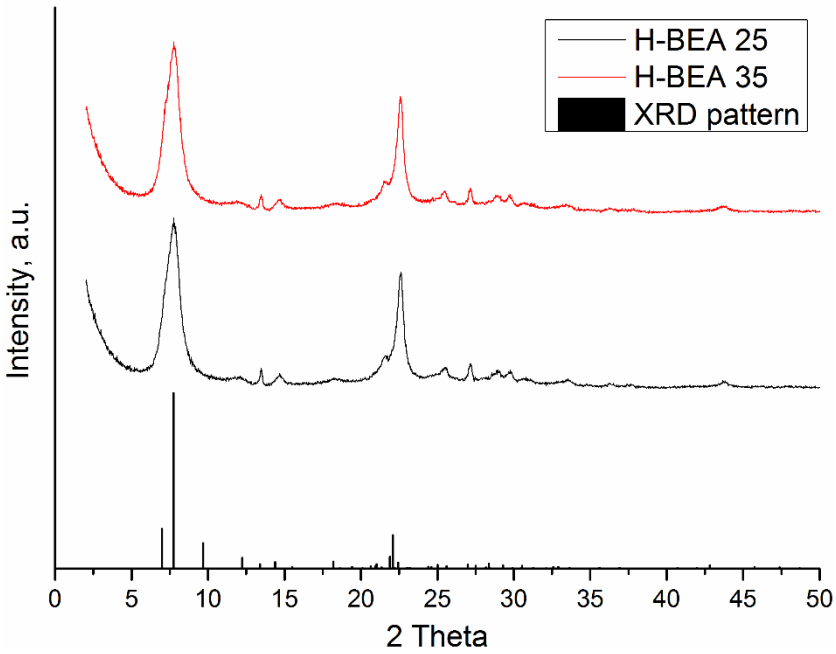

Figure 9.5 X-ray diffraction (XRD) of H-BEA 25 and H-BEA 35 compared to reported powder pattern by International Zeolite Association (www.iza-structure.org)

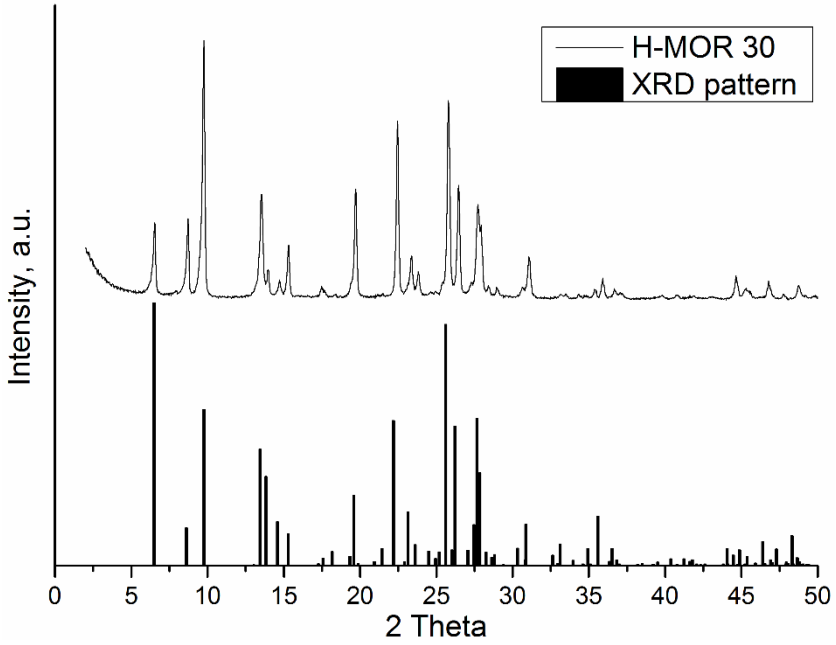

Figure 9.6 X-ray diffraction (XRD) of H-MOR 30 compared to reported powder pattern by International Zeolite Association (www.iza-structure.org)

9.4.1.3. Nitrogen adsorption at 77 K

The adsorption of nitrogen at 77 K over the three samples is presented in Figure 9.7. It is observed a significant level of mesoporosity on H-BEA 25, this is due to the very small particle size resulting in agglomeration (see Figure 9.2) from which the intercrystalline space provides said mesoporosity. The aforementioned is also seen in Table 9.1 where although H-BEA 25

presents larger surface area than H-MOR 30 it shows smaller micropore area and volume. Moreover Beta zeolite with higher Si/Al ratio presents larger surface area as concluded by Shirazi et al. [12]; H-BEA 35 is then able to provide larger catalytic surface although the difference is less than 10%.

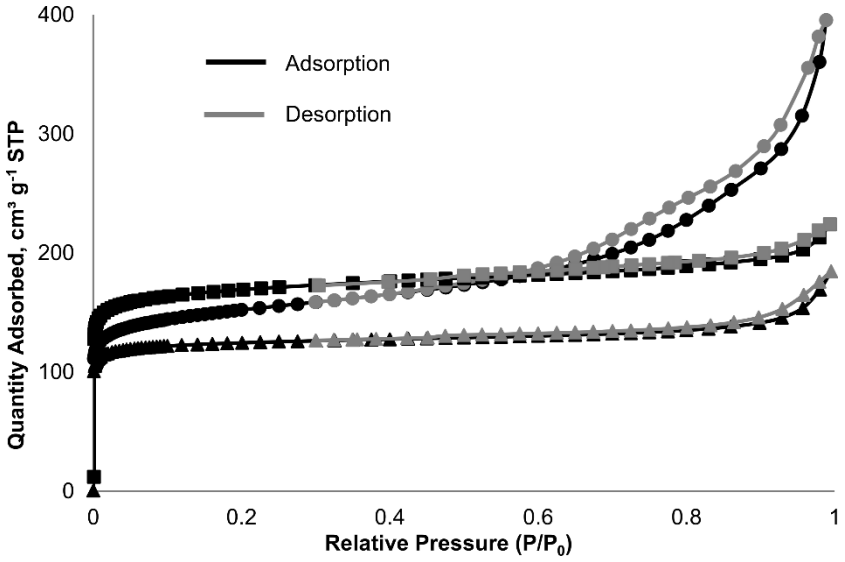

Figure 9.7 Nitrogen adsorption of H-BEA 25 (●), H-MOR 30 (▲), and H-BEA 35 (■) at 77 K (P_0 = 1 atmosphere)

Table 9.1 Surface area and micropore area and volume of H-BEA 25, H-MOR 30, and H-BEA 35

	H-BEA 25	H-MOR 30	H-BEA 35
BET Surface Area, $m^2\ g^{-1}$	518	417	568
Micropore area, $m^2\ g^{-1}$	346	393	522
Micropore volume, $cm^3\ g^{-1}$	0.157	0.184	0.247

9.4.2. *o*-Xylene conversion over the three catalysts

The conversion of *o*-xylene and the water content before use of each zeolite is presented in Table 9.2. The hydrophilic character increases with the presence of aluminum within the zeolite (i.e., lower Si/Al ratio) [12,39]. However, H-MOR 30 retained more water than H-BEA 25 although it has a higher Si/Al ratio, the acidity of the first might be higher as a result of the interactions between acid sites due to the separation given by their different topologies. For the same structure, the zeolite with lower Si/Al ratio exhibits higher water content as expected.

Even though xylene isomerization is catalyzed by acid sites, the highest *o*-xylene conversion is obtained over the catalyst demonstrating lower acidity; the reason may be explained in terms of diffusion constraints inside the channels of the zeolites together with the slightly larger surface area. Diffusion and adsorption are highly correlated, the movement of the molecules can be seen

as a succession of discrete jumps from site to site, thus physical chemistry process of sorption and desorption cannot be neglected [35,40,41]. Therefore, the diffusion of molecules with higher dipole moment are more hindered due to stronger adsorption on high acid catalysts [27,40,42]. The dipole moment for *o*-, *m*-, and *p*-xylene are 0.62, 0.36, and 0.00 D respectively [43]; this might explain the lower diffusivity of *o*-xylene in large-pore zeolites. On the other hand, in medium-pore zeolites the size of the molecule outweighs the dipole moment making *m*-xylene the slowest isomer inside the channels [44]; the critical size of *o*-, *m*-, and *p*-xylene are 0.73, 0.74, and 0.67 nm [27].

Table 9.2 *o*-Xylene conversion after 8 hours for 10 g of catalyst and 250 ml (initial concentration 8.2 mol L^{-1})

Catalyst	H-BEA 25	H-BEA 35	H-MOR 30
H_2O wt %	2.7	2.0	3.1
Conversion %	3.7	30.4	0.6
Final concentration, mol L^{-1}			
o-Xylene	7.90	5.71	8.15
m-Xylene	0.30	2.07	0.05
p-Xylene	0.00	0.35	0.00
Toluene	0.00	0.03	0.00
Trimethylbenzenes	0.00	0.04	0.00

According to Čejka and Wichterlová [35], zeolites with lower acidity can provide higher activity under specific reaction conditions as it has been seen in this work. There is an increase in both extra-framework and framework aluminum as Si/Al ratio decreases promoting the formation of Brønsted and Lewis acid sites [12]. As indicated before, Lewis acid sites do not participate in xylene isomerization but they can strengthen the acidity of Brønsted sites [5]; therefore, an optimum balance between both types of acid sites is the goal in tailoring the catalyst for a particular service [8,13]. For instance, Nayak and Choudhary [10] found maximum conversion but minimum selectivity over ZSM-5 at Si/Al ratio of 17.2.

Pérez-Pariente et al. [45] studied zeolite Beta with Si/Al from 11 to 42 and found maximum activity between 14 and 15 corresponding to the previously referred optimum between Lewis and Brønsted acid sites. In this work the Si/Al ratio is higher due to the lower temperatures in the reaction conditions; Celik et al. [46] observed lower temperatures for maximum rates while increasing the Si/Al ratio.

9.4.3. Kinetic study and modeling

H-BEA 35 is used for the kinetic study due to its higher conversion of *o*-xylene at 493 K. The experimental concentrations of each species at different extent of the reaction for the three

temperatures studied are presented in Table 9.3. The concentration of toluene is fairly constant throughout the experiments, the presence of xylene inhibits the disproportionation of toluene and also the lower number of alkyl groups on the benzene ring reduces its reactivity [9].

The experimental data presented in Table 9.3 is used to determine the kinetic parameters for both scheme 1 and 2 by means of the maximum likelihood method with constant variance and tolerance of 10^{-5} on the commercial software gPROMS v3.7.1 from Process Systems Enterprise (www.psenterprise.com) using equations (9.1) to (9.5).

Table 9.3 Experimental concentration (mol L^{-1}) of xylenes and toluene at different extents of the reaction for temperatures 473, 493, and 513 K

t, h	OX	MX	PX	Tol	OX	MX	PX	Tol	OX	MX	PX	Tol
						473 K						
0	5.27	0.00	0.00	3.39	0.01	4.99	0.01	3.57	0.00	0.01	4.98	3.58
2	5.26	0.06	0.01	3.32	0.02	4.97	0.03	3.57	0.00	0.05	4.94	3.58
4	5.18	0.08	0.02	3.37	0.04	4.90	0.06	3.59	0.00	0.13	4.86	3.58
6	5.11	0.15	0.02	3.37	0.07	4.82	0.10	3.60	0.01	0.30	4.68	3.58
8	5.00	0.23	0.03	3.40	0.20	4.61	0.31	3.45	0.01	0.44	4.54	3.58
						493 K						
0	5.09	0.08	0.03	3.47	0.09	4.83	0.13	3.53	0.00	0.07	4.95	3.54
2	4.96	0.28	0.04	3.37	0.26	4.40	0.40	3.53	0.00	0.26	4.76	3.55
4	4.50	0.69	0.09	3.36	0.44	3.96	0.64	3.54	0.02	0.61	4.38	3.56
6	4.04	1.06	0.15	3.38	0.64	3.49	0.91	3.55	0.05	0.93	3.99	3.60
8	3.48	1.49	0.27	3.38	0.78	3.20	1.06	3.55	0.11	1.48	3.43	3.56
						513 K						
0	4.51	0.75	0.11	3.26	0.20	4.61	0.29	3.48	0.00	0.93	4.08	3.56
2	3.54	1.48	0.33	3.26	0.47	3.91	0.68	3.54	0.16	1.45	3.34	3.63
4	2.72	2.01	0.58	3.28	0.79	3.34	0.93	3.54	0.52	2.13	2.33	3.60
6	2.06	2.38	0.82	3.31	0.85	3.06	1.08	3.61	0.76	2.45	1.75	3.64
8	1.62	2.60	1.00	3.37	1.02	2.86	1.12	3.61	0.83	2.60	1.48	3.71

The estimated parameters are presented in Table 9.4; the uncertainty associated with each value corresponds to the 95 % confidence interval. Clearly scheme 1 is a better representation of the reaction under the experimental conditions since the uncertainty associated with the direct conversion between *o*- and *p*-xylene (i.e., $E_{a,6}$ and $k_{0,6}$) is significantly high. Moreover, the uncertainties of the parameters ($\leq$ 10 %) and the Chi-Squared Goodness-of-Fit Test at 95 % verifies accurate representation of the experimental data by the kinetic model of scheme 1 [47]. Additionally, the experimental concentrations and their predicted values using the estimated parameters corresponding to scheme 1 are presented in Figure 9.8.

It can be seen from the values of Cappellazzo et al. [18] that there are some diffusional constraints in the conversion between *o*- and *m*-xylene based on its lower activation energy ($E_{a,1}$).

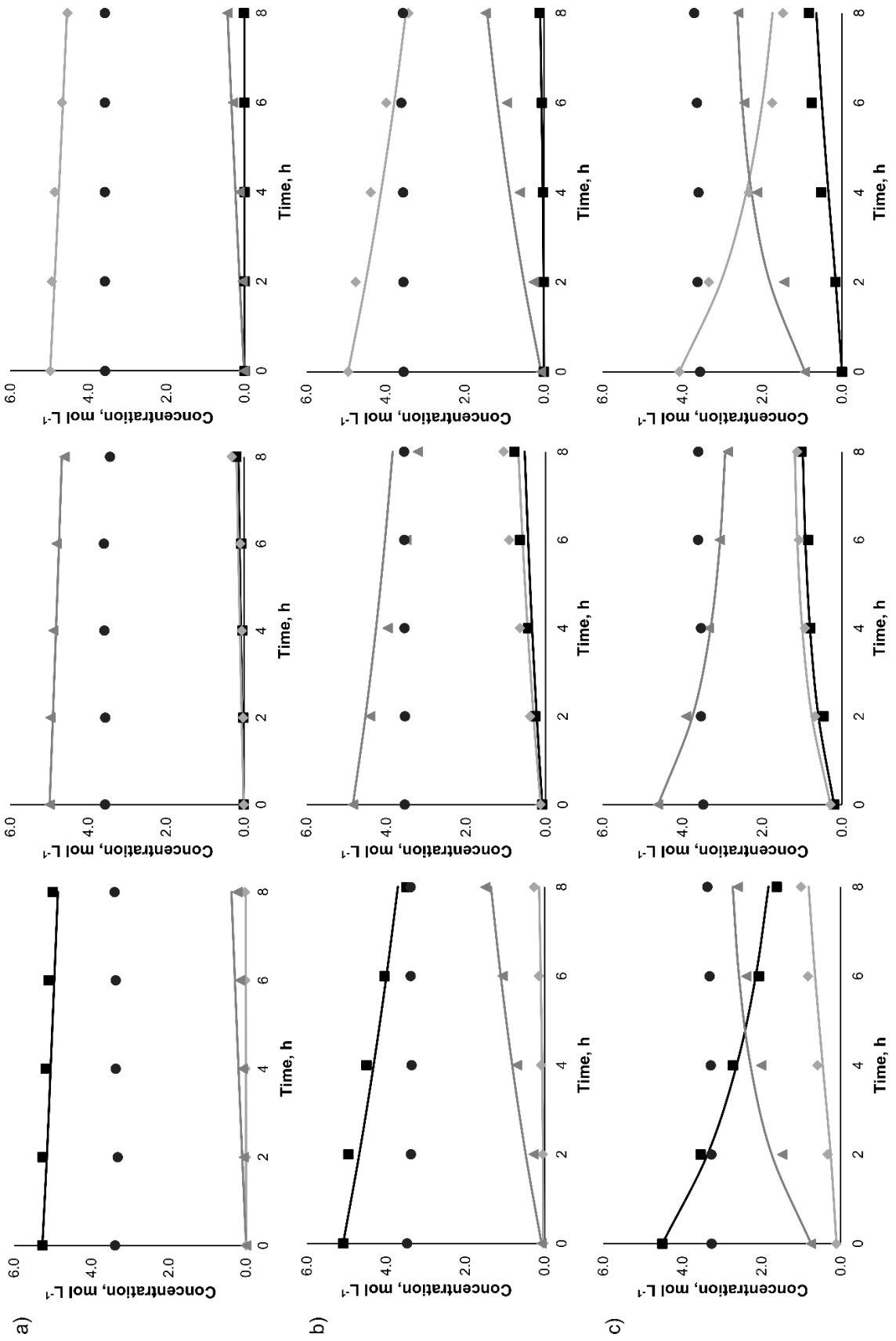

Figure 9.8 Experimental (symbol) and predicted (solid line) concentrations of *o*-xylene (■), *m*-xylene (▲), *p*-xylene (♦), and toluene (●) for each reaction at temperatures: a) 473 K b) 493 K c) 513 K

Such a difference is not observed in the activation energies of H-BEA 35 suggesting similar diffusion among the isomers inside the channels which is essential for high conversion in isomerization reactions. On the other hand, diffusional constraints on *o*- and *m*-xylene provides selectivity towards the *para*-isomer.

Table 9.4 Kinetic parameters for scheme 1, 2, and those obtained by Cappellazzo et al. [18]

Parameter	Scheme 1[a]	Scheme 2[a]	Cappellazzo et al. [18][b]
$E_{a,1}$, kJ mol^{-1}	144 ± 13	139 ± 16	98.8
$E_{a,3}$, kJ mol^{-1}	140 ± 13	134 ± 15	136
$E_{a,6}$, kJ mol^{-1}	-	203 ± 146	158
$k_{0,1}$ × 10^8, m^3 kg^{-1}s^{-1}	29 ± 3[c]	27 ± 3[c]	63.6[d]
$k_{0,3}$ × 10^8, m^3 kg^{-1}s^{-1}	14.4 ± 1.3[c]	13.7 ± 1.4[c]	106[d]
$k_{0,6}$ × 10^8, m^3 kg^{-1}s^{-1}	-	2 ± 2[c]	57.8[d]

[a] This work. [b] The authors worked between 523 and 573 K. [c] Kinetic constant at 493 K. [b] Kinetic constant at 553 K

Even though scheme 2 is not an adequate representation of the system, it is noted a significant higher activation energy for the conversion between *o*- and *p*-xylene; this was also observed by Iliyas and Al-Khattaf [33] over USY zeolite. The aforementioned suggest that even over large-pore zeolite, apparent direct conversion between *o*- and *p*-xylene is expected at higher temperatures. With the purpose of analyzing said conversion, the kinetic constants are estimated separately at each temperature and presented in Table 9.5. The conversion between *o*- and *p*-xylene starts to appear as the temperature increases; this behavior was also noted by Young et al. [16] in the temperature range from 473 to 533 K in liquid phase.

Table 9.5 Kinetic constants at each temperature for scheme 2

Parameter	473 K	493 K	513 K
k_1 × 10^8, m^3 kg^{-1}s^{-1}	3.7 ± 0.8	32 ± 5	89 ± 8
k_3 × 10^8, m^3 kg^{-1}s^{-1}	3.1 ± 0.4	14 ± 2	46 ± 4
k_6 × 10^8, m^3 kg^{-1}s^{-1}	0	0	19 ± 6

9.4.4. Comparison with ZSM-5

Minceva et al. [48] developed a model of a fixed-bed catalytic reactor for xylene isomerization with based on the model parameters of Cappellazzo et al. [18]. The model included axial dispersion and external and internal mass-transfer resistance coupled in a single mass-transfer coefficient based on the Linear Driving Force (LDF) model. The authors found excellent agreement with the steady-state outlet compositions reported by Cappellazzo et al. [18]. In this work, the same model is used to compare the catalysts H-BEA 35 and ZSM-5 in the

isomerization of xylenes in liquid phase. The kinetic data used is that presented in Table 9.4 combined with the thermodynamic equilibrium from Chapter 3.

The model is solved using the commercial software gPROMS v3.7.1 from Process Systems Enterprise (www.psenterprise.com) through the discretization of the axial domain using second-order orthogonal collocation on 50 finite elements with 10^{-5} as tolerance. Table 9.6 presents the reactor outlet weight fractions for several LWHSV (liquid weight hourly space velocity) at temperatures 493, 513, and 533 K keeping the same feed composition of 27.5 wt% *o*-xylene, 60.4 wt% *m*-xylene, and 12.1 wt% *p*-xylene as used by the authors. H-BEA 35 exhibits higher xylene conversion due to less constrained diffusion of all three isomers within the catalyst channels; the difference between *o*- and *p*-xylene diffusivity is much higher on ZSM-5 than that on Beta [28].

Table 9.6 Reactor outlet weight fractions based on the kinetics from Cappellazzo et al. [18] and this work.

LWHSV, h^{-1}	Cappellazzo et al. [18] (ZSM-5)			This work (H-BEA 35 – Scheme 1)		
	OX, wt%	MX, wt%	PX, wt%	OX, wt%	MX, wt%	PX, wt%
			493 K			
20	27.5	60.3	12.2	27.4	60.1	12.5
10	27.4	60.3	12.3	27.2	59.8	13.0
4.7	27.3	60.1	12.6	26.9	59.2	13.9
2.5	27.2	59.8	13.0	26.4	58.3	15.3
1.7	27.0	59.6	13.4	26.0	57.6	16.4
			513 K			
20	27.4	60.1	12.5	27.0	59.3	13.7
10	27.3	59.8	12.9	26.5	58.4	15.1
4.7	27.0	59.2	13.8	25.5	57.0	17.5
2.5	26.5	58.4	15.1	24.2	55.7	20.1
1.7	26.1	57.7	16.2	23.2	55.1	21.7
			533 K			
20	27.1	59.5	13.4	26.0	57.7	16.3
10	26.7	58.7	14.6	24.8	56.2	19.0
4.7	26.0	57.2	16.8	23.0	54.9	22.1
2.5	25.0	55.6	19.4	21.7	54.4	23.9
1.7	24.2	54.7	21.1	21.3	54.4	24.3

9.5. Conclusions

Three large-pore zeolites are studied in the conversion of *o*-xylene at 493 K in liquid phase. Beta zeolite with Si/Al ratio of 35 exhibits the highest conversion due to its appropriate acidity providing active sites for xylene isomerization without restricting the diffusion of the species

inside the catalyst channels. A kinetic model based on reaction experiments carried out between 473 and 513 K in the presence of toluene is developed and compared to zeolite ZSM-5 kinetics from the literature; zeolite Beta shows higher performance in a fixed-bed catalytic reactor in the isomerization of xylenes at low temperatures.

9.6. Nomenclature

C_i = Concentration of component i, mol L^{-1}

$E_{a,j}$ = Activation energy of reaction j, kJ mol^{-1}

k_j = Kinetic constant of reaction j, m^3 $kg^{-1}s^{-1}$

$k_{0,j}$ = Kinetic constant at centered temperature T_0, m^3 $kg^{-1}s^{-1}$

LWHSV = Liquid weight hourly space velocity, s^{-1}

R_i = Reaction rate of component i, mol $kg^{-1}s^{-1}$

R = Ideal gas constant, kJ $mol^{-1}K^{-1}$

T = Temperature, K

T_0 = Centered temperature, K

t = Time, s

V_l = Liquid volume inside the batch reactor, m^3

W_c = Mass of catalyst, kg

Abbreviations

LDF = Linear Driving Force

MX = *m*-Xylene

OX = *o*-Xylene

PX = *p*-Xylene

SEM = Scanning electron microscopy

SMBR = Simulated Moving Bed Reactor

Tol = Toluene

XRD = X-ray diffraction

9.7. References

[1] Perego, C., and P. Pollesel. 2009. "Advances in Aromatics Processing Using Zeolite Catalysts." In *Advances in Nanoporous Materials*, edited by Stefan Ernst, 97-149. Amsterdam: Elsevier.

[2] Hodala, J. L., A. B. Halgeri, and G. V. Shanbhag. 2014. "Phosphate modified ZSM-5 for the shape-selective synthesis of para-diethylbenzene: Role of crystal size and acidity." *Applied Catalysis A: General* no. 484:8-16.

[3] Corma, A., and A. Cortes. 1980. "Kinetics of the Gas-Phase Catalytic Isomerization of Xylenes." *Industrial & engineering chemistry process design and development* no. 19 (2):263-267.

[4] Gonçalves, J. C., and A. E. Rodrigues. 2013. "Industrial xylene/ethylbenzene isomerization unit using a radial-flow reactor and euo-type zeolite." *Chemical Engineering and Technology* no. 36 (10):1658-1664.

[5] Derouane, E. G., J. C. Védrine, R. Ramos Pinto, P. M. Borges, L. Costa, M. A. N. D. A. Lemos, F. Lemos, and F. Ramôa Ribeiro. 2013. "The acidity of zeolites: Concepts, measurements and relation to catalysis: A review on experimental and theoretical methods for the study of zeolite acidity." *Catalysis Reviews: Science and Engineering* no. 55 (4):454-515.

[6] Akpolat, O., and G. Gündüz. 2005. "Isomerization of M-xylene." *Journal of Applied Sciences* no. 5 (2):236-248.

[7] Alabi, W., L. Atanda, R. Jermy, and S. Al-Khattaf. 2012. "Kinetics of toluene alkylation with methanol catalyzed by pure and hybridized HZSM-5 catalysts." *Chemical Engineering Journal* no. 195–196 (0):276-288.

[8] Caillot, M., A. Chaumonnot, M. Digne, and J. A. Vanbokhoven. 2014. "Creation of Brønsted acidity by grafting aluminum isopropoxide on silica under controlled conditions: Determination of the number of Brønsted Sites and their turnover frequency for m-xylene isomerization." *ChemCatChem* no. 6 (3):832-841.

[9] Al-Khattaf, S., M. N. Akhtar, T. Odedairo, A. Aitani, N. M. Tukur, M. Kubů, Z. Musilová-Pavlačková, and J. Čejka. 2011. "Catalytic transformation of methyl benzenes over zeolite catalysts." *Applied Catalysis A: General* no. 394 (1-2):176-190.

[10] Nayak, V. S., and V. R. Choudhary. 1982. "Isomerization of m-xylene on H-ZSM-5: Part I: Influence on catalytic activity and selectivity of si/al ratio, degree of cation exchange, deammoniation conditions and poisoning of stronger acid sites." *Applied Catalysis* no. 4 (4):333-352.

[11] Waziri, S. M., A. M. Aitani, and S. Al-Khattaf. 2010. "Transformation of toluene and 1,2,4-trimethylbenzene over ZSM-5 and mordenite catalysts: A comprehensive kinetic model with reversibility." *Industrial and Engineering Chemistry Research* no. 49 (14):6376-6387.

[12] Shirazi, L., E. Jamshidi, and M. R. Ghasemi. 2008. "The effect of Si/Al ratio of ZSM-5 zeolite on its morphology, acidity and crystal size." *Crystal Research and Technology* no. 43 (12):1300-1306.

[13] Osman, M., L. Atanda, M. M. Hossain, and S. Al-Khattaf. 2013. "Kinetics modeling of disproportionation and ethylation of ethylbenzene over HZSM-5: Effects of SiO2/Al2O3 ratio." *Chemical Engineering Journal* no. 222:498-511.

[14] Karge, H. G. 2008. "Concepts and Analysis of Acidity and Basicity." In *Handbook of Heterogeneous Catalysis*, edited by Gerhard Ertl, Helmuth Knözinger, Ferdi Schüth and Jens Weitkamp. Weinheim, Germany: Wiley-VCH.

[15] Norman, G. H., D. S. Shigemura, and J. R. Hopper. 1976. "Isomerization of Xylene over Hydrogen Modernite. A Comprehensive Model." *Industrial & Engineering Chemistry Research* no. 15 (1):41-45.

[16] Young, L. B., S. A. Butter, and W. W. Kaeding. 1982. "Shape selective reactions with zeolite catalysts. III. Selectivity in xylene isomerization, toluene-methanol alkylation, and toluene disproportionation over ZSM-5 zeolite catalysts." *Journal of Catalysis* no. 76 (2):418-432.

[17] Collins, D. J., R. J. Medina, and B. H. Davis. 1983. "Xylene Isomerization by ZSM-5 Zeolite Catalyst." *Canadian Journal of Chemical Engineering* no. 61 (1):29-35.

[18] Cappellazzo, O., G. Cao, G. Messina, and M. Morbidelli. 1991. "Kinetics of Shape-Selective Xylene Isomerization over a ZSM-5 Catalyst." *Industrial & Engineering Chemistry Research* no. 30 (10):2280-2287.

[19] Bergeot, G., D. Leinekugel-Le-Cocq, P. Leflaive, C. Laroche, L. Muhr, and M. Bailly. 2009. "Simulated moving bed reactor for paraxylene production." *CHemical ENgineering Transactions* no. 17:87-92.

[20] Wise, J. J. 1968. *Isomerization and disproportionation of alkyl aromatics.* US 3,377,400. Mobil Oil Corporation

[21] Burress, G. T. 1974. *Xylene isomerization.* US 3,856,873. Mobil Oil Corporation

[22] Morrison, R. A., and S. A. Tabak. 1980. *Manufacture of aromatic compounds.* US 4,224,141. Mobil Oil Corporation

[23] Mohr, G. D. 2004. *Xylene Isomerization.* U.S. 6,770,792 B2. ExxonMobil Chemical Company

[24] Bresler, L., and R. B. Larson. 2009. *Energy-efficient process for para-xylene production.* US 7,553,998-B2. UOP LLC

[25] Magne-Drisch, J., F. Alario, J.-F. Joly, A. Minkkinen, and E. Merlen. 2002. *Process for the production of paraxylene that comprises an adsorption stage, a liquid phase isomerization stage and a gas phase isomerization stage with an EUO-type zeolite.* US 6,448,459-B1. Institut Français du Pétrole

[26] Bejblová, M., N. Zilková, and J. Cejka. 2008. "Transformation of aromatic hydrocarbons over zeolites." *Research on Chemical Intermediates* no. 34 (5-7):439-454.

[27] Choudhary, V. R., V. S. Nayak, and T. V. Choudhary. 1997. "Single-Component Sorption/Diffusion of Cyclic Compounds from Their Bulk Liquid Phase in H-ZSM-5 Zeolite." *Industrial & Engineering Chemistry Research* no. 36 (5):1812-1818.

[28] Al-Khattaf, S., S. A. Ali, A. M. Aitani, N. Žilková, D. Kubička, and J. Čejka. 2014. "Recent advances in reactions of alkylbenzenes over novel zeolites: The effects of zeolite structure and morphology." *Catalysis Reviews: Science and Engineering* no. 56 (4):333-402.

[29] Llopis, F., G. Sastre, and A. Corma. 2004. "Xylene isomerization and aromatic alkylation in zeolites NU-87, SSZ-33, β, and ZSM-5: molecular dynamics and catalytic studies." *Journal of Catalysis* no. 227 (1):227-241.

[30] Llopis, F., G. Sastre, and A. Corma. 2006. "Isomerization and disproportionation of m-xylene in a zeolite with 9- and 10-membered ring pores: Molecular dynamics and catalytic studies." *Journal of Catalysis* no. 242 (1):195-206.

[31] Fernandez, C., I. Stan, J. P. Gilson, K. Thomas, A. Vicente, A. Bonilla, and J. Pérez-Ramírez. 2010. "Hierarchical ZSM-5 zeolites in shape-selective xylene isomerization: Role of mesoporosity and acid site speciation." *Chemistry - A European Journal* no. 16 (21):6224-6233.

[32] Oldshue, J. Y. 1983. "Fluid Mixing Technology and Practice." *Chemical Engineering (New York)* no. 90 (12):82-108.

[33] Iliyas, A., and S. Al-Khattaf. 2004. "Xylene transformation over USY zeolite: An experimental and kinetic study." *Applied Catalysis A: General* no. 269 (1-2):225-236.

[34] Guisnet, M., N. S. Gnep, and S. Morin. 2000. "Mechanisms of xylene isomerization over acidic solid catalysts." *Microporous and Mesoporous Materials* no. 35-36:47-59.

[35] Čejka, J., and B. Wichterlová. 2002. "Acid-Catalyzed Synthesis of Mono- and Dialkyl Benzenes over Zeolites: Active Sites, Zeolite Topology, and Reaction Mechanisms." *Catalysis Reviews* no. 44 (3):375-421.

[36] Jones, C. W., S. I. Zones, and M. E. Davis. 1999. "m-Xylene reactions over zeolites with unidimensional pore systems." *Applied Catalysis A: General* no. 181:289-303.

[37] Al Khattaf, S. 2005. "Modeling xylene reactions over ZSM-5 zeolite in a riser simulator: 1,3-versus 1,2-methyl shift." *Industrial & Engineering Chemistry Research* no. 44 (21):7957-7968.

[38] Froment, G. F., and K. B. Bischoff. 1979. *Chemical reactor analysis and design*: Wiley.

[39] Čejka, J., and D. Kubička. 2007. "Zeolites and Other Micro- and Mesoporous Molecular Sieves." In *Kirk-Othmer Encyclopedia of Chemical Technology*, edited by Arza Seidel, 1-30. New York: John Wiley & Sons, Inc.

[40] Li, Y.-G., X. Chang, and Z. Zeng. 1992. "Kinetics Study of the Isomerization of Xylene on HZSM-5 Zeolite. 1. Kinetics Model and Reaction Mehanism." *Industrial & Engineering Chemistry Research* no. 31 (1):187-192.

[41] Sundaresan, S., and C. K. Hall. 1986. "Mathematical modelling of diffusion and reaction in blocked zeolite catalysts." *Chemical Engineering Science* no. 41 (6):1631-1645.

[42] Iliyas, A., and S. Al-Khattaf. 2004. "Xylene Transformation over USY Zeolite in a Riser Simulator: A Comprehensive Kinetic Model." *Industrial & Engineering Chemistry Research* no. 43:1349-1358.

[43] Yaws, C. L. 2003. *Yaws' Handbook of Thermodynamic and Physical Properties of Chemical Compounds*. First ed. Norwich: Knovel.

[44] Mirth, G., J. Cejka, and J. A. Lercher. 1993. "Transport and Isomerization of Xylenes over HZSM-5 Zeolites." *Journal of Catalysis* no. 139 (1):24-33.

[45] Pérez-Pariente, J., E. Sastre, V. Fornés, J. A. Martens, P. A. Jacobs, and A. Corma. 1991. "Isomerization and disproportionation of m-xylene over zeolite β." *Applied Catalysis* no. 69 (1):125-137.

[46] Celik, F. E., T. J. Kim, and A. T. Bell. 2010. "Effect of zeolite framework type and Si/Al ratio on dimethoxymethane carbonylation." *Journal of Catalysis* no. 270 (1):185-195.

[47] Soong, T. T. 2004. *Fundamentals of Probability and Statistics for Engineers*. First ed. New York: Wiley.

[48] Minceva, M., P. S. Gomes, V. Meshko, and A. E. Rodrigues. 2008. "Simulated moving bed reactor for isomerization and separation of p-xylene." *Chemical Engineering Journal* no. 140 (1-3):305-323.

Chapter 10: Conclusions and suggestions for future work

The main conclusion of this thesis along with the accomplishment of several specific objectives are briefly described in this chapter. In addition, suggestions for future work related to the subject are also presented, that is different catalysts for xylene isomerization in liquid phase, development of a single material capable of adsorbing and converting the isomers into *p*-xylene, different operating conditions and even different aromatics complex scheme are proposed.

10.1. Conclusions

A simulated moving bed reactor for the production of *p*-xylene is developed in the framework of a proposal to modify the current aromatics complex in Portugal; it is verified that a purity constraint of 0.70 in the extract guarantees a *p*-xylene feed above 75 wt% to a crystallization unit leading to a recovery of 95% in a single stage unit. The production of benzene and *p*-xylene within the aromatics complex is increased in 170% and 72% respectively compared to the current production. The simulated moving bed reactor unit is also capable of handling twice the current feed to the complex since the recycle loop is significantly reduced due to the fact that a significant part of the isomers are isomerized within the unit and therefore the charge to the isomerization unit is reduced.

The unit is designed based on the existing simulated moving bed for separation of *p*-xylene. Maintaining the same physical dimensions of the columns it is found that the best configuration is two columns in the first zone, six in the second zone, fourteen in the third, and two in the fourth zone where each column comprises a first bed with a homogeneous mixture with an adsorbent to adsorbent plus catalyst weight ratio of 0.4 occupying 15% of the column followed by a second bed filled with adsorbents. The unit exhibits at 473 K a productivity of 226 kg $m^{-3}h^{-1}$, a desorbent consumption of 0.07 m^3 h^{-1}, and a deviation from the equilibrium of 2.08 which results in *p*-xylene in the extract to *p*-xylene in the feed ratio of 1.75. The unit also demonstrated flexibility to process more feed by reducing the portion of the first bed with a still high deviation from the equilibrium of 2.02. Therefore, it is concluded that it is feasible to turn an existing simulated moving bed unit into a simulated moving bed reactor unit.

Even though the unit does not present uniform bed structure, the true moving bed reactor approach proves to be a valuable tool in the design of the dual-bed simulated moving bed reactor. Optimal particle size is determined by analyzing the unit for several sizes using less-time consuming true moving bed reactor approach. It is verified that the optimal distribution of columns within the zones does not depend on the particle size, however it is recommended to set said distribution with a relative small particle diameter. Moreover, it is noticed that the larger amount of desorbent needed in this type of unit is due to the continuous xylene isomerization rather than mass-transfer resistance; therefore, optimum column configuration tends to have fewer columns in zones one and four. The aforementioned together with milder constraint in the extract product allow to use more columns in zone three where in fact more *p*-xylene is produced because its lower concentration.

The main disadvantage is the large amount of desorbent needed which may increase circulating and desorbent recovery costs. Nevertheless, the maximum pressure drop of the unit is

not affected due to fewer columns in the first zone which somewhat compensates the higher desorbent rate. Furthermore, the distillation column for the recovery of desorbent from the extract stream is combined with the column to separate unreacted toluene from the selective toluene disproportionation unit providing another advantage of the integrated process in the proposed aromatics complex. Also, the reduction in the recycle loop might outweighs the cost due to circulation of toluene based on the decreased energy consumed within the furnace of the isomerization unit.

Additionally, isomerization of xylenes in liquid phase is analyzed. Initially, three expressions to determine the equilibrium between 250 and 550 K are developed based on experimental data in the literature. Afterwards, three large-pore zeolites are experimentally studied as potential candidates to be used in the simulated moving bed reactor where conversion is preferred over selectivity. Beta zeolite with Si/Al ratio of 35 exhibits the highest conversion of *o*-xylene at 493 K due to its optimum level of acidity without compromising the diffusion of the species inside the channels. Reaction experiments are carried out between 473 and 513 K with the purpose of developing a kinetic model of said zeolite in the presence of toluene, absence of diffusional constraints is verified based on the activation energies obtained.

Finally, a mathematical model based on the operation of the existing isomerization unit is developed; the model effectively simulates the operation of the radial reactor which is later used in the mass balance of the proposed aromatics complex.

10.2. Suggestions for future work

Since xylene isomerization is not industrially performed in liquid phase there is a long path to select the appropriate catalyst for a simulated moving bed reactor. It has been noticed that there is an optimum Si/Al ratio, however that value may vary for different zeolites. It has also been seen that zeolite with large pores might be suitable for this purpose due to diffusion constraints in liquid phase at low temperatures and the fact that the presence of adsorbents provides selectivity and toluene shifts disproportionation reactions towards the xylene side. Normally, 12 membered-ring zeolites possess large pores (e.g., Beta), nevertheless there are other zeolites that could provide the required xylene conversion. For instance, the structures of MCM-22 and NU-87 are between 10 and 12 membered-ring, TNU-9 possesses three-dimensional 10 membered-ring systems with slightly larger pores than MFI. Moreover, hierarchical zeolites, specifically MFI treated with NaOH and washed by mild HCl, present the combination of micropores and mesopores enhancing the diffusion within the zeolite crystals while maintaining

or even increasing their Brønsted acidity. An extensive experimental study shall be carried out in order to choose the optimum catalyst.

The influence of temperature has not been addressed in this thesis, since adsorption decreases and reaction increases with higher temperatures there is an optimum value for the operation of the simulated moving bed reactor. Adsorption and reaction data for several temperatures are required for this purpose; temperature is to be above around industrial separation of *p*-xylene (i.e., ~180 ºC) and below 300 ºC which is near to the operation of gas phase isomerization units. Optimum temperature can be determined together with column arrangement and particle size using the less-time consuming true moving bed reactor approach. After that, the dual-bed system can be developed with the appropriate ratio of adsorbents and catalysts using the method proposed in Chapter 7.

Up to this point, adsorbents and catalysts have been treated as separate solids; the appropriate zeolite catalyst may be combined with one of the well-studied adsorbents at the previously determined ratio within a single pellet with γ-alumina as binder. Not only packing process would be simpler but the path between adsorption and reaction sites is significantly reduced.

Although adsorption and reaction data are obtained experimentally, the unit should also be evaluated experimentally through some sort of pilot unit in order to confirm the mathematical model and prove the feasibility of the unit. Some parameters, such as dispersion and molecular diffusivities among others, used in this thesis are obtained from published correlations, small variations on these parameters could cause significant deviations from actual operation from which is highly recommended to verify said parameters.

Mass and energy balances should be calculated within the proposed aromatics complex. Operating costs should be estimated and the separation within the distillation columns should be verified due to the large amount of toluene. Moreover, a different scheme where an isomerization unit with ethylbenzene dealkylation catalyst type is placed upstream the simulated moving bed reactor unit could present better performance through the withdrawal of a significant portion of ethylbenzene before the simulated moving bed reactor.

Annex A: Properties

A.1. General

Critical constants and acentric factors of ethylbenzene (EB), *o*-xylene (OX), *m*-xylene (MX), *p*-xylene (PX), ethylcyclohexane (ECH), hydrogen (H_2), toluene (Tol), and benzene (Ben) used throughout the thesis are presented in Table A.1:

Table A.1 Properties of the species involved throughout the thesis from Poling et al. [1]

	P_c, kPa	T_c, K	ω	ρ_c, kg m^{-3}	M, g mol^{-1}
EB	3609	617.15	0.3035	283.86	106.165
OX	3732	630.3	0.3101	286.93	106.165
MX	3541	617	0.3265	283.12	106.165
PX	3511	616.2	0.3218	280.86	106.165
ECH	3040	609.15	0.2455	260.96	112.213
H_2	1313	33.19	-0.2160	31.428	2.016
Tol	4108	591.75	0.2640	291.56	92.138
Ben	4895	562.05	0.2103	305.13	78.112

A.2. Gas phase

The molar volume (V) for the aromatics and naphthenes (ethylcyclohexane) used in Chapter 4 is calculated using the virial equation truncated after the second virial coefficient [1]:

$$V = \frac{RT}{P}\left(1 + \frac{B}{V}\right) \tag{A.1}$$

$$\frac{BP_c}{RT_c} = B^{(0)} + \omega B^{(1)} \tag{A.2}$$

$$B^{(0)} = 0.1445 - \frac{0.330}{T_r} - \frac{0.1385}{T_r^2} - \frac{0.0121}{T_r^3} - \frac{0.000607}{T_r^8} \tag{A.3}$$

$$B^{(1)} = 0.0637 + \frac{0.331}{T_r^2} - \frac{0.423}{T_r^3} - \frac{0.008}{T_r^8} \tag{A.4}$$

where critical parameters are presented in Table A.1 and reduced temperature (T_r) is calculated with the critical value ($T_r = T/T_c$).

A.3. Liquid phase

The molecular diffusivity D_m (cm^2 s^{-1}) used for mass-transfer in Chapters 5 to 7 is calculated through the Wilke-Chang method modified to include the mixed solvent case by Perkins and Geankoplis [2]:

$$D_{im}^{0} = 7.4 \times 10^{-8} \frac{(\phi M)^{1/2} T}{\mu_m V_i^{0.6}} \quad \text{with} \quad \phi M = \sum_{\substack{j=1 \\ j \neq i}} x_j \phi_j M_j \tag{A.5}$$

where ϕ_j depends on the solvent and in this case is 1. The mixture viscosity μ_m (cP) is calculated with the method of Grunberg and Nissan for ideal mixtures [2]:

$$\mu_m = \prod_j \mu_j^{x_j} \tag{A.6}$$

where x_j is the mole fraction of species j. The viscosity of pure components μ_j (cP) are taken from Yaws [3] and presented in Table A.2:

Table A.2 Viscosity of pure components [3]

	$\log \mu = \mathrm{A} + \mathrm{B}/T + \mathrm{C}T + \mathrm{D}T^2$					μ, cP at 200 ºC
	A	B	C	D	T, K	
PX	-9.4655	1.44×10^{3}	1.991×10^{-2}	-1.6994×10^{-5}	288-616	0.156
MX	-6.0517	9.246×10^{2}	1.2583×10^{-2}	-1.185×10^{-5}	225-617	0.160
OX	-7.8805	1.25×10^{3}	1.6116×10^{-2}	-1.3993×10^{-5}	268-630	0.179
EB	-5.2585	8.3065×10^{2}	1.0784×10^{-2}	-1.0618×10^{-5}	210-617	0.167
Tol	-5.1649	8.1068×10^{2}	1.0454×10^{-2}	-1.0488×10^{-5}	200-592	0.140

V_i is the molar volume (cm^3 mol^{-1}) of solute i at its normal boiling point T_b. Molar volume of each component at different conditions is estimated using the Yamada and Gunn method [2]:

$$V = V_{ref}(0.29056 - 0.08775\omega)^{(1-T/T_c)^{2/7} - (1-T_{ref}/T_c)^{2/7}} \tag{A.7}$$

where the reference value is the molar volume at 25 ºC. The molar volume is also used to calculate the density of each component. The molar volumes at different temperatures are presented in Table A.3:

Table A.3 Molar volumes of each species at different conditions

	V_{ref}, cm^3 mol^{-1}	V, cm^3 mol^{-1} at T_b	V, cm^3 mol^{-1} at 200 ºC
PX	123.93	141.29	155.37
MX	123.47	140.90	154.73
OX	121.25	138.48	150.18
EB	123.08	139.77	154.03
Tol	106.87	118.26	136.72

A.4. Crystallization

The heat of fusion (ΔH^{fusion}) and difference of solid and liquid heat capacity (ΔC_p) of each species at their melting point (T_m) is presented in Table A.4:

Table A.4 Heat of fusion and difference of solid and liquid heat capacity of each species at melting point [3]

	ΔH^{fusion}, kJ mol^{-1}	ΔC_p, J mol^{-1}K^{-1}	T_m, K
PX	17.113	40.912	286.41
MX	11.569	48.385	225.30
OX	13.598	34.067	247.98
EB	9.184	60.250	178.20

Table A.5 and Table A.6 present the solid heat capacity (C_p^{sol}) and liquid heat capacity (C_p^{liq}) respectively:

Table A.5 Solid heat capacity of each species [3]

	$C_p^{sol} = A + BT + CT^2$				C_p^{sol},
	A	B	C	T, K	J mol^{-1}K^{-1} at T_m
PX	0.872	8.0786×10^{-1}	-9.5350×10^{-4}	153-286	154.035
MX	3.913	8.4357×10^{-1}	-1.4305×10^{-3}	80-225	121.357
OX	0.302	7.8782×10^{-1}	-8.1442×10^{-4}	20-247	145.584
EB	-4.874	1.0061	-2.2358×10^{-3}	20-170	103.415

Values are used even if outside of temperature range in the absence of more reliable data

Table A.6 Liquid heat capacity of each species [3]

	$C_p^{liq} = A + BT + CT^2 + DT^3$					C_p^{liq},
	A	B	C	D	T, K	J mol^{-1}K^{-1} at T_m
PX	-11.035	1.5158	-3.9039×10^{-3}	3.9193×10^{-6}	287-555	194.947
MX	70.916	8.0450×10^{-1}	-2.1885×10^{-3}	2.5061×10^{-6}	226-555	169.742
OX	56.460	9.4926×10^{-1}	-2.4902×10^{-3}	2.6838×10^{-6}	249-567	179.651
EB	102.111	5.5959×10^{-1}	-1.5609×10^{-3}	2.0149×10^{-6}	179-555	163.665

Values are used even if outside of temperature range in the absence of more reliable data

A.5. Nomenclature

C_p = Heat capacity, J mol^{-1}K^{-1}

D_m = Molecular diffusivity, m^2 s^{-1}

H^{fusion} = Heat of fusion, kJ mol^{-1}

M = Molecular weight, g mol^{-1}

P = Pressure, kPa

T = Temperature, K

T_b = Normal boiling point, K

T_m = Melting point, K

V = molar volume, $cm^3\ mol^{-1}$

x_i = Mole fraction of component i

Greek letters

μ = Viscosity, cP

ρ = Fluid density, $kg\ m^{-3}$

ϕ = Association factor

ω = Acentric factor

Abbreviations

Ben = Benzene

EB = Ethylbenzene

ECH = Ethylcyclohexane

MX = m-Xylene

OX = o-Xylene

PX = p-Xylene

Tol = Toluene

Superscripts and subscripts

c = Critical property

liq = Liquid

m = Mixture

r = Reduced property

ref = Reference

sol = Solid

A.6. References

[1] Poling, B. E., G. H. Thomson, D. G. Friend, R. L. Rowley, and W. V. Wilding. 2008. "Physical and Chemical Data." In *Perry's Chemical Engineers' Handbook*, edited by Don W. Green and Robert H. Perry. McGraw-Hill.

[2] Poling, B. E., J. M. Prausnitz, and J. J. P. O'Connell. 2001. *The Properties of Gases and Liquids*. 5th ed. New York: The McGraw-Hill Companies.

[3] Yaws, C. L. 2003. *Yaws' Handbook of Thermodynamic and Physical Properties of Chemical Compounds*. First ed. Norwich: Knovel.

Annex B: Optimizations

B.1. Separation regions and separation volumes

Table B.1 to Table B.4 present the vertex points for several values of γ_1 and γ_4, 6-9-6-3 configuration, and 69 s switching time with the four particle diameters studied in Section 6.3.1 in Chapter 6 from which an optimum value is chosen for each size.

Table B.1 Vertex points of the separation regions for γ_1 values between 3.5 and 6.0 and γ_4 values between 0.1 and 0.8 for 6-9-6-3 configuration, 69 s switching time and 0.5 mm particle diameter

γ_4	γ_2	γ_3	PR, kg $m^{-3}h^{-1}$	DC, m^3 kg^{-1}	DE
			$\gamma_1 = 3.5$		
0.1	1.20	1.41	118.71	0.092	1.39
0.2	1.20	1.40	115.77	0.091	1.42
0.3	1.18	1.40	141.43	0.072	1.54
0.4	1.17	1.39	150.60	0.066	1.63
0.5	1.16	1.38	159.39	0.060	1.71
0.6	1.16	1.37	155.38	0.060	1.74
0.7	1.16	1.35	146.49	0.061	1.81
0.8	1.16	1.32	130.66	0.066	1.90
			$\gamma_1 = 4.0$		
0.1	1.18	1.43	150.86	0.083	1.47
0.2	1.18	1.42	148.46	0.082	1.50
0.3	1.16	1.42	173.67	0.068	1.60
0.4	1.15	1.41	183.18	0.063	1.67
0.5	1.15	1.39	176.67	0.063	1.73
0.6	1.14	1.38	185.34	0.059	1.81
0.7	1.14	1.36	177.03	0.060	1.87
0.8	1.14	1.34	167.39	0.061	1.94
			$\gamma_1 = 4.5$		
0.1	1.17	1.44	166.62	0.084	1.49
0.2	1.17	1.43	164.48	0.084	1.53
0.3	1.15	1.42	187.03	0.072	1.64
0.4	1.14	1.41	196.46	0.067	1.72
0.5	1.14	1.40	193.25	0.066	1.75
0.6	1.14	1.38	186.19	0.067	1.82
0.7	1.13	1.36	190.34	0.064	1.92
0.8	1.13	1.34	180.60	0.065	1.98
			$\gamma_1 = 5.0$		
0.1	1.17	1.44	167.15	0.094	1.50
0.2	1.16	1.43	177.78	0.086	1.58
0.3	1.15	1.42	187.61	0.080	1.65
0.4	1.14	1.41	197.06	0.075	1.72
0.5	1.13	1.40	206.36	0.070	1.79

γ_4	γ_2	γ_3	PR, kg $m^{-3}h^{-1}$	DC, m^3 kg^{-1}	DE
0.6	1.13	1.38	199.32	0.071	1.86
0.7	1.13	1.36	190.95	0.072	1.92
0.8	1.13	1.34	181.20	0.074	1.99
			$\gamma_1 = 5.5$		
0.1	1.16	1.44	180.35	0.096	1.55
0.2	1.16	1.43	178.19	0.095	1.58
0.3	1.14	1.43	202.98	0.082	1.66
0.4	**1.13**	**1.41**	**209.99**	**0.078**	**1.76**
0.5	1.13	1.40	206.81	0.077	1.80
0.6	1.13	1.38	199.77	0.078	1.86
0.7	1.13	1.36	191.40	0.080	1.93
0.8	1.13	1.34	181.65	0.083	2.00
			$\gamma_1 = 6.0$		
0.1	1.16	1.44	180.67	0.104	1.55
0.2	1.15	1.44	193.33	0.096	1.59
0.3	1.14	1.43	203.32	0.090	1.66
0.4	1.13	1.41	210.34	0.085	1.76
0.5	1.13	1.40	207.15	0.085	1.80
0.6	1.13	1.38	200.11	0.086	1.87
0.7	1.13	1.36	191.74	0.088	1.93
0.8	1.12	1.34	194.09	0.086	2.03

Bold indicates optimum

Table B.2 Vertex points of the separation regions for γ_1 values between 3.5 and 6.0 and γ_4 values between 0.1 and 0.8 for 6-9-6-3 configuration, 69 s switching time, and 0.7 mm particle diameter

γ_4	γ_2	γ_3	PR, kg $m^{-3}h^{-1}$	DC, m^3 kg^{-1}	DE
			$\gamma_1 = 3.5$		
0.1	1.19	1.28	60.17	0.181	1.60
0.2	1.18	1.29	79.03	0.133	1.70
0.3	1.18	1.29	79.00	0.129	1.70
0.4	1.17	1.30	97.62	0.102	1.77
0.5	1.17	1.29	91.29	0.105	1.79
0.6	1.17	1.28	84.67	0.109	1.80
0.7	1.17	1.26	70.51	0.127	1.83
0.8	1.17	1.24	55.28	0.156	1.84
			$\gamma_1 = 4.0$		
0.1	1.17	1.31	104.82	0.119	1.76
0.2	1.16	1.32	123.01	0.099	1.80
0.3	1.16	1.31	117.15	0.101	1.82
0.4	1.16	1.31	117.13	0.098	1.83
0.5	1.15	1.30	123.29	0.091	1.90
0.6	1.15	1.30	123.33	0.088	1.91

γ_4	γ_2	γ_3	PR, kg $m^{-3}h^{-1}$	DC, m^3 kg^{-1}	DE
0.7	1.15	1.29	116.89	0.090	1.93
0.8	1.15	1.27	103.04	0.099	1.98
			$\gamma_1 = 4.5$		
0.1	1.15	1.35	156.94	0.090	1.83
0.2	1.15	1.34	152.00	0.090	1.86
0.3	1.14	1.35	169.20	0.079	1.88
0.4	1.14	1.34	164.28	0.080	1.91
0.5	1.14	1.33	159.03	0.080	1.94
0.6	1.14	1.32	153.46	0.081	1.97
0.7	1.14	1.31	147.56	0.082	2.00
0.8	1.14	1.30	141.33	0.084	2.04
			$\gamma_1 = 5.0$		
0.1	1.14	1.36	174.69	0.090	1.85
0.2	1.14	1.35	170.05	0.090	1.88
0.3	1.13	1.34	177.35	0.085	1.95
0.4	1.13	1.35	182.23	0.081	1.92
0.5	1.13	1.34	177.32	0.081	1.95
0.6	1.13	1.33	172.08	0.082	1.99
0.7	1.13	1.32	166.51	0.083	2.02
0.8	1.13	1.30	154.26	0.087	2.08
			$\gamma_1 = 5.5$		
0.1	1.14	1.36	175.28	0.098	1.86
0.2	**1.13**	**1.36**	**187.52**	**0.090**	**1.90**
0.3	1.13	1.35	182.87	0.091	1.93
0.4	1.13	1.34	177.92	0.092	1.96
0.5	1.13	1.34	177.91	0.090	1.96
0.6	1.13	1.33	172.67	0.091	1.99
0.7	1.13	1.32	167.08	0.092	2.03
0.8	1.13	1.30	154.81	0.097	2.09
			$\gamma_1 = 6.0$		
0.1	1.13	1.36	188.06	0.100	1.90
0.2	1.13	1.36	188.01	0.099	1.90
0.3	1.13	1.35	183.34	0.099	1.93
0.4	1.13	1.34	178.38	0.100	1.96
0.5	1.13	1.34	178.38	0.099	1.97
0.6	1.12	1.33	185.07	0.093	2.03
0.7	1.12	1.32	179.58	0.094	2.06
0.8	1.12	1.31	173.72	0.096	2.10

Bold indicates optimum

Table B.3 Vertex points of the separation regions for γ_1 values between 4.0 and 6.5 and γ_4 values between 0.1 and 0.8 for 6-9-6-3 configuration, 69 s switching time, and 0.8 mm particle diameter

γ_4	γ_2	γ_3	PR, kg $m^{-3}h^{-1}$	DC, m^3 kg^{-1}	DE
		$\gamma_1 = 4.0$			
0.1	1.17	1.27	74.14	0.168	1.75
0.2	1.17	1.26	67.09	0.181	1.75
0.3	1.16	1.26	79.10	0.150	1.84
0.4	1.16	1.27	86.23	0.133	1.83
0.5	1.16	1.27	86.30	0.130	1.83
0.6	1.16	1.26	79.23	0.137	1.85
0.7	1.16	1.24	64.24	0.164	1.87
0.8	1.16	1.22	48.32	0.212	1.88
		$\gamma_1 = 4.5$			
0.1	1.16	1.28	93.78	0.150	1.82
0.2	1.15	1.28	105.95	0.130	1.89
0.3	1.15	1.29	112.59	0.119	1.87
0.4	1.15	1.29	112.62	0.116	1.87
0.5	1.15	1.28	106.01	0.121	1.90
0.6	1.15	1.27	99.14	0.126	1.92
0.7	1.15	1.26	92.00	0.132	1.94
0.8	1.15	1.24	76.79	0.154	1.97
		$\gamma_1 = 5.0$			
0.1	1.15	1.30	119.57	0.131	1.86
0.2	1.15	1.29	113.17	0.136	1.88
0.3	1.14	1.30	131.80	0.114	1.91
0.4	1.14	1.30	131.82	0.112	1.91
0.5	1.14	1.29	125.46	0.115	1.94
0.6	1.14	1.28	118.83	0.118	1.96
0.7	1.14	1.27	111.91	0.123	1.99
0.8	1.14	1.26	104.71	0.128	2.01
		$\gamma_1 = 5.5$			
0.1	1.14	1.31	138.43	0.125	1.89
0.2	1.14	1.30	132.30	0.128	1.92
0.3	1.14	1.30	132.31	0.126	1.92
0.4	1.14	1.30	132.30	0.123	1.92
0.5	1.14	1.29	125.96	0.127	1.94
0.6	1.13	1.28	131.47	0.119	2.01
0.7	1.13	1.28	131.57	0.117	2.02
0.8	1.13	1.27	124.64	0.121	2.05
		$\gamma_1 = 6.0$			
0.1	1.14	1.31	138.84	0.136	1.90
0.2	1.13	1.30	144.96	0.128	1.96
0.3	1.13	1.31	151.08	0.121	1.94

γ_4	γ_2	γ_3	PR, kg $m^{-3}h^{-1}$	DC, m^3 kg^{-1}	DE
0.4	**1.13**	**1.31**	**151.10**	**0.118**	**1.95**
0.5	1.13	1.30	145.01	0.121	1.97
0.6	1.13	1.29	138.63	0.125	2.00
0.7	1.13	1.28	131.96	0.128	2.03
0.8	1.13	1.27	125.02	0.133	2.05
			$\gamma_1 = 6.5$		
0.1	1.13	1.32	157.28	0.130	1.92
0.2	1.13	1.31	151.44	0.133	1.95
0.3	1.13	1.31	151.42	0.131	1.95
0.4	1.13	1.30	145.31	0.134	1.97
0.5	1.13	1.30	145.35	0.132	1.98
0.6	1.13	1.29	138.96	0.136	2.00
0.7	1.13	1.28	132.28	0.140	2.03
0.8	1.13	1.27	125.32	0.145	2.06

Bold indicates optimum

Table B.4 Vertex points of the separation regions for γ_1 values between 4.5 and 7.0 and γ_4 values between 0.1 and 0.8 for 6-9-6-3 configuration, 69 s switching time and 0.9 mm particle diameter

γ_4	γ_2	γ_3	PR, kg $m^{-3}h^{-1}$	DC, m^3 kg^{-1}	DE
			$\gamma_1 = 4.5$		
0.1	1.16	1.24	60.70	0.232	1.78
0.2	1.16	1.24	60.71	0.226	1.78
0.3	1.16	1.23	53.13	0.253	1.78
0.4	1.16	1.22	45.36	0.289	1.78
0.5	1.16	1.21	37.48	0.341	1.76
0.6	1.15	1.16	7.27	1.715	1.71
0.7	1.15	1.16	7.29	1.666	1.72
			$\gamma_1 = 5.0$		
0.1	1.15	1.26	87.65	0.179	1.86
0.2	1.15	1.26	87.66	0.175	1.86
0.3	1.15	1.25	80.42	0.187	1.87
0.4	1.15	1.25	80.47	0.183	1.87
0.5	1.15	1.24	73.00	0.197	1.89
0.6	1.15	1.23	65.28	0.215	1.90
0.7	1.15	1.22	57.39	0.240	1.91
0.8	1.14	1.16	16.84	0.797	1.94
			$\gamma_1 = 5.5$		
0.1	1.15	1.26	88.01	0.196	1.86
0.2	1.14	1.27	107.13	0.158	1.91
0.3	1.14	1.27	107.16	0.155	1.91
0.4	1.14	1.27	107.21	0.152	1.92
0.5	1.14	1.26	100.19	0.160	1.94

γ_4	γ_2	γ_3	PR, kg $m^{-3}h^{-1}$	DC, m^3 kg^{-1}	DE
0.6	1.14	1.25	92.93	0.169	1.95
0.7	1.14	1.24	85.40	0.180	1.97
0.8	1.14	1.22	69.51	0.216	2.00
			$\gamma_1 = 6.0$		
0.1	1.14	1.28	114.27	0.165	1.90
0.2	1.14	1.27	107.47	0.173	1.92
0.3	1.14	1.27	107.49	0.170	1.92
0.4	1.14	1.27	107.54	0.166	1.92
0.5	1.14	1.26	100.52	0.175	1.94
0.6	1.14	1.25	93.23	0.185	1.96
0.7	1.14	1.24	85.67	0.198	1.98
0.8	1.13	1.22	81.54	0.204	2.07
			$\gamma_1 = 6.5$		
0.1	1.14	1.27	107.73	0.190	1.92
0.2	1.13	1.26	112.68	0.179	1.99
0.3	1.13	1.28	126.70	0.156	1.95
0.4	**1.13**	**1.28**	**126.75**	**0.154**	**1.96**
0.5	1.13	1.27	119.97	0.160	1.98
0.6	1.13	1.26	112.92	0.167	2.00
0.7	1.13	1.25	105.62	0.176	2.03
0.8	1.13	1.24	98.05	0.186	2.05
			$\gamma_1 = 7.0$		
0.1	1.13	1.28	126.91	0.174	1.96
0.2	1.13	1.28	126.93	0.171	1.96
0.3	1.13	1.28	126.95	0.169	1.96
0.4	1.13	1.28	127.01	0.166	1.96
0.5	1.13	1.27	120.21	0.173	1.98
0.6	1.13	1.26	113.16	0.181	2.01
0.7	1.13	1.25	105.84	0.190	2.03
0.8	1.13	1.24	98.26	0.202	2.06

Bold indicates optimum

B.2. Arrangement of columns

Table B.5 presents the optimum points corresponding to the separation regions presented in Figure 6.2 for each particle size with productivity, desorbent consumption, and deviation from the equilibrium.

Table B.5 Optimum points for several configurations and 69 s switching time for each particle diameter.

Size, mm	Config	γ_2	γ_3	PR, kg $m^{-3}h^{-1}$	DC, m^3 kg^{-1}	DE
	2-4-16-2	1.11	1.65	253.33	0.064	1.19
	3-4-15-2	1.11	1.63	253.00	0.064	1.23
	2-5-15-2	1.11	1.63	252.17	0.065	1.22
	3-5-14-2	1.11	1.61	251.87	0.065	1.26
	3-4-14-3	1.12	1.62	243.97	0.067	1.23
	2-6-14-2	1.12	1.61	241.33	0.068	1.24
	3-6-13-2	1.12	1.58	241.03	0.068	1.31
0.5[a]	4-6-12-2	1.12	1.55	240.73	0.068	1.38
	3-7-11-3	1.12	1.53	239.79	0.068	1.43
	3-7-12-2	1.12	1.55	239.39	0.068	1.37
	4-7-11-2	1.12	1.52	239.01	0.068	1.46
	3-8-11-2	1.12	1.51	237.36	0.069	1.48
	5-7-9-3	1.13	1.47	226.65	0.072	1.60
	5-8-8-3	1.13	1.45	222.16	0.073	1.65
	5-9-7-3	1.13	1.43	216.17	0.075	1.70
	2-4-16-2	1.13	1.42	213.48	0.079	1.73
	2-5-15-2	1.13	1.41	210.96	0.080	1.77
	3-4-15-2	1.13	1.41	210.71	0.080	1.77
	2-6-14-2	1.13	1.40	207.79	0.082	1.80
	3-5-14-2	1.13	1.40	207.77	0.082	1.80
	3-4-14-3	1.13	1.39	204.75	0.083	1.83
	3-6-13-2	1.13	1.39	204.17	0.083	1.83
0.7[b]	4-5-13-2	1.13	1.39	204.17	0.083	1.83
	4-5-12-3	1.13	1.38	200.36	0.085	1.87
	4-6-12-2	1.13	1.38	200.09	0.085	1.86
	3-7-12-2	1.13	1.38	199.95	0.085	1.86
	4-8-10-2	1.13	1.37	194.16	0.087	1.88
	3-9-10-2	1.13	1.37	193.83	0.087	1.88
	2-10-10-2	1.13	1.37	193.42	0.088	1.88
	5-9-7-3	1.13	1.34	175.69	0.096	1.93
	2-5-15-2	1.13	1.35	186.25	0.096	1.96
	2-6-14-2	1.13	1.35	185.64	0.096	1.95
	3-5-14-2	1.13	1.34	180.96	0.099	1.99
	3-5-13-3	1.13	1.34	180.31	0.099	1.98
	3-6-13-2	1.13	1.34	180.20	0.099	1.98
	3-7-12-2	1.13	1.34	179.22	0.100	1.97
0.8[c]	3-8-11-2	1.13	1.34	178.02	0.101	1.96
	2-9-11-2	1.13	1.34	177.78	0.101	1.96
	4-5-12-3	1.13	1.33	174.40	0.103	2.01
	3-7-11-3	1.13	1.33	173.13	0.103	2.00
	4-7-11-2	1.13	1.33	173.06	0.103	1.99
	2-4-16-2	1.14	1.34	170.29	0.105	1.97

Size, mm	Config	γ_2	γ_3	PR, kg $m^{-3}h^{-1}$	DC, m^3 kg^{-1}	DE
	4-8-9-3	1.13	1.33	170.17	0.105	1.97
	5-7-9-3	1.13	1.32	164.90	0.109	2.00
	5-9-7-3	1.13	1.31	154.23	0.116	1.98
	2-4-16-2	1.14	1.32	156.90	0.124	2.01
	2-5-15-2	1.14	1.32	156.26	0.125	2.00
	2-6-14-2	1.14	1.32	155.35	0.126	1.99
	3-4-15-2	1.14	1.31	150.59	0.130	2.04
	3-4-14-3	1.14	1.31	149.86	0.130	2.03
	3-5-14-2	1.14	1.31	149.78	0.130	2.03
	3-5-13-3	1.14	1.31	148.93	0.131	2.02
0.9[d]	4-5-13-2	1.14	1.31	148.89	0.131	2.02
	4-5-12-3	1.14	1.31	148.89	0.131	2.02
	3-6-13-2	1.14	1.31	148.70	0.131	2.02
	4-8-9-3	1.13	1.30	148.55	0.131	2.01
	5-8-9-2	1.13	1.30	148.51	0.131	2.01
	5-8-8-3	1.13	1.30	146.32	0.133	1.99
	5-7-9-3	1.13	1.29	142.37	0.137	2.04
	5-9-7-3	1.13	1.29	136.90	0.142	1.98

[a] γ_1=5.5 and γ_4=0.4. [b] γ_1=5.5 and γ_4=0.2. [c] γ_1=6.0 and γ_4=0.4. [d] γ_1=6.5 and γ_4=0.4

B.3. Optimization without maximum pressure drop constraint

Table B.6 presents the optimization results for each particle diameter from Section 6.3.3 in Chapter 6 without maximum pressure drop constraint.

Table B.6 Optimization for several configurations at different desorbent consumptions for each particle size

Config	γ_1	γ_2	γ_3	γ_4	PR, kg $m^{-3}h^{-1}$	DE	Switching time, s
0.5 mm							
DC = 0.08 m^3 kg^{-1}							
2-6-14-2	4.85	1.11	1.32	0.27	1282.20	2.00	10
2-5-15-2	4.83	1.11	1.32	0.25	1235.91	2.00	10
3-5-14-2	4.60	1.12	1.32	0.22	1224.89	1.98	10
2-4-16-2	4.78	1.12	1.33	0.22	1153.92	2.00	11
3-4-15-2	4.62	1.12	1.32	0.21	1137.53	1.99	11
3-4-14-3	4.62	1.12	1.32	0.24	1095.80	1.99	11
DC = 0.07 m^3 kg^{-1}							
2-6-14-2	4.35	1.11	1.32	0.32	1211.15	1.99	11
2-5-15-2	4.32	1.12	1.33	0.30	1165.21	1.99	11

Config	γ_1	γ_2	γ_3	γ_4	PR, kg $m^{-3}h^{-1}$	DE	Switching time, s
3-5-14-2	4.16	1.12	1.32	0.29	1149.96	1.98	11
2-4-16-2	4.29	1.12	1.33	0.28	1085.03	1.99	12
3-4-15-2	4.18	1.12	1.33	0.28	1065.58	1.98	12
3-4-14-3	4.17	1.12	1.33	0.30	1026.98	1.98	12
DC = 0.06 m^3 kg^{-1}							
2-6-14-2	3.85	1.12	1.33	0.39	1107.55	1.99	11
2-5-15-2	3.84	1.12	1.33	0.38	1061.96	1.98	12
3-5-14-2	3.75	1.12	1.33	0.38	1040.36	1.97	12
2-4-16-2	3.82	1.12	1.34	0.36	984.89	1.97	13
3-4-15-2	3.76	1.12	1.34	0.37	961.76	1.97	13
3-4-14-3	3.75	1.12	1.33	0.38	927.00	1.98	13
DC = 0.05 m^3 kg^{-1}							
2-6-14-2	**3.39**	**1.12**	**1.34**	**0.49**	**943.80**	**1.97**	**14**
2-5-15-2	3.39	1.12	1.34	0.48	900.08	1.97	14
3-5-14-2	3.35	1.12	1.34	0.48	871.86	1.97	15
2-4-16-2	3.38	1.13	1.35	0.46	829.66	1.96	16
3-4-15-2	3.35	1.13	1.34	0.49	803.38	1.96	16
3-4-14-3	3.37	1.13	1.34	0.48	773.85	1.97	16
DC = 0.04 m^3 kg^{-1}							
2-6-14-2	3.00	1.13	1.35	0.63	647.24	1.96	20
2-5-15-2	3.01	1.13	1.36	0.61	617.47	1.94	21
3-5-14-2	3.01	1.13	1.36	0.62	586.43	1.95	22
2-4-16-2	3.02	1.13	1.37	0.58	571.09	1.91	24
3-4-15-2	3.02	1.13	1.37	0.59	543.21	1.92	25
3-4-14-3	3.01	1.13	1.36	0.60	518.73	1.93	26
0.7 mm							
DC = 0.10 m^3 kg^{-1}							
2-6-14-2	5.19	1.13	1.31	0.23	425.80	2.02	26
2-5-15-2	5.17	1.13	1.31	0.24	405.04	2.02	27
3-5-14-2	5.20	1.13	1.31	0.25	389.53	2.02	28
2-4-16-2	5.22	1.13	1.32	0.22	372.41	2.01	30
3-4-15-2	5.14	1.14	1.31	0.23	359.41	2.01	30
3-4-14-3	5.16	1.13	1.31	0.28	344.51	2.02	31
DC = 0.09 m^3 kg^{-1}							
2-6-14-2	4.79	1.13	1.31	0.31	393.38	2.01	28
2-5-15-2	4.78	1.13	1.32	0.29	374.45	2.01	29
3-5-14-2	4.77	1.13	1.32	0.30	358.99	2.01	31
2-4-16-2	4.77	1.14	1.32	0.24	344.22	1.99	32
3-4-15-2	4.76	1.14	1.32	0.28	331.27	2.00	33
3-4-14-3	4.74	1.14	1.32	0.33	317.30	2.01	34

Config	γ_1	γ_2	γ_3	γ_4	PR, kg $m^{-3}h^{-1}$	DE	Switching time, s
DC = 0.08 m^3 kg^{-1}							
2-6-14-2	4.42	1.13	1.32	0.37	347.89	2.00	32
2-5-15-2	4.41	1.14	1.32	0.35	331.61	1.99	34
3-5-14-2	4.40	1.14	1.32	0.36	316.59	1.99	35
2-4-16-2	4.40	1.14	1.33	0.28	306.08	1.96	37
3-4-15-2	4.40	1.14	1.33	0.33	292.93	1.97	38
3-4-14-3	4.41	1.14	1.33	0.37	279.73	1.98	40
DC = 0.07 m^3 kg^{-1}							
2-6-14-2	**4.09**	**1.14**	**1.33**	**0.44**	**278.05**	**1.96**	**41**
2-5-15-2	4.09	1.14	1.34	0.40	268.68	1.95	43
3-5-14-2	4.09	1.14	1.34	0.42	252.39	1.95	46
2-4-16-2	4.10	1.14	1.35	0.34	252.06	1.90	47
3-4-15-2	4.09	1.14	1.35	0.36	237.52	1.91	49
3-4-14-3	4.07	1.14	1.34	0.41	223.73	1.93	52
DC = 0.06 m^3 kg^{-1}							
2-4-16-2	3.82	1.15	1.41	0.36	167.26	1.69	76
2-5-15-2	3.82	1.15	1.40	0.39	154.00	1.70	82
2-6-14-2	3.77	1.15	1.40	0.42	138.02	1.69	89
3-4-15-2	3.79	1.15	1.42	0.40	132.45	1.62	94
3-5-14-2	3.78	1.15	1.41	0.41	129.82	1.66	95
3-4-14-3	3.79	1.16	1.41	0.46	117.15	1.67	104
0.8 mm							
DC = 0.12 m^3 kg^{-1}							
2-6-14-2	5.83	1.13	1.30	0.22	293.60	2.02	35
3-7-12-2	5.78	1.13	1.30	0.24	285.32	2.02	36
3-6-13-2	5.78	1.13	1.30	0.23	280.36	2.02	36
2-5-15-2	5.89	1.13	1.31	0.24	279.40	2.03	37
3-5-14-2	5.78	1.14	1.30	0.21	268.12	2.02	38
3-5-13-3	5.78	1.13	1.30	0.27	255.21	2.03	40
DC = 0.11 m^3 kg^{-1}							
2-6-14-2	5.44	1.13	1.31	0.26	275.61	2.01	38
3-7-12-2	5.44	1.13	1.30	0.28	266.50	2.01	39
2-5-15-2	5.42	1.14	1.31	0.23	262.42	2.01	40
3-6-13-2	5.41	1.13	1.31	0.26	262.33	2.01	39
3-5-14-2	5.38	1.14	1.31	0.24	251.65	2.01	41
3-5-13-3	5.41	1.14	1.31	0.31	238.90	2.02	43
DC = 0.10 m^3 kg^{-1}							
2-6-14-2	5.06	1.14	1.31	0.30	251.37	2.00	42
3-7-12-2	5.06	1.13	1.31	0.33	241.05	2.00	43
2-5-15-2	5.06	1.14	1.32	0.27	240.21	1.99	44
3-6-13-2	5.05	1.14	1.31	0.31	238.23	2.00	44

Config	γ_1	γ_2	γ_3	γ_4	PR, kg $m^{-3}h^{-1}$	DE	Switching time, s
3-5-14-2	5.05	1.14	1.32	0.28	228.83	1.99	46
3-5-13-3	5.04	1.14	1.31	0.34	217.07	2.00	48
DC = 0.09 m^3 kg^{-1}							
2-6-14-2	**4.72**	**1.14**	**1.32**	**0.34**	**217.24**	**1.97**	**49**
2-5-15-2	4.72	1.14	1.33	0.31	209.58	1.96	52
3-6-13-2	4.71	1.14	1.32	0.36	203.43	1.97	52
3-7-12-2	4.72	1.14	1.32	0.39	202.96	1.97	52
3-5-14-2	4.71	1.14	1.33	0.32	197.56	1.96	54
3-5-13-3	4.69	1.14	1.32	0.38	185.67	1.98	57
DC = 0.08 m^3 kg^{-1}							
2-5-15-2	4.42	1.15	1.35	0.32	163.74	1.89	69
2-6-14-2	4.41	1.15	1.34	0.37	161.46	1.90	69
3-5-14-2	4.41	1.15	1.35	0.34	147.30	1.88	76
3-6-13-2	4.38	1.15	1.35	0.38	138.29	1.88	80
3-5-13-3	4.39	1.15	1.35	0.41	128.91	1.88	85
3-7-12-2	4.29	1.15	1.35	0.41	117.88	1.84	90
0.9 mm							
DC = 0.13 m^3 kg^{-1}							
2-6-14-2	6.03	1.14	1.30	0.21	201.59	2.01	49
2-5-15-2	6.02	1.14	1.30	0.20	192.47	2.01	51
3-5-14-2	6.00	1.14	1.30	0.21	183.81	2.01	53
2-4-16-2	6.03	1.14	1.31	0.17	177.61	2.00	56
3-4-15-2	6.01	1.14	1.31	0.19	170.21	2.00	58
3-4-14-3	5.96	1.14	1.30	0.27	161.71	2.02	60
DC = 0.12 m^3 kg^{-1}							
2-6-14-2	5.64	1.14	1.31	0.24	187.41	2.00	53
2-5-15-2	5.67	1.14	1.31	0.22	179.53	1.99	56
3-5-14-2	5.64	1.14	1.31	0.23	170.74	2.00	58
2-4-16-2	5.59	1.15	1.31	0.19	166.34	1.98	60
3-4-15-2	5.65	1.15	1.31	0.21	158.81	1.98	63
3-4-14-3	5.63	1.15	1.31	0.29	150.24	2.00	65
DC = 0.11 m^3 kg^{-1}							
2-6-14-2	5.31	1.14	1.31	0.27	168.45	1.98	60
2-5-15-2	5.31	1.14	1.32	0.24	162.59	1.97	63
3-5-14-2	5.29	1.14	1.32	0.26	153.36	1.97	66
2-4-16-2	5.33	1.15	1.32	0.21	151.93	1.95	68
3-4-15-2	5.28	1.15	1.32	0.22	143.97	1.95	71
3-4-14-3	5.28	1.15	1.32	0.31	135.11	1.97	74
DC = 0.10 m^3 kg^{-1}							
2-6-14-2	**4.98**	**1.15**	**1.33**	**0.30**	**140.82**	**1.94**	**73**
2-5-15-2	4.99	1.15	1.33	0.27	139.09	1.93	75

Config	γ_1	γ_2	γ_3	γ_4	PR, kg $m^{-3}h^{-1}$	DE	Switching time, s
2-4-16-2	5.01	1.15	1.34	0.22	132.82	1.90	80
3-5-14-2	4.97	1.15	1.33	0.28	128.30	1.93	81
3-4-15-2	4.99	1.15	1.34	0.24	123.67	1.90	85
3-4-14-3	4.96	1.15	1.33	0.33	113.28	1.92	90
DC = 0.09 m^3 kg^{-1}							
2-4-16-2	4.73	1.16	1.37	0.24	106.07	1.79	104
2-5-15-2	4.69	1.16	1.36	0.27	102.61	1.80	106
3-4-15-2	4.69	1.16	1.37	0.25	92.40	1.76	118
2-6-14-2	4.56	1.16	1.37	0.28	83.40	1.74	126
3-5-14-2	4.58	1.16	1.38	0.28	76.97	1.71	137
3-4-14-3	4.56	1.17	1.38	0.36	64.36	1.68	159

Bold indicates optimum

B.4. Optimization subject to maximum pressure drop constraint

Table B.7 presents the results of the alternative optimization from Section 6.3.4 in Chapter 6 with the three best configurations.

Table B.7 Optimization for the best three configurations at different productivity values for each particle diameter (Alternative approach).

Config	Size, mm	γ_1	γ_2	γ_3	γ_4	PR, kg m^3h^{-1}	DE	Switching Time, s	DC, m^3 kg^{-1}
2-6-14-2	0.5	2.97	1.14	1.44	0.68	202.41	1.62	70	0.036
		3.58	1.13	1.47	0.65	220.00	1.60	72	0.041
	0.62	3.46	1.15	1.40	0.52	184.94	1.74	70	0.050
		3.48	1.14	1.39	0.53	200.37	1.78	65	0.050
		3.50	1.14	1.38	0.52	220.00	1.81	59	0.051
		3.54	1.14	1.38	0.50	240.00	1.84	54	0.051
		3.87	**1.13**	**1.41**	**0.32**	**260.00**	**1.75**	**56**	**0.054**
	0.7	3.75	1.15	1.40	0.41	137.19	1.69	88	0.061
		3.78	1.15	1.39	0.40	160.23	1.76	76	0.062
		3.86	1.15	1.37	0.44	180.00	1.84	67	0.062
		3.92	1.14	1.36	0.45	200.00	1.87	60	0.063
		3.95	1.14	1.35	0.46	220.00	1.91	54	0.065
		3.99	1.14	1.34	0.46	240.00	1.93	49	0.066
		4.39	1.13	1.36	0.27	260.00	1.90	50	0.070
	0.8	4.14	1.16	1.39	0.35	97.99	1.68	113	0.075
		4.23	1.15	1.37	0.36	120.01	1.78	94	0.076
		4.33	1.15	1.36	0.35	140.01	1.85	81	0.078

Config	Size, mm	γ_1	γ_2	γ_3	γ_4	PR, kg m^3h^{-1}	DE	Switching Time, s	DC, m^3 kg^{-1}
		4.41	1.15	1.34	0.37	160.01	1.90	70	0.080
		4.49	1.14	1.33	0.37	180.00	1.93	61	0.083
		4.60	1.14	1.33	0.36	200.01	1.96	54	0.086
		4.73	1.14	1.32	0.34	220.00	1.97	49	0.091
		5.00	1.14	1.32	0.29	240.00	1.99	45	0.096
		4.49	1.17	1.38	0.28	73.31	1.67	141	0.090
		4.68	1.16	1.35	0.29	100.00	1.82	106	0.092
		4.81	1.15	1.34	0.30	120.00	1.89	87	0.095
	0.9	4.95	1.15	1.33	0.31	140.00	1.94	73	0.100
		5.19	1.14	1.32	0.29	160.00	1.97	64	0.106
		5.51	1.14	1.31	0.26	180.00	1.99	56	0.116
		5.98	1.14	1.30	0.22	200.00	2.01	49	0.129
		6.86	1.13	1.30	0.16	220.00	2.03	45	0.149
	0.5	2.94	1.14	1.45	0.69	205.17	1.61	70	0.034
		3.33	1.13	1.47	0.68	220.00	1.61	72	0.037
		3.38	1.15	1.43	0.50	162.48	1.62	80	0.049
		3.44	1.15	1.42	0.50	180.00	1.66	74	0.049
	0.62	3.46	1.14	1.41	0.49	200.01	1.71	67	0.049
		3.48	1.14	1.40	0.48	220.00	1.76	60	0.050
		3.49	1.14	1.39	0.48	240.00	1.80	55	0.051
		3.86	**1.13**	**1.42**	**0.32**	**260.00**	**1.72**	**56**	**0.054**
		3.73	1.16	1.43	0.42	123.46	1.58	100	0.059
		3.76	1.15	1.41	0.40	140.03	1.65	89	0.059
		3.83	1.15	1.40	0.39	160.00	1.72	79	0.060
	0.7	3.87	1.15	1.38	0.39	180.01	1.78	69	0.061
		3.90	1.14	1.37	0.39	200.00	1.84	61	0.063
2-5-15-2		3.94	1.14	1.36	0.40	220.00	1.88	55	0.065
		4.00	1.14	1.35	0.41	240.00	1.91	49	0.067
		4.43	1.13	1.37	0.24	260.00	1.88	50	0.071
		4.08	1.17	1.42	0.34	89.54	1.56	128	0.072
		4.15	1.16	1.41	0.32	100.01	1.63	116	0.073
		4.24	1.15	1.39	0.31	120.02	1.73	98	0.074
		4.32	1.15	1.37	0.31	140.00	1.81	83	0.076
	0.8	4.40	1.15	1.35	0.32	160.00	1.88	71	0.079
		4.50	1.15	1.34	0.32	180.01	1.92	62	0.083
		4.64	1.14	1.33	0.31	200.01	1.95	55	0.088
		4.82	1.14	1.32	0.29	220.00	1.97	49	0.093
		5.20	1.14	1.32	0.23	240.00	1.99	46	0.100
		4.39	1.17	1.41	0.29	66.29	1.56	159	0.086
	0.9	4.53	1.16	1.39	0.27	80.01	1.67	136	0.086
		4.68	1.16	1.36	0.26	100.00	1.79	109	0.089

Config	Size, mm	γ_1	γ_2	γ_3	γ_4	PR, kg m^3h^{-1}	DE	Switching Time, s	DC, m^3 kg^{-1}
2-4-16-2	0.5	4.81	1.15	1.34	0.27	120.00	1.87	89	0.094
		5.00	1.15	1.33	0.26	140.01	1.93	75	0.100
		5.27	1.15	1.32	0.25	160.00	1.97	64	0.109
		5.65	1.14	1.31	0.22	180.00	2.00	55	0.120
		6.29	1.14	1.30	0.18	200.00	2.02	49	0.137
		2.90	1.14	1.46	0.70	205.14	1.59	71	0.033
		3.26	1.13	1.46	0.70	220.00	1.62	72	0.036
	0.62	3.39	1.15	1.45	0.53	153.20	1.55	86	0.048
		3.40	1.15	1.44	0.52	160.00	1.57	83	0.048
		3.42	1.15	1.43	0.49	180.01	1.62	74	0.048
		3.44	1.15	1.42	0.47	200.00	1.66	67	0.049
		3.46	1.14	1.41	0.45	220.00	1.71	61	0.050
		3.48	1.14	1.40	0.44	240.00	1.75	55	0.051
		3.93	**1.13**	**1.44**	**0.31**	**260.00**	**1.67**	**57**	**0.054**
	0.7	3.65	1.16	1.44	0.44	115.94	1.52	106	0.058
		3.75	1.15	1.43	0.40	140.02	1.60	91	0.058
		3.80	1.15	1.41	0.37	160.00	1.67	80	0.059
		3.85	1.15	1.40	0.35	180.02	1.74	70	0.061
		3.91	1.15	1.38	0.35	200.00	1.79	62	0.063
		3.97	1.14	1.37	0.34	220.01	1.84	55	0.066
		4.04	1.14	1.36	0.34	240.00	1.88	50	0.068
		4.63	1.14	1.38	0.19	260.00	1.86	51	0.074
	0.8	4.05	1.17	1.44	0.37	83.99	1.50	138	0.070
		4.12	1.16	1.42	0.32	100.00	1.58	119	0.071
		4.22	1.16	1.40	0.29	120.00	1.69	99	0.073
		4.32	1.15	1.38	0.28	140.00	1.78	84	0.076
		4.43	1.15	1.36	0.27	160.00	1.85	72	0.080
		4.57	1.15	1.35	0.26	180.01	1.90	62	0.085
		4.78	1.14	1.33	0.25	200.01	1.94	55	0.091
		5.04	1.14	1.32	0.23	220.00	1.97	49	0.099
		5.97	1.14	1.33	0.12	240.00	1.98	48	0.112
	0.9	4.38	1.17	1.43	0.29	66.00	1.49	166	0.082
		4.50	1.16	1.40	0.26	80.00	1.62	139	0.084
		4.67	1.16	1.37	0.24	100.00	1.75	111	0.088
		4.89	1.15	1.35	0.22	120.00	1.85	91	0.095
		5.12	1.15	1.33	0.22	140.00	1.92	75	0.103
		5.51	1.15	1.32	0.20	160.00	1.97	64	0.115
		6.13	1.14	1.31	0.17	180.00	2.00	55	0.132
		7.17	1.14	1.30	0.13	200.01	2.03	49	0.160

Bold indicates optimum

B.5. Nomenclature

DC = Desorbent consumption, $m^3\ kg^{-1}$

DE = Deviation from the equilibrium

PR = Productivity, $kg\ m^{-3}h^{-1}$

Greek letters

γ_j = Velocity ratio in zone *j*